

LIGHT HIDDEN SECTORS:
DARK MATTER AND LEPTON JETS

JOSHUA THOMAS RUDERMAN

A DISSERTATION PRESENTED
TO THE FACULTY OF
PRINCETON UNIVERSITY IN
CANDIDACY FOR THE DEGREE
OF DOCTOR OF PHILOSOPHY

RECOMMENDED FOR ACCEPTANCE
BY THE DEPARTMENT OF PHYSICS
ADVISOR: NIMA ARKANI-HAMED

MAY 2011

© Copyright by Joshua Thomas Ruderman, 2011.

All Rights Reserved.

ABSTRACT

A new generation of experiments, including the Large Hadron Collider, is leading particle physics into the data-driven era. This era may bring the discovery of new physics at higher energies than the particle masses of the Standard Model. An equally exciting possibility is the existence of new physics at low energies, such as the GeV scale, with the new physics very weakly coupled to the Standard Model. We focus on the second scenario in this thesis, and we address the question: how could the possible existence of a new, light, hidden sector of particles modify upcoming experimental results? In the first part of the thesis, we build a series of models where dark matter resides in a light hidden sector. We consider scenarios where dark matter annihilates into hidden sector particles, decays into hidden sector particles, or carries an asymmetry under a conserved quantum number of the hidden sector. Each of these cases has exciting consequences for the direct or indirect detection of dark matter. In the second part of the thesis, we consider how a light hidden sector can be discovered in a high-energy collider, such as the Large Hadron Collider. Standard Model particles can decay into highly-boosted hidden sector particles, that manifest themselves as collimated bunches of leptons, known as lepton jets. The discovery of an excess of these new objects would constitute a smoking-gun signature of the existence of a light hidden sector. Lepton jets are now being searched for at the Tevatron and Large Hadron Collider.

ACKNOWLEDGEMENTS

I am grateful to the many people whose help and support have made this thesis possible. First and foremost, I would like to thank my advisor, Nima Arkani-Hamed. His ideas, inspiration, and advice are behind most of my work at Princeton, and he has assembled a large and vibrant phenomenology community here, which includes many of my collaborators. I would also like to thank Liantao Wang, who has provided me with great support and advice throughout graduate school. Liantao collaborated with me on much of the work in this thesis, and provided me with strong encouragement from the very beginning.

I am also especially grateful to the collaborators that have taken the time to teach me the ropes. Clifford Cheung, who worked with me on my first few projects, really got me started. And Tomer Volansky picked up from there, he is the ideal collaborator and has taught me much of what I know (and thanks to Elinor and Segev Volansky for welcoming me over to their apartment for many late nights of working!). More recently, I have benefited greatly from working with David Shih, who has helped bring my work closer to experimentalists. I also learned a lot from Itay Yavin and Adam Falkowski, two wonderful collaborators who worked with me on much of the content in this thesis.

I would also like to thank all of my other collaborators on various projects, including Matt Baumgart, Michael Graesser, David Krohn, Mariangela Lisanti, Philip Schuster, Jessie Shelton, Tracy Slatyer, Scott Thomas, Natalia Toro, Neal Weiner, and Jure Zupan; you all taught me a lot. And I have benefited enormously from conversations with many other great physicists, including Nathaniel Craig, JiJi Fan, Patrick Fox, Dan Green, Jared Kaplan, Ami Katz, Zohar Komargodski, Paul Langacker, Patrick Meade, Michele Papucci, Matt Reece, Nati Seiberg, and Matt Strassler. And I have learned everything I know about real physics from talking to many excellent experimentalists, in-

cluding Yuri Gerstein, Eva Halkiadakis, Cristiano Galbiati, Valerie Halyo, Henry Lubatti, Sunil Somalwar, and Chris Tully. I thank Herman Verlinde for sitting on my thesis committee, along with Nima and Chris. I apologize to the people that I forgot to list, but should be here.

Finally, I would like to thank the people that make my life more interesting. Meixia Zhang provides much support and motivation (she, above anyone else, makes sure that I always raise my standards), as do my parents and sister, who this thesis is dedicated to. My grandfather, Thomas O'Hara was also always a strong supporter of my academic pursuits, and although he passed away during my time at graduate school, I know he would have been proud of me now. Princeton was much more fun because of my academic brother Jacob Bourjaily (thanks for letting me keep the bigger desk in our office!), my older academic siblings Cliff, Jared, and Matt, and my other classmates, John Appel, Alex Dahlen, XinXin Du, Colin Parker, Silviu Pufu, Richard Saldanha, Audrey Sederberg, Tibi Tesileanu, and many others!

To my parents Maureen and Stephen, and sister Danielle.

RELATION TO PREVIOUSLY PUBLISHED WORK

Chapters 2 and 6 come from ref. [1], chapter 3 from ref. [2], chapter 4 from ref. [3], chapter 5 from ref. [4], chapter 7 from ref. [5], chapter 8 from ref. [6], and chapter 9 from ref. [7]. Portions of this thesis were presented by the author at the following workshops and conferences: *Phenomenology*, University of Wisconsin-Madison, May 2009; *The Dark Side of the Universe*, University of Melbourne, June 2009; *Implications of Neutrino Flavor Oscillations*, Sante Fe, July 2009; *Giving New Physics a Boost*, SLAC, July 2009; and *Dark Forces Workshop*, SLAC, September 2009.

Contents

Abstract	iii
Acknowledgements	iv
Relation to Previously Published Work	vii
1 Introduction and Conclusions	1
Part I: Models of Hidden Sector Dark Matter	9
2 Non-Abelian Models	10
2.1 The Dark Sector and Symmetry Breaking	13
I. Doublet Models	15
II. Doublet/Triplet Models	16
2.2 Dark Matter Mass Splitting	17
I. Radiative Splitting	19
II. Mass splitting from higher dimensional operator	20
2.3 Generation of the Dark Sector Mass Scale	23
I. SUSY Breaking from Kinetic Mixing	25
II. SUSY Breaking From $\mathbf{5} + \bar{\mathbf{5}}$ Messengers	27
2.4 Benchmark Models	29
I. Non-SUSY Benchmark Models	30
II. SUSY Benchmark Models	33

3	A Minimal $U(1)$ Model	38
3.1	Introduction	38
3.2	New Scales in the Dark Sector via Kinetic Mixing	40
3.3	A Model for the Dark Sector	41
	I. Coupling to the Standard Model	42
	II. Mass Spectrum	43
	III. Supersymmetry Breaking Effects	44
3.4	Observations and Predictions	45
3.5	Conclusions	47
4	Decaying into the Hidden Sector	49
4.1	Introduction	49
4.2	Tools for Modeling Decaying Dark Matter	52
	I. Framework	52
	II. Model Building Dangers	54
	III. GUT Scale: Decay Operators	56
	IV. Weak Scale: Dark Matter Mass and Communicating SUSY Breaking	58
	V. GeV Scale: Breaking the Dark Sector	60
	VI. MeV Scale: Dark Matter Splitting	62
4.3	Models	64
	I. $U(1)_d$: The Minimal Model	65
	II. $SU(2)_d \rightarrow U(1)_d$: GUT Scale Symmetry Breaking	67
	III. $SU(5)_{\text{SM}} \times U(1)_d$: SM Charged-DM and Correlated Neutrinos . .	70
	IV. $U(1)_\chi \times U(1)_d$: No Mass Splitting	72
4.4	Cosmology of the Dark Sector	74
	I. Thermal DM Abundance	75
	II. The Lightest Dark Sector Fermion	77
4.5	Discussion	80
5	Asymmetric Dark Matter from Leptogenesis	82
5.1	Introduction	82

5.2	Toy Model for Two-Sector Thermal Leptogenesis	86
	I. Toy Model	86
	II. Decay Asymmetry	87
	III. Boltzmann Equations	88
	IV. Washout Effects	91
5.3	Towards a Complete Model	95
5.4	Symmetric Dark Matter from an Asymmetry	99
	I. Restoring Symmetric Dark Matter with Late Decays	100
	II. Asymmetric Sterile Neutrinos from Leptogenesis	104
5.5	Cosmology and Light Dark Matter	109
5.6	Outlook	113
Part II: Lepton Jets		115
6	Introduction to Lepton Jets	116
6.1	Lepton Jets from a Non-Abelian Dark Sector	116
	I. Production and decay of dark gauge bosons and Higgses	117
	II. Collider signals of supersymmetric models	126
7	Lepton Jet Showering and Experimental Definition	135
7.1	Introduction	135
7.2	Electroweak Production	138
	I. Rare Z^0 Decays	139
	II. Electroweak-ino Pair Production	141
	III. Neutralino Decays into the Dark Sector	142
7.3	Dark Sector Dynamics	145
	I. Dark Showering	146
	II. Decay of dark states back into leptons and pions	149
	III. Lepton jets' morphology	150
7.4	Lepton Jets and Experimental Searches	151
	I. Lepton jets from rare Z^0 decays	152

II.	Lepton jets from neutralino cascades	152
III.	Experimental Searches	156
7.5	Conclusions	160
8	Hiding the Higgs with Lepton Jets	163
8.1	Introduction	163
8.2	The Hidden Sector	167
I.	Portals	167
II.	A Minimal Model	170
8.3	Higgs Decays to the Hidden Sector	171
I.	Neutralino Channel	171
II.	Sneutrino Channel	174
III.	Singlet Channel	176
8.4	Collider Phenomenology	177
I.	Lepton Jets and Neutralino Jets	178
II.	Experimental Observables	179
8.5	Can Lepton Jets Really Hide the Higgs?	184
8.6	Experimental Constraints	185
I.	LEP-1 Searches	186
II.	LEP-2 Searches	187
III.	Tevatron Searches	190
8.7	Hiding the Higgs	191
I.	Methodology	192
II.	Constraints on Experimental Observables	192
III.	Benchmarks Models	195
8.8	Suggested Search Strategies	199
8.9	Conclusions and Outlook	202
9	Discovering Higgs Decays to (Electronic) Lepton Jets	205
9.1	Introduction	205
9.2	Models	206

9.3	Electron jets vs. QCD jets	208
9.4	Analysis and Results	209
9.5	Higgs Mass	212
A	Appendices	214
A.1	Kinetic Mixing	214
A.2	Charge Breaking in the Dark Sector	216
A.3	Hidden \mathbb{Z}_2 Symmetry in the $\tan\beta = 1$ Limit	218
A.4	SUSY Contribution to DM Mass Splitting	218
A.5	Decaying Models: Superpotentials and Charges	221
A.6	Notation for Hidden Higgs	225
A.7	Efficiencies of Existing Searches for Hidden Higgs	226

Introduction and Conclusions

The data-driven age of particle physics has begun. The Large Hadron Collider (LHC) is rapidly collecting proton-proton collision data at a center of mass energy of 7 TeV, and the Tevatron is completing its final run. A new generation of dark matter detectors have unprecedented sensitivity to directly detect the scattering of dark matter particles against nuclei. Meanwhile, a suite of ground and space based detectors are looking to the sky, improving our understanding of the cosmic ray, gamma ray, and neutrino spectra in our Galaxy. Experimental particle physics is advancing dramatically on many fronts, and the data collected over the next decade have the potential to revolutionize our understanding of the Universe.

There are good reasons to expect that the next decade will bring the discovery of new particles at higher energies. The Standard Model (SM) [8] provides an excellent description of particle physics that is consistent with many experimental tests across many orders of magnitude of energies up to the electroweak scale of about 100 GeV. But so far, the observed particle content is incomplete, because new degrees of freedom, such as the higgs boson, are required to unitarize W^+W^- scattering at the TeV energy scale. And even with the higgs, the SM suffers a fine tuning problem, and new particles are probably required at the electroweak scale in order to explain the large hierarchy between this scale and the Planck scale of 10^{19} GeV, where gravity becomes strongly coupled. Supersymmetry (see [9] for a review with original references) is a leading candidate to explain the hierarchy problem, and predicts the presence of many new particles at the energies that will be probed by the LHC.

For the reasons just outlined, most of the recent theoretical and experimental efforts in particle physics have focused on the search for new dynamics at higher energy scales. This thesis is concerned with a different, complementary, program. What if there are new, light, degrees of freedom that remain undetected because they are very weakly coupled to the Standard Model? If the field content of our Universe is non-minimal,

then there may exist entire new sectors of particles with their own gauge symmetries, and with masses lighter than the electroweak scale. We will learn throughout this thesis that new, light, hidden sector particles are within reach of emerging experiments. And we will learn that light hidden sectors can modify phenomenology, beyond the SM, in interesting and nontrivial ways.

The possible importance of a light hidden sector for collider phenomenology was recently stressed by Refs. [10, 11, 12, 13]. These papers consider the possibility that there exists a hidden sector, called a *Hidden Valley*, with a gauge group that confines below the electroweak scale, $\Lambda_h \ll m_Z$. In their setup, SM particles (or superpartners) can decay into hidden sector partons, which shower, hadronize, and decay back to SM particles, such as displaced b-jets. Whereas most previous model building, beyond the SM, has focused on solving problems of the SM at higher energies, the Hidden Valley papers point out that it is also interesting to consider non-minimal models because they can qualitatively modify signals at the LHC.

The Hidden Valley models were unmotivated, in the sense that they did not attempt to explain anything, but instead were designed to highlight interesting signals. More recently, a series of astrophysical anomalies have provided a motivation for light hidden sectors, and a connection to Dark Matter (DM).

The PAMELA satellite [14] observed an excess, shown to the left of figure 1.1, in the ratio of positron to electron cosmic rays at energies of 10 to 100 GeV, relative to the predicted astrophysical background. This background comes from proton cosmic rays colliding with interstellar material, and this background rate is estimated from models of cosmic ray diffusion [15, 17]. Soon after, the FERMI satellite observed an excess, shown to the right of figure 1.1, of electron plus positron cosmic rays extending up to energies of 1 TeV. The PAMELA and FERMI excesses are both compatible with a new source that injects an equal number of electron and positron cosmic rays at the TeV energy scale [18]. Dark matter annihilations, in our Galaxy, can be this new source of leptonic cosmic rays. The lightest supersymmetric particle (LSP) provides a possible dark matter candidate (for a review see [19]). However it is very challenging for vanilla dark matter candidates, like the LSP, to explain the cosmic ray anomalies for two reasons, (1) the annihilation

rate must be several orders of magnitude larger than the annihilation rate that produces the correct DM relic abundance, and (2) DM must annihilate predominantly into leptons and not hadrons, since PAMELA observes no corresponding excess in antiproton cosmic rays.

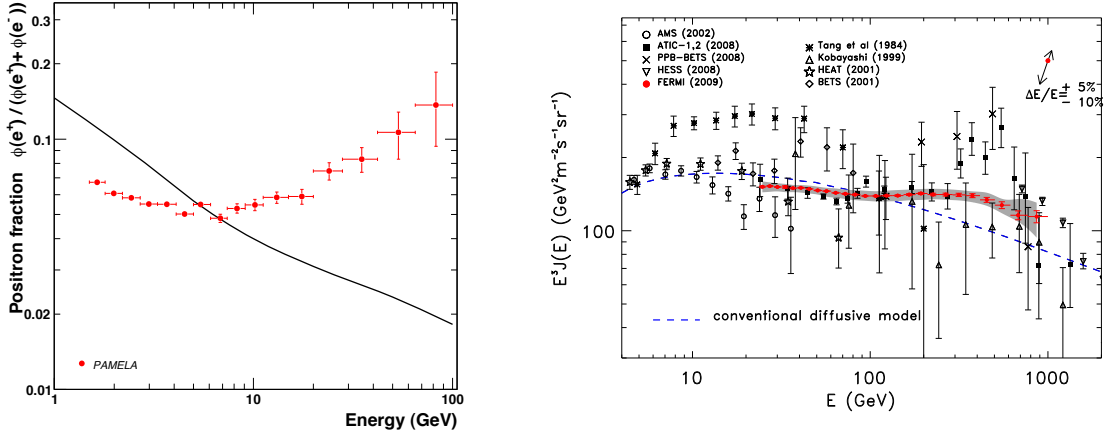


Figure 1.1: The plot on the *left* shows the positron fraction of e^\pm cosmic rays, measured by the PAMELA satellite [14]. The data (red points) rise above the predicted astrophysical background (black curve), using a model for cosmic ray diffusion [15]. The plot on the *right* shows the total electron plus positron cosmic ray spectrum measured by the FERMI satellite [16]. The data (red points) show a mild excess above the the prediction (dashed blue line) of a diffusion model [17].

A compelling explanation of these cosmic ray anomalies was put forth by refs. [20,21]. Instead of residing in the SM sector, dark matter may be charged under a hidden sector gauge symmetry. Then, dark matter may annihilate into hidden sector gauge bosons, γ_d . If the hidden sector is light, $m_{\gamma_d} \lesssim \text{GeV}$, then the annihilation rate is Sommerfeld enhanced [22] at low velocities, providing a mechanism to explain the large rate needed to account for the PAMELA and FERMI anomalies described above. The hidden photons can decay to leptons if they kinetically mix with SM photons, and for $m_{\gamma_d} \lesssim \text{GeV}$, antiprotons are kinematically disallowed. Therefore, DM annihilations into a light hidden sector provide an economical solution to the two challenges, described above, for DM to account for the lepton cosmic ray anomalies. These models also naturally in-

clude the possibility that there are several DM states with small mass splittings on the order of 100 keV, such that DM can scatter inelastically against nuclei into an excited state. This inelastic DM [23] provides a mechanism to reconcile the modulation observed by the DAMA/LIBRA experiment, shown in figure 1.2, with the null results of other experiments. We have seen that not only can hidden sectors lead to dramatic changes in collider phenomenology, as emphasized by the Hidden Valley program, but they can account for anomalies in astrophysics and direct detection experiments, if DM interacts with the light hidden sector.

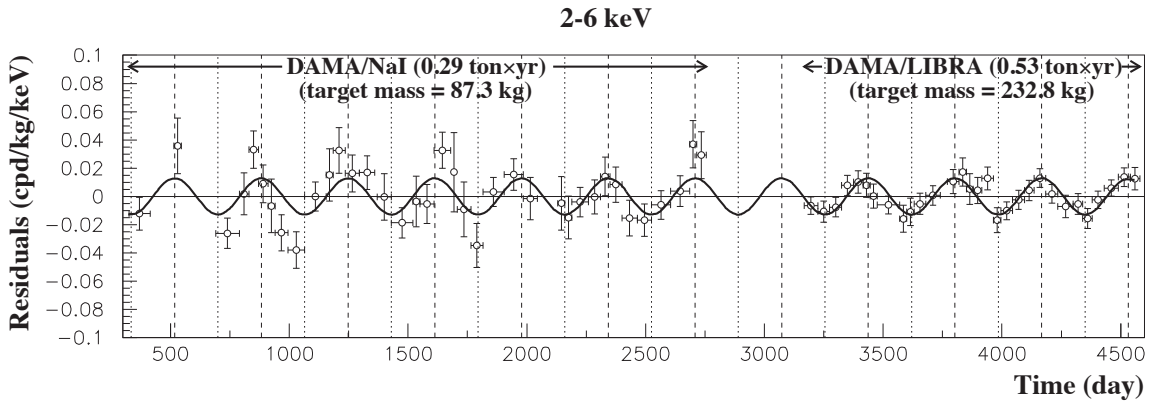


Figure 1.2: The modulation of scintillation events observed by the DAMA/LIBRA experiment, shown with a superimposed sinusoid with period of one year and a phase of June 2nd [24].

In this thesis, we explore more details of light hidden sectors, and their possible relation to DM or collider physics. The thesis is divided into two parts. In the first part, we construct a series of models where DM resides in a light hidden sector. Similarly to the discussion above, we will see that these models will modify the indirect and direct detection of DM, in interesting ways. In the second part of the thesis, we introduce and study a new collider physics object, *lepton jets*, which were proposed by ref [21] to follow from the same light hidden sector models that can explain astrophysical anomalies. SM particles decay into hidden sector particles, which can cascade decay into yet more hidden sector particles, including hidden photons. Since the hidden sector mass scale is light, all

of the hidden particles are highly boosted in the lab-frame, and therefore form collimated groups. Then, the hidden photons can decay back to the SM, through kinetic mixing, to leptons. The final result is bunches of collimated electrons, muons, and pions, which form jet-like objects called lepton jets.

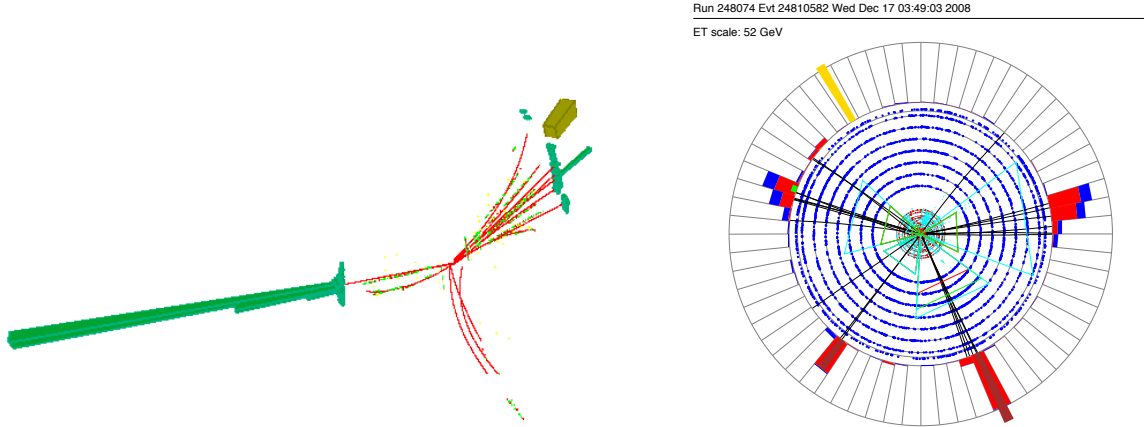


Figure 1.3: Lepton jets at LEP and the Tevatron. The *left* plot shows an L3 simulation of a higgs decaying to two lepton jets composed of multiple collimated electrons. We thank Chris Tully for providing this plot. The *right* plot shows an event display of an event passing the $D0$ search for 2 lepton jets plus missing energy [25], here each candidate lepton jet contains an electron and at least one nearby companion track.

We are happy to point out that the proposal of [21], followed by the work in this thesis, has led to a broad experimental program to detect lepton jets in high-energy colliders. It is possible that lepton jets were produced, and missed, at the LEP electron-positron collider. The left plot of figure 1.3 shows an L3 detector simulation of a Higgs boson decaying to two lepton jets composed of electrons. Lepton jets have now been searched for explicitly at the $D0$ detector at the Tevatron, and the right plot of figure 1.3 shows a real event that passes the selection, with two candidate lepton jets plus missing energy. There are SM processes that produce collimated leptons, including heavy flavor decays and meson decays, so it is important to point out that this event probably does not constitute new physics since no excess above SM expectations was observed. Lepton jet searches are now under way at the ATLAS and CMS detectors at the LHC. Figure 1.4

shows CMS event displays of simulated lepton jets composed of collimated muons. CMS has already set preliminary limits on colored SUSY production of muonic lepton jets with 35 pb^{-1} of data [26].

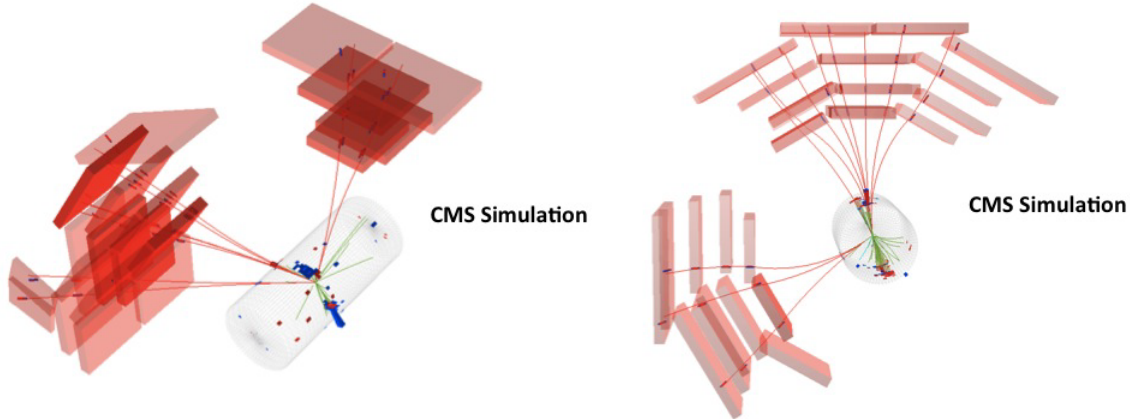


Figure 1.4: CMS event displays of SUSY production of simulated lepton jets composed of collimated muons. We thank Valerie Halyo for providing these plots.

We now summarize the contents of the rest of this thesis. In chapter 2, we construct explicit models where DM annihilates into a non-abelian GeV-scale hidden sector, along the lines proposed by ref. [21]. We place a special emphasis on two model-building issues, (1) naturally generating the GeV scale, and (2) arranging the field content so that the hidden sector is completely broken and so that DM mass splittings are radiatively generated with couplings that can account for inelastic DM. In order to address issue (1), we show that supersymmetric models, with kinetic mixing automatically generate the GeV scale through mixing of the hidden sector and hypercharge D -terms. We also solve issue (2) and present a series of workable hidden sectors and benchmark models.

We continue to consider models where DM annihilates into a light hidden sector, in chapter 3. Here, we present a minimal, complete, hidden sector model that can account for the astrophysical anomalies. In this chapter, the hidden sector includes only a $U(1)_d$ gauge symmetry, which is broken at the GeV scale due to D -term mixing. A DM mass splitting, that can account for inelastic DM, is generated by a higher dimension operator. This minimal model features a small number of parameters, and is therefore predictive.

In chapter 4, we propose a new class of models where DM decays, instead of annihilates, into a light hidden sector. The correct decay rate to account for the PAMELA and FERMI anomalies is naturally generated by dimension 6 operators suppressed by the GUT scale. These models avoid certain astrophysical tensions of the annihilating models, and predict correlated signals in gamma rays and neutrinos, which, if found, would suggest that the leptonic cosmic rays are due to DM decays, instead of annihilations.

In chapter 5, we consider an alternative paradigm for explaining the DM abundance. Instead of DM being a thermal relic with abundance determined by the annihilation rate, DM may carry an asymmetry under a conserved quantum number, similar to baryons. We propose a new implementation of this idea, with two-sector leptogenesis, where DM resides in a hidden sector. Right handed neutrinos decay out of equilibrium into both the SM and hidden sector, producing a lepton asymmetry and a DM asymmetry at the same time. This model simultaneously explains the baryon asymmetry, DM abundance, and neutrino masses. The DM mass can range from 1 keV to 10 TeV, and this model includes new mechanisms for generating a large annihilation rate in the present epoch, allowing for an explanation of the cosmic ray anomalies.

Part 2 of the thesis begins in chapter 6, where we introduce lepton jets within the context of non-Abelian hidden sectors, at the GeV scale. We discuss the production of lepton jets from Z -boson decays and from the decays of SM superpartners, and we survey the features of their phenomenology, including production cross-section and lepton multiplicities, opening angles, and p_T spectra.

We continue with a more detailed study of lepton jets in chapter 7. Here, we discuss the effects of hidden sector showering on the production of lepton jets. We present a Monte Carlo simulation of this effect. We also propose an experimental definition of lepton jets, which can serve as a search strategy in high-energy colliders.

In chapter 8, we propose that the higgs boson may decay dominantly into lepton jets. We also consider, in detail, how existing LEP and Tevatron searches constrain lepton jets. We find that the higgs may be as light as 100 GeV, and have been produced copiously but missed by existing searches at LEP and the Tevatron.

Finally, in chapter 9, we suggest a concrete search strategy for finding a light higgs boson that decays to lepton jets composed of electrons. Such lepton jets can be differentiated from QCD jets by looking at the fraction of jet energy deposited in the electromagnetic calorimeter, and the fraction of jet p_T carried by charged tracks. We find that a light higgs decaying to lepton jets can be discovered, or ruled out, by searching for this signal at the Tevatron or 7 TeV LHC.

PART I: MODELS OF HIDDEN SECTOR
DARK MATTER

Non-Abelian Models

Several intriguing observational results from high-energy astrophysics have motivated an exciting new proposal [20] in which a WIMP-like dark matter (DM) particle at 500-800 GeV annihilates primarily into leptons and is charged under a new “dark” force carrier. ATIC [27] detects an abundance of cosmic ray electrons between 300 – 800 GeV, while PAMELA [14] sees an excess of positrons (but not anti-protons [28]) at 10-100 GeV. Together with the CMB haze [29, 30, 31], these observations paint a consistent picture whereby DM annihilates primarily into muons and/or electrons [32].

There are two sources of tension between these results and more conventional models of WIMP dark matter. First, assuming thermal freeze-out, the standard relic abundance calculation implies an annihilation cross-section that is at least a hundred times too small to explain the lepton excesses observed in astrophysical experiments. A “boost factor,” typically attributed to local over-densities of dark matter, is often evoked in this case. A second difficulty is the non-observation of corresponding excesses in anti-protons [28] and gamma rays [33], which puts strong bounds on hadronic channels that are present in many dark matter models.

Motivated by the above considerations, the authors of Ref. [20] outline a scenario in which these apparent contradictions are reconciled. They introduce a 500-800 GeV WIMP that couples to a GeV scale dark gauge boson that kinetically mixes with the photon of the Standard Model (SM) [34]¹ (see Ref. [36] for another recent suggestion with similar ingredients). A schematic illustration of this scenario is presented in Fig. 2.1. The ATIC and PAMELA data are explained by DM annihilation into the dark gauge boson which subsequently decays into electrons and muons. Elegantly enough, the $\mathcal{O}(1)$ GeV scale plays two independent roles. First, the new dark force carrier at \lesssim GeV introduces a Sommerfeld enhancement [37, 38, 39, 40], giving a boost factor of the right size to enhance

¹Ref. [35] analyzes particle physics bounds on such a light vector field and its possible connection to the HyperCP anomaly.

the DM annihilation cross-section². Second, the absence of anti-protons in the PAMELA observations is now simply a result of kinematics [42].

The gauge group, G_{dark} , is a priori unspecified. However, it was observed in Ref. [20] that a non-abelian G_{dark} nicely accommodates the excited dark matter (XDM) [43] and inelastic dark matter (iDM) [23] mechanisms. XDM was proposed in order to explain the INTEGRAL [44] measurement of the 511 keV gamma-ray line at the center of the galaxy. The iDM scenario can accommodate the DAMA/LIBRA measurement of WIMP-nuclei scattering with other direct detection experiments [45, 46, 47]. Both XDM and iDM are non-standard WIMP scenarios in which a DM ground state can transition to and from new excited states via the emission of some field that couples back to the SM. If the DM lives in a multiplet of a non-abelian G_{dark} , then these ground and excited states can be the components of this multiplet, and transitions will emit dark gauge bosons that couple weakly to the SM. Independent of the results from INTEGRAL and DAMA, we find the possibility of a non-abelian dark sector to be intriguing in its own right, with direct implications for the collider phenomenology. Thus throughout this chapter we consider a dark sector with a non-abelian gauge symmetry that is completely broken by some dark Higgs sector³.

In Section 2.1, we construct a catalog of explicit minimal models. Since G_{dark} needs to include a $U(1)$ factor for kinetic mixing with SM hypercharge, we take $G_{\text{dark}} = SU(2) \times U(1)$. Our models differ only in their dark Higgs sectors, which are constructed to break G_{dark} completely and induce all the necessary couplings between the different states of the DM multiplet.

In Section 2.2, we discuss the mass splittings between the dark matter states. In order to obtain the small mass splittings needed for XDM and iDM, we consider DM that is a doublet or a triplet under $SU(2)_{\text{dark}}$. The splittings may be generated radiatively from dark gauge boson loops. Another possibility is to generate them through higher-dimensional couplings between the dark matter and a single dark Higgs.

²See Ref. [41] for an alternative, but related way for producing a large boost factor.

³There are strong astrophysical constraints on a long range interaction from unbroken gauge symmetry with an unsuppressed coupling [48, 49, 50].

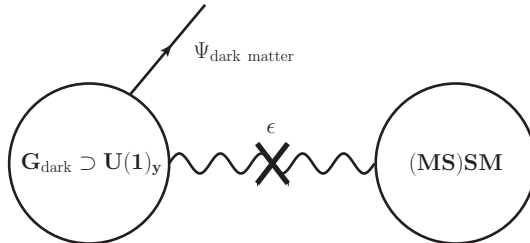


Figure 2.1: A schematic illustration of the minimal setup we consider in this chapter. The dark sector and the SM are connected through kinetic mixing term suppressed by $\epsilon \lesssim 10^{-3}$. The dark matter multiplet may or may not couple directly to the SM. Supersymmetric extensions of this scenario are also discussed.

In Section 2.3, we consider the addition of SUSY to the dark sector. We observe that the minimal assumption of kinetic mixing between dark sector and SM hypercharge generates an effective FI term in the dark sector that is naturally of the desired scale, $\mathcal{O}(\text{GeV})$. This term can break SUSY, or even more interestingly can generate a super-Higgs mechanism that leaves a supersymmetric dark sector with a ~ 1 GeV gap. Both of these scenarios typically result in light fermions that may have an influence on collider physics. We emphasize that this is a *leading* contribution which must be included in any SUSY scenario that includes kinetic mixing. Furthermore, within this scheme the DM can easily be a SM singlet, and so DM annihilations do not produce SM W^\pm bosons that would dangerously decay to anti-protons that have not been observed by PAMELA. We also investigate the gauge mediation scenario originally proposed in Ref. [21] where DM is charged under the SM gauge group. An additional complication we address arises because SUSY restricts the form of the scalar potential which is responsible for breaking G_{dark} completely. We provide several examples to overcome this difficulty.

In Section 2.4, we present several benchmark models for the dark Higgs sector. The resulting spectra of light vector bosons and scalars are explicitly computed and the relevant couplings are discussed.

Finally, let us briefly comment on the notational conventions used in this chapter. In general, symbols referring to elements of the SM will be capitalized—so for example the

SM hypercharge gauge coupling, gauge field, and field strength will be denoted by g_Y , B_μ and $B_{\mu\nu}$. In contrast, lowercase symbols will refer to elements of the dark sector, so the dark sector gauge coupling, gauge field, and field strength will be denoted by g_y , b_μ and $b_{\mu\nu}$. We will use h , or h' to denote dark Higgses. We denote the dark matter states by Ψ and we denote the SM and dark photon by γ and γ' , respectively.

2.1 The Dark Sector and Symmetry Breaking

Let us begin by discussing the basic structure of the dark sector models that we will consider in this chapter. We take the DM to be the lightest (and stable) component of some multiplet of the non-abelian group G_{dark} . As we will discuss in Section 2.2, such a multiplet is necessary if we wish to explain the INTEGRAL and/or DAMA signals along the lines of the XDM and iDM proposals of [43, 23, 51].

Furthermore, we follow the proposal of [20] in which the SM is coupled to the dark sector via a kinetic mixing term between SM hypercharge and a dark sector $U(1)$ gauge field:

$$\mathcal{L}_{\text{gauge}} = -\frac{1}{4}B_{\mu\nu}B^{\mu\nu} - \frac{1}{4}b_{\mu\nu}b^{\mu\nu} + \frac{\epsilon}{2}B_{\mu\nu}b^{\mu\nu} \quad (2.1.1)$$

where $B_{\mu\nu}$ and $b_{\mu\nu}$ are the SM and dark sector hypercharge field strengths, respectively. Because this marginal operator preserves all of the symmetries of the SM, it is relatively unconstrained phenomenologically. For a detailed analysis of kinetic mixing and the couplings it induces between SM and dark sector fields, see appendix A.1.

Since G_{dark} must contain a $U(1)$ factor⁴, the minimal choice is of course $G_{\text{dark}} = SU(2) \times U(1)$. Furthermore, if G_{dark} is broken completely at a scale of $\sim \text{GeV}$, then the resulting mass gap will relieve constraints from BBN on the number of relativistic degrees of freedom. However, in order to fully break charge, it is necessary to appropriately

⁴It is actually possible to achieve mixing without an abelian factor through an S parameter type operator $\text{Tr}[\Phi w_{\mu\nu}]B^{\mu\nu}$, where Φ is some operator that transforms as an adjoint of the non-abelian group. In this chapter we keep the abelian factor in order to investigate the collider signatures of the more general gauge group structure and ignore the existence of such operators. That is certainly justified in the case where no fundamental adjoints are present and the contribution is subleading.

engineer a dark Higgs sector. As we shall see shortly, these scalars must also break a custodial $SU(2)$ in order to be phenomenologically viable. The necessity of breaking these symmetries demands a fairly elaborate dark Higgs sector.

First, let us consider the issue of charge breaking. Even for the simplest two Higgs doublet model, the criterion for charge breaking is quite complicated [52], for theories with more exotic Higgs representations, the space of charge breaking vacua is not even known. In appendix A.2, we present a straightforward method for deriving necessary conditions for charge breaking in two higgs doublet sectors, which we applied in order to obtain viable dark sector benchmark models.

Now let us explain the problem of the custodial symmetry. In the spirit of [20], we will assume that the DM is a multiplet of G_{dark} whose components are split in mass. The resulting excited and ground states have transitions mediated by dark gauge bosons that need to couple to the SM electric current if they are to realize the XDM and/or iDM scenarios (see Section 2.2). However, this mixing can be forbidden by a custodial symmetry of the dark Higgs sector. To see why this is the case, consider a model of two scalar doublets. We define $w_{a\mu}$ and b_μ to be the gauge bosons of G_{dark} , where b_μ is the abelian field which mixes with the SM hypercharge, B_μ . Assuming arbitrary vevs for the scalars, G_{dark} is broken, and in the $\{w_1, w_2, w_3, b\}$ basis, the gauge boson mass matrix takes the form

$$M_{\text{dark gauge}}^2 = \begin{pmatrix} m_w^2 & 0 & 0 & \Delta_1 \\ 0 & m_w^2 & 0 & \Delta_2 \\ 0 & 0 & m_w^2 & \Delta_3 \\ \Delta_1 & \Delta_2 & \Delta_3 & m_b^2 \end{pmatrix} \quad (2.1.2)$$

As a consequence of the custodial symmetry present in any theory of only scalar doublets, the diagonal entries w_i are all equal. Applying a custodial $SU(2)$ transformation, we can rotate the components Δ_i completely into the w_3 direction. This yields a mass matrix which has a manifest $U(1)$ symmetry that acts as a phase rotation on $w_\pm = w_1 \pm iw_2$ (note that the gauged “electromagnetism” can still be broken while preserving this $U(1)$). Under this $U(1)$ the components of the DM multiplet have distinct charges—consequently the gauge bosons that mediate transitions among these states must also be charged, so

they can only be the w_{\pm} . However, w_{\pm} have no components in the b direction, so they do not kinetically mix with SM hypercharge and thus cannot decay to SM particles.

Because the custodial symmetry is broken explicitly by the dark hypercharge, the couplings to the SM that are excluded at tree-level by this symmetry will be generated at one loop. Indeed, this may actually be desirable, since it generates an effective coupling for the DAMA transition that is suppressed beyond the ϵ^2 from the kinetic mixing. Another possibility, considered below, is to include additional Higgses that break custodial symmetry at tree-level.

In the case of SUSY models, we will be forced to significantly enlarge the Higgs sector. This is because many of the difficulties that arise in the non-SUSY case are exacerbated with the additional constraints imposed by SUSY. Moreover, in SUSY, all scalars are complex, which forces us to promote real Higgs triplets to complex Higgs triplets. This, along with the constraint of anomaly cancellation implies somewhat of a proliferation of Higgses in these theories.

In what follows, we enumerate several types of scalar sectors that break dark charge as well as custodial symmetry. We focus on models with the intention of later extending them with supersymmetry.

I. Doublet Models

A theory of one Higgs doublet is incapable of breaking charge, so we consider two doublets h_1 and h_2 with quantum numbers $\mathbf{2}_{-1/2}$ and $\mathbf{2}_{1/2}$ under $G_{\text{dark}} = SU(2) \times U(1)$. A general renormalizable scalar potential that breaks charge is given by⁵,

$$\begin{aligned}
 V(h_1, h_2) &= \frac{\lambda_1}{2} (|h_1|^2 - |v_1|^2)^2 + \frac{\lambda_2}{2} (|h_2|^2 - |v_2|^2)^2 \\
 &+ \lambda_4 |h_1^T \epsilon h_2 - v_1 v_2 \cos \alpha|^2 + \lambda_3 (|h_1|^2 - |v_1|^2) (|h_2|^2 - |v_2|^2)
 \end{aligned}
 \tag{2.1.3}$$

⁵This is not the most general renormalizable scalar potential possible. One can add three more terms, $|h_1|^2 |h_2|^2$, $|h_1|^2 h_1^T \epsilon h_2$, and $|h_2|^2 h_1^T \epsilon h_2$ which are consistent with all the symmetries. However, these simply complicate the potential and are not required for breaking charge. A more general analysis of the vacuum structure can be found in Ref. [52]

with,

$$\lambda_1 > 0, \quad \lambda_2 > 0, \quad \sqrt{\lambda_1 \lambda_2} + \lambda_3 > 0, \quad \lambda_4 > 0 \quad (2.1.4)$$

v_2 is complex and charge is broken when $0 < |\cos \alpha| < 1$.

In the MSSM the conditions of Eq. (2.1.4) are violated at tree level. From the D-term contributions to the scalar potential we have $\lambda_1 = \lambda_2 = -\lambda_3 = (g^2 + g'^2)/8$. The inequality is saturated and the potential in Eq. (2.1.3) degenerates and contains a flat direction. To avoid such flat directions in the MSSM one must usually evoke a condition on the quadratic terms in the potential. Such potentials cannot be placed in the form of Eq. (2.1.3) and charge is not broken. Therefore the usual supersymmetric two doublets model will not suffice and we need additional contributions to the scalar potential in order to satisfy the condition, Eq. (2.1.4).

In addition, since this model has a custodial symmetry, it fails to have proper mixings between the gauge bosons. Nonetheless, since the custodial symmetry is broken by dark hypercharge, the gauge boson mixing receives one-loop radiative corrections that break the custodial symmetry. From this point of view there is also no reason not to include higher dimension custodial violating operators that can be generated if heavy (triplet) states have been integrated out. In fact, we include such irrelevant operators in the benchmark model of Section I.

Here we also note the presence of an unfortunate \mathbb{Z}_2 symmetry that is present in the $\tan \beta = 1$ limit. This symmetry needs to be broken since it prevents two of the dark gauge bosons from coupling to SM electric charge (see appendix A.3).

II. Doublet/Triplet Models

An obvious way to break custodial $SU(2)$ at tree-level is to augment the two doublet model with a light triplet of $SU(2)$. For instance, consider a model of one doublet, h , and one real triplet, Φ , with dark quantum numbers $\mathbf{2}_{1/2}$ and $\mathbf{3}_0$, respectively. In order to realize a charge breaking angle between the doublet and triplet, we include the following two operators: $h^\dagger \Phi h$ and $h^T \epsilon \Phi h$. Since the latter has nonzero hypercharge, we must

multiply it by a new hypercharged singlet, S , in order to include it in the potential:

$$\begin{aligned}
V(h, \Phi, S) &= \frac{\lambda_h}{2} (|h|^2 - |v_h|^2)^2 + \frac{\lambda_\Phi}{2} (\text{Tr} [\Phi\Phi] - |v_\Phi|^2)^2 \\
&+ \frac{\lambda_S}{2} (|S|^2 - |v_S|^2)^2 + c_1 h^\dagger \Phi h + (c_2 S h^T \epsilon \Phi h + \text{h.c.})
\end{aligned}
\tag{2.1.5}$$

Alternatively, we might consider a model with two doublets and one triplet. This is more natural if we wish to eventually include SUSY. The scalar potential takes the form:

$$\begin{aligned}
V(h_1, h_2, \Phi) &= V(h_1, h_2) + \frac{\lambda_\Phi}{2} (\text{Tr} [\Phi\Phi] - |v_\Phi|^2)^2 \\
&+ c_1 h_1^\dagger \Phi h_1 + c_2 h_2^\dagger \Phi h_2 + (c_3 h_1^T \epsilon \Phi h_2 + \text{h.c.})
\end{aligned}
\tag{2.1.6}$$

where $V(h_1, h_2)$ is the contribution from doublets alone defined in eq 2.1.3.

We can impose an additional \mathbb{Z}_2 symmetry $\Phi \rightarrow -\Phi$, that forbids tree-level couplings between the triplet and doublets: $c_1 = c_2 = c_3 = 0$. This enhanced global symmetry implies the existence of two pseudo-Goldstone bosons which obtain masses at one-loop ~ 10 MeV. These pseudo-Goldstone bosons will be produced at the bottom of dark sector cascades. They decay into leptons through either two off-shell dark gauge bosons or at one-loop (see Fig. 6.2 and the discussion in Section I.). Either way, the long lifetime causes the pseudo-Goldstone boson to escape the detector at colliders. Since those are pseudo-scalars they will not contribute to the Sommerfeld enhancement of DM annihilations in the early universe and their mass is therefore not bounded by the limits derived in Ref. [53].

2.2 Dark Matter Mass Splitting

The authors of [20] observed that a DM multiplet of some non-abelian G_{dark} , given appropriate mass splittings, can in principle realize the XDM explanation of INTEGRAL [43] and also the iDM mechanism for reconciling the DAMA annual modulation with the null result of other direct detection experiments [23, 51]. In this section we briefly review these proposals, and discuss concrete ways of generating the appropriate mass splittings within concrete theories.

The INTEGRAL collaboration has provided an extremely refined measurement of the 511 keV line of positronium annihilation coming from the galactic center. In the XDM scenario, WIMPs in the galactic center scatter into an excited state, lying ~ 1 MeV above the ground state. The excited state then de-excites into e^+e^- which provides the excess positrons needed. In terms of model-building we need a splitting of ~ 1 MeV between two states in the DM multiplet. Transitions between these two states are mediated by a dark gauge boson with some component of the dark hypercharge (which in turn couples to SM leptons).

In contrast, DAMA is a direct detection experiment which seeks to measure the scattering of galactic WIMPs off of NaI(Tl). Assuming a standard WIMP with elastic scattering, several other experiment such as CDMS [45, 46], XENON [47], and ZEPLIN [54] exclude DAMA's measured annual modulation by many orders of magnitude. The iDM proposal reconciles these experiments by proposing that the WIMP can only scatter off of nuclei through an inelastic process by which the the DM is converted into a slightly excited state. Since the WIMP kinetic energy is fixed and the threshold for the inelastic transition is dependent on the atomic number of the nuclei, this iDM scenario can simultaneously predict a null result at CDMS and a positive result at DAMA⁶. Considering fermionic DM, this scenario can be accommodated by including a mass splitting of around ~ 100 -150 keV [23, 51] between the lightest two Majorana states of the fermion. The bottom line for model building is that to evade CDMS and CRESST [55] bounds, the DM must be split from the next heaviest Majorana state by at least 100 keV.

Before we consider mechanisms for generating the required splittings, we must ascertain that there is no elastic scattering which would have been seen in direct detection experiments. One possibility is to begin with Majorana dark matter in a real representation of the dark gauge symmetry. Gauge bosons then couple different states of the multiplet and radiative corrections, to be discussed in Section I., can split the masses of these states. But if the dark matter begins in a complex representation, for example if it has dark or SM U(1) charge, then it must be Dirac-like at high-energies. Then the

⁶XENON and ZEPLIN, which both use Xe as a target should be able to exclude the iDM scenario, but at the moment these experiments are background limited [51]

model is already excluded by direct detection experiments since the elastic scattering of Dirac-like dark matter is not sufficiently suppressed unless $\epsilon \lesssim 10^{-6}$. However, it is possible to split the masses of the Majorana components of the Dirac fermions by using the same scalar sector that is responsible for breaking dark gauge symmetry. For instance, if we imagine that ϕ is some scalar singlet whose vev breaks global fermion number and $U(1)_y$, we can add a term such as,

$$\mathcal{L}_{\text{Majorana}} = \phi\Psi\Psi + \phi^*\Psi^c\Psi^c \quad (2.2.7)$$

where Ψ and Ψ^c are the Weyl components of some DM multiplet. If ϕ develops a vev of order $\sim \text{GeV}$, it will generate a Majorana mass splitting that forbids any elastic scattering and evades direct detection bounds.

Another possibility is to use a higher dimensional operator with a dark sector doublet, h ,

$$\mathcal{L}_{\text{Majorana}} = \frac{1}{M_X} h\Psi\Psi h, \quad (2.2.8)$$

where $M_X \sim \text{TeV}$. In this case, the Majorana splitting is of order $\sim \text{MeV}$ which again kinematically forbids elastic scattering. If DM is charged under the SM as part of a $\mathbf{5} + \bar{\mathbf{5}}$ multiplet, then a dimension 6 operator is required to contract both dark hypercharge and SM quantum numbers. For example, we can use the operator $1/M_X^2 H\Psi\Psi H\phi$, where H is the SM Higgs, ϕ is a singlet that soaks up Ψ 's dark hypercharge and gets a vev at $\sim 1 \text{ GeV}$, and $M_X \sim \text{TeV}$. This leads to Majorana splitting of order $\sim \text{GeV}$, which forbids elastic scattering.

Any of the possibilities mentioned above can be employed to evade direct detection from CDMS. In the next subsection, we consider two possible way for generating the appropriate $\sim 1 \text{ MeV}$ and $\sim 100 \text{ keV}$ mass splittings necessary for XDM and iDM.

I. Radiative Splitting

As is well-known [56], spontaneous symmetry breaking of a non-abelian gauge group generates radiative mass splittings within a multiplet of the symmetry. We take the DM multiplet to have mass $\sim 500 - 800 \text{ GeV}$, and to be charged under the dark $SU(2) \times U(1)$. As discussed in section 2.1, realistic dark sectors must break charge and custodial

$SU(2)$, but to develop some intuition about the radiative mass splittings, we will begin by considering the limit where these symmetries are preserved. In this limit the mass splittings among the multiplet take a particularly simple form,

$$\begin{aligned} \Delta m_{ij} &= \frac{\alpha^{\text{dark}}}{2}(q_i^2 - q_j^2)M_z \\ &- \frac{\alpha_2^{\text{dark}}}{2}((T_i^3)^2 - (T_j^3)^2)(M_z - M_w), \end{aligned} \tag{2.2.9}$$

where we define α_2^{dark} , and α^{dark} as usual with respect to $SU(2) \times U(1)$ couplings. The charges are $q_i = T_i^3 + Y$ and T_i^3 is the i^{th} eigenvalue of the third $SU(2)$ generator. In the more general limit where charge and custodial symmetry are broken, one must use the appropriate vector boson mass eigenstates and their couplings to the fermions in order to compute the mass correction (Eqs. 1.4.15). This is a straightforward computation, however, in general it does not yield a simple analytic result. Nevertheless, it is clear that there are two factors which control the mass splitting: first, the differences between masses of the vector bosons; and second, the couplings of the different members of the representation to the vector bosons.

As a simple example with all the required splittings and couplings we can consider a triplet with hypercharge $y = 1/2 - \delta$. We generate both large, $\Delta M \sim \alpha^{\text{dark}}M_z$ and small $\Delta m \sim \delta\alpha^{\text{dark}}M_z$ splittings. The correct couplings to account for the XDM and iDM scenarios are induced when charge and custodial breaking corrections are included. A realistic model certainly need not be based on such odd charge assignments, however, this example serves to illustrate how straightforward it is to obtain the correct splittings and couplings. In Figs. 2.2 and 2.3, we consider some of the more general models of Section 2.1, which include charge and custodial symmetry breaking, and we plot the exact ratio of the two splittings relevant to XDM and iDM as a function of the parameters. The corrections induced in supersymmetric models are discussed in appendix A.4.

II. Mass splitting from higher dimensional operator

It is also possible to generate the INTEGRAL and DAMA mass splittings from higher dimension operators alone. The key observation is that $\delta m \sim \Lambda_{\text{dark}}^2/M_X \sim \text{MeV}$, which is of the desired range.

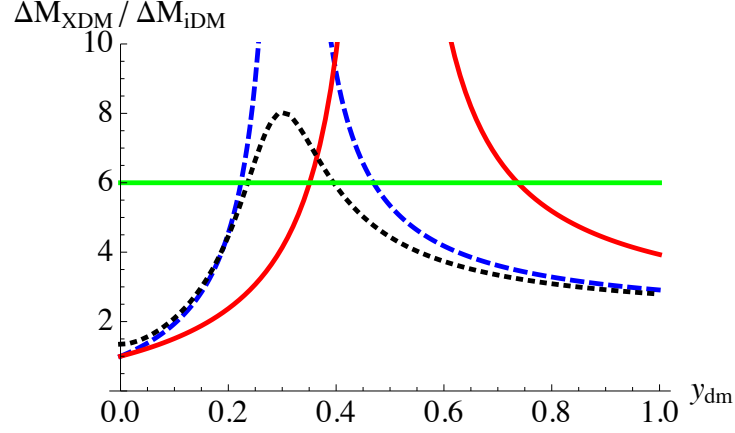


Figure 2.2: The ratio of the XDM splitting to the iDM splitting as a function of triplet dark matter $U(1)_y$ hypercharge. The green horizontal line indicates the minimum ratio for simultaneously achieving both splittings. Red (line) is an example of two Higgs doublets with charge preserved, blue (dashed) represents two Higgs doublets with charge broken, and black (dots) adds a Higgs triplet to the previous case. For this example, the gauge couplings are $g = 0.97$ and $g_y = 0.26$, and in terms of Eq. 2.1.3 we have for all three models $v_1 = 0.9$ GeV, $v_2 = 1.1$ GeV and $\lambda_{1,2,3,4} = 1$. Red (line) and black (dots) add charge breaking with $\cos \alpha = 0.75$, and for black (dots), in terms of Eq. 2.1.6, $\lambda_\Phi = 1$, $v_\Phi = 1$ GeV and the triplet is decoupled from the doublets at tree-level by imposing the discrete symmetry: $\Phi \rightarrow -\Phi$.

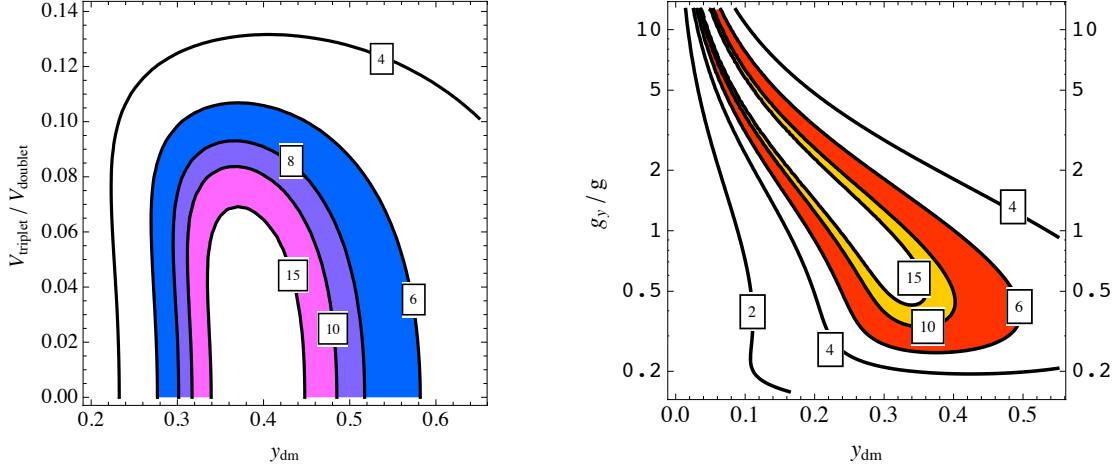


Figure 2.3: Two contour plots of the ratio of the XDM splitting to the iDM splitting for triplet dark matter with two Higgs doublets and one Higgs triplet. The shaded regions represent splitting ratios where XDM and iDM can be achieved simultaneously. In both plots, the horizontal axis is the dark matter $U(1)_y$ hypercharge. The vertical axis of the left plot represents the ratio of the triplet to doublet VEVs, v_Φ/v , where $v^2 = v_u^2 + v_d^2$ and $\langle\Phi\rangle = v_\Phi T_3$. The vertical axis of the right plot represents the ratio of dark hypercharge and $SU(2)$ couplings, g'/g . For both plots, the triplet is decoupled from the doublets at tree-level by imposing the discrete symmetry: $\Phi \rightarrow -\Phi$, and in terms of Eq. 2.1.3 we have $v_1 = 0.9$ GeV, $v_2 = 1.1$ GeV, $\cos\alpha = 0.9$ and $\lambda_{1,2,3,4} = 1$. For the left plot, the gauge couplings are $g = 0.97$ and $g_y = 0.26$. For the right plot, we have also chosen, in terms of Eq. 2.1.6, $\lambda_\Phi = 1$ and $v_\Phi = 1$ GeV.

As an example, we consider two Weyl fermions Ψ, Ψ^c which are $\mathbf{2}_{1/2}$ and $\bar{\mathbf{2}}_{-1/2}$ under G_{dark} . It is possible to achieve all the required splittings and transitions with a single scalar doublet,

$$\mathcal{L} \supset M_{\Psi} \Psi \Psi^c + \frac{\lambda_1}{M_X} \Psi h \Psi h + \frac{\lambda_2}{M_X} \Psi^c h^c \Psi^c h^c + \frac{\lambda_3}{M_X} \Psi^c h^c \Psi h + h.c. \quad (2.2.10)$$

with $\Psi = (\psi_{\nu}, \psi_e)$ and $\Psi h \equiv \psi_i \epsilon_{ij} h_j$ and $h_i^c = \epsilon_{ij} h_j^*$. Once the scalar doublet gets a vev, $\langle h \rangle = (0, v)$, the ‘‘neutrino’’ components of Ψ and Ψ^c mix through the following matrix,

$$M = \begin{pmatrix} \lambda_1 \bar{v} & M_{\Psi} + \lambda_3 \bar{v} \\ M_{\Psi} + \lambda_3 \bar{v} & \lambda_2 \bar{v} \end{pmatrix}, \quad (2.2.11)$$

where $\bar{v} = v^2/M_X \sim \text{MeV}$. In the limit where $\lambda_1 = \lambda_2 = 0$ the states are maximally mixed, $\psi^{\pm} = (\psi_{\nu} \pm \psi_{\nu}^c)/\sqrt{2}$, and form a Dirac pair of mass $M_{\Psi} + \lambda_3 \bar{v}$ which provides the XDM splitting when compared with the ψ_e, ψ_e^c states of mass M_{Ψ} .

With non-zero λ_1 and λ_2 we have,

$$\begin{aligned} \psi'_1 &= \cos \theta \psi^+ + \sin \theta \psi^- & m_1 &= M_{\Psi} + \frac{\bar{v}}{2}(2\lambda_3 + \lambda_1 + \lambda_2) \\ \psi'_2 &= -\sin \theta \psi^+ + \cos \theta \psi^- & m_2 &= -M_{\Psi} - \frac{\bar{v}}{2}(2\lambda_3 - \lambda_1 - \lambda_2) \end{aligned} \quad (2.2.12)$$

with $\sin \theta \approx (\lambda_1 - \lambda_2)\bar{v}/4M_{\Psi}$. The mass difference between the two states is $|\Delta m_{12}| = (\lambda_1 + \lambda_2)\bar{v}$. So, by tuning λ_1 against λ_2 we can achieve $\Delta m_{12} \sim 0.1 \text{ MeV} = 100 \text{ keV}$ as required by iDM. The coupling of the mass eigenstates to the dark gauge boson is given by,

$$\begin{aligned} g_y \bar{\Psi} \not{b} \Psi - g_y \bar{\Psi}^c \not{b} \Psi^c &= g_y \sin \theta \cos \theta (\bar{\psi}'_2 \not{b} \psi'_2 - \bar{\psi}'_1 \not{b} \psi'_1) \\ &- g_y \cos^2 \theta \bar{\psi}'_1 \not{b} \psi'_2 + h.c. \end{aligned} \quad (2.2.13)$$

In this case the ratio of the elastic to inelastic coupling is approximately $\sin \theta = (\lambda_1 - \lambda_2)(\bar{v}/M_{\Psi}) \sim 10^{-7}$, which is sufficiently suppressed. The spectrum relevant for this case is shown in Fig. 2.4.

2.3 Generation of the Dark Sector Mass Scale

As noted in [21], a particularly nice feature of a SUSY dark sector is that the GeV scale is naturally generated by gauge mediated SUSY breaking from the SM. In this section,

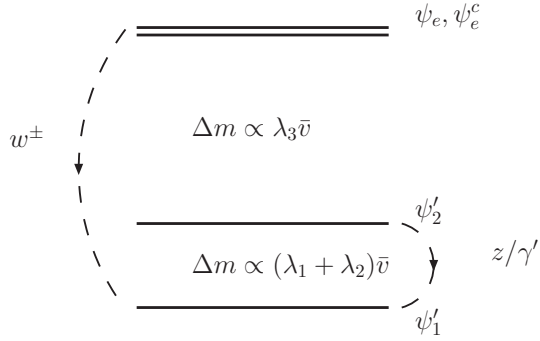


Figure 2.4: The resulting spectrum for a Dirac doublet with majoron coupling.

we elaborate on this scenario in detail. Furthermore, we propose an even more minimal alternative in which “kinetic mixing mediation” breaks SUSY or induces a super-Higgs mechanism at a scale of several GeV in the dark sector. As we will discuss, these theories typically have light fermions which affect the collider physics.

For gauge mediation, dark matter itself can act as the messenger if we take it to be charged under the SM as part of a $\mathbf{5} + \bar{\mathbf{5}}$ multiplet. Dark matter annihilations then also produce SM electroweak gauge bosons, resulting in hadronic channels. But since the GeV scale can be generated by kinetic mixing mediation alone, there is no need to charge dark matter under the SM.

Although we focus on kinetic mixing mediation and gauge mediation for the rest of this section, and when we construct benchmarks in Section 2.4, there are other ways to break SUSY in the dark sector. We would like to stress that the rest of our chapter, in particular the model-independent discussion of collider signatures in Section 6.1, does not depend on how SUSY is broken in the dark sector. One alternative is that there is high-scale gauge mediation and a GeV scale gravitino [21]. Then SUSY is broken in the dark sector at the GeV scale by a “Planck slop.” Another possibility is that the dark matter mass is related to the mechanism that sets the MSSM μ parameter, for example due to a superpotential of the form: $\lambda SH_u H_d + \lambda' S\Psi\Psi^c$. A vev for F_S is communicated to the dark sector through gauge mediation with dark matter as messengers.

I. SUSY Breaking from Kinetic Mixing

In [57] it was observed that mixing of gauge boson kinetic terms will induce mixed D-term contributions to the action that can communicate SUSY breaking between two sectors that are otherwise decoupled.⁷ There the authors noted new, possibly dangerous contributions to SUSY breaking to the MSSM from this effect. In this section, we use this effect to our advantage in order to mediate SUSY breaking from the SM to the dark sector. We should note that while we can choose to make this the dominant mechanism for breaking SUSY in the dark sector, it is always present at the GeV scale.⁸

As was originally proposed in [20], we have been assuming that the dark sector and the SM are coupled via a marginal gauge kinetic mixing between the dark hypercharge, $U(1)_y$ and the SM hypercharge, $U(1)_Y$. If both $U(1)$'s are fundamental, then the kinetic mixing is a UV boundary condition, sensitive to physics at the highest scales. Instead, if either $U(1)$ is embedded in a GUT, then the kinetic mixing is only induced below the scale of GUT breaking by integrating out fields charged under both $U(1)$'s. In this case we can estimate its size. In particular, heavy fields charged under both the SM and the dark sector will induce a gauge kinetic mixing:

$$\mathcal{L}_{\text{gauge}} = \frac{1}{4} \int d^2\theta (W_Y W_Y + W_y W_y - 2\epsilon W_Y W_y + \text{h.c.}) \quad (2.3.14)$$

$$\epsilon \sim -\frac{g_Y g_y}{16\pi^2} \log\left(\frac{M^2}{M'^2}\right) \quad (2.3.15)$$

where g_y and g_Y are the gauge couplings for the dark and SM hypercharges, respectively, M and M' are the masses of components of the heavy particle multiplet. Assuming that these mass scales are not too separated and that the gauge couplings are of reasonable size, this gives an estimate of $\epsilon \sim 10^{-3} - 10^{-4}$. Interestingly, this not only gives the right scale to explain the DAMA cross-section, but also generates a scale of around a GeV in the dark sector. Eq. (2.3.14), along with the Kahler potential, implies a D-term

⁷Strictly speaking, this is a form of gauge mediation according to the definition of Ref. [58]

⁸Kinetic mixing mediation is neglected in some recent $U(1)$ dark sector papers, for instance Ref. [59] focuses on a form of mediation that is sub-leading in ϵ .

potential:

$$V_{\text{gauge}} = \frac{1}{2}D_Y^2 + \frac{1}{2}D_y^2 - \epsilon D_Y D_y + g_Y D_Y \sum_i Q_i |H_i|^2 + g_y D_y \sum_i q_i |h_i|^2 \quad (2.3.16)$$

where H_i and h_i denote the SM and dark sector Higgs, respectively, and Q_i and q_i denote their SM and dark sector hypercharges. Integrating out the SM fields, H_i and D_Y , generates a cross term $\epsilon D_y \langle D_Y \rangle$ in the low-energy theory. Thus, in the infrared, this induces an effective Fayet-Iliopolous D-term for D_y , for which

$$V_{\text{gauge}} \supset \epsilon D_y \langle D_Y \rangle = \xi D_y \quad (2.3.17)$$

$$\xi = \epsilon \langle D_Y \rangle = \epsilon \frac{g_Y}{2} \cos 2\beta v^2 \quad (2.3.18)$$

where in the last equality we have substituted in for $\langle D_Y \rangle$ from the MSSM. For $\epsilon \sim 10^{-3} - 10^{-4}$, ξ is at the GeV^2 scale. Thus, given the minimal assumption of kinetic mixing and SUSY, we obtain precisely the right scale to account for PAMELA and ATIC with the Sommerfeld enhancement.

With an effective FI term at low energies, it is straightforward to break SUSY in the dark sector. In particular, a generic superpotential for the dark Higgses, h_i , will break SUSY because the F and D terms cannot be simultaneously set to zero. While this SUSY breaking generates scalar soft masses, it does not generate soft masses for gauginos. Moreover, since SUSY is broken within the dark sector this will typically introduce a massless dark sector Goldstino⁹, assuming the absence of explicit SUSY breaking operators. So, within this mechanism there are light fermions. We present a concrete model of this type in Section 2.4, and mention the possibility of associated missing energy signals in Section I.

In the opposite extreme, we can take the superpotential to be less generic, or perhaps even trivial, and so the dark Higgs potential is dominated by D-terms. Here the dark Higgses simply align to set the dark hypercharge D-term to zero. In this limit SUSY is actually preserved in the dark sector, but a super-Higgs mechanism will generate a GeV scale dark sector that may still be consistent with a Sommerfeld enhancement and αm_z

⁹The gravitino will eat a linear combination of this field and the Goldstino associated with SUSY breaking in the MSSM

mass splittings for DM. A more minimal superpotential also can imply the existence of light pseudo-Goldstone fields and their superpartners. Finally, we note that unlike the SUSY breaking case, this super-Higgs scenario will also generate GeV scale gaugino masses.

II. SUSY Breaking From $\mathbf{5} + \bar{\mathbf{5}}$ Messengers

In this section, we elaborate on the gauge mediation proposal of [21] in which a multiplet of $\mathbf{5} + \bar{\mathbf{5}}$ messengers is charged directly under both the dark sector and SM, thereby communicating SM SUSY breaking to the dark sector. We consider the additional possibility that the lightest component of the messenger supermultiplet is in fact the DM.

Let us determine the various contributions which set the scale of masses for the scalar and fermion components of the DM $\mathbf{5} + \bar{\mathbf{5}}$ multiplet. First, we assume that the fermions have a SUSY mass, $m_f^{(2,3)}$, that splits the doublet and triplet components. Second, in the case where low-scale gauge mediation explains SUSY breaking in the MSSM, then the doublet and triplet scalars of the $\mathbf{5} + \bar{\mathbf{5}}$ receive identical soft mass contributions to that of the sleptons and right-handed down squarks of the MSSM. We denote this contribution by $m_s^{(2,3)} \sim 100$ GeV. Finally, the scalar DM can in principle also receive soft mass contributions from whatever dynamics set its μ and $B\mu$ terms, which we denote by $B\mu^{(2,3)}$. Instead of specifying these dynamics, we will choose a model-independent parameterization for the DM supermultiplet masses. The scalar doublets and triplets of the $\mathbf{5} + \bar{\mathbf{5}}$ have a scalar mass matrix given by:

$$M_{2,3}^2 = \begin{pmatrix} \left[m_f^{(2,3)} \right]^2 + \left[m_s^{(2,3)} \right]^2 & B\mu^{(2,3)} \\ B\mu^{(2,3)} & \left[m_f^{(2,3)} \right]^2 + \left[m_s^{(2,3)} \right]^2 \end{pmatrix} \quad (2.3.19)$$

whose eigenvalues, $m_{\pm}^{(2,3)}$, are given by

$$\left(m_{\pm}^{(2,3)} \right)^2 = \left(m_f^{(2,3)} \right)^2 + \left(m_s^{(2,3)} \right)^2 \pm B\mu^{(2,3)}. \quad (2.3.20)$$

The lightest component of the doublet supermultiplet corresponds to dark matter, and we choose it to have mass $\sim 500 - 800$ GeV, which is favored by ATIC.

Note that the messenger supertrace of the $\mathbf{5} + \bar{\mathbf{5}}$ mass matrix is non-zero, and proportional to $m_s^{(2,3)}$. As discussed in [60], this non-zero supertrace generates a logarithmically

UV sensitive soft mass for the dark sector scalars. Indeed, since the messenger supertrace is positive, this implies a negative soft mass for the dark Higgs:

$$m_h^2 \approx -8 \left(\frac{\alpha}{4\pi} \right)^2 \left(2 [M_s^{(2)}]^2 + 3 [M_s^{(3)}]^2 \right) \log \left(\frac{\Lambda_{UV}^2}{m_f^2} \right) C_a S_q \quad (2.3.21)$$

where C_a is the dark scalar's quadratic Casimir, S_Q is dark matter's Dynkin index, and Λ_{UV} is set by the messenger scale of SUSY breaking to the SM. The negative soft mass squared allows for G_{dark} to break. This gives us a way to break the symmetries, independent of the effect of RGE running. It is our assumption that the contributions due to running are suppressed. For low-scale gauge mediation, $\Lambda_{UV} \sim 30 - 100$ TeV, and because of this logarithmic enhancement and the combined effect of five messengers, we find that our desired scale of $m_h^2 \sim 1 \text{ GeV}^2$ implies that $m_s^{(2,3)} \sim 50 \text{ GeV}$. This indicates a bit of tension numerically because we expect that $m_s^{(2,3)}$ is set by the SM soft mass scale of hundreds of GeV.

Additionally, if we want fermionic DM, then there is the additional constraint that the fermion is the lightest component of the dark matter supermultiplet: thus $(B\mu^{(2)})^{1/2} < m_s^{(2)} \ll m_f^{(2)}$. Since the DM $B\mu$ contribution breaks the dark sector R-symmetry, the gaugino soft masses are suppressed if we assume that the triplet component satisfies the same condition:

$$m_\lambda \approx \frac{\alpha}{2} S_q \left(2 \frac{B\mu^{(2)}}{m_f^{(2)}} + 3 \frac{B\mu^{(3)}}{m_f^{(3)}} \right) \quad (2.3.22)$$

This implies light gauginos and the generic prediction is that fermionic dark matter implies that the lightest dark sector particle is a mostly-gaugino fermion. This conclusion can be avoided by raising $B\mu^{(3)}$ while maintaining $(B\mu^{(2)})^{1/2} \ll m_f^{(2)}$.

The dark sector Higgses require GeV scale μ and $B\mu$ terms to help break dark gauge symmetry and lift runaway directions. These terms can be generated by additional dynamics that communicate SM SUSY breaking to the dark Higgses, in general also resulting in new two-loop contributions to the dark scalar masses. We will assume that these contributions to m_h^2 are subdominant to the usual gauge mediation contributions of Eq. 2.3.21. A recent paper identifies a class of general gauge mediation models that satisfy this assumption [61].

Let us note that while Eqs. 2.3.21 and 2.3.22 are approximations, our benchmark model of gauge mediation in Section II. employs the full expressions of Ref. [60].

2.4 Benchmark Models

In this section, we present four detailed benchmark dark sector models and their spectra. The models break dark gauge symmetry and custodial symmetry, generating the dark matter splittings and couplings necessary to explain the astrophysical data, as explained in Section 2.1. These examples illustrate some of the theoretical issues discussed above, and their spectra and couplings serve as starting points for thinking about the types of cascades that can occur in GeV scale dark sectors. We begin in Section I. with two non-SUSY models, where the GeV scale is put into the scalar potential by hand. We then consider two SUSY examples in Section II., where the GeV scale is generated radiatively in the dark sector from interactions with the Standard Model.

For each example we consider an $SU(2) \times U(1)_y$ dark sector and triplet dark matter. We take the Majorana components of the dark matter fermions to be split by enough to avoid direct detection bounds, for example by one of the mechanisms discussed in Section 2.2. We then calculate the radiative splittings among the triplet, induced by dark symmetry breaking, as in Section I.. We take the ground state to correspond to dark matter, the heaviest excited state to allow for the XDM explanation of INTEGRAL, and the first excited state to allow for the iDM explanation of DAMA. We allow complex parameters to carry imaginary parts in order to avoid unbroken CP symmetry in the dark sector which may lead to stable states. This is not necessarily a problem and may actually have additional interesting signatures, but we'd like to keep the spectrum as general as possible for the present discussion.

I. Non-SUSY Benchmark Models

Non-SUSY 1: Two Doublets

We begin with the two doublet model of Section I., where h_1 and h_2 have dark quantum numbers $\mathbf{2}_{-1/2}$, $\mathbf{2}_{1/2}$. We have chosen a benchmark which breaks charge and radiatively generates the XDM and iDM splittings, and we have calculated its mass spectrum (Fig. 2.5). As discussed in section 2.1, the custodial $SU(2)$ symmetry of the Higgs sector determines the tree-level gauge boson spectrum. The gauge bosons that couple between the different dark matter mass eigenstates, w_{\pm} , do not mix with the b and are degenerate in mass. Custodial symmetry is broken at one-loop and in general due to higher-dimensional operators. The DAMA inelastic scattering is therefore suppressed relative to models where custodial symmetry is broken at tree-level. For this benchmark, we induce the iDM coupling by including the dimension 6 custodial-breaking operators $c_1^T |h_1 D h_1|^2$ and $c_2^T |h_2 D h_2|^2$, with coefficients c_1^T and c_2^T expressing the loop-suppression.

For the benchmark, we choose the gauge couplings: $g = 0.46$ and $g_y = 0.19$. The dark matter hypercharge is chosen to be $y_{\text{dm}} = 1/2$. In the limit of small charge breaking, this choice leads to one small and one large dark matter splitting, as discussed in Section I.. In terms of the potential of Eq. 2.1.3, the parameters are: $v_1 = 1.5$ GeV, $v_2 = (1.5 + 3.2i)$ GeV, $\lambda_1 = 0.5$, $\lambda_2 = 0.3$, $\lambda_3 = -0.031$, $\lambda_4 = 0.5$, and $\cos \alpha = 0.8$. The coefficients of the custodial-breaking dimension 6 operators are chosen to be $c_1^T = 2.8 \times 10^{-4}$ GeV⁻² and $c_2^T = -5.7 \times 10^{-4}$ GeV⁻².

Non-SUSY 2: Two Doublets and One Complex Triplet

We now add a complex triplet Higgs Φ to the two doublet model, with dark quantum numbers $\mathbf{3}_0$. The triplet vev breaks custodial symmetry, causing all gauge bosons to mix with the b and inducing the iDM coupling at tree-level. We take the triplet to be complex. While not the minimal possible choice, it has a more straightforward SUSY extension. We again choose a benchmark that breaks charge in the doublet sector and radiatively generates the XDM and iDM dark matter splittings. We have calculated its spectrum (Fig. 2.6).

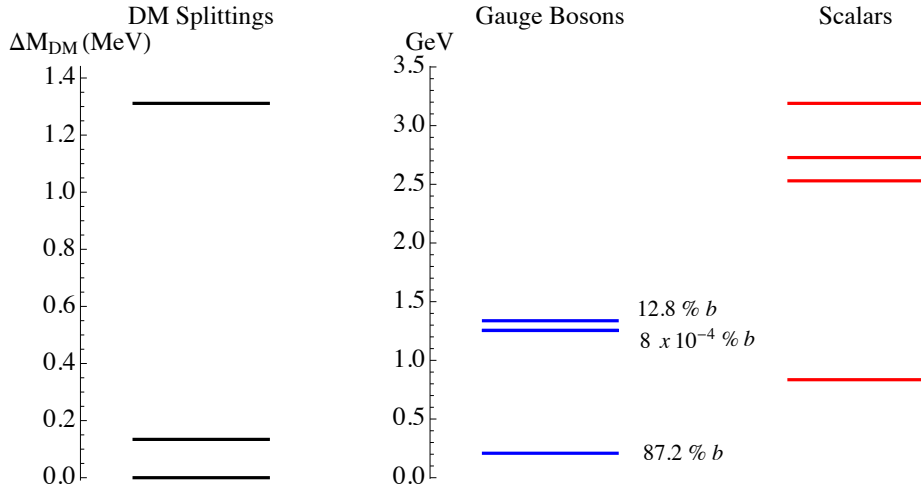


Figure 2.5: The spectrum of **Non-SUSY 1**, our two doublet non-SUSY benchmark. The left side shows the radiative mass splittings of the components of the dark matter triplet, measured from the ground state. The splittings allow for the XDM and iDM explanations of INTEGRAL and DAMA, respectively. The right side displays the spectrum of the GeV-scale dark sector. The b fractions of the gauge bosons are indicated and determine how strongly each gauge boson couples to Standard Model electromagnetic current. Because of custodial $SU(2)$, two of the gauge bosons are degenerate and do not mix with the b at tree-level, and these are the gauge bosons that couple between different dark matter states. They do mix with the b at one-loop, inducing a suppressed iDM coupling, and we include the dimension 6 operators $c_1^T |h_1 D h_1|^2$ and $c_2^T |h_2 D h_2|^2$ in order to parametrize custodial breaking corrections. The parameters of this benchmark are listed in the text.

For this benchmark, we choose the gauge couplings $g = 0.23$ and $g_y = 0.75$, and the dark matter hypercharge is chosen to be $y_{\text{dm}} = 0.3$. The potential is similar to Eq. 2.1.6 except we take Φ to be complex:

field	h_1	h_2	Φ	(2.4.23)
charge	$\mathbf{2}_{-1/2}$	$\mathbf{2}_{1/2}$	$\mathbf{3}_0$	

$$\begin{aligned}
V(h_1, h_2, \Phi) &= V(h_1, h_2) + \frac{\lambda_\Phi}{2} (\text{Tr} [\Phi^\dagger \Phi] - |v_\Phi|^2)^2 \\
&+ \left(c_1 h_1^\dagger \Phi h_1 + c_2 h_2^\dagger \Phi h_2 + c_3 h_1^T \epsilon \Phi h_2 + \text{h.c.} \right)
\end{aligned}
\tag{2.4.24}$$

where the first term is the two doublet potential of Eq. 2.1.3. For the two doublet sector we choose the parameters: $v_1 = 1.8$ GeV, $v_2 = (1.8 + 1.4i)$ GeV, $\lambda_1 = 0.71$, $\lambda_2 = 0.47$, $\lambda_3 = 0.33$, $\lambda_4 = 0.099$, and $\cos \alpha = 0.052$. The parameters involving the triplet are chosen to be: $v_\Phi = (1.1 + 0.61i)$ GeV, $\lambda_\Phi = 0.51$, $c_1 = (0.054 + 0.47i)$ GeV, $c_2 = (0.74 + 0.69i)$ GeV, and $c_3 = (0.61 + 0.81i)$ GeV.

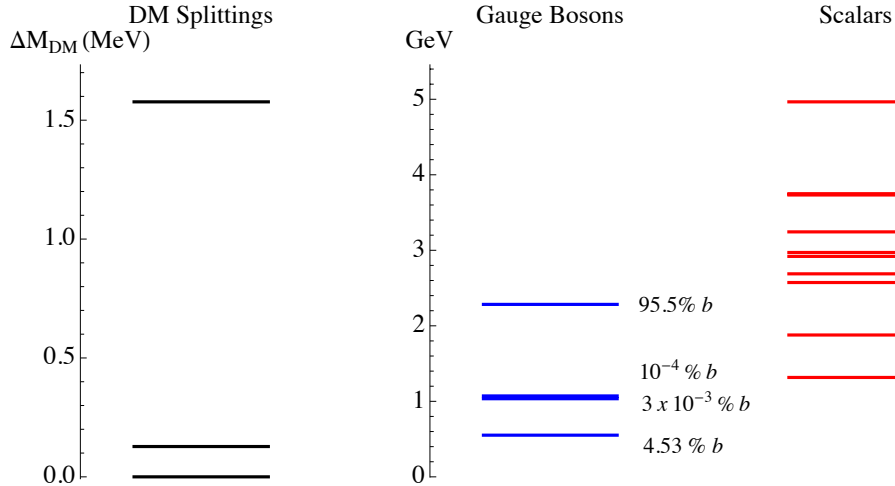


Figure 2.6: The spectrum of **Non-SUSY 2**, our two doublet and one complex triplet non-SUSY benchmark. The left side displays the radiative mass splittings of the dark matter triplet, measured from the ground state. The splittings can account for the XDM and iDM explanations of INTEGRAL and DAMA, respectively. The right side shows the dark sector spectrum, and the b fractions of the gauge bosons are indicated. The triplet vev breaks custodial $SU(2)$, and all 4 gauge boson mass eigenstates mix with the b at tree-level, although for this example most of the b is contained in two of the mass eigenstates. The parameters of this benchmark are listed in the text.

II. SUSY Benchmark Models

Now we consider two SUSY benchmarks, where the GeV scale is generated radiatively from interactions with the Standard Model, as discussed in Section 2.3. Since our models all employ a kinetic mixing, they all receive SUSY breaking contributions from kinetic mixing mediation, as discussed in Section I. In our first example, **SUSY 1**, this the only source of SUSY breaking, however as noted in appendix A.2, it is difficult within this framework to break charge with only one hypercharge neutral triplet. We circumvent this in this example by adding a second complex triplet and taking the triplets to have dark hypercharge. For our second example, **SUSY 2**, we add an additional gauge mediation source for GeV-scale SUSY breaking by taking dark matter to be charged as a $\mathbf{5} + \bar{\mathbf{5}}$ of the SM. Dark matter then acts as a messenger of gauge mediation, as discussed in section II. For this setup, we can break charge with two doublets and one hypercharge neutral triplet.

SUSY 1: Kinetic Mixing Mediation with Two Doublets and Two Triplets

For this benchmark, we have two doublets, h_1 and h_2 , and two complex triplets, Φ_1 and Φ_2 , with dark quantum numbers $\mathbf{2}_{-1/2}$, $\mathbf{2}_{1/2}$, $\mathbf{3}_1$, and $\mathbf{3}_{-1}$. We have chosen triplet hypercharge assignments that allow Yukawa couplings between doublets and triplets, otherwise there may be pseudo-Goldstone bosons in the spectrum. The GeV scale is generated in the dark sector from kinetic mixing, as described in Section I. The most general renormalizable superpotential for two doublets and two triplets with these charge assignments is:

$$\begin{array}{c|c|c|c|c}
 \text{field} & h_1 & h_2 & \Phi_1 & \Phi_2 \\
 \hline
 \text{charge} & \mathbf{2}_{-1/2} & \mathbf{2}_{1/2} & \mathbf{3}_1 & \mathbf{3}_{-1}
 \end{array} \tag{2.4.25}$$

$$W = \mu_h h_1^T \epsilon h_2 + \mu_\Phi \text{Tr} [\Phi_1 \Phi_2] + \lambda_1 h_1^T \epsilon \Phi_1 h_1 + \lambda_2 h_2^T \epsilon \Phi_2 h_2 \tag{2.4.26}$$

We include GeV scale μ and $B\mu$ terms for the doublets and triplets because they help break the dark gauge symmetry and lift runaway directions. We do not include the effects of running from the TeV scale to the GeV scale, which we take to be subdominant. Kinetic

mixing mediation already gives negative scalar soft mass squareds at tree-level, leading to the breaking of dark gauge symmetry.

We include a kinetic mixing coefficient of $\epsilon = 2 \times 10^{-4}$, in terms of Eq. 2.1.1, which automatically generates the GeV scale in the dark sector. Our benchmark radiatively generates the XDM splitting, but unfortunately the smaller dark matter splitting is too large to account for iDM. We have calculated the mass spectrum (Fig. 2.7). The triplet vevs break custodial $SU(2)$ at tree-level and all gauge bosons mix with the b . The gauginos and Higgsinos are strongly mixed after dark symmetry breaking, but for this example the lightest fermion is a mostly gaugino-like Goldstino with a mass of only ~ 2 MeV. Such a field is present because SUSY is broken within the dark sector itself. The second lightest fermion, with mass ~ 190 MeV, is lighter than the lightest gauge boson. Thus, the dark gauge bosons will cascade into these light fermions, rather than SM lepton pairs. The second lightest fermion decays to the lightest fermion and a SM lepton pair through a 3-body decay, which can account for the astrophysical lepton production and lead to visibly displaced vertices at colliders. Another possibility, not realized in this example, is to have an approximately supersymmetric dark sector, with a kinetic mixing mediation induced super-Higgs mechanism at a GeV. Gauginos then reside in massive vector supermultiplets and get GeV scale masses.

For this benchmark, we have chosen the gauge couplings $g = 0.22$ and $g_y = 1.2$, and dark matter hypercharge $y_{\text{dm}} = 1/5$. The superpotential Yukawa couplings are chosen to be $\lambda_1 = 1.7 + 0.022i$ and $\lambda_2 = 0.5 + 1.8i$. For the doublets we choose $\mu_h = (0.11 + 0.63i)$ GeV and $(B\mu)_h = (0.74 + 0.69i)$ GeV². For the triplets we choose $\mu_\Phi = (0.51 + 0.83i)$ GeV and $(B\mu)_\Phi = (0.57 + 0.59i)$ GeV².

SUSY 2: Gauge Mediation with Two Doublets and One Triplet

For this benchmark, we supersymmetrize the Higgs content of our **Non-SUSY 2** benchmark, including SUSY breaking contributions from both kinetic mixing mediation and gauge mediation with dark matter messengers. The most general renormalizable super-

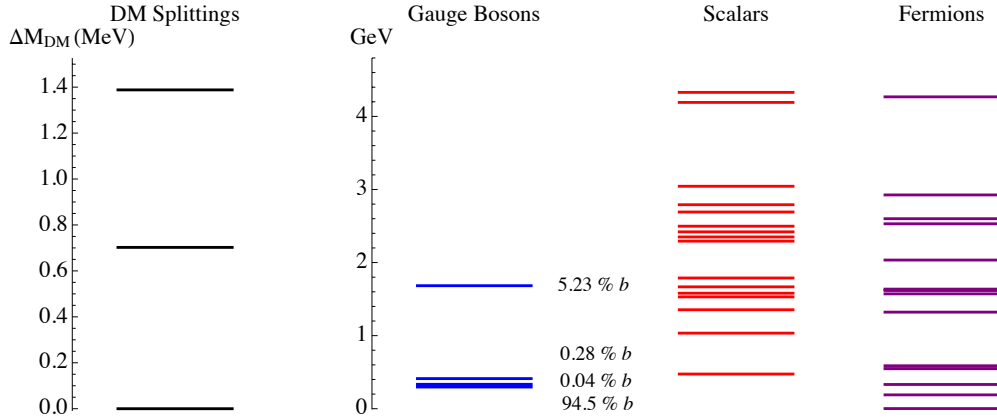


Figure 2.7: The spectrum of **SUSY 1**, our two doublet and two complex triplet SUSY benchmark with kinetic mixing mediation. The left side displays the radiative mass splittings of the dark matter triplet, measured from the ground state. The larger splitting allows for the XDM explanation of INTEGRAL, but the smaller splitting is too large to explain DAMA with iDM. The right side shows the dark sector spectrum, and the b fractions of the gauge bosons are indicated. The triplet vevs break custodial symmetry, and all four gauge boson mass eigenstates are part b at tree-level. The gauginos and Higgsinos are strongly mixed after dark symmetry breaking. The lightest fermion, with mass ~ 2 MeV, is mostly gaugino and light because gauginos get no soft masses from kinetic mixing mediation. The second lightest fermion has a 3-body decay to the lightest fermion and a SM lepton pair, which can account for astrophysical lepton production and lead to a visibly displaced vertex at colliders.

potential for two doublets and one triplet is the following:

$$\begin{array}{c|c|c|c}
 \text{field} & h_1 & h_2 & \Phi \\
 \hline
 \text{charge} & \mathbf{2}_{-1/2} & \mathbf{2}_{1/2} & \mathbf{3}_0
 \end{array} \tag{2.4.27}$$

$$W = \mu_h h_1^T \epsilon h_2 + \mu_\Phi \text{Tr} [\Phi^2] + \lambda h_1^T \epsilon \Phi h_2 \tag{2.4.28}$$

As in the **SUSY 1** benchmark, we include GeV scale μ terms for the doublets and triplet and do not include the effects of running from the TeV scale to the GeV scale. There are already negative scalar soft mass squareds at tree-level because of the nonzero

dark matter supertrace [60], leading to the breaking of dark gauge symmetry. For this example, it is not necessary to include GeV scale $B\mu$ terms for the doublets or triplet.

We have chosen a benchmark which generates a GeV scale dark sector with charge breaking and custodial breaking, and which leads to radiative XDM and iDM splittings. We have calculated the mass spectrum (Fig. 2.8). The gauginos and Higgsinos are strongly mixed after dark symmetry breaking, but the three heaviest fermions with masses near ~ 5.5 GeV are almost pure Higgsino mixtures. The spectrum is slightly split by a small separation between the dark μ and soft mass scales. The gauge couplings are chosen to be $g = 0.3$ and $g_y = 0.37$ and the dark matter hypercharge is $y_{\text{dm}} = 1/2$. The kinetic mixing is $\epsilon = 7 \times 10^{-5}$ in terms of equation 2.1.1. The messenger scale of SUSY breaking to the Standard Model, which enters the log divergence of Eq. 2.3.21, is chosen to be $\Lambda_{UV} = 30$ TeV, corresponding to low-scale gauge mediation. The standard model doublet dark matter mass components, in terms of Eq. 2.3.19, are given by $m_f^{(2)} = 800$ GeV, $m_s^{(2)} = 50$ GeV, and $B\mu^{(2)} = (40 \text{ GeV})^2$. As discussed in section II., the small soft mass is needed to generate the GeV scale in the dark sector, and we choose a small $B\mu$, keeping dark matter fermionic. For the standard model triplet components of the dark matter $\mathbf{5} + \bar{\mathbf{5}}$, we choose the parameters $m_f^{(3)} = 840$ GeV, $m_s^{(3)} = 50$ GeV, and $B\mu^{(3)} = (300 \text{ GeV})^2$. The larger $B\mu$ for the triplet leads to GeV scale gaugino soft masses in the dark sector (see Eq. 2.3.22 and the surrounding discussion). The superpotential parameters are $\mu_h = (0.27 + 0.28 i)$ GeV, $\mu_\Phi = (2.52 + 3.48 i)$ GeV, and $\lambda = 0.29 + 1.51 i$.

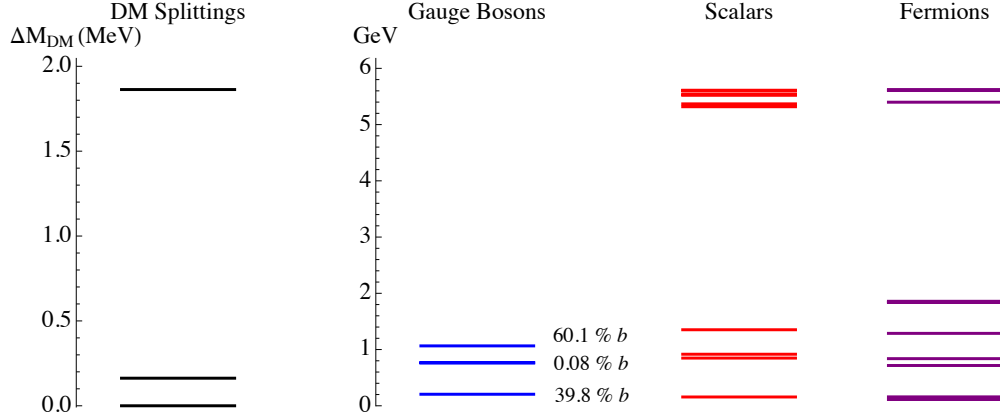


Figure 2.8: The spectrum of **SUSY 2**, our two doublet and one complex triplet SUSY benchmark with both kinetic mixing mediation and dark matter messengers charged under the Standard Model. The left side displays the radiative mass splittings of the dark matter triplet, measured from the ground state. The splittings can allow for the XDM and iDM explanations of INTEGRAL and DAMA, respectively. The right side shows the dark sector spectrum, and the b fractions of the gauge bosons are indicated. The triplet vev breaks custodial $SU(2)$ and three of the gauge boson mass eigenstates are part b at tree-level. The dark spectrum now includes GeV scale fermions, and the gauginos and Higgsinos are strongly mixed after dark symmetry breaking. The three heaviest fermions, with masses near ~ 5.5 GeV, are almost pure Higgsino mixtures. The spectrum is slightly split by a small separation between the dark μ and soft mass scales. The parameters of this benchmark are listed in the text.

A Minimal $U(1)$ Model

3.1 Introduction

A number of intriguing results from astronomical and cosmic ray data may be evidence for dark matter (DM) annihilation in our galaxy [28, 14, 27]. In addition, the DAMA direct detection experiment reports a signal which may be the first instance of DM interaction with normal matter [24]. Interestingly, if interpreted as coming from dark matter interactions and annihilations these signals span an enormous hierarchy of length scales, 100 keV - 1 TeV, making dark matter model building a challenging enterprise. Along these lines, Arkani-Hamed et. al. have suggested a broad framework [20, 21] in which 500 - 800 GeV dark matter is charged under a dark gauge group, $G_d \supset U(1)_d$, whose abelian factor kinetically mixes with the Standard Model (SM) photon [36]. Assuming that G_d is non-abelian and broken at a GeV, then loops of the resulting GeV scale dark gauge bosons will generate 100 keV - 1 MeV mass splittings within the dark matter multiplet.

This approach resolves several of the puzzles raised by recent observations: 1) a Sommerfeld enhancement from GeV scale dark gauge bosons boosts the dark matter annihilation rate today, reconciling the large flux of e^+e^- observed in the PAMELA and ATIC data with the weak cross-section inferred from the dark matter relic abundance. 2) Dark gauge bosons have kinematically suppressed hadronic decays, explaining the lack of excess anti-protons at PAMELA. 3) The DAMA signal arises from inelastic nuclei-dark matter (iDM) scattering coming from ~ 100 keV mass splittings in the dark matter multiplet [23]. 4) A slightly larger splitting of ~ 1 MeV can explain the INTEGRAL 511 keV line using the proposal of exciting dark matter (XDM) [43, 72, 42].

In this chapter, we propose a simple and predictive setup that differs from the original proposal in two important ways. First, we demonstrate that an abelian gauge group, $G_d = U(1)_d$, is sufficient to generate a multiplet of states with 100 keV - 1 MeV mass

splittings. This is a considerable simplification over non-abelian models, which generally need large numbers of dark Higgses [1]. Second, we argue that supersymmetric theories acquire a scale of $\sim \text{GeV}$ as a dynamical consequence of kinetic mixing alone. D-term mixing between $U(1)_d$ and the Minimal Supersymmetric SM (MSSM) hypercharge induces an effective Fayet-Iliopoulos (FI) term for $U(1)_d$ of order GeV^2 . In the presence of a single $U(1)_d$ charged dark Higgs, the dark gauge symmetry is broken at a GeV .

Our model is also distinct from a number of alternative proposals for $U(1)_d$ charged dark matter. An earlier treatment has neglected D-term mixing completely, even though it is dominant to the effects being considered [59]. Another approach considers gauge mediation in the limit of negligible kinetic mixing [73]. Also, during the completion of this work we learned of an interesting forthcoming proposal [74] which utilizes anomaly mediation to generate additional GeV scale contributions.

The model presented in this chapter is remarkably simple and has a small number of free parameters that can be fixed by observations. For instance, the dark matter mass, M , may be fixed by a possible future observation of a shoulder in the PAMELA positron excess (alternatively, the feature seen in ATIC may already fix that scale). Assuming thermal freeze-out, the dark gauge coupling, g_d , determines the relic abundance and is thus fixed in terms of M . Furthermore, the size of the kinetic mixing, ϵ , is constrained by the boost factor required to explain the PAMELA positron excess. Quite interestingly, our model implies a direct relation between the DAMA scattering cross-section and the hypercharge D-term of the MSSM. This is a generic prediction of any theory whose only origin of scales is the kinetic mixing. Also, the dark photon should be copiously produced in SUSY cascades at particle colliders, yielding clusters of closely packed collimated energetic leptons, which has been referred to in Ref. [20, 21, 1] as “lepton jets”. At high energy colliders, dark photons are produced with energies of 10s – 100s GeV . As the dark photon decays through its mixing with the photon it produces a pair of leptons that are highly collimated $\Delta R_{\ell\ell} \sim 0.1 - 0.01$, forming lepton jets. Cascade decays in the GeV dark sector will result in more leptons and hence richer lepton jets, see [1] for a detailed discussion. We note that the dark photon can also have significant decay branching ratios to light mesons. Presence of such mesons certainly alters the phenomenology, and it is

therefore possible to define several sub-classes of lepton jets. Since our focus is not on the collider phenomenology, we will not make this distinction in this chapter.

3.2 New Scales in the Dark Sector via Kinetic Mixing

Throughout this letter we assume a weak scale mass for the dark matter supermultiplet. All of the light scales in the dark sector will be generated dynamically through kinetic mixing between hypercharge and the dark force carrier. In particular, the action contains a term

$$\mathcal{L} \supset -\frac{\epsilon}{2} \int d^2\theta W_Y W_d \quad (3.2.1)$$

where W_Y (W_d) is the supersymmetric field strength for the SM hypercharge (dark abelian group) and ϵ is a small parameter. Integrating out heavy fields charged under both hypercharge and $U(1)_d$ will induce this operator and we can estimate the size of the mixing to be,

$$\epsilon = -\frac{g_Y g_d}{16\pi^2} \sum_i Q_i q_i \log\left(\frac{M_i^2}{\mu^2}\right) \quad (3.2.2)$$

which can naturally be of order $10^{-3} - 10^{-4}$. As observed in ref. [1], the kinetic mixing includes

$$V_{\text{D-term mixing}} = \epsilon D_Y D_d \quad (3.2.3)$$

After electroweak symmetry breaking, D_Y gets a vacuum expectation value (VEV)

$$\langle D_Y \rangle = \frac{g'}{2} (|H_u|^2 - |H_d|^2) + \xi_Y \quad (3.2.4)$$

where $H_{u,d}$ are the MSSM Higgs doublets and g' is the hypercharge coupling. We included, ξ_Y , which is an effective FI term for the SM hypercharge group since this is a relevant operator allowed by all the symmetries and there is no reason to a priori exclude it from the low energy action that defines the MSSM [75, 76, 77, 78]. From the low energy perspective, ξ_Y is only constrained to not be so large as to destabilize the electroweak scale.

The expectation value of D_Y induces an effective FI term for the dark abelian group via the kinetic mixing

$$\xi = \epsilon \langle D_Y \rangle = \epsilon \left(-\frac{g'v^2 \cos 2\beta}{4} + \xi_Y \right) \quad (3.2.5)$$

where v is the electroweak vacuum expectation value. With $\epsilon = 10^{-4} - 10^{-3}$ and $\langle D_Y \rangle$ of order the weak scale, we find that $\xi = (1 - 5 \text{ GeV})^2$. Thus the GeV scale in the dark sector is a fortuitous byproduct of the kinetic mixing. If there are any light degrees of freedom charged under $U(1)_d$, the vacuum can break the gauge group and/or supersymmetry at the GeV scale. We focus on the possibility that SUSY is preserved and $U(1)_d$ is broken, resulting in a $\sim \text{GeV}$ mass for the vector supermultiplet. If dark matter has a superpotential coupling to a light field that gets a VEV, then the vacuum can dynamically generate an MeV sized splitting between dark matter supermultiplets, as we now demonstrate with a concrete model.

3.3 A Model for the Dark Sector

We take DM to be a pair of chiral supermultiplets, (Φ, Φ^c) , oppositely charged under the dark gauge group, $U(1)_d$. The superpotential for chiral multiplets is given by,

$$W = M\Phi\Phi^c + \lambda N h h^c + \frac{1}{4\Lambda} \Phi^2 h^c{}^2 \quad (3.3.6)$$

h and h^c are oppositely charged and N is neutral under $U(1)_d$. Here $\Lambda \sim \text{TeV}$ and is associated with new physics at the electroweak scale¹. We choose a discrete symmetry to forbid dimensionful operators involving the light fields: N , N^2 , and $h h^c$. Depending on the choice of discrete symmetry, there may be marginal and irrelevant operators in addition to the ones included in equation 3.3.6, but they will not be relevant to the following discussion. The neutral field is included in order to avoid any massless degrees of freedom at low energies.

¹This can come in the form of TeV scale states which couple to both Φ and h^c . Then the operator $\frac{1}{4\Lambda} \Phi^2 h^c{}^2$ can be generated after integrating out the heavy states. One simple possibility is to introduce an additional pair of chiral supermultiplets S, S^c with Dirac mass $\sim \text{TeV}$, and couplings $\lambda_\Phi S \Phi^2 + \lambda_{h^c} S^c h^c{}^2$.

The scalar potential for this theory is given by:

$$\begin{aligned}
V &= V_D + V_F \\
V_D &= \frac{1}{2} \left[\frac{g_d}{2} (|h|^2 - |h^c|^2 + |\Phi|^2 - |\Phi^c|^2) + \xi \right]^2 \\
V_F &= \left| M\Phi^c + \frac{1}{2\Lambda} \Phi h^c \right|^2 + |M\Phi|^2 \\
&\quad + \left| \lambda N h + \frac{1}{2\Lambda} h^c \Phi^2 \right|^2 + |\lambda N h^c|^2 + |\lambda h h^c|^2
\end{aligned} \tag{3.3.7}$$

There is a SUSY vacuum (with vanishing F and D-terms) with broken $U(1)_d$ at $\langle h^c \rangle = \sqrt{\frac{2\xi}{g_d}}$ and all other scalar VEVs set to zero.

I. Coupling to the Standard Model

The supersymmetric field strength mixing, Eq. (3.2.1), also contains the gauge-boson kinetic mixing,

$$\mathcal{L}_{\text{gauge mixing}} = \frac{\epsilon}{2} B_{\mu\nu} b^{\mu\nu} \tag{3.3.8}$$

where $B_{\mu\nu}$ and $b_{\mu\nu}$ denote the SM and dark field strengths. As argued in [20, 21], this is the leading marginal operator that couples the dark sector to the standard model. Moreover, since it does not violate any SM symmetries, it is relatively unconstrained phenomenologically, and $\epsilon = 10^{-4} - 10^{-3}$ is consistent with current bounds [35].

The primary effect of this mixing is to induce an ϵ suppressed coupling between the electromagnetic current of the SM and the dark vector-boson [34]. Dark matter annihilations produce dark vector-bosons that subsequently decay into light leptons or pions via this kinetic mixing. Decay into heavier particles is kinematically disallowed. This injection of leptons can explain the excesses observed at PAMELA and ATIC. Another consequence of the kinetic mixing is that the SM Z boson and bino couple to the $U(1)_d$ current, which has implications for collider phenomenology [1].

II. Mass Spectrum

Next, let us consider the spectrum of the dark sector. The vector supermultiplet gets a mass of

$$m_b^2 = g_d \xi \quad (3.3.9)$$

which is naturally \sim GeV scale. As pointed out in Refs. [42, 20, 21], a vector-boson of this mass elegantly explains why decay channels into anti-protons are kinematically disfavored. It also serves as a light force carrier capable of enhancing the annihilation cross-section via the Sommerfeld enhancement mechanism to produce the necessary annihilation rate for PAMELA or ATIC.

The masses of the dark matter states Φ and Φ^c are affected as well. To leading order in $m_b/M \lesssim 10^{-3}$, the mass eigenstates are given by $\Phi_{\pm} = (\Phi \pm \Phi^c)/\sqrt{2}$, and Φ_- , being the lighter of the two, is identified with our (fully supersymmetric) dark matter candidate. The mass splitting between the two states is,

$$\begin{aligned} \Delta m &= m_+ - m_- = \frac{m_b^2}{g_d^2 \Lambda} \\ &= 0.8 \text{ MeV} \left(\frac{30^{-1}}{\alpha_d} \right) \left(\frac{m_b}{\text{GeV}} \right)^2 \left(\frac{3 \text{ TeV}}{\Lambda} \right) \end{aligned} \quad (3.3.10)$$

Depending on the precise values of the parameters involved, this scale can be used to explain either DAMA or INTEGRAL using the iDM or XDM scenarios, respectively. Either way, the mass splitting can be fixed by fitting to the experimental signature. Furthermore, since the states are almost maximally mixed, the transitions among mass eigenstates are strongly inelastic. The elastic couplings are suppressed by $m_b^2/M\Lambda$ and bounds from direct detection are easily evaded. If $\Delta m < 2m_{electron}$, then the life-time of the excited state is longer than the age of the universe². Direct detection bounds may be relevant if a cosmological abundance of the excited state is still present today.

²We thank N. Arkani-Hamed and M. Pospelov for pointing this out to us. See Ref. [79] for details and lifetime estimates.

Lastly, we consider the spectrum of dark Higgses. h^c is eaten via the super-Higgs mechanism. h and N pair-up and become massive:

$$m_h^2 = m_N^2 = \frac{2\lambda^2\xi}{g_d} = 2\left(\frac{\lambda}{g_d}\right)^2 m_b^2 \quad (3.3.11)$$

As long as $\lambda > g_d/2\sqrt{2}$, then $m_h > m_b/2$ and decays of the dark photon into dark Higgses are kinematically forbidden. At this level, these states are exactly stable since the potential respects $N - h$ number as an exact symmetry.

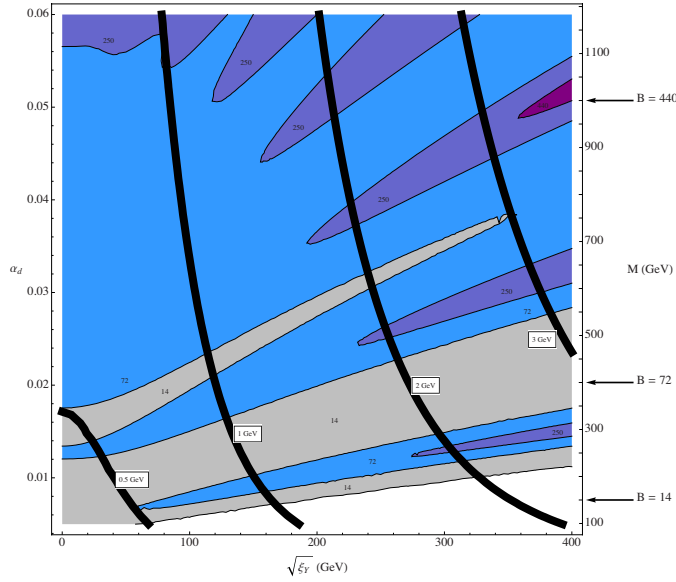


Figure 3.1: A contour plot of the Sommerfeld enhancement [20] as a function of M (or α_d , related through Eq. (3.4.12)) and $\sqrt{\xi_Y}$, with $\epsilon = 10^{-4}$ and $\tan\beta = 40$. The solid black lines correspond to fixed m_b . The dark matter velocity is taken to be $v = 150$ km/s. On the right we indicate the boost required for PAMELA for three reference values of M , for the process $\Phi\Phi \rightarrow \gamma'\gamma'$ followed by $\gamma' \rightarrow e^+e^-$ [32]. The boost is relative to $\langle\sigma v\rangle = 3 \times 10^{-26} \text{ cm}^3 \text{ s}^{-1}$, assuming local dark matter density $\rho_0 = 0.3 \text{ GeV cm}^{-3}$.

III. Supersymmetry Breaking Effects

This setup is interesting because the origin of scales is centered on the mixed D-term. For this reason we have assumed there are no large SUSY breaking effects, for example from gravity mediation. Instead, we consider low-scale gauge mediation such that the dark

sector only receives SUSY breaking contributions from the MSSM via kinetic mixing. As such, the dark sector is supersymmetric only at leading order in ϵ . For example, since the dark Higgs couples to the MSSM bino, it receives a positive soft mass of order $m^2 \sim \epsilon^2 g_d^2 M_{\tilde{B}}^2 / 16\pi^2 \sim (10 - 100 \text{ MeV})^2$ from bino loops. This has a negligibly small effect on the dark matter supermultiplet, since it lifts the scalars from the fermions by $m^2/M \sim \mathcal{O}(1) \text{ keV}$. The dark matter is effectively supersymmetric because transitions among the supermultiplet occur on timescales longer than the age of the universe.

In contrast, the scalar h is heavier than its superpartner by an amount $m^2/m_h \sim \mathcal{O}(1) \text{ MeV}$, while the scalar N is lighter by a tenth of that due to a *negative* mass² contribution from the Yukawa coupling, $\lambda N h h^c$. Furthermore, an A-term of size $\lambda \epsilon^2 g'^2 M_{\tilde{B}} / 16\pi^2$ is generated which mixes N and h once h^c condenses. The resulting spectrum consists of the scalar N as the lightest state, the fermionic N and h about $100 \text{ keV} - \text{MeV}$ above that, and the scalar h as the heaviest state. While these MeV splittings imply interesting possibilities for model building, we leave this for future work.

3.4 Observations and Predictions

In this section we discuss the parameters of our model and their relation to observations in astrophysics and direct detection.

The mass of the WIMP can be determined through the electron/positron excess seen in ATIC/PAMELA. Since the leptons are produced as byproducts of the annihilation into dark photons, $\Phi\Phi \rightarrow \gamma'\gamma'$, followed by a leptonic decay of γ' , the excess should have an endpoint at the WIMP's mass.

The relic abundance of dark matter is fixed by the thermal annihilation cross-section of Φ during freeze-out. The dominant annihilation channel is $\Phi\Phi \rightarrow \gamma'\gamma'$, which fixes the dark gauge coupling in terms of the dark matter mass ³:

$$\langle\sigma v\rangle_{\text{freeze}} \sim \alpha_d^2/M^2 \tag{3.4.12}$$

with $\langle\sigma v\rangle_{\text{freeze}} = 3 \times 10^{-26} \text{ cm}^3 \text{ s}^{-1}$.

³We leave a more detailed calculation of the relic abundance to a future publication.

Next, let us consider the effects of the GeV scale states on cosmology. Although N and h are stable, their relic abundance can be sufficiently depleted assuming that they are heavier than the vector multiplet. In this case they annihilate efficiently into the vector multiplet, which in turn annihilates into SM fields via the kinetic mixing. Since this cross-section is small, the states in the vector multiplet have large abundances at freeze-out, but all decay safely before Big Bang Nucleosynthesis (BBN). In particular, the dark photon decays promptly to e^+e^- , while the radial dark Higgs decays either into e^+e^- through a loop or into $e^+e^-e^+e^-$ through two off-shell dark photons. The dark photino has the longest lifetime because it has to decay to a photon and gravitino. This decay can occur before BBN:

$$\tau_{\tilde{\gamma}' \rightarrow \gamma \tilde{G}} \sim 0.3 \text{ s} \left(\frac{10^{-3}}{\epsilon} \right)^2 \left(\frac{\text{GeV}}{m_b} \right)^5 \left(\frac{\sqrt{F}}{10 \text{ TeV}} \right)^4 \quad (3.4.13)$$

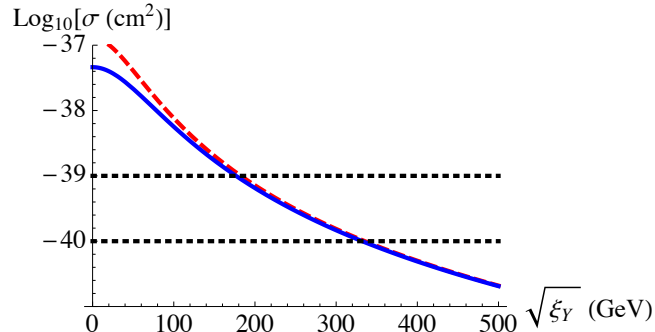


Figure 3.2: The DAMA cross-section as a function of the effective FI parameter with $\tan \beta = 2$ (red, dashed) and ∞ (blue, line). The horizontal lines indicate the preferred range for the WIMP-nucleon cross-section [23].

The dark photon, γ' , provides the Sommerfeld enhancement of the annihilation cross-section needed for PAMELA [14] and ATIC [27]. In Fig. 3.1, we present a contour plot of the Sommerfeld enhancement, S , as a function of ξ_Y and M .

Our model can reconcile DAMA with the limits of other direct detection experiments, if Λ is such that the mass splitting between Φ_+ and Φ_- is $\Delta m \sim 100 \text{ keV}$, providing a realization of the iDM scenario of Ref. [23, 51, 71]. Interestingly enough, the cross-section

per nucleon in this model is sensitive to $\langle D_Y \rangle$ only,

$$\sigma = \frac{4Z^2 \mu_{ne}^2}{A^2} \frac{\alpha \cos^2 \theta_W}{\langle D_Y \rangle^2} \quad (3.4.14)$$

Notice that any dependence on the dark sector couplings have cancelled completely. This type of cancellation will occur in *any theory in which the mass scale of the dark sector is fixed entirely by D-term kinetic mixing*. Thus, for this class of models the measured DAMA cross-section, if confirmed, yields a definitive prediction about electroweak physics. Fig. 3.2 shows the dependence of the DAMA cross-section on ξ_Y , where we have also denoted the range of cross-sections preferred by iDM [23, 51, 71].

A determination of ξ and α_d yields a prediction for m_b , the mass of the vector supermultiplet, as shown in Fig. 3.1. Furthermore, since the MSSM bino couples directly to the dark photon and photino, dark photons should be produced in SUSY cascades from the MSSM at high energy colliders. Such a signal, very distinct from the collider signatures of the conventional MSSM, is generic in GeV dark sector models with supersymmetry [1]. Dark state production at the LHC provides a promising avenue for probing the dark sector and its interactions [1, 80].

3.5 Conclusions

In this letter we considered a supersymmetric dark sector involving a massive and stable matter field which constitute the WIMP and is coupled to an abelian gauge field. The sector also contains light matter fields which ultimately spontaneously break the gauge symmetry at \sim GeV. Similarly to recently proposed scenarios, the abelian group is weakly mixed with hypercharge through the kinetic terms. The main point of our discussion is that, in supersymmetry, the existence of kinetic mixing, together with the breaking of hypercharge in the SM, also breaks the dark abelian gauge symmetry at \sim GeV in a natural and unavoidable fashion.

We find the extreme simplicity of this setup and the natural generation of all the scales involved the most attractive feature of this scenario. However, as it stands, it suffers from two main difficulties. The first is related to the lifetime of the dark gaugino given in Eq.

(3.4.13). In order to decay before BBN it requires a rather low supersymmetry breaking scale. This can easily be relaxed with a slightly heavier gauge boson or larger mixing parameter. Moreover, the injection of electromagnetic energy during BBN is not as strongly constrained as hadronic energy injection [81]. The second issue, and the more serious one, is associated with the cross-section of WIMP-nucleon scattering in the iDM model as given in Eq. (3.4.14). The model's simplicity leads to an unambiguous relation between this cross-section and the MSSM hypercharge D-term, $\langle D_Y \rangle$. In the simplest case, where $\langle D_Y \rangle$ is given by the higgs' VEV alone, the cross-section is too large by about an order of magnitude. It is certainly possible for $\langle D_Y \rangle$ to enjoy from additional contributions, however, some of the model's allure is marred.

Despite these shortcomings, both of which can be alleviated with the slightest extensions, this model serves as an example for an incredibly simple dark sector which *naturally* generates all the necessary scales recently discussed in the literature. It exhibits a rich structure originating from the single inclusion of supersymmetric kinetic mixing between hypercharge and a dark abelian gauge group. Most importantly, it is predictive in its content and results in unambiguous relations between its parameters and measurable quantities.

Decaying into the Hidden Sector

4.1 Introduction

The existence of a low energy hidden sector, weakly coupled to the Standard Model (SM), is an exciting possibility that will be tested by upcoming experiments. Hidden sector particles can be produced in high energy colliders, as stressed in the context of ‘Hidden Valley’ models [10] and models where gauge kinetic mixing results in ‘lepton jets’ [21, 1]. Such hidden sectors can also be probed with low energy e^+e^- colliders and fixed target experiments [35]. Here, we point out that the existence of a low energy hidden sector, together with weakly interacting DM (WIMP) and gauge coupling unification, implies the generic possibility that DM may decay directly into the hidden sector through operators suppressed by the GUT scale. These decays, followed by decays into SM particles through kinetic mixing, provide the intriguing possibility of using astrophysical observations to study the hidden sector spectrum, complementing direct production experiments. This decaying DM framework provides a simple and natural explanation for the recent cosmic ray (CR) anomalies [14, 16, 85, 86], while avoiding the tensions and pitfalls of many previously proposed models.

A DM explanation of the electronic CR excess requires a DM mass greater than a TeV [18, 87, 88], and predominantly leptonic production [89, 90]. Consequently, the vanilla MSSM WIMP scenario is disfavored, and many new models have been proposed, bifurcating into annihilating models [20, 91] and decaying models [92, 93, 94, 95, 96, 97, 98, 99, 100, 101, 102, 103, 104, 105, 106, 107]. Annihilating models are difficult to reconcile with the FERMI and HESS CR data, because the softening of the spectrum above a few TeV requires an annihilation cross-section $\mathcal{O}(1000)$ times larger than that of the standard thermal WIMP [18, 87, 88]. Such a large cross-section is in tension with constraints from photon and neutrino measurements from the Galactic Center (GC) [18, 87, 88, 108, 109, 110, 111], extragalactic emissions [53, 112, 113, 114], and

the CMB [115, 116, 117]. There is also model building tension for achieving such a large cross-section. Possible mechanisms include non-perturbative Sommerfeld enhancements [22, 118, 39, 41, 20], or a resonance [119, 120, 121, 122, 123]. In the latter case, a very narrow resonance and degenerate states are required, while in the former, either large ($\gtrsim 1$) gauge or Yukawa couplings to the light mediator or tuned parameters are necessary [20]. As we discuss below, the required large couplings conflict with a need for Yukawa interactions that generate a DM splitting, necessary in many models to avoid constraints from direct detection [124]. Indeed, the mechanism that generates the splitting typically opens up new annihilation channels that can parametrically dominate at freeze out. As a consequence, in order to achieve the correct relic abundance, the couplings responsible for the Sommerfeld enhancement are constrained and cannot produce a large enough enhancement.

Decaying models replace the need for a large annihilation cross-section. Since the DM lifetime is much longer than the age of the Universe, its decays do not affect the attractive features of the thermal WIMP and leave no signature on the CMB radiation. Moreover, constraints from the GC or subhalos are easily evaded [93], since the emission rate depends on one power of the DM density, ρ , as opposed to the ρ^2 dependence in the annihilating case. Interestingly, the correct lifetime to explain the anomalies, $\mathcal{O}(10^{26}$ sec), is obtained if the decays are induced by dimension-6 operators suppressed by the GUT scale [92]. Still, it is non-trivial to construct a decaying DM model that does not overproduce antiprotons, and many existing models are fine tuned or have small and ad hoc parameters.

In this chapter we study a new and natural class of models, where DM decays into a light hidden ‘dark sector’, with gauge group G_d . Working in the supersymmetric framework appropriate in the context of GUTs, the dark sector has a stable mass gap at the GeV scale, and communicates with the supersymmetric SM (SSM) through kinetic mixing [34]. The GeV gauge bosons decay into light SM fermions, explaining the lack of antiproton production [42]. The dark sector is close in spirit to the models discussed in [20, 21]. Nonetheless, it is more general in the sense that the DM may or may not be charged under G_d and/or the SM. This opens the door for a wider range of models and is

potentially simpler. Dimension-6 decay operators appear naturally, and are expected to be present at low energy unless forbidden by global symmetries. For related work where DM decays into light states, see [95, 96].

Models of the type studied here involve several scales. Physics at the GUT scale, M_{GUT} , is responsible for producing the decay operators. More formally, in the limit $M_{\text{GUT}} \rightarrow \infty$, the DM is completely stable due to a preserved global symmetry. Fields at the GUT scale then break that symmetry, inducing the required decays. It is important that dimension-5 operators which would trigger a fast DM decay are not generated. Below we show several mechanisms that prevent such operators from showing up at low energy. The TeV scale generates the DM mass which can be naturally related to the supersymmetry (SUSY) breaking scale, thereby avoiding the usual μ -problem. The GeV scale which controls the branching fractions of the DM decays into SM fields, is generated either by communicating supersymmetry breaking to the dark sector indirectly through the SM [21] or through D-term mixing [1, 71, 2]. Finally, splittings between DM states may be required to avoid direct detection. Such splittings are naturally of order an MeV, thereby accommodating the inelastic DM (iDM) [23] and eXciting DM (XDM) scenarios [43]. Below we study mechanisms that can appear at each of these scales, stressing the modular nature of such models, which significantly simplifies the model building.

The models studied here predict distinctive signatures in many upcoming experiments, and unique indirect signals which will complement the direct production experiments mentioned above. For instance, if the dark sector is approximately supersymmetric, or if the dark gaugino is lighter than the dark gauge boson, $m_{\tilde{\gamma}_d} \lesssim m_{\gamma_d}$, it typically decays into a gravitino and a SM photon. Such primary photons will show up as sharp features in the measured flux. If the DM is also charged under the SM, its decays are accompanied by primary neutrinos, again admitting a sharp and hard spectral feature. In the corresponding annihilating models, these decay channels are excluded due to the excess of primary photons or neutrinos produced, for example, at the GC. Both possibilities are studied in [125], where it was shown that current and future experiments will have the ability to measure these signatures and thereby differentiate between the

annihilating and decaying DM scenarios. In sections 4.2 and 4.3 we provide detailed examples that illustrate the presence of these signatures.

The chapter is organized as follows. In section 4.2 we discuss the tools for constructing decaying DM models. We first list the dangerous pitfalls of these models, and then discuss solutions, organized by energy scale. In section 4.3 we apply these tools to study four distinct example models. In I. we show the simplest $U(1)$ model, which is UV completed in II.. In III. we construct a model where the DM is charged under the SM and decays into primary neutrinos, and in section IV. we demonstrate how one can evade direct detection without splitting the DM multiplets. In section 4.4 we discuss the cosmology of these models. In particular, we show that a supersymmetric dark sector can have long lived gauginos which decay into photons, without violating constraints from big bang nucleosynthesis (BBN). We conclude in section 4.5. In appendix A.5 we revisit the symmetries of the four models, showing that these forbid the presence of any dangerous operators.

4.2 Tools for Modeling Decaying Dark Matter

In this section we describe our strategy for building models of hidden sector decaying DM. After briefly introducing our framework and notations, we list several potential dangers for models of this type, which arise from cosmological and experimental constraints. We then introduce a series of model building tools, organized by energy scale, that address these dangers and can be used to build viable models. We stress that these tools are modular, and can be used to construct a variety of models. We demonstrate the use of these tools to build some example models in section 4.3.

I. Framework

We consider models where weak-scale DM, χ , decays into a hidden sector with a gauge group, G_d , through a dimension-6 operator suppressed by the GUT scale, M_{GUT} . We take this ‘dark sector’ to be weakly coupled with a GeV mass gap, in resemblance to the annihilating models proposed in Ref. [20]. Throughout this chapter we work in the

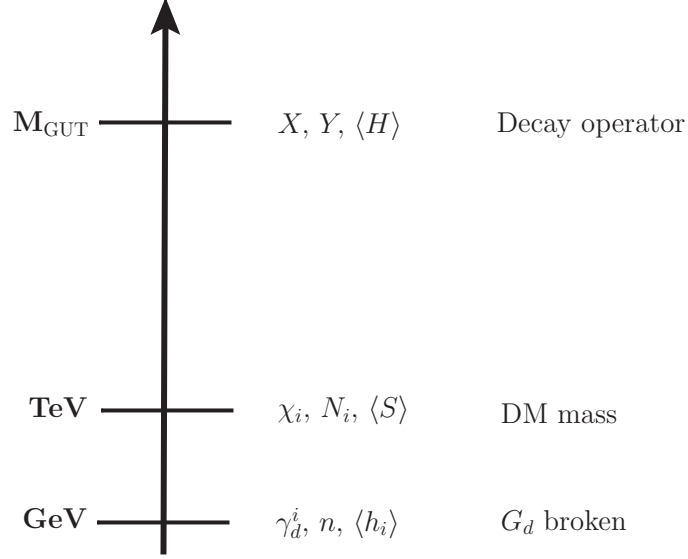


Figure 4.1: We summarize our notations, organized by energy scale. X and Y denote GUT scale fields that are integrated out to generate dimension-6 operators that induce DM decays. We use $\langle H \rangle$ to denote a GUT scale VEV, which can partially break the dark gauge group, $G'_d \rightarrow G_d$, as demonstrated in section II.. The DM may be composed of multiple species, χ_i , with mass at the TeV scale. This scale is naturally generated through the VEV of a singlet, S , that communicates with the SUSY breaking sector. Here, N_i denote electroweak scale fields that participate in the mechanism that generates a DM mass splitting. Such splittings can help evade the bounds from direct detection, as we discuss in section VI.. The dark gauge group, with gauge bosons γ_d^i , is entirely broken at the GeV scale by the VEVs of light Higgses. DM decays by dimension-6 operators into these GeV scale states. We use h_i to denote light fields charged under the dark gauge group, at least some of which will receive VEVs, and we use n to denote a light singlet.

supersymmetric framework which comes naturally with GUT models, and can stabilize the GeV scale. Furthermore, we assume the breaking of supersymmetry to be mediated through gauge interactions, allowing for a low scale of mediation. This assumption can be somewhat relaxed, if the breaking is sequestered from the dark sector [74]. The dark sector consists of massive gauge bosons, γ_d^i , gauginos, $\tilde{\gamma}_d^i$, Higgses, h_i , and Higgsinos, \tilde{h}_i . We couple it to the SM through gauge kinetic mixing, and consequently dark sector particles decay through the mixing to SM particles. Due to the low dark gauge boson mass, it decays predominantly into light leptons. Within this framework, DM decays can naturally explain the PAMELA and FERMI measurements. Our notations are summarized in Fig. 4.1.

II. Model Building Dangers

- **Dimension-5 DM Decay**

As we discuss in section III., dimension-6 decay operators suppressed by the GUT scale induce DM decays with a lifetime of $\tau_6 \simeq 10^{26}$ sec, the correct timescale to account for the PAMELA and FERMI signals. Alternatively, dimension-5 operators suppressed by the GUT scale correspond to a lifetime of $\tau_5 \simeq 1$ sec, and must be avoided.

- **Sommerfeld Enhancement**

If DM is directly charged under the light dark sector, the annihilation cross-section is Sommerfeld-enhanced [20]. It is important that this enhancement is not too large, since there are various strong constraints on the annihilation rate. These include constraints from gamma rays and neutrinos from the Galactic Center and Galactic Ridge (GR) [108, 18, 109, 110, 111], diffuse gammas from extragalactic DM annihilations [112, 113, 114], and modified CMB radiation from DM annihilation during recombination [115, 116, 117].

- **Direct Detection**

There are strong limits from direct detection on models in which a weak-scale DM couples elastically to a light gauge boson that kinetically mixes with the photon.

One finds a DM-nucleon cross-section of the order [20]:

$$\sigma_0 \simeq 10^{-37} \text{ cm}^2 \left(\frac{\epsilon}{10^{-3}} \right)^2 \left(\frac{\alpha_d}{0.01} \right) \left(\frac{m_{\gamma_d}}{1 \text{ GeV}} \right)^{-4}, \quad (4.2.1)$$

where ϵ parametrizes the size of the kinetic mixing. Current measurements rule out a cross-section of this size by 6 orders of magnitude [46, 47]. There are also strong limits from direct detection on DM that couples elastically to the Z . For example, models where DM is the neutral component of an $SU(2)_W$ doublet are excluded by 2-3 orders of magnitude [126].

- **Inelastic Capture in the Sun**

As we discuss in section VI., one way to avoid the above constraints from direct detection is to split the mass between the DM states, $\delta M_{\text{DM}} \gtrsim 100 \text{ keV}$, and couple inelastically to γ_d or Z [124]. It was recently demonstrated that if $\delta M_{\text{DM}} \simeq 100 - 500 \text{ keV}$, there are strong constraints on the inelastic capture of DM in the sun which is followed by annihilations into W^+W^- , ZZ , $\tau^+\tau^-$, or $t\bar{t}$ [127, 128]. This constraint is particularly important if DM is charged under $SU(2)_W$.

- **Long-Lived GeV Scale Fields**

The dark sector may contain light long-lived fields, and one must make sure that their cosmology is safe. On the one hand, stable particles must not overclose the universe, $\Omega_x h^2 < 0.1$. On the other hand, the dark sector may contain long-lived particles that decay electromagnetically through the kinetic mixing. For such decays, lifetimes of order $\tau \simeq 10^4 - 10^{12} \text{ sec}$ are constrained by Big Bang Nucleosynthesis [81] and decays after recombination, $\tau \gtrsim 10^{13} \text{ sec}$, are constrained by diffuse gamma rays [129].

- **Long-Lived Colored Particles**

If the DM is charged under the GUT gauge group, then there is a colored component χ_3 . There are strong constraints on colored particles with lifetimes $\tau \gtrsim 10^{17} \text{ sec}$ as they form exotic atoms [130, 131]. χ_3 must therefore have a much shorter lifetime than χ .

III. GUT Scale: Decay Operators

We consider models where weak-scale DM decays through dimension-6 operators suppressed by the GUT scale, into the dark sector. The GeV-scale dark fields then decay through gauge kinetic mixing to leptons. We focus on two possible scenarios, both of which include multiple, non-degenerate DM states: (i) One of the TeV fields receives a VEV, breaking part of G_d at the weak scale, and (ii) none of the states obtain VEVs and G_d is fully broken at the GeV scale. For scenario (ii), transitions between the TeV fields can be induced by the three body decay operators,

$$\frac{1}{M_{\text{GUT}}^2} \int d^4\theta \chi_1^\dagger \chi_2 h_1^\dagger h_2, \quad \frac{1}{M_{\text{GUT}}^2} \int d^2\theta \chi_1 \bar{\chi}_2 \mathcal{W}_d^2, \quad \frac{1}{M_{\text{GUT}}^2} \int d^2\theta \chi \bar{\mathbf{5}}_f \mathcal{W}_d^2. \quad (4.2.2)$$

For the first two operators, χ_1 and χ_2 are both weak-scale with $m_{\chi_2} > m_{\chi_1}$. Consequently, the DM is dominantly composed of χ_2 which generically has a larger density than χ_1 . For the third operator χ is a $\mathbf{5}$ of $SU(5)_{\text{SM}}$. We will consider examples that generate each of these operators in section 4.3. The decay rate of these operators is given parametrically by:

$$\tau \simeq \left(\frac{M_{\text{DM}}^5}{16\pi^2 M_{\text{GUT}}^4} \right)^{-1} \simeq 10^{26} \text{ sec} \left(\frac{M_{\text{DM}}}{1 \text{ TeV}} \right)^{-5} \left(\frac{M_{\text{GUT}}}{5 \times 10^{15} \text{ GeV}} \right)^4. \quad (4.2.3)$$

This is the correct timescale to account for the PAMELA and FERMI signals, as was first noticed by Ref. [92]. For scenario (i), two body decays will typically dominate. An example operator that we will consider in section IV. follows from inserting a $\langle \chi_1 \rangle$ VEV into the second operator of Eq. (4.2.2),

$$\frac{1}{M_{\text{GUT}}^2} \int d^2\theta \langle \chi_1 \rangle \bar{\chi}_2 \mathcal{W}_d^2. \quad (4.2.4)$$

As mentioned in the introduction, in the $M_{\text{GUT}} \rightarrow \infty$ limit, the DM is completely stable. This is typically achieved by a \mathbb{Z}_2^i discrete symmetry under which χ_i and $\bar{\chi}_i$ are charged. The superpotential at the GUT scale breaks this symmetry, destabilizing the DM. We demonstrate the existence of these symmetries in the models of section 4.3. Still, such symmetries do not ensure that the DM is sufficiently long-lived. Indeed, when integrating out GUT fields to generate the above dimension-6 decays, it is important to make sure that no dimension-5 decay operators are generated. This can follow from

symmetries at the GUT scale. For each specific model of section 4.3 we identify these symmetries in appendix A.5. To demonstrate that this is possible, we now discuss two general mechanisms for generating dimension-6 decays that do not generate dimension-5 decays. One simple possibility is that the hidden sector gauge group is broken at the GUT scale, $G'_d \rightarrow G_d$, without breaking supersymmetry. By going to Unitary gauge and integrating out the massive G'_d/G_d vector superfields, it is simple to check that dimension-6 decay operators, of the form of the first operator in Eq. (4.2.2), are generated in the Kähler potential [132]. Moreover, if the DM and light Higgses have a canonical Kähler potential at the GUT scale, no dimension-5 terms are generated. We will discuss this in more detail for a specific example in section II.

A second way to generate dimension-6 operators without generating dimension-5 ones is by coupling canonical GUT-scale fields to the DM in a chiral manner,

$$W \supset M_{\text{GUT}} X \bar{X} + X \chi h. \quad (4.2.5)$$

Integrating out X and \bar{X} , and allowing for a weak-scale VEV for the DM, results in the dimension-6 Kähler potential operator in Eq. (4.2.4). It is straightforward to see from the equations of motion that no dimension-5 operators are generated in the superpotential or Kähler potential. More generally, global symmetries prevent quantum corrections from generating dimension-5 decays in the Kähler potential, as we discuss in appendix A.5.

When the DM is charged under $SU(5)_{\text{SM}}$, as for the third operator of Eq. (4.2.2), one must ensure that its colored partner decays on a timescale shorter than the current age of the universe. For example, suppose that the DM is the neutral component of the doublet of a $\mathbf{5} + \bar{\mathbf{5}}$. The model is viable if the triplet can decay through a dimension-5 operator that does not induce DM decays. This is straightforward to achieve since the triplet is typically heavier than the doublet at the weak scale, due to the RG evolution of their masses. Example triplet decay operators include:

$$\frac{1}{M_{\text{GUT}}} \int d^2\theta \chi^2 \bar{\mathbf{5}}_f^2, \quad \frac{1}{M_{\text{GUT}}} \int d^2\theta \chi \mathbf{10}_f^2 s, \quad \frac{1}{M_{\text{GUT}}} \int d^4\theta \bar{\chi} \bar{\mathbf{5}}_f^\dagger s, \quad (4.2.6)$$

where in the first operator the triplet partner decays into the DM while in the other two the triplet decays into a singlet, s , with $m_{\chi_2} < m_s < m_{\chi_3}$.

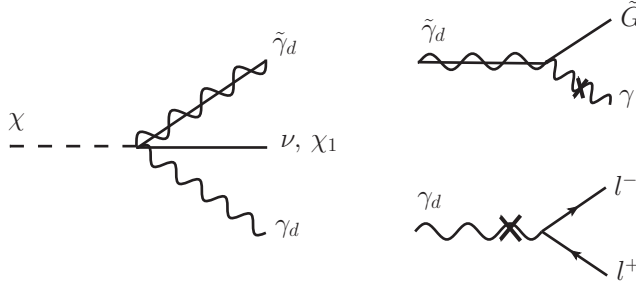


Figure 4.2: A sample DM 3-body decay induced by one of the two last operators of Eq. (4.2.2). The DM decays to a GeV-scale gauge boson, gaugino, and a neutrino or the lighter field, χ_1 . The gauge boson decays through the kinetic mixing to a lepton pair and the gaugino decays through the kinetic mixing to a photon and gravitino, assuming that the gaugino is lighter than, or degenerate with, the dark photon. The resulting leptons can explain the PAMELA and FERMI excesses while the gamma rays and neutrinos lead to hard and sharp spectral features that can be probed by upcoming experiments [125].

IV. Weak Scale: Dark Matter Mass and Communicating SUSY Breaking

As we discuss in the sections V. and 4.5, sharp spectral features in the photon flux may exist, depending on the light dark spectrum. As a consequence, the low lying excitations, and indirectly the SUSY-breaking effects in that sector, may be probed in the near future [125]. Below, we briefly discuss the possible effects which may influence the spectrum.

In our framework, the DM has a weak-scale mass. A GUT-scale one can be avoided by imposing a PQ or R symmetry that is spontaneously broken at the weak scale by a neutral scalar, S . The DM mass term then takes the form,

$$y\langle S\rangle\chi\bar{\chi}. \quad (4.2.7)$$

This is similar to the well-known μ -problem, and we present no new solution. Instead, we simply assume the coupling above, with a VEV induced by the SUSY-breaking sector.

In principle, S may have a soft mass which arises from coupling to the SUSY-breaking sector. We distinguish between two cases,

- **χ is not charged under G_d** and couples to the light sector only through GUT suppressed couplings. Examples of such a scenario are given in sections III. and IV.. In this case, SUSY-breaking effects are primarily communicated to the light sector through the kinetic mixing, as is worked out in [133]. The leading contribution to the soft mass squared of the light Higgses is generated as a threshold effect at the gauge messenger scale and is proportional to ϵ^2 ,

$$\delta m_h^2 \simeq \epsilon^2 \frac{g_d^2}{g_Y^2} M_{\tilde{E}}^2 = (100 \text{ MeV})^2 \left(\frac{\epsilon}{5 \times 10^{-4}} \right)^2 \left(\frac{g_d}{g_Y} \right)^2 \left(\frac{M_{\tilde{E}}}{200 \text{ GeV}} \right)^2. \quad (4.2.8)$$

Here g_Y is the hypercharge gauge coupling and $M_{\tilde{E}}$ is the soft mass of the right-handed selectron. As we show in the next subsection, this is parametrically smaller by one power of ϵ compared to the supersymmetric mass squared of the dark vector boson. The corresponding contribution to the gaugino soft masses is even smaller [133] and may be neglected. The GeV scale, which we discuss below, is therefore approximately supersymmetric.

- **χ is charged under G_d** and may couple directly to the light Higgses. Such examples are given in sections I. and II.. Here the SUSY-breaking effects can be communicated either through S or through the kinetic mixing as discussed above. Below, for simplicity we assume the latter. We stress that S can be naturally supersymmetric and still solve the μ -problem. This can be achieved for example through retrofitting [134]. We postpone the details of such a scenario to future work. If, on the other hand, S is accompanied by a soft mass, SUSY breaking effects in the light sector are expected to be of order GeV, and therefore dominate over the kinetic mixing contributions.

In the above discussion we assumed the absence of TeV-scale messengers that couple to both the dark sector and SM. If such states exist, SUSY breaking is mediated as in gauge mediation and the supermultiplets are split at the GeV scale [21]. Finally, we note that when the DM is approximately supersymmetric, both the fermion and boson components

are cosmologically long-lived and constitute order one fractions of the DM relic density. On the other hand, when there is large splitting within the DM supermultiplet, either the fermion or scalar component dominates the relic density, in a model-dependent fashion. The analysis that follows does not depend on the spin of the DM.

V. GeV Scale: Breaking the Dark Sector

In correspondence to the discussion above, there are two ways to naturally generate the GeV scale in the dark sector. One is with the use of D-term mixing which results from supersymmetric kinetic mixing [57]. In such a case, the light dark sector is approximately supersymmetric, at the GeV scale. We review this mechanism below. The second way to generate the GeV scale is by communicating weak scale SUSY breaking as mentioned above. For simplicity, below we only consider a $U(1)_d$ model with the D-term mixing mechanism. The approximate supersymmetry in the light dark sector simplifies the analysis, since we do not need to consider GeV-scale soft terms. Nevertheless, we stress that this is only a simplifying assumption, which can easily be relaxed. Indeed, introducing GeV SUSY-breaking may change the low energy spectrum and consequently the astrophysical signatures, but does not affect the discussions below in a significant way.

The GeV scale of our theory resembles that of [20, 21]. We assume that the SM and dark sector interact with each other through gauge kinetic mixing. The kinetic mixing between $U(1)_d$ and hypercharge is given by:

$$-\frac{\epsilon}{2} \int d^2\theta \mathcal{W}_d \mathcal{W}_Y. \quad (4.2.9)$$

ϵ is naturally of order $10^{-3} - 10^{-4}$ and arises from integrating out heavy fields charged under both sectors. Supersymmetric kinetic mixing of this size automatically generates the GeV scale in the dark sector [1, 2]. To see this, we expand Eq. (4.2.9) in components. One finds D-term mixing, $V \supset \epsilon D_{\text{dark}} D_Y$, which upon electroweak symmetry breaking generates a Fayet-Illiopolous (FI) term for $U(1)_d$. Such a term triggers the breaking of

the dark sector at the GeV scale:

$$m_{\gamma_d}^2 = \epsilon g_d \langle D_Y \rangle = (1 \text{ GeV})^2 \left(\frac{\epsilon}{5 \times 10^{-4}} \right) \left(\frac{g_d}{0.35} \right) \left(\frac{\sqrt{\langle D_Y \rangle}}{75 \text{ GeV}} \right)^2. \quad (4.2.10)$$

As discussed in the previous section, the dark sector spectrum is approximately supersymmetric when kinetic mixing is the only form of low-energy communication between the two sectors.

When produced, the GeV scale particles can decay through the kinetic mixing to SM particles. The dark photon, γ_d , decays directly through the kinetic mixing to pairs of SM leptons, l^+l^- . If the dark Higgs, h , is too light to decay to two dark photons, it decays at one loop to lepton pairs. Both of these decays are prompt on galactic scales for typical values of the parameters:

$$\begin{aligned} \gamma_d \rightarrow l^+l^- & \quad \tau \simeq (\epsilon^2 \alpha_{\text{EM}} m_{\gamma_d})^{-1} \simeq 10^{-16} \text{ sec}, \\ h \rightarrow l^+l^- & \quad \tau \simeq 4\pi(\epsilon^4 \alpha_{\text{EM}}^2 m_h)^{-1} \simeq 10^{-6} \text{ sec}, \end{aligned} \quad (4.2.11)$$

where for the last step we have chosen the representative values $m_{\gamma_d}, m_h = 1 \text{ GeV}$ and $\epsilon = 5 \times 10^{-4}$.

The decay of the lightest fermion in the dark sector has important consequences for the astrophysical signals of our model. If the lightest fermion mixes with the dark gaugino, it can always decay through the kinetic mixing to the SM photon and the gravitino¹, $\tilde{\gamma}_d \rightarrow \gamma \tilde{G}$. The lifetime is found to be:

$$\tau_{\tilde{\gamma}_d \rightarrow \gamma \tilde{G}} \simeq \epsilon^{-2} \left(\frac{m_{\tilde{\gamma}_d}^5}{16\pi F^2} \right)^{-1} = 10^4 \text{ sec} \left(\frac{5 \times 10^{-4}}{\epsilon} \right)^2 \left(\frac{1 \text{ GeV}}{m_{\tilde{\gamma}_d}} \right)^5 \left(\frac{\sqrt{F}}{100 \text{ TeV}} \right)^4. \quad (4.2.12)$$

This decay is prompt on galactic scales for low-scale SUSY breaking, and leads to a hard gamma ray signature. If the lightest fermion is significantly heavier than its bosonic superpartner, it can also decay to its superpartner and the gravitino, $\tilde{\gamma}_d \rightarrow \gamma_d \tilde{G}$, or

¹We only consider models where gravity mediation is not the dominant source of scale generation in the dark sector, such that $m_{\tilde{G}} \simeq F/M_p < \text{GeV}$. This is the case for the general framework of low-scale gauge mediation.

$\tilde{h} \rightarrow h \tilde{G}$, with lifetime:

$$\begin{aligned} \tau_{\tilde{\gamma}_d \rightarrow \gamma_d \tilde{G}} &\simeq \left(\frac{m_{\tilde{\gamma}_d}^5}{16\pi F^2} \right)^{-1} \left(1 - \frac{m_{\gamma_d}^2}{m_{\tilde{\gamma}_d}^2} \right)^{-4} \\ &= 3 \times 10^{-3} \text{ sec} \left(\frac{1 \text{ GeV}}{m_{\tilde{\gamma}_d}} \right)^5 \left(\frac{\sqrt{F}}{100 \text{ TeV}} \right)^4 \left(1 - \frac{m_{\gamma_d}^2}{m_{\tilde{\gamma}_d}^2} \right)^{-4}. \end{aligned} \quad (4.2.13)$$

Due to the phase space suppression above, the decay into the dark photon is subdominant when the dark sector is approximately supersymmetric as in our case. Consequently DM decays into γ_d and h produce hard leptons, while decays into $\tilde{\gamma}_d$ produce hard gamma rays. Since the DM decays into both bosonic and fermionic states in the dark sector, we are led to the generic conclusion that the hard lepton signals may be correlated with hard gamma ray signals. These signatures are studied in detail in [125].

The dark spectrum and lifetimes are constrained by the requirement that the GeV scale cosmology is safe. We discuss the dark sector cosmology and the resulting constraints in section 4.4.

VI. MeV Scale: Dark Matter Splitting

It is important for DM to evade the strong constraints on direct detection mentioned in section II. There are three possible solutions:

1. Very small kinetic mixing, ϵ , between the dark sector and the SM.
2. The DM does not directly couple to γ_d or Z .
3. The DM multiplets are split.

The first solution applies when DM is charged under the light dark sector. As we can see from equation (4.2.1), the DM evades direct detection if the kinetic mixing is small enough, $\epsilon \lesssim 10^{-6}$. Interestingly, as discussed in section 4.4, mixing of this size may be insufficient to keep the dark sector in thermal equilibrium thereby interfering with the usual WIMP cosmology.

The second solution can be realized by keeping the DM neutral under both the SM and the light gauge group. For example, in section IV., we consider a $U(1)_\chi \times U(1)_d$

model where DM is charged only under $U(1)_\chi$, which is broken at the weak scale, while $U(1)_d$ is broken at the GeV scale. Kinetic equilibrium is maintained between DM and the SM through double kinetic mixing, as we discuss in section 4.4.

The third possibility is to introduce a DM splitting $\delta M_\chi \gtrsim 100$ keV. Indeed in such a case the DM couples inelastically together with an excited state, χ' , to the dark gauge boson, γ_d , or Z , suppressing direct detection [124]. This bound is all that is necessary to evade the current constraints, but there are two special values for the splitting that are of experimental significance. If the splitting is of order 100 keV, the DAMA signal [24] can be reconciled with the bounds from other experiments through the inelastic DM scenario (iDM) [23] (see however [135]). If, on the other hand, the splitting is of size $\delta M_\chi \gtrsim 1$ MeV, it can account for the anomalous production of positrons observed by the INTEGRAL satellite close to the Galactic Center [44]. This is the eXciting DM (XDM) proposal [43] (see however [136]). If there are enough DM states, both scenarios can be realized.

Suppose first, that DM is charged under G_d . Splittings with the right parametric size for iDM or XDM are generated by direct couplings between DM and the light Higgses [2]:

$$W \supset S (y_N N^2 + y_\chi \chi \bar{\chi}) + y_{\text{split}} N \chi h. \quad (4.2.14)$$

As discussed above, we assume that S interacts with the SUSY breaking sector and gets a weak scale VEV. N is a singlet and stability of DM requires N to be heavier than χ , $|y_N| > |y_\chi|$. In this limit, we integrate out N and find a DM splitting of size:

$$\delta m_\chi = \frac{y_{\text{split}}^2 \langle \bar{h} \rangle^2}{4m_N} = 100 \text{ keV} \left(\frac{y_{\text{split}}}{1} \right)^2 \left(\frac{\langle \bar{h} \rangle}{1 \text{ GeV}} \right)^2 \left(\frac{m_N}{2.5 \text{ TeV}} \right)^{-1}. \quad (4.2.15)$$

If χ is charged under the SM, the last term in Eq. (4.2.14) can be replaced with a coupling to the SM Higgs. In that case the splitting is expected to be larger.

There is an important caveat to the above mechanism. If S gets a weak-scale F -term, the χ scalars receive a weak-scale splitting and the dark gauge boson couples across the splitting. This SUSY-breaking splitting provides another mechanism for evading the constraint from direct detection, but the splitting is generically too large to account for iDM or XDM. If we wish to include these proposals, S must receive a weak-scale VEV but

should have no F-term to leading order². Consequently, S cannot be the NMSSM singlet. We note that there are more options other than Eq. (4.2.14) for generating an MeV size DM splitting, and we will employ a slightly different mechanism in appendix A.5.

Another possibility is that the DM is charged under a non-Abelian hidden sector. In this case, the splittings among the DM multiplet are generated radiatively after dark sector symmetry breaking [20]. In practice, non-Abelian dark sectors are more difficult to construct and often require elaborate Higgs sectors [1]. In the explicit models that we study below, we will instead focus on the simplest possibility of a $U(1)_d$ hidden sector at low energies. This is for illustrative purposes only, and more complicated dark sectors remain a valid possibility.

4.3 Models

In this section we use the tools described above to construct four explicit models of hidden sector decaying DM. There are many possible models within this framework, and these should be viewed only as illustrative examples. The models are roughly ordered by increasing complexity. We begin with a minimal $U(1)_d$ dark sector which includes all of the main ideas. The second model embeds $U(1)_d$ into $SU(2)_d$ at the GUT scale. The $SU(2)_d$ breaking generates dimension 6 DM decay. For the third model, we consider DM charged under the SM, and find that there is always an associated hard neutrino signal. The reader who is primarily interested in the new correlated signals that we propose may want to skip directly to this model. All four models can produce hard gammas that are correlated with the astrophysical leptons, but only the third model also produces hard neutrinos. Finally, we consider a $U(1)_\chi \times U(1)_d$ model, where no splitting is required to evade direct detection. In section 4.4, we discuss the constraints that cosmology places on these models. In appendix A.5, we discuss some further technical details for each model.

²An alternative possibility is to introduce another source of SUSY breaking that lifts both χ scalars above the fermions so that the fermions constitute DM.

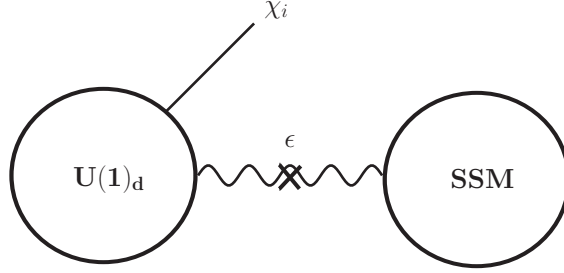


Figure 4.3: The setup of our minimal model. DM is charged under the hidden sector, $U(1)_d$, and decays through dimension-6 GUT scale suppressed operators into the dark sector gauge multiplet. $U(1)_d$ kinetically mixes with hypercharge, and this kinetic mixing has three important effects: (i) D-term mixing causes $U(1)_d$ to break at the GeV scale, (ii) dark gauge bosons decay through the kinetic mixing to leptons while decays into antiprotons are kinematically forbidden, and (iii) DM stays in kinetic equilibrium with the SM through the kinetic mixing, allowing for the usual ‘WIMP Miracle’ cosmology (see section 4.4).

In the last two models the DM is not charged under the GeV-scale dark sector. Consequently no Sommerfeld enhancement is present at all, so the astrophysical constraints are automatically avoided. Such models are in sharp contrast to the annihilating models of [20].

I. $U(1)_d$: The Minimal Model

We begin by considering the simplest possibility, $G_d = U(1)_d$. This model captures the main ideas of our framework and serves as an example for the models that follow. We assume a kinetic mixing between $U(1)_d$ and hypercharge, as in equation (4.2.9). The field content is listed in table 4.1 and the setup is illustrated in Fig. 4.3. All fields are assumed to have canonical Kähler potential at the GUT scale. In order to stress the modularity of the model, we split up the superpotential into three pieces,

$$W = W_{\text{decay}} + W_{\text{DM}} + W_{\text{split}}. \quad (4.3.16)$$

	GUT				TeV				GeV		
	X	\bar{X}	Y	\bar{Y}	χ_i	$\bar{\chi}_i$	S	N_i	h	\bar{h}	n
$U(1)_d$	0	0	1	-1	1	-1	0	0	1	-1	0

Table 4.1: The matter content of the $U(1)_d$ model, where $i = 1, 2$. We stress the modularity of the model by grouping the fields according to their scales.

The first term leads to DM decay:

$$W_{\text{decay}} = (M_{\text{GUT}} + X) Y \bar{Y} + M_{\text{GUT}} X \bar{X} + \bar{X} \chi_1 \bar{\chi}_2. \quad (4.3.17)$$

Integrating out the GUT scale fields generates the second operator of equation (4.2.2), at one loop [94]. Meanwhile, it is straightforward to see from the equations of motion that no dimension-5 decays are generated in the superpotential.

The second term of equation (4.3.16) determines the DM and dark sector spectrum:

$$W_{\text{DM}} = S (y_1 \chi_1 \bar{\chi}_1 + y_2 \chi_2 \bar{\chi}_2) + n h \bar{h}. \quad (4.3.18)$$

We assume that S obtains a weak-scale VEV, possibly through interactions with the SUSY breaking sector. The different Yukawa couplings $y_{1,2}$ generate masses for χ_1 and χ_2 with $m_{\chi_2} > m_{\chi_1}$. Both χ_i are stable on cosmological timescales and contribute to the relic density, however, DM is mostly composed of χ_2 , whose larger mass leads to a smaller annihilation cross-section and therefore to a larger abundance. The dimension-6 decay operator in Eq. (4.2.2), leads to three body decays of χ_2 into χ_1 and dark sector gauge bosons, γ_d , and/or gauginos, $\tilde{\gamma}_d$. γ_d and $\tilde{\gamma}_d$ then decay to SM leptons and photons through the channels described in section V..

At the GeV scale, this model resembles the low-energy $U(1)$ construction of Ref. [2]. The D-term mixing, described in section V., generates an effective FI term for the $U(1)_d$, which triggers one of the light Higgses to get a VEV at the GeV scale. Without loss of generality, we take \bar{h} to be the one with a non-vanishing VEV. Expanding around $\langle \bar{h} \rangle$, h and n obtain a GeV mass through the last term of Eq. (4.3.18). Consequently, all fields are lifted, forming a GeV scale mass gap.

	GUT				TeV				GeV		
	H	X	$\bar{\Phi}$	\bar{n}	χ	$\bar{\chi}$	Φ	S_Φ	h	n'	s_n
$SU(2)_d$	Adj	\square	Adj	Adj	\square	\square	Adj	1	\square	Adj	1

Table 4.2: The matter content for the $SU(2)_d \rightarrow U(1)_d$ model.

The last term of Eq. (4.3.16) corresponds to two copies of the splitting mechanism described by Eqs. (4.2.14),(4.2.15),

$$W_{\text{split}} = \sum_{i=1}^2 (SN_i^2 + N_i\chi_i\bar{h}) . \quad (4.3.19)$$

Splittings are generated for both χ_i , evading the constraints from direct detection. The two splittings are of different sizes, and we note that both iDM and XDM can be incorporated in this model if $\delta M_{\chi_1} \sim 100$ keV and $\delta M_{\chi_2} \sim 1$ MeV, or vica versa. It would be interesting to conduct a more detailed study of this multi-species DM model to see if indeed the two scenarios can be accommodated.

That χ_1 and χ_2 are long-lived follows from an unbroken $\mathbb{Z}_2^1 \times \mathbb{Z}_2^2$, as $M_{\text{GUT}} \rightarrow \infty$. $\chi_i, \bar{\chi}_i$, and N_i are charged under \mathbb{Z}_2^i , respectively. This symmetry is broken by Eq. (4.3.17), resulting in DM decays. In appendix A.5, we verify that dimension-5 decays are forbidden by a GUT scale symmetry.

We conclude by remarking that with this field content, the absence of Landau poles below the GUT scale places a bound on the dark gauge coupling at the GeV scale, $\alpha_d \lesssim 1/30$.

II. $SU(2)_d \rightarrow U(1)_d$: GUT Scale Symmetry Breaking

We now consider a UV completion of the previous model, by embedding $U(1)_d$ into $SU(2)_d$ which is broken at the GUT scale. In the following discussion, we focus on the two new features of this model: (i) heavy gauge bosons generate the dimension-6 DM decay, and (ii) the low-energy theory contains split $SU(2)_d$ multiplets. The field content is summarized in table 4.2. Again, we assume a canonical Kähler potential and group

the terms in the superpotential according to their role,

$$W = W_{\text{decay}} + W_{\text{GUT}} + W_{\text{DM}}. \quad (4.3.20)$$

The first term above, triggers the GUT-scale breaking $SU(2)_d \rightarrow U(1)_d$,

$$W_{\text{decay}} = f(H) + HX^2. \quad (4.3.21)$$

Here $H = H^a T^a$ is a triplet and $T^a = \sigma^a/2$ are the generators of $SU(2)_d$. In most of what follows we suppress color indices. We take $f(H)$ to be a potential for H with a minimum at $\langle H \rangle = M_{\text{GUT}} T^3$. Consequently, X , which is introduced to cancel $SU(2)$ anomalies [137], obtains a GUT-scale mass and is integrated out.

To see the effect of the breaking, we integrate out the broken $SU(2)_d/U(1)_d$ generators. Going to the Unitary gauge and solving for the massive vector superfields, $V_{\pm} = V_1 \mp iV_2$, one finds an additional contribution to the Kähler potential [132],

$$\delta K_{\text{eff}} = -(\varphi_i^\dagger T^+ \varphi_i) \lambda_{\pm}^{-1} (\varphi_j^\dagger T^- \varphi_j), \quad (4.3.22)$$

where φ_i collectively denote all fields (subject to the Unitary gauge constraint), $T^{\pm} = T^1 \pm iT^2$ are the broken generators in the corresponding representation and

$$\lambda^{\pm} = \frac{1}{2} H^\dagger \{T^+, T^-\} H = M_{\text{GUT}}^2. \quad (4.3.23)$$

Substituting the DM states, $\chi_\alpha = (\chi_1, \chi_2)$, $\bar{\chi}^\alpha = (\bar{\chi}_1, \bar{\chi}_2)$ and light Higgs, $h_\alpha = (h_1, h_2)$ into Eq. (4.3.22) one finds the contributions,

$$-\frac{1}{M_{\text{GUT}}^2} \int d^4\theta \left(\chi_1^\dagger \chi_2 h_2^\dagger h_1 + \bar{\chi}_1^\dagger \bar{\chi}_2 h_1^\dagger h_2 \right) + (1 \rightarrow 2). \quad (4.3.24)$$

These operators are precisely of the form of the first operator in Eq. (4.2.2). As in the $U(1)_d$ model, we will require $m_{\chi_2} > m_{\chi_1}$. In this case, DM is mostly composed of χ_2 and Eq. (4.3.24) generates 3-body decay of χ_2 into χ_1 and the lights Higgses h_1 and h_2 . We again assume that there is kinetic mixing between the low-energy $U(1)_d$ and hypercharge, generated by integrating out fields charged under both the dark sector and SM, so that D-term mixing generates a GeV-scale VEV for h_2 , which is eaten by the gauge multiplet and decays to SM leptons and photons as we describe in section V..

In order to minimize the low-energy field content so that it matches the $U(1)_d$ model of the previous section, and in order to give different masses to χ_1 and χ_2 , we work with split $SU(2)_d$ multiplets. We can split the triplets Φ and n by coupling them to H and GUT scale singlets, denoted by S_Φ and s_n :

$$W_{\text{GUT}} = \text{Tr} [g(H) (\Phi\bar{\Phi} + S_\Phi\bar{\Phi} + n'\bar{n} + s_n\bar{n})] . \quad (4.3.25)$$

For generic $g(H)$ ³, the VEV of H generates GUT scale masses for all component fields except for one linear combination of Φ_3 and S_Φ , which we denote by S , and one linear combination of n'_3 and s_n , which we denote n . The specific linear combinations that remain light depend on $g(H)$. In appendix A.5, we use a discrete symmetry to prove that S and n remain light and to show that dimension-5 DM decays can be forbidden for generic superpotentials.

The low-energy theory is dictated by the superpotential terms:

$$W_{\text{DM}} = (\Phi + S_\Phi)\chi\bar{\chi} + (n' + s_n)h^2 . \quad (4.3.26)$$

After the $SU(2)_d$ breaking splits the multiplets, the low-energy effective superpotential is of the form:

$$W_{\text{eff}} = S(y_1 \chi_1\bar{\chi}_1 + y_2 \chi_2\bar{\chi}_2) + nh_1h_2 , \quad (4.3.27)$$

with y_i couplings of order one that depend on $g(H)$. The projection onto the light state S results in couplings that are not $SU(2)$ invariant, and the TeV scale VEV of S therefore generates different masses for χ_1 and χ_2 . As before, the DM is long-lived because as $M_{\text{GUT}} \rightarrow \infty$, there is an unbroken $\mathbb{Z}_2^1 \times \mathbb{Z}_2^2$ symmetry, under which χ_i and $\bar{\chi}_i$ are separately charged for $i = 1, 2$. The third term is the same as the last term of Eq. (4.3.18), and the low-energy dark sector is thus the same as the $U(1)_d$ model. It is also straightforward to induce small DM splittings, in order to evade the constraints from direct detection and possibly incorporate iDM and XDM. This is shown in appendix A.5.

³There is in general a different polynomial of H in front of each term of Eq. (4.3.25), which we have suppressed to keep our notation compact.

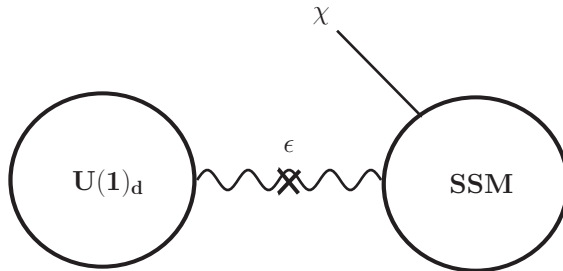


Figure 4.4: A model with DM charged under the SM. DM is the neutral component of a $\mathbf{5} + \bar{\mathbf{5}}$ representation of $SU(5)_{\text{SM}} \supset SU(3)_C \times SU(2)_W \times U(1)_Y$. DM decays through a dimension-6 operator into the gauge multiplet of $U(1)_d$, which kinetically mixes with hypercharge. The conservation of hypercharge (at the GUT scale) implies that this decay must be accompanied by the associated production of a neutrino. This results in a primary neutrino spectrum that is correlated with the leptonic cosmic rays, and will be tested by upcoming experiments such as IceCube/DeepCore [125].

III. $SU(5)_{\text{SM}} \times U(1)_d$: SM Charged-DM and Correlated Neutrinos

We now consider a model where DM is charged under the SSM and decays through a dimension-6 operator into the dark sector. In this model, DM itself is not charged under the GeV sector, avoiding the constraints due to Sommerfeld enhancement discussed in section II. We take $\chi + \bar{\chi}$ to be charged under an $SU(5)$ GUT gauge group, residing in a $\mathbf{5} + \bar{\mathbf{5}}$. A schematic description of the model is shown in Fig. 4.4. By gauge invariance, decay into the dark sector must be accompanied by associated SM particle production⁴. If one SM particle is produced, it must be a neutrino or Higgs. The latter produces antiprotons, which are constrained by PAMELA, and thus we focus on the possibility that DM decays produce hard neutrinos that accompany dark sector production. The discovery of such neutrinos is discussed in [125].

An important requirement for this model is that the colored partner of DM decays faster than the current age of the universe. This is because there are strong constraints

⁴We thank N. Arkani-Hamed for drawing our attention to this point.

	GUT				TeV					GeV		
	X	\bar{X}	Y	\bar{Y}	χ	$\bar{\chi}$	S	s_1	N	h	\bar{h}	n'
$SU(5)_{\text{SM}}$	1	1	1	1	\square	$\bar{\square}$	1	1	1	1	1	1
$U(1)_d$	0	0	1	-1	0	0	0	0	0	1	-1	0

Table 4.3: The matter content for our model with DM charged under $SU(5)_{\text{SM}} \supset SU(3)_C \times SU(2)_W \times U(1)_Y$.

on stable colored particles, as discussed in section II.. These constraints are evaded if the triplet DM decays through a dimension-5 operator. For this model, we assume that the canonical Kähler potential is supplemented by one irrelevant operator, generated at the GUT scale,

$$K_{\text{DM}} = \frac{1}{M_{\text{GUT}}} \int d^4\theta \chi \bar{\mathbf{5}}_f^\dagger s_1, \quad (4.3.28)$$

where s_1 is a singlet with mass: $m_{\chi_2} < m_{s_1} < m_{\chi_3}$. This mechanism can be easily arranged since the triplet partner is expected to be heavier than the DM, due to the RG evolution of their masses below the GUT scale.

We list the field content in table 4.3, and again we group the superpotential terms according to their roles:

$$W = W_{\text{decay}} + W_{\text{DM}} + W_{\text{split}}. \quad (4.3.29)$$

The first term generates dimension-6 DM decay using the same mechanism as our $U(1)_d$ model of section I.:

$$W_{\text{decay}} = (M_{\text{GUT}} + X)Y\bar{Y} + M_{\text{GUT}}X\bar{X} + \bar{X}\chi\bar{\mathbf{5}}_f. \quad (4.3.30)$$

Integrating out X and Y generates the third dimension-6 decay operator of Eq. (4.2.2) at one-loop:

$$\frac{1}{M_{\text{GUT}}^2} \int d^2\theta \frac{\alpha_d}{4\pi} \chi \bar{\mathbf{5}}_f \mathcal{W}_d^2. \quad (4.3.31)$$

This operator results in three-body decay, with DM decaying into one neutrino or sneutrino and two dark gauge bosons or gauginos, which subsequently decay to SM leptons and photons through the operators discussed in section V..

At low energies, this model resembles the constructions above:

$$W_{\text{DM}} = S (\chi\bar{\chi} + s_1^2) + nh\bar{h} \quad (4.3.32)$$

We assume that S , which may be the NMSSM singlet, gets a weak-scale VEV. This generates a mass for the DM and the singlet s_1 , which plays a role in the triplet decay of Eq. (4.3.28). As in the models above, we take $U(1)_d$ to kinetically mix with hypercharge, and the D-term mixing generates a GeV-scale VEV for \bar{h} . With no DM splitting, this model would be ruled out because the DM couples strongly to the SM Z boson. This constraint is evaded by coupling the DM to the Higgs, which generates a small splitting:

$$W_{\text{split}} = SN^2 + \chi H_d N. \quad (4.3.33)$$

Here N is a singlet that must be heavier than χ , to ensure its stability. The resulting splitting is too large to account for iDM or XDM. In fact, iDM is already ruled out for this model by the constraints from inelastic capture in the sun, as discussed in section II.. Finally, the DM is long-lived due to an unbroken \mathbb{Z}_2 at the renormalizable level, under which $\chi, \bar{\chi}$, and N are charged.

If the DM relic density is only determined by its $SU(2)_W$ gauge interaction, its mass is fixed to be: $m_\chi \simeq 1.1$ TeV [126]. This mass is too small to fit the FERMI excess with DM decays [18]. Fortunately, the second operator of the above splitting mechanism, Eq. (4.3.33), opens up a new annihilation channel into SM Higgses. This raises the DM annihilation cross-section, allowing for heavier masses which can fit FERMI. We discuss the DM relic density further in section 4.4.

IV. $U(1)_\chi \times U(1)_d$: No Mass Splitting

We now consider a model with a $U(1)_\chi \times U(1)_d$ hidden sector. We illustrate the basic idea in Fig. 4.5. The DM, χ_2 , is charged under $U(1)_\chi$, which is broken at the weak scale by the VEV of a different species χ_1 . It decays through a dimension-6 operator into the $U(1)_d$ gauge multiplet. There are two advantages to this setup. First, this model does not have a strong constraint from direct detection, because DM does not couple directly to the Z boson or γ_d . Therefore, unlike the previous models, no DM splitting is required.

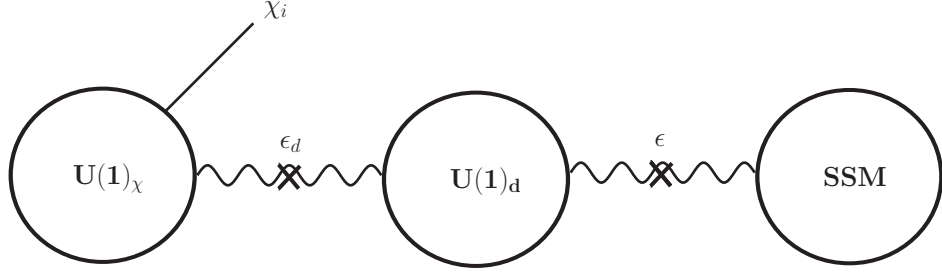


Figure 4.5: A model with double kinetic mixing. DM, χ_2 , is charged under $U(1)_\chi$, which is broken by a different species, χ_1 , at the TeV scale. Decays are induced by a dimension-6 GUT suppressed operator into the $U(1)_d$ gauge multiplet, which kinetically mixes with both hypercharge and $U(1)_\chi$. This double kinetic mixing is sufficient to keep DM in kinetic equilibrium with the SM, preserving the usual WIMP cosmology (see section 4.4). There is no strong constraint from direct detection because the DM does not couple directly to the Z or $U(1)_d$ gauge boson, and therefore no DM splitting is required.

Second, there is no constraint from photon or neutrino measurements, as in the model of section III., since DM is not charged under $U(1)_d$. Another unique feature of this model is that 2-body decays dominate over 3-body decays because the decay operator contains a field, χ_1 , which obtains a weak scale VEV.

The field content of this model is listed in table 4.4. We assume a canonical Kähler potential, and we group the superpotential terms according to their role,

$$W = W_{\text{decay}} + W_{\text{DM}}. \quad (4.3.34)$$

The first term is identical to the GUT scale interactions of the $U(1)_d$ model, Eq. (4.3.17),

$$W_{\text{decay}} = (M_{\text{GUT}} + X) Y \bar{Y} + M_{\text{GUT}} X \bar{X} + \bar{X} \chi_1 \bar{\chi}_2,$$

generating the second decay operator of Eq. (4.2.2). Integrating out bifundamentals generates kinetic mixing between $U(1)_d$ and $U(1)_\chi$,

$$-\frac{\epsilon_d}{2} \int d^2\theta \mathcal{W}_\chi \mathcal{W}_d, \quad (4.3.35)$$

	GUT				TeV			GeV		
	X	\bar{X}	Y	\bar{Y}	χ_i	$\bar{\chi}_i$	S_i	h	\bar{h}	n
$U(1)_\chi$	0	0	0	0	1	-1	0	0	0	0
$U(1)_d$	0	0	1	-1	0	0	0	1	-1	0

Table 4.4: The matter content for the $U(1)_\chi \times U(1)_d$ model, where $i = 1, 2$.

of the same size as the kinetic mixing between $U(1)_d$ and hypercharge, $\epsilon_d \sim \epsilon \sim 10^{-3} - 10^{-4}$. A mixing of this size is small enough to keep the $U(1)_d$ mass gap at a GeV, but large enough to keep the $U(1)_\chi$ sector in thermal equilibrium with the $U(1)_d$ sector. The latter guarantees, through the double kinetic mixing, that $U(1)_\chi$ is in thermal equilibrium with the SM. We discuss the cosmology of this model in more detail in section 4.4.

The terms in the superpotential relevant at low energies are:

$$W_{\text{DM}} = S_2 \chi_2 \bar{\chi}_2 + S_1 (\chi_1 \bar{\chi}_1 + S_2^2) + n h \bar{h}, \quad (4.3.36)$$

where S_2 receives a weak scale VEV from communicating with the SUSY breaking sector, giving the DM a mass. Solving for the F -term of S_1 , one finds VEVs for χ_1 and $\bar{\chi}_1$ of order $\langle S_2 \rangle$. This breaks $U(1)_\chi$ at the weak scale, and the dominant DM decay is 2-body, with a χ_1 VEV insertion resulting in the operator of Eq. (4.2.4). DM is long-lived because as $M_{\text{GUT}} \rightarrow \infty$ there is an unbroken \mathbb{Z}_2 symmetry, $(\chi_2, \bar{\chi}_2) \rightarrow -(\chi_2, \bar{\chi}_2)$. As in the previous models, \bar{h} gets a VEV at the GeV scale due to the D-term mixing between hypercharge and $U(1)_\chi$. The last term of Eq. (4.3.36) generates a GeV scale mass gap.

4.4 Cosmology of the Dark Sector

In this section we discuss the cosmology of the dark sector and the resulting constraints on our framework. We find constraints on the size of the kinetic mixing between the dark sector and SM, ϵ , on the DM interactions, and on the spectrum of the GeV scale states. The cosmology of our model resembles the cosmology of the annihilating DM framework of Ref. [20]. For related discussions of the cosmology of GeV scale hidden

sectors, see Refs. [43, 21, 2, 79, 133]. Below we include several new observations and a novel emphasis on the aspects of the cosmology that are important for decaying DM. We begin this section by discussing the relic density of DM, and end with a discussion on the cosmology of light dark sector fermions, which can decay to observable gamma rays providing a smoking gun signature of decaying DM [125].

I. Thermal DM Abundance

A model of DM must of course reproduce the observed relic density, $\Omega_\chi h^2 \simeq 0.1$. The ‘WIMP Miracle’ implies that the correct abundance is achieved if DM is in kinetic equilibrium with the SM when it freezes out, with a WIMP cross-section, $\langle\sigma_\chi v\rangle \simeq 3 \times 10^{-26} \text{ cm}^3 \text{ s}^{-1}$. The same cosmology applies for decaying DM, as mentioned in the introduction, since the decay rate is much longer than the age of the Universe. We now discuss how our model can satisfy these requirements.

DM retains the usual thermal history by interacting with dark gauge bosons which are in kinetic equilibrium with the SM [43, 21, 79]. The kinetic equilibrium is maintained by interacting with the SM thermal bath through the kinetic mixing, $\gamma_d \psi_{\text{SM}} \leftrightarrow \gamma \psi_{\text{SM}}$, where ψ_{SM} denotes any relativistic SM particle with hypercharge. This reaction remains efficient for temperatures in the range $m_{\gamma_d} \lesssim T_{\text{kin}} \lesssim (\epsilon^2 \alpha_{\text{EM}}^2 / \pi^2 g_*^{1/2}) M_{\text{pl}}$, where g_* is the number of relativistic degrees of freedom at temperature T_{kin} . For the DM to be a thermal relic with a WIMP cross-section, T_{kin} must be larger than the DM decoupling temperature, $T_{\text{dec}} \simeq m_\chi/20$. The thermal history therefore places a lower-bound on the size of the kinetic mixing:

$$\epsilon \gtrsim 10^{-5} - 10^{-6}. \quad (4.4.37)$$

There is tension between this constraint, and the constraint on ϵ from direct detection when DM couples elastically to the dark photon, Eq. (4.2.1). One way to evade the constraint of Eq. (4.4.37) is to introduce weak scale particles charged under both the dark sector and the SM. Particles charged under both sectors can maintain kinetic equilibrium, but they must be very light, $\mathcal{O}(100 \text{ GeV})$, in order to do so until T_{dec} .

Another way to alleviate this tension is to introduce a DM splitting, which evades the constraint from direct detection.

The introduction of a DM splitting can change the DM annihilation cross-section in an interesting way. A splitting can be generated radiatively or through Yukawa interactions, as we discuss in section VI. Radiative splittings are generated after breaking non-Abelian dark sectors with specific matter content, however such models are significantly more complicated to construct [1]. A simpler alternative, when the DM is charged under $U(1)_d$, is to couple it directly to the light Higgses, as in Eq. (4.2.14). In addition to introducing splittings, these interactions provide the DM a direct annihilation channel into light Higgses. This Yukawa annihilation rate, σ_y , can be parametrically related to the annihilation rate into dark gauge bosons, σ_g , as

$$\frac{\sigma_y}{\sigma_g} \simeq \left(\frac{m_\chi}{m_{\gamma_d}}\right)^4 \left(\frac{\delta m_\chi}{m_\chi}\right)^2 = \left(\frac{0.5 \text{ GeV}}{m_{\gamma_d}}\right)^4 \left(\frac{m_\chi}{2.5 \text{ TeV}}\right)^2 \left(\frac{\delta m_\chi}{100 \text{ keV}}\right)^2. \quad (4.4.38)$$

Here δm_χ is the size of the DM splitting, Eq. (4.2.15). We see that the Yukawa annihilation channel parametrically dominates the DM relic density when $m_{\gamma_d} \lesssim 500 \text{ MeV}$ or when the splitting is sufficiently large. In this regime, the DM gauge coupling must be small in order for the DM to have the correct relic density. This implies that non-perturbative Sommerfeld enhancements to the annihilation cross-section are $\lesssim \mathcal{O}(100)$. Decaying DM models in this regime evade the constraints from the Sommerfeld enhancements discussed in section II., and annihilating models of this type cannot achieve a large enough Sommerfeld enhancement to fit FERMI [18].

A similar analysis applies when DM is charged under the SM and couples to the Z , as in the model of section III.. A splitting is required to evade the constraints from direct detection, which can be introduced by coupling the DM to the SM Higgs. This opens up a new annihilation channel of DM into SM Higgses, which allows for a larger annihilation cross-section and heavier DM masses, as discussed in section III..

An interesting example that has no tension between the thermal history and direct detection, and does not require a DM splitting, is our $U(1)_\chi \times U(1)_d$ model of section IV.. Here, the DM is charged under $U(1)_\chi$, which is broken at the weak scale and kinetically mixes with the GeV-scale dark sector, $U(1)_d$, with mixing of order $\epsilon_d \sim 10^{-3}$. There is

no strong constraint on this model from direct detection because DM does not couple directly to the Z or the light dark photon. The light dark sector, $U(1)_d$, stays in kinetic equilibrium with the SM through kinetic mixing, as discussed above. The kinetic mixing between $U(1)_\chi$ and $U(1)_d$ keeps $U(1)_\chi$, and therefore the DM, in kinetic equilibrium with $U(1)_d$ through the interaction $\gamma_\chi h \leftrightarrow \gamma_d h$, with h corresponding to any of the light Higgses or Higgsinos charged under the $U(1)_d$. The DM is thus kept in kinetic equilibrium with the SM through double kinetic mixing, yielding the correct relic abundance⁵.

II. The Lightest Dark Sector Fermion

The dark sector may contain light particles that are long-lived. Such fields are constrained by cosmology, as we discuss now. There is typically no constraint on light scalars and gauge bosons since both can decay through the kinetic mixing with cosmologically fast timescales, as in Eq. (4.2.11). An exception to this are stable light scalars due to an unbroken discrete symmetry, which we discuss below. The lightest fermion, on the other hand, must decay to the gravitino, if kinematically allowed, which can lead to cosmologically long lifetimes. In what follows, we focus on the situation where the lightest fermion mixes with the gaugino, and we consider separately the cases where it is heavier than, approximately degenerate with, or lighter than the dark gauge boson. We show that the last two scenarios require the lightest fermion to decay to a photon and a gravitino on sub-galactic length scales, leading to observable gamma ray signatures [125].

- $m_{\tilde{\gamma}_d} > m_{\gamma_d}$

This regime applies when there is sizeable SUSY breaking in the dark sector \gtrsim GeV. The fermions can annihilate into dark gauge boson pairs, with cross-section $\sigma \simeq g_d^4/(8\pi\text{GeV}^2)$ which leads to an abundance $\Omega_{\tilde{\gamma}_d} h^2 \simeq 10^{-6}$. After freezeout, the fermion can decay to the dark gauge boson and a gravitino, which is kinematically allowed for low scale SUSY breaking, $\sqrt{F} \lesssim 10^9$ GeV. The dark gauge boson then

⁵For this model, the DM does kinetically decouple from the SM during freezeout at $T_{\text{kin}} = m_{\gamma_\chi} \lesssim m_\chi$. After decoupling, the DM temperature scales as $T = T_\gamma^2/T_{\text{kin}}$, but this only modifies the relic density by an $\mathcal{O}(1)$ amount.

decays through the kinetic mixing to leptons. The corresponding fermion lifetime is given by Eq. (4.2.13). For an abundance this small, there is no constraint from BBN for electromagnetic decays [81, 187]. There are, on the other hand, strong constraints on electromagnetic decays after recombination [129], however the decay discussed above always proceeds before recombination and hence evades the bound. An analogous discussion applies if the lightest dark fermion is a Higgsino that is heavier than its scalar superpartner. We conclude that the dark sector is not constrained by the lightest fermion when it is heavier than its superpartner.

- $m_{\tilde{\gamma}_d} \sim m_{\gamma_d}$

Let us now consider the regime where the dark gaugino is approximately degenerate with the dark gauge boson. This is the case when the dark sector spectrum is approximately supersymmetric, for instance when D-term mixing dominates as discussed in section V. When the temperature is above m_{γ_d} , the dark sector is in kinetic equilibrium with the SM and the number density of the dark bosons and fermions are of the same order of magnitude. When the temperature drops below m_{γ_d} , the dark gauge bosons cannot be created from the thermal bath, and they decay instantly to SM leptons through the kinetic mixing, on a timescale much faster than the Hubble rate, as in Eq. (4.2.11). The dark gauginos, on the other hand, are long lived with abundance controlled by their available annihilation channels. As long as $m_{\tilde{\gamma}_d} > \mathcal{O}(0.85) m_{\gamma_d}$, the finite temperature allows dark gauginos to annihilate into a dark gauge boson pairs [123], with cross-section

$$\langle \sigma_{\tilde{\gamma}_d} v \rangle \simeq \mathcal{O}(0.1) \times \frac{g_d^4}{8\pi m_{\tilde{\gamma}_d}^2} \simeq 10^4 \langle \sigma_{\chi} v \rangle \left(\frac{g_d}{0.35} \right)^4 \left(\frac{1 \text{ GeV}}{m_{\tilde{\gamma}_d}} \right)^2, \quad (4.4.39)$$

where the $\mathcal{O}(0.1)$ suppression results from thermal averaging, and σ_{χ} is the DM annihilation cross-section.

For the above parameters, the resulting relic density is $\Omega_{\tilde{\gamma}_d} h^2 \simeq 10^{-5}$. The gauginos will decay to photons and gravitinos with lifetime given by Eq. (4.2.12). For an abundance of this size, there is no constraint from BBN on the resulting electromagnetic decays (see Fig. 9 from the first reference of [81]), but the gauginos

must decay before recombination, $\tau < 10^{13}$ sec, to avoid constraints from diffuse gammas [129]. Amusingly, there is a coincidence in which the time of recombination roughly equals the amount of time it takes light to cross our Galaxy. As a consequence, the constraint from recombination guarantees that dark gauginos produced in our galaxy decay to observable gamma rays. The resulting constraint on the size of the kinetic mixing is $\epsilon \gtrsim 10^{-9}$ and fixing $\epsilon \simeq 5 \times 10^{-4}$, the constraint on the SUSY breaking scale is $\sqrt{F} \lesssim 2 \times 10^7$ GeV. A possible caveat in the above argument, is that by the time the fermions decouple, the gauge boson are already kinetically decoupled from the thermal bath. This may alter the final abundance by some (order one) amount. A better understanding requires solving the exact Boltzmann equations, which is beyond the scope of this chapter.

- $m_{\tilde{\gamma}_d} < \mathcal{O}(0.85) m_{\gamma_d}$

Lastly, we consider the regime where the dark gaugino is significantly lighter than the dark gauge boson, which as in the first case requires GeV-scale SUSY breaking in the dark sector. If $m_{\tilde{\gamma}_d} \gtrsim 0.5 m_{\gamma_d}$, a gaugino pair can annihilate into one dark gauge boson, and an e^+e^- pair, through kinetic mixing. The resulting cross-section is suppressed by ϵ^2 ,

$$\langle \sigma_{\tilde{\gamma}_d} v \rangle \simeq \epsilon^2 \alpha_{\text{EM}} \frac{g_d^4}{8\pi m_{\tilde{\gamma}_d}^2} 10^{-4} \langle \sigma_{\chi} v \rangle \left(\frac{\epsilon}{5 \times 10^{-4}} \right)^2 \left(\frac{g_d}{0.35} \right)^4 \left(\frac{1 \text{ GeV}}{m_{\tilde{\gamma}_d}} \right)^2. \quad (4.4.40)$$

The abundance is $\Omega_{\tilde{\gamma}_d} h^2 \simeq 10^3$, and the BBN constraint now requires $\tau_{\tilde{\gamma}_d} \lesssim 10^4$ sec. This constraint is rather strong and can be marginally satisfied for the parameters of Eq. (4.2.12). We see that rather large kinetic mixing and a low SUSY breaking scale are both necessary. Again, the gaugino decays to an observable gamma ray. Finally, we note that when $m_{\tilde{\gamma}_d} < m_{\gamma_d}/2$, the gauginos must annihilate into $2e^+2e^-$, with cross-section suppressed by an additional $\epsilon^2 \alpha_{\text{EM}}$ relative to Eq. (4.4.40), ruling out models where the lightest fermion is lighter than $m_{\gamma_d}/2$.

To summarize our findings, we see that our model is unconstrained by the lightest fermion when $m_{\tilde{\gamma}_d} \gtrsim m_{\gamma_d}$, and that otherwise cosmological constraints imply that the

dark gaugino must decay to gamma rays with short lifetimes compared to galactic length scales, leading to observable gamma ray signatures. These constraints are manifest as limits on the size of kinetic mixing, ϵ , and the SUSY breaking scale \sqrt{F} , as we discuss above.

We conclude this section by noting that there may be light particles that are completely stable. For example, in the model of section I., h and n are stable, which follows from their charges under an unbroken \mathbb{Z}_2 . If h and n are heavier than the dark gauge boson, they have a large annihilation cross-section which is parametrically similar to the heavy gaugino case discussed above, thus resulting in a small relic density, $\Omega_h \simeq 10^{-6}$. On the other hand, if h and n are lighter than the dark gauge boson, they will have a large abundance and the model is excluded. In general, light fields that are stable due to discrete symmetries must be heavier than, and annihilate into, the unstable and lighter dark sector fields.

4.5 Discussion

The decaying DM models proposed in this chapter predict a number of signals at upcoming experiments. The light dark sector particles can be produced in colliders, resulting in lepton jets, as in the annihilating models of [20, 21, 1]. The dark sector can also be probed at low energy e^+e^- colliders and fixed target experiments [82, 83, 84]. These direct production experiments have the potential to discover the dark sector, but probably cannot tell apart decaying and annihilating models. On the other hand, astrophysical signals can differentiate between the two scenarios and provide a complementary means to probe the dark spectrum [125]. As we discuss above, primary photons are produced when the dark gaugino is degenerate with or lighter than the dark photon. This results in a hard gamma ray spectrum that can be discovered by HESS, AGIS, and CTA and possibly FERMI [125]. Moreover, if DM is charged under the SM, as in the model of section III., decays produce primary neutrinos, resulting in a hard neutrino spectrum that can be measured at upcoming experiments such as IceCube/DeepCore. The situation is distinct from the annihilating models. For those, measurements from the GC

exclude the production of primary photons and neutrinos with sizeable branching fractions [18, 87, 88, 108, 109].

We conclude with two further directions that can be explored in these models.

- It would be interesting to construct a model that is more directly related to the SUSY breaking sector. We have taken DM to receive a weak scale mass by coupling it to a singlet. Since the DM is not required to be charged under the SM or under the dark sector, another interesting possibility is for the DM to reside in the SUSY breaking sector, for example as a pseudomodulus [138, 139].
- The $U(1)_d$ and $SU(2)_d$ models in sections I. and II. respectively, include two species of DM χ_1 and χ_2 . The existence of several species has several interesting implications. First, there can be ‘Wimponium’ [140, 141] bound states, $\chi_1\bar{\chi}_2$ and $\chi_2\bar{\chi}_1$, which are cosmologically long-lived. Second, it may be possible to include both the iDM and XDM proposals since we have shown that both species can have MeV-sized DM splittings. The viability of these ideas requires further study.

Asymmetric Dark Matter from Leptogenesis

5.1 Introduction

The neutrino masses, the baryon asymmetry of the universe, and the existence of Dark Matter (DM) are the three experimental facts that clearly point to physics beyond the Standard Model (SM). Interestingly, it is plausible that all three are related. On the one hand, neutrino masses suggest the existence of heavy sterile neutrinos, whose decays in the early universe can naturally produce the baryon asymmetry via leptogenesis [142] (for reviews with further references see e.g. [143, 144]). On the other hand, the baryon and DM energy densities are of the same order, $\Omega_{\text{DM}}/\Omega_{\text{b}} \sim 5$, suggesting that they may have a common origin.

One framework that relates the baryon and DM relic densities is Asymmetric DM (ADM) [145, 146]. In this framework, the DM particle is distinct from its antiparticle and carries a conserved quantum number. An asymmetry in the particle-antiparticle number densities is generated in the early universe. Subsequently, the symmetric component is annihilated away by sufficiently fast CP-conserving interactions, leaving the asymmetric component to dominate the relic density. Thus, the relic DM abundance is determined by the asymmetry, rather than by the annihilation cross-section, in close analogy to SM baryogenesis, and in stark contrast to the thermal DM scenario.

The ADM scenario has been extensively studied in the literature [147, 148, 149, 150, 151, 152, 153, 93, 154, 155, 156, 157, 158, 159, 160, 161, 162, 163, 164]. In many existing realizations, an asymmetry is first produced in one sector, either in the SM or in the DM sector, and is then transferred to the other sector at later times by contact interactions. Such a scenario typically predicts similar baryon and DM number densities, $n_{\text{DM}} \sim n_{\text{b}}$ (see however [145, 165, 166]), which then allows one to explain the observed $\Omega_{\text{DM}}/\Omega_{\text{b}}$ ratio for

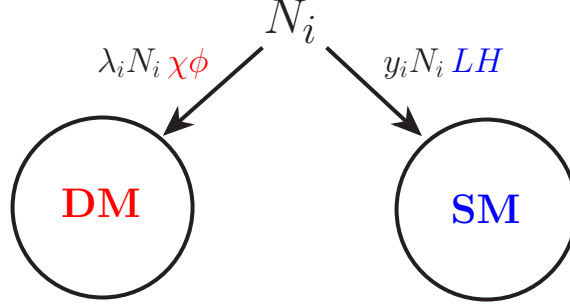


Figure 5.1: A schematic view of our framework: the SM and DM sectors are indirectly connected via Yukawa interactions with the same heavy right-handed neutrinos, N_i . The complex couplings, λ_i and y_i , lead to CP violation in N_i decays, and consequently particle-antiparticle asymmetries for DM and leptons.

dark matter mass in the GeV ballpark. However, the lepton and DM asymmetries may be produced simultaneously at a very high temperature. This scenario, which we refer to as *two-sector leptogenesis*, may profoundly alter the standard ADM predictions. Several authors have previously considered generating the DM asymmetry from leptogenesis [167, 168, 169, 170, 171], however in the context of more specific models that predict $n_{\text{DM}} \sim n_b$. In this chapter we define a general framework for two-sector leptogenesis and demonstrate that it may naturally lead to a large hierarchy between n_{DM} and n_b . Thus, a wide range of DM masses, from about 1 keV to 10 TeV, can be obtained within the ADM paradigm.

The general framework we consider is sketched in Fig. 5.1. DM resides in a hidden sector indirectly connected to the SM via Yukawa interactions with heavy Majorana neutrinos, N_i . In this set-up, the SM leptons and the DM particle are charged under an approximate lepton number, which is broken by the Majorana masses of N_i . The Yukawa couplings can be complex, leading to CP violation in the decays of N_i . Throughout this chapter we work within the framework of thermal leptogenesis. Resonant leptogenesis [172], Dirac leptogenesis [173, 174], or soft leptogenesis [175, 176] could also be considered in this context and would be interesting to pursue.

The generation of the DM abundance adheres to the following steps,

- A population of (at least) the lightest Majorana neutrino, N_1 , is generated in the early universe.
- At temperatures below M_{N_1} , these neutrinos decay out of equilibrium to both sectors. The CP-violating decays lead to a lepton number asymmetry in both the SM and hidden sector.
- As the universe cools well below M_{N_1} , the washout of lepton asymmetry, and its transfer between the 2 sectors, becomes inefficient and the asymmetries are frozen-in. The asymptotic asymmetry can, in general, be different in the two sectors due to different branching fractions and/or washout effects.
- As usual, the SM lepton asymmetry is transferred into baryon asymmetry via electroweak sphalerons. The symmetric baryon component is almost entirely wiped out by hadronic annihilations, and only the asymmetric component survives.
- Similarly, the symmetric component of the DM number density is annihilated away in the hidden sector. The relic abundance of DM is set by the remaining asymmetric component. DM receives a Dirac mass, $m_\chi\chi\tilde{\chi}$, with another fermion state in the hidden sector, $\tilde{\chi}$.

We present a simple model that realizes the scenario described above. The hidden sector contains a chiral fermion χ - the DM candidate - and a complex scalar ϕ . The two are coupled to heavy sterile neutrinos via Yukawa interactions, $\lambda_i N_i \chi \phi$. We assume that any asymmetry carried by ϕ is immediately washed out by fast interactions, $\phi \leftrightarrow \phi^\dagger$, however only interactions mediated by the sterile neutrinos can turn χ into its antiparticle. In this way, an asymmetry $n_{\Delta\chi} = n_\chi - n_{\tilde{\chi}}$ can survive at low temperatures below M_{N_1} . We also assume that additional interactions are present that allow the symmetric component of DM to annihilate. For example, there may be a hidden $U(1)_d$ gauge symmetry, in which case χ and $\tilde{\chi}$ can annihilate into hidden photons, $\chi + \tilde{\chi} \rightarrow \gamma_d + \gamma_d$, as in Ref. [148]. Within this framework we study the range of asymmetries, in the SM and DM sectors, that can be generated during the 2-sector leptogenesis. In particular, we demonstrate that the asymmetries in the two sectors may end up being vastly different,

that is to say, $n_{\Delta\chi} \ll n_{\Delta L}$ or $n_{\Delta\chi} \gg n_{\Delta L}$. In such cases, the dark matter mass must be much larger, or much smaller, than a GeV, in order to recover $\Omega_{\text{DM}} \sim \Omega_b$. We argue that, within this framework, DM masses in the keV - 10 TeV range are easily obtained without violating any phenomenological constraints. Of particular interest is that ADM can accommodate very light dark matter, in the cold as well as in the warm regimes.

The scenario we have outlined may be varied in many ways. In this chapter, we discuss two simple variations of the hidden sector in more detail. In one realization the ϕ asymmetry, generated by N_1 decays, is *not* washed out during leptogenesis, but instead survives together with the χ asymmetry. We will see that the two asymmetries have about the same size, $n_{\Delta\chi} \simeq n_{\Delta\phi}$. Then, at later times, when annihilations are already too slow to significantly reduce the DM abundance, ϕ decays to $\bar{\chi}$ (plus SM states) through an interaction generated by integrating out the right-handed neutrinos, and cancels out the DM asymmetry. Thus, in this scenario, the DM relic density is set by the primordial asymmetry, but today DM is symmetric. This fact has important consequence for phenomenology, notably for indirect detection of DM, as DM particles in our Galaxy may annihilate with a large cross-section.

In another realization, ϕ obtains a VEV. Consequently, through N_i interactions, χ mixes with the left-handed neutrinos of the SM. This scenario is a novel realization of the sterile neutrino framework for DM (for a review and references, see [177]), admitting a new and simple mechanism to populate its density. The mixing with neutrinos opens up decay modes of DM into SM states. As we show below, for sufficiently small $\lambda \langle \phi \rangle$, χ has a long enough lifetime to be consistent with current bounds, while the decays may be observable in the near future. The VEV of ϕ also generates a Majorana mass for χ , leading to particle/antiparticle oscillations for DM, $\chi \leftrightarrow \bar{\chi}$. We show that these oscillations can lead to a large annihilation cross-section in our Galaxy.

The chapter is organized as follows. In Sec. 5.2, we explain the workings of 2-sector leptogenesis. To this end we construct a simple toy model that captures most of the physics and discuss washout and transfer effects that influence the final asymmetries. Sec. 5.3 describes the complete SM plus hidden sector scenario. In Sec. 5.4, we discuss the variations of our scenario in which, although the DM relic density is set by the

$\chi - \bar{\chi}$ asymmetry, we can repopulate symmetric DM at the present epoch. In Sec. 5.5, we discuss some additional constraints on our scenario that arise when the DM particle is lighter than the GeV scale. Our concluding discussion appears in Sec. 5.6. In the Appendix we discuss some technical details of the Boltzmann equations of 2-sector leptogenesis. We note that readers who are most interested in dark matter model building, and less familiar with the technicalities of leptogenesis, may prefer to read sections I.-III. where we describe the toy model, and the discussion around Eqs. 5.3.17 and 5.3.18, where we discuss how the generated asymmetries relate to the DM mass. It is then possible to skip to sections 5.4 and 5.5, where we discuss model building issues. On the other hand, readers who are already familiar with leptogenesis may prefer to skip directly to section 5.3, where we discuss the full model.

5.2 Toy Model for Two-Sector Thermal Leptogenesis

In this section we discuss the simultaneous generation of matter-antimatter asymmetries in the SM and hidden sector during thermal leptogenesis. In order to highlight the relevant physics of 2-sector leptogenesis, we start with a simple toy model. The extension of the theory to accommodate the full SM is straightforward, and we highlight the ingredients in Sec. 5.3.

I. Toy Model

Consider two fermion (matter) fields l, χ and two complex scalars h, ϕ coupled to two Majorana neutrinos $N_i, i = 1, 2$,

$$-\mathcal{L} \supset \frac{1}{2}M_i N_i^2 + y_i N_i l h + \lambda_i N_i \chi \phi + h.c. \quad (5.2.1)$$

As the notation suggests, l, h is a proxy for the SM sector, while χ, ϕ represent the DM sector. At low energy, the theory admits an approximate global “lepton” symmetry under which l and χ are charge +1 while N_i are charged -1 . The symmetry is exact in the limit $M_i \rightarrow \infty$. On the other hand, we assume here that the quantum numbers carried by h and ϕ are rapidly washed out by some other interactions. We take both

χ and ϕ to get masses at low energies, and DM stability follows from $m_\chi < m_\phi$, and an assumed \mathbb{Z}_2 symmetry under which both χ and ϕ are charged. The DM mass must be Dirac in order to preserve lepton number, so we assume that DM gets a mass with another fermion, $m_\chi \chi \tilde{\chi}$, where $\tilde{\chi}$ has lepton number -1 . Furthermore, we assume the presence of additional lepton conserving interactions that rapidly thermalize l, h, χ, ϕ and ultimately annihilate the symmetric component $l + \bar{l}, \chi + \bar{\chi}$.¹ We will discuss these important model building issues later in this chapter, but for the moment we focus on the mechanism generating asymmetries in the two sectors. The key point of this example is to demonstrate that l and χ can easily have different asymmetries, allowing for a large range of DM masses.

II. Decay Asymmetry

In order to generate an asymmetry in leptons and in DM, there must be CP -violation in the decays of N_i . While one Yukawa phase in each sector can be removed by field redefinitions, the remaining 2 Yukawa phases are physical and lead to CP violation. We use the basis where y_1 and λ_1 are real and positive while $y_2 = |y_2|e^{i\phi_\chi}$ and $\lambda_2 = |\lambda_2|e^{i\phi_l}$. We take the hierarchal approximation, $M_1 \ll M_2$ and assume that we can integrate out N_2 and only include N_1 in the Boltzmann equations. We're interested in asymmetries in the decays of N_1 ,

$$\epsilon_\chi = \frac{\Gamma(N_1 \rightarrow \chi\phi) - \Gamma(N_1 \rightarrow \bar{\chi}\phi^\dagger)}{\Gamma_{N_1}} \quad , \quad \epsilon_l = \frac{\Gamma(N_1 \rightarrow lh) - \Gamma(N_1 \rightarrow \bar{l}h^\dagger)}{\Gamma_{N_1}} \quad , \quad (5.2.2)$$

where $\Gamma_{N_1} = (y_1^2 + \lambda_1^2)M_{N_1}/16\pi$ is its total width. The asymmetries are straightforward to compute,

$$\epsilon_\chi \simeq \frac{M_1}{M_2} \frac{1}{16\pi(y_1^2 + \lambda_1^2)} (2\lambda_1^2|\lambda_2|^2 \sin(2\phi_\chi) + y_1 y_2 \lambda_1 |\lambda_2| \sin(\phi_l + \phi_\chi)) \quad , \quad (5.2.3)$$

$$\epsilon_l \simeq \frac{M_1}{M_2} \frac{1}{16\pi(y_1^2 + \lambda_1^2)} (2y_1^2|y_2|^2 \sin(2\phi_l) + y_1 y_2 \lambda_1 |\lambda_2| \sin(\phi_l + \phi_\chi)) \quad . \quad (5.2.4)$$

¹The canonical example for such interactions is a $U(1)_d \times G_{\text{SM}}$ gauge symmetry under which each sector is charged separately. Washout of h and ϕ asymmetries can be due to Yukawa interactions with other light fermions in the theory.

We see immediately that the 2 sectors may have different asymmetries, and in particular,

$$\frac{\epsilon_l}{\epsilon_\chi} \simeq \frac{2r \sin(2\phi_l) + \sin(\phi_l + \phi_\chi)}{2r^{-1} \sin(2\phi_\chi) + \sin(\phi_l + \phi_\chi)}, \quad r = \frac{y_1 |y_2|}{\lambda_1 |\lambda_2|}. \quad (5.2.5)$$

Therefore $\epsilon_l/\epsilon_\chi \simeq r$ for generic phases. When the couplings of matter fields to both right handed neutrinos are similar, $y_1 \simeq y_2$ and $\lambda_1 \simeq \lambda_2$, the asymmetry for each sector scales as the branching ratio of N_1 decays into that sector. Of course, when Yukawa couplings within one sector are hierarchical, e.g. $y_1 \gg y_2$ and/or $\lambda_1 \ll \lambda_2$, the decay asymmetries do not have to be correlated with the branching ratios.

The final asymmetry in each sector is determined not only by the decay asymmetries ϵ_x , but also by washout effects and transfer effects that may change the asymmetry in one or both of the sectors. These may change the simple dependence on the branching ratios quite drastically and may even result with a *larger* asymmetry in the sector with the *smaller* branching fraction and decay asymmetry. The range of possible asymmetry patterns is therefore very rich.

III. Boltzmann Equations

The cosmological evolution of the sterile neutrinos and the asymmetries are described by the Boltzmann Equations (BEs). We introduce the abundance yield $Y_x = n_x/s$ where n_x is the number density of the particle x and s is the entropy density. We are interested in the evolution of the asymmetries $Y_{\Delta l, \chi} = Y_{l, \chi} - Y_{\bar{l}, \bar{\chi}}$ as a function of time (or temperature T), assuming these asymmetries vanish at early times. To this end we solve the BEs that include the N_1 decays, inverse decays, and 2-to-2 scattering of matter in both sectors. For the initial conditions we assume that the matter in the two sectors is in equilibrium with the same temperature, while for N_1 we consider two cases: either equilibrium or zero abundance at early times. For the toy model at hand the BEs take the schematic

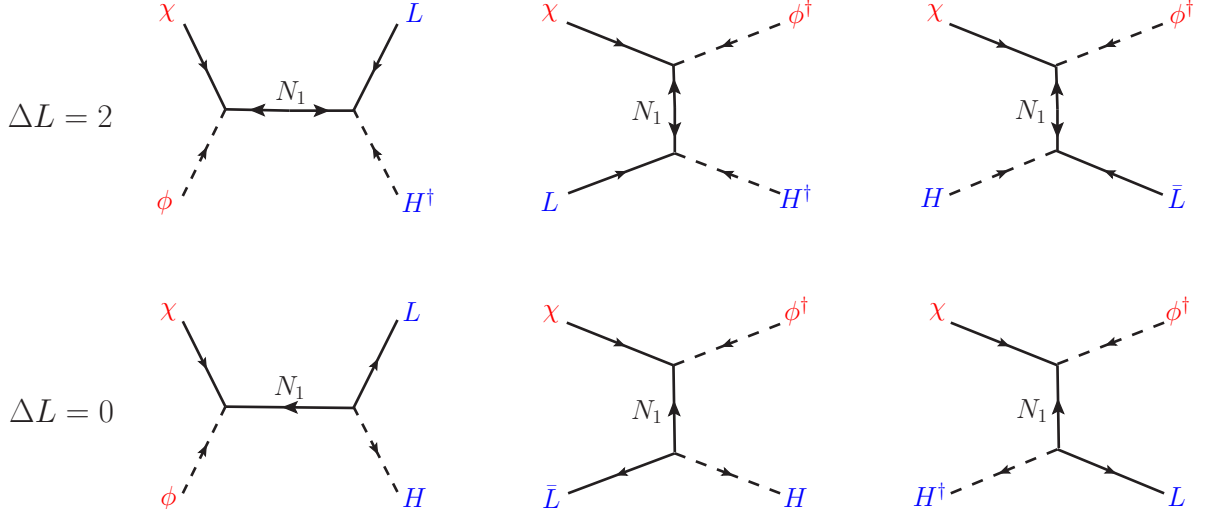


Figure 5.2: *Feynman diagrams contributing to the 2-to-2 terms in the Boltzmann Eqs. (5.2.7) and (5.2.8), that transfer the lepton asymmetry between the two sectors. The top row shows diagrams that violate lepton number, while the transfer diagrams in the bottom row conserve lepton number.*

form,

$$\frac{sH_1}{z}Y'_{N_1} = -\gamma_D \left(\frac{Y_{N_1}}{Y_N^{\text{eq}}} - 1 \right) + (2 \leftrightarrow 2), \quad (5.2.6)$$

$$\frac{sH_1}{z}Y'_{\Delta\chi} = \gamma_D \left[\epsilon_\chi \left(\frac{Y_{N_1}}{Y_{N_1}^{\text{eq}}} - 1 \right) - \frac{Y_{\Delta\chi}}{2Y_\chi^{\text{eq}}} \text{Br}_\chi \right] + (2 \leftrightarrow 2 \text{ washout} + \text{transfer}), \quad (5.2.7)$$

$$\frac{sH_1}{z}Y'_{\Delta l} = \gamma_D \left[\epsilon_l \left(\frac{Y_{N_1}}{Y_{N_1}^{\text{eq}}} - 1 \right) - \frac{Y_{\Delta l}}{2Y_l^{\text{eq}}} \text{Br}_l \right] + (2 \leftrightarrow 2 \text{ washout} + \text{transfer}). \quad (5.2.8)$$

Here $z = M_{N_1}/T$, H_1 is the Hubble parameter at $T = M_{N_1}$, s is the entropy density, $Y_{N_1, l, \chi}^{\text{eq}}$ are the equilibrium number densities, and $\text{Br}_{\chi, l}$ denote the branching fractions of N_1 into the two sectors. Finally, γ_D is the thermally averaged N_1 decay density,

$$\gamma_D = \frac{m_{N_1}^3 K_1(z)}{\pi^2 z} \Gamma_{N_1}. \quad (5.2.9)$$

Further details and the complete set of equations are given in the Appendix.

The first equation describes the evolution of N_1 abundance due to decays and inverse decays. The strength of these interactions is set by γ_D (or more appropriately Γ_{N_1}/H_1), which thus controls the departure of N_1 from thermal equilibrium. We will always assume

that Γ_{N_1}/H_1 is not too small, so that N_1 decays before dominating the energy density of the universe. In the other two equations, the terms proportional to $\epsilon_{l,\chi}$ source the asymmetries $Y_{\Delta\chi,\Delta l}$ once N_1 drops out of thermal equilibrium. The terms proportional to Br_x describe the effect of $2 \rightarrow 1$ inverse decay processes $aa \rightarrow N_1$ ($a = l, \chi$ or the corresponding scalars) which lead to a washout of the asymmetries. The ($2 \leftrightarrow 2$ washout) stands for $\Delta L = 2$ processes $aa \leftrightarrow \bar{a}\bar{a}$ with an off-shell N_1 , while the ($2 \leftrightarrow 2$ transfer) terms stand for $\Delta L = 0$ or 2 processes, $aa \leftrightarrow bb, \bar{b}\bar{b}$, that transfer the asymmetries from one sector to the other. The Feynman diagrams contributing to these (2 -to- 2 transfer) terms, are shown in Fig. 5.2.

There are two basic regimes of the BEs (5.2.6-5.2.8)

- The **narrow-width approximation**: $\Gamma_{N_1} \ll M_{N_1}$ and $\Gamma_{N_1}^2/M_{N_1}H_1 \ll 1$. Here, the inverse decays are the dominant source of the washout and the 2-to-2 contribution can be neglected. Consequently, the last two equations decouple from each other and the asymmetries evolve independently in each sector. One can further distinguish the *weak washout* regime, $\Gamma_{N_1} \ll M_{N_1}$, and the *strong washout* regime $\Gamma_{N_1} \gtrsim M_{N_1}$. In the latter, the asymmetries can be sizably reduced by the inverse decays.
- The **large washout/transfer regime**: $\Gamma_{N_1} \simeq M_{N_1}$ or $\Gamma_{N_1}^2/M_{N_1}H_1 \gtrsim 1$. Here the 2-to-2 contributions are important and may change the final asymmetries by many orders of magnitude. The last two BEs never decouple, and the 2 asymmetries get correlated due to strong washout and transfer effects.

To describe these washout effects, it is convenient to parametrize the asymptotic asymmetries,

$$Y_{\Delta x}^\infty = \eta_x \epsilon_x Y_{N_1}^{eq}(0). \quad (5.2.10)$$

In the narrow-width approximation, $Y_{\Delta x}^\infty$ is proportional to ϵ_x which parametrizes the CP-asymmetry of N_1 decays, as discussed earlier. In addition, the washout efficiencies, η_x , defined through the above parametrization, capture the washout effects occurring during the thermal evolution. Note however that, while intuitive, these definitions need

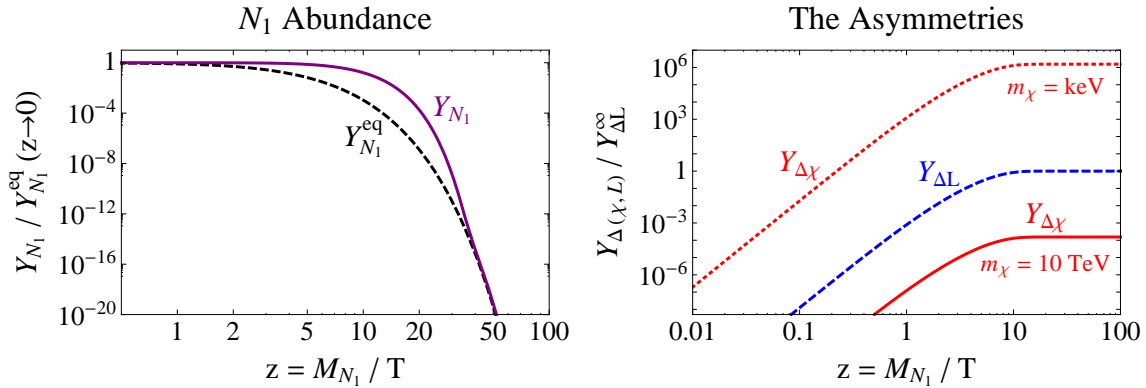


Figure 5.3: *Solutions to the Boltzmann equations for a 2-sector toy model with both sectors in the weak washout regime, $\Gamma_{N_1} \text{Br}_{l,\chi}/H_1 \ll 1$ (and consequently in the narrow-width limit), assuming the initial condition $Y_{N_1} = Y_{N_1}^{\text{eq}}$. In this limit, the washout efficiencies are $\eta_{l,\chi} = 1$ and the final lepton and DM abundances depend only on $\epsilon_{l,\chi}$ as in Eq. (5.2.10). The **left** plot shows the N_1 abundance (purple line) as a function of $z = M_{N_1}/T$, with its equilibrium value, $Y_{N_1}^{\text{eq}}$, plotted for reference (black dashed). The **right** plot shows the asymmetry abundances normalized to the asymptotic lepton abundance for ΔL (blue dashed) and $\Delta\chi$ with $m_\chi = \text{keV}$ (red dotted) and $m_\chi = 10 \text{ TeV}$ (red line).*

not imply that N_1 ever reaches its equilibrium abundance. In Sec. IV. we highlight some effects of the 2-to-2 scatterings. We comment that in the narrow-width limit, since the BEs for the two asymmetries are decoupled, the efficiencies are bounded, $\eta_x < 1$. However, more generally, we will see that 2-to-2 transfer effects can dominate one of the asymmetries, leading to $\eta_x > 1$. For now, we show in Fig. 5.3 simple solutions to the BEs for which $\eta_{L,\chi} = 1$, occurring in the narrow-width limit and the weak-washout regime $\Gamma_{N_1}/H_1 \ll 1$. The solutions assume an initial thermal abundance of N_1 and demonstrates the two viable DM mass limits of keV and $\sim 10 \text{ TeV}$.

IV. Washout Effects

Washout effects may play an important role in one or both sectors. For a given sector, one can distinguish between weak, $\text{Br}_x \Gamma_{N_1}/H_1 \ll 1$, and strong, $\text{Br}_x \Gamma_{N_1}/H_1 \gg 1$ washout. We now briefly highlight a few interesting washout effects. To classify the spectrum

of possibilities it is convenient to divide the discussion into three cases depending on whether each sector is in the weak or strong washout regime.

Weak/Weak

In this case $\text{Br}_{L,\chi}\Gamma_{N_1}/H_1 \ll 1$. It follows that for $M_{N_1} \lesssim 10^{18}$ GeV, the two sectors are in the narrow-width regime, $\text{Br}_{L,\chi}\Gamma_{N_1}/M_{N_1} \ll 1$, and are therefore decoupled. Consequently, washout is negligible and the final asymmetry strongly depends on whether N_1 thermalizes before decaying. In the case that it does the final asymmetries are set by ϵ_x and one has,

$$\eta_L \simeq 1, \quad \eta_\chi \simeq 1. \quad (5.2.11)$$

This situation is depicted in Fig. 5.3. The ratio of the asymmetries,

$$R_\Delta \equiv Y_{\Delta L}^\infty/Y_{\Delta\chi}^\infty, \quad (5.2.12)$$

is then simply $R_\Delta \simeq \epsilon_L/\epsilon_\chi$, which can be extracted from Eqs (5.2.3) and (5.2.4). In particular, for our toy model, $R_\Delta \simeq y_1 y_2/\lambda_1 \lambda_2$. A hierarchical R_Δ may appear if the Yukawa couplings display a hierarchy between the 2 sectors.

If $Y_{N_1}(0) = 0$, the asymmetry vanishes in the first approximation, as a negative asymmetry generated at $z \ll 1$ (when Y_{N_1} is still less than $Y_{N_1}^{eq}$) cancels against the positive asymmetry generated at $z > 1$ (when $Y_{N_1} > Y_{N_1}^{eq}$). A small asymmetry arises thanks to the washout effects being different at small and at large z . One can estimate,

$$\eta_L \simeq \frac{\Gamma_{N_1}^2}{H_1^2} \text{Br}_L, \quad \eta_\chi \simeq \frac{\Gamma_{N_1}^2}{H_1^2} \text{Br}_\chi. \quad (5.2.13)$$

Thus $R_\Delta \simeq \epsilon_L \text{Br}_L/\epsilon_\chi \text{Br}_\chi$, which, again for the toy model, gives $y_1^3 y_2/\lambda_1^3 \lambda_2$. In this case even a small hierarchy between the Yukawa couplings of the 2 sectors to heavy neutrinos may be amplified into a hierarchical R_Δ . In Fig. 5.4 we demonstrate the above scaling with a solution in the weak/weak limit for both $Y_{N_1}(0) = 0$ and $Y_{N_1}(0) = Y_{N_1}^{eq}(0)$.

Strong/Strong

For large $\text{Br}_{L,\chi}\Gamma_{N_1}/H_1 \gg 1$ there is no significant dependence on initial conditions for N_1 , however there is a qualitative dependence on whether the narrow-width approximation

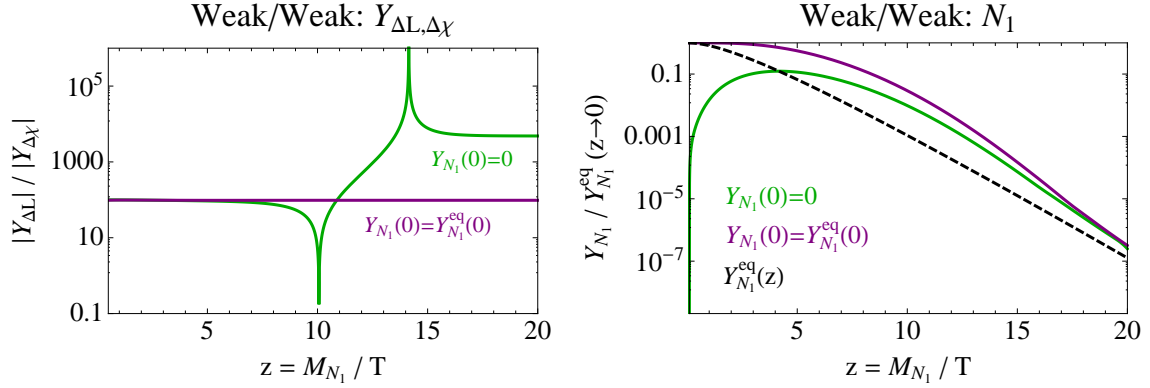


Figure 5.4: *Solutions to the Boltzmann equations in the case where both sectors are in the weak washout regime $\Gamma_{N_1} \text{Br}_{L,\chi} / H_1 \ll 1$ (which implies the narrow-width approximation), for $\text{Br}_\chi = 10^{-2}$ and $\epsilon_{L,\chi} = 10^{-5} \times \text{Br}_{L,\chi}$. Two solutions are shown, assuming thermal and zero initial conditions for N_1 . The former implies washout efficiency of order one, $\eta_{L,\chi} = 1$ as in Fig. 5.3. On the other hand, in the latter case N_1 never thermalizes and consequently the efficiencies are smaller, as predicted in Eq. (5.2.13). The **left** plot shows the ratio of lepton to dark matter abundance as a function of $z = M_{N_1} / T$ while the **right** plot shows the normalized N_1 abundance.*

holds. For $\Gamma_{N_1} \ll M_{N_1}$ and $\Gamma_{N_1}^2 \ll M_{N_1} H_1$ transfer and $2 \leftrightarrow 2$ washout effects are suppressed, and the asymmetry in each sector evolves independently. One can estimate the washout efficiencies as

$$\eta_L \simeq \frac{H_1}{\Gamma_{N_1}} \frac{1}{\text{Br}_L}, \quad \eta_\chi \simeq \frac{H_1}{\Gamma_{N_1}} \frac{1}{\text{Br}_\chi}. \quad (5.2.14)$$

The asymmetry ratio now scales as $R_\Delta \simeq \epsilon_L \text{Br}_\chi / \epsilon_\chi \text{Br}_L \simeq \lambda_1 y_2 / y_1 \lambda_2$. This is of order one unless the couplings to N_1 and N_2 display a hierarchy in at least one of the sectors. Thus, assuming no hierarchy of Yukawa couplings within each sector in this case, one predicts comparable asymmetries in the two sectors. In the ADM scenario that would translate to a prediction that the DM mass is comparable to the baryon mass. Thus the strong-strong case without Yukawa hierarchies may be linked to the ADM scenarios in the literature that predict $Y_b / Y_{DM} \sim 1$. In reality, however, the Yukawa couplings in the SM sector typically do display a hierarchy to match the observed neutrino masses, which destroys this prediction.

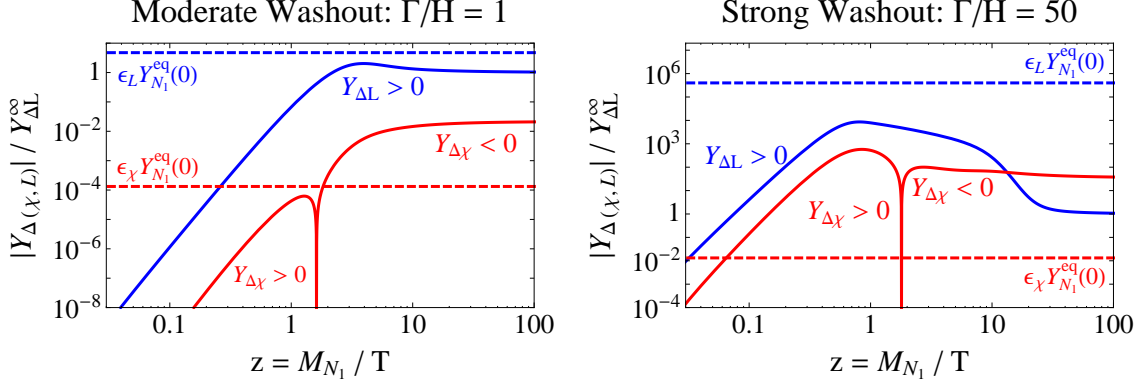


Figure 5.5: Normalized abundances of lepton and DM asymmetries as a function of $z = M_{N_1}/T$. The dashed curves show the expected asymptotic asymmetries for unit washout efficiencies, $\eta_{L,\chi} = 1$. The **left** plot shows the solution in the case $\Gamma_{N_1}/H_1 = 1$. The DM asymmetry changes sign due to the significant washout and transfer effects. The final asymmetry in that sector is greater than one. Here $\Gamma_{N_1}/M_{N_1} = 0.1$ and $\text{Br}_L = 0.9$. On the **right** plot, the solution is shown with identical parameters except for $\Gamma_{N_1}/H_1 = 50$. The corresponding theory is in the strong/strong regime with wide N_1 width. As can be seen, the large washout and transfer effects reverse the ratio of lepton to DM abundance, rendering a larger number density in the dark sector. As discussed in Sec. IV, the ratio of the asymptotic abundances is independent of $\epsilon_{L,\chi}$.

For $\Gamma_{N_1} \simeq M_{N_1}$ and/or $\Gamma_{N_1}^2 \ll M_{N_1} H_1$ washout gets amplified due to the contribution of 2-to-2 processes, which may change the efficiency estimates in Eq. (5.2.14) by many orders of magnitude. See the Appendix for details. The asymmetries in the two sectors can then get correlated due to transfer effects and since the transfer terms in Eqs. (5.2.7), (5.2.8) are proportional to the branching fraction, one expects $R_\Delta \propto \text{Br}_\chi/\text{Br}_L$ independently of ϵ_x . Interestingly, these results imply that far from the narrow-width limit, it is generic to have a *larger* density in the sector with *smaller* branching fraction. This is demonstrated on the right side of Fig 5.5: R_Δ is indeed found to be independent of ϵ_x and the density in the DM sector dominates. One can also note that the DM density changes sign due to the strong transfer effects.

Strong/Weak

An intermediate case occurs when only one sector (say the SM), is in the strong washout regime while the other (here the DM sector) is in the weak washout regime. In the narrow-width approximation one then finds

$$\eta_L \simeq \frac{H_1}{\Gamma_{N_1} \text{Br}_L}, \quad \eta_\chi \simeq \begin{cases} 1 & Y_{N_1}(0) = Y_{N_1}^{eq} \\ \frac{\Gamma_{N_1}}{H_1} \text{Br}_\chi & Y_{N_1}(0) = 0 \end{cases}. \quad (5.2.15)$$

In the first case R_Δ is suppressed from the naive value ϵ_L/ϵ_χ by a small factor $H_1/\Gamma_{N_1} \text{Br}_L$ (while in the other case the factor is $H_1^2/\Gamma_{N_1}^2 \text{Br}_L \text{Br}_\chi$ which may or may not be small). As in the strong/strong case, the above suppression may allow for a situation where the density is larger in the sector with smaller branching fraction. For instance, for $\epsilon_L/\epsilon_\chi = 1$, $\Gamma_{N_1}/H_1 = 10$ and $\text{Br}_\chi = 10^{-2}$, one finds an order of magnitude larger density in the hidden sector. For $\Gamma_{N_1} \ll M_{N_1}$ and $\Gamma_{N_1}^2 \ll M_{N_1} H_1$ the washout of $Y_{\Delta l}$ becomes even larger, further strengthening the aforementioned effect, while loosing the ϵ_x dependence of the ratio.

5.3 Towards a Complete Model

Let us now briefly discuss how the above model is modified when we replace one of the sectors with the complete SM,

$$- \mathcal{L} \supset \frac{1}{2} M_i N_i^2 + Y_{i\alpha} N_i L_\alpha H + \lambda_i N_i \chi \phi + h.c., \quad (5.3.16)$$

where $\alpha = 1 \dots 3$ counts the SM generation. As in in the toy model, we assume that DM pairs up with another fermion, $\tilde{\chi}$, to receive a Dirac mass at low energies, $m_\chi \chi \tilde{\chi}$. We define the decay asymmetry into the SM as the sum of decay asymmetries into each generation, $\epsilon_L = \sum_\alpha \epsilon_{L_\alpha}$. χ is now the asymmetric DM candidate. To match observation, the asymptotic asymmetries should have the numerical values,

$$Y_{\Delta L}^\infty = \epsilon_L \eta_L Y_{N_1}^{eq}(0) \simeq 2.6 \times 10^{-10} \quad (5.3.17)$$

$$Y_{\Delta \chi}^\infty = \epsilon_\chi \eta_\chi Y_{N_1}^{eq}(0) \simeq 4 \times 10^{-10} \left(\frac{\text{GeV}}{m_\chi} \right) \quad (5.3.18)$$

where $Y_{N_1}^{eq}(0) = 135\zeta(3)/4\pi^4 g_*$ and $g_* \sim 100$ counts the total number of relativistic degrees of freedom at $T \sim M_{N_1}$. On the right-hand side, we show the asymmetries that are required to reproduce the observed baryon and DM abundances, assuming $Y_B = 12Y_{\Delta L}/37$.

The value for $\epsilon_L \eta_L$ is fixed by experiment (up to a small dependence on g_* at $T \sim M_{N_1}$). On the other hand, a prediction for $\epsilon_\chi \eta_\chi$ translates into a prediction for the DM mass required to match the observed abundance. For example, if the set-up predicts $Y_{\Delta L}^\infty/Y_{\Delta\chi}^\infty \sim 1$, the required DM mass is in the GeV ballpark. However, as we discussed in the toy model, such a relation between the asymmetries is not a generic prediction of two-sector leptogenesis in most of the parameter space: the ratio of the decay asymmetries ϵ_L/ϵ_χ depends on arbitrary Yukawa couplings, and moreover there is a wide spectrum of possible washout efficiencies $\eta_{L,\chi}$. All this implies that a large range of dark matter masses are possible.

If the SM neutrino masses are generated through the see-saw mechanism, a generalized Davidson-Ibarra (DI) bound [178] on M_{N_1} can be derived. Working in the hierarchical limit, $M_{N_1} \ll M_{N_{2,3}}$, we can express $\epsilon_{L,\chi}$ as,

$$\epsilon_L \simeq \frac{M_{N_1}}{8\pi} \frac{\text{Im}[(3Y^*Y^T + \lambda^*\lambda)M^{-1}YY^\dagger]_{11}}{[2YY^\dagger + \lambda\lambda^*]_{11}}, \quad (5.3.19)$$

$$\epsilon_\chi \simeq \frac{M_{N_1}}{8\pi} \frac{\text{Im}[(Y^*Y^T + \lambda^*\lambda)M^{-1}\lambda\lambda^*]_{11}}{[2YY^\dagger + \lambda\lambda^*]_{11}}, \quad (5.3.20)$$

where above $M = \text{diag}(M_{N_1}, M_{N_2}, M_{N_3})$. Concentrating on ϵ_L and using the relation $[YY^\dagger]_{ij} = M_{N_i}^{1/2} M_{N_j}^{1/2} [R m_\nu R^\dagger]_{ij}/v_{EW}^2$ with R an arbitrary orthogonal complex matrix, an upper bound is found,

$$\epsilon_L \leq \frac{3M_{N_1} m_\nu^{\max}}{16\pi v_{EW}^2} C \simeq 10^{-7} \left(\frac{M_{N_1}}{10^9 \text{ GeV}} \right) C. \quad (5.3.21)$$

Here $v_{EW} = 174 \text{ GeV}$ is the VEV of the SM Higgs and m_ν^{\max} is the heaviest neutrino which was taken to be 0.05 eV on the RHS. C is a function of M and the Yukawa matrices. It is simply expressed in the limit where the N_1 branching fraction into one of

the sectors dominates²,

$$C \simeq \begin{cases} 1 & \text{Br}_L \gg \text{Br}_\chi \\ (\lambda_2^2 M_{N_1} / \lambda_1^2 M_{N_2})^{1/2} & \text{Br}_L \ll \text{Br}_\chi \end{cases} \quad (5.3.22)$$

In deriving the small Br_L limit above, we assumed R is a matrix with order one coefficients, to avoid tuning or non-perturbative Yukawa couplings. We see that the standard DI bound is recovered when N_1 decays mostly to the SM. A large enough asymmetry in the SM requires $\epsilon_L \gtrsim 10^{-7}$ which then implies $M_{N_1} \gtrsim 10^9$ GeV. In the opposite limit the DI bound is multiplied by a factor depending on the ratio of the Yukawa couplings in the dark sector, and on the ratio of the sterile neutrino masses. This typically leads to an additional suppression and the bound becomes stronger, unless there is a large hierarchy $|\lambda_2/\lambda_1| \gg M_{N_2}/M_{N_1}$ accompanied by $|\lambda_1| > |Y_{1\alpha}| \gtrsim 10^{-2}(M_{N_1}/10^9\text{GeV})^{1/2}$. The modified DI bound is clearly visible in the scatter plot in Fig. 5.6.

An additional consequence of thermal leptogenesis with see-saw masses is that the SM sector typically lies in the strong washout regime, $\text{Br}_L \Gamma_{N_1} / H_1 \gg 1$. Indeed, one finds,

$$\frac{\text{Br}_L \Gamma_{N_1}}{H_1} = \frac{M_{\text{Pl}}}{\sqrt{g_*/90}} \frac{[R m_\nu R^\dagger]_{11}}{8\pi^2 v_{\text{EW}}^2} \simeq 25 \frac{m_\nu^{\text{max}}}{0.05 \text{ eV}}, \quad (5.3.23)$$

where $g_* \sim 100$ and a generic R was assumed (weaker washout may however arise for $R_{12}, R_{13} \ll 1$). The hidden sector, on the other hand, may lie either in the weak washout regime for $\text{Br}_\chi \ll 1$, or in the strong washout regime for $\text{Br}_\chi \sim 1$. Note that $\text{Br}_L \ll 1$ implies that washout in the hidden sector becomes extremely strong. The multiplicity of available scenarios thus allows for a wide range of the asymmetries that can be generated. In particular, it is straightforward to make the dark sector asymmetry subdominant $Y_{\Delta\chi}^\infty \ll Y_{\Delta L}^\infty$, corresponding to DM mass larger than GeV. For this the hidden Yukawa couplings have to be small, in which case, ϵ_χ is suppressed. A theoretical bound on the DM mass, $m_\chi \lesssim 10$ TeV, then arises from the perturbativity bound on the annihilation rate of the symmetric DM component.³

²Here Br_L denotes the total branching ratio of N_1 into the sum of the SM flavors.

³However larger DM masses may be possible when dark matter is composite and there is a hierarchy between the confining scale and the DM mass [179, 180].

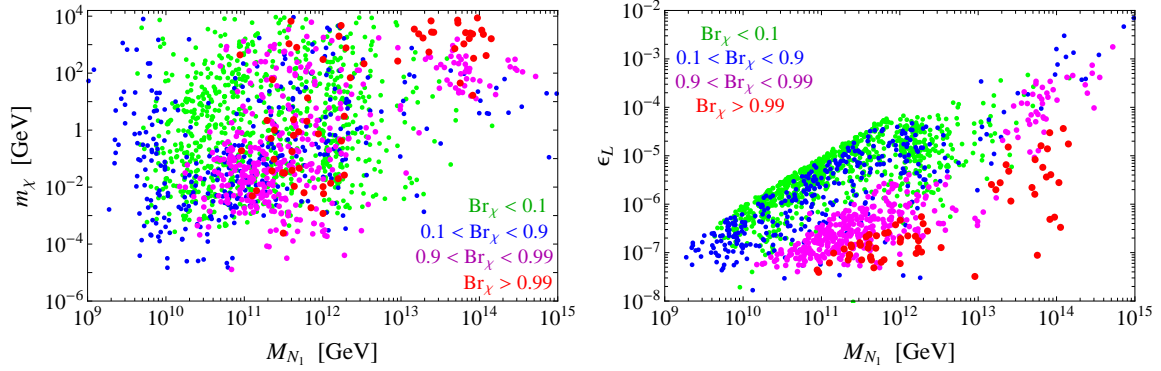


Figure 5.6: Scatter plots for realistic 2-sector thermal leptogenesis, scanning over models that generate the correct SM lepton asymmetry, Eq. (5.3.17), while at the same time producing the correct spectrum and mixing angles for the active neutrinos. The **left** plot shows the spread of DM masses as a function of the mass of the lightest right-handed neutrino, assuming $M_{N_3}/M_{N_2} = M_{N_2}/M_{N_1} = 10$. The coloring of points indicate the branching fraction of N_1 into the hidden sector. 10 keV to 10 TeV masses are accommodated within the thermal leptogenesis framework. Very light DM is typically obtained for smaller M_{N_1} and for hidden sector branching fractions of order 0.1 – 0.9. The **right** plot demonstrates the attainable values for the CP violating parameter, ϵ_L , as a function of the lightest right-handed neutrino mass. For a given mass, M_{N_1} , a maximal value for ϵ_L is clearly visible, in accordance with the DI bound. For both plots, we assume that N_1 starts with a thermal abundance.

A lower limit on the DM mass in the 2-sector thermal leptogenesis scenario follows from perturbativity, which requires $\epsilon_\chi \lesssim 10^{-1}$. Since $Y_{N_1}^{eq} \simeq 4 \times 10^{-3}$, it follows $Y_{\Delta\chi}^\infty \lesssim 4 \times 10^{-4}$ and Eq. 5.3.18 yields the lower bound of $m_\chi \gtrsim$ keV. Coincidentally, the rough astrophysical bound on hot DM is also of order keV [181]. In reality, however, keV DM mass is hard to obtain in thermal leptogenesis since washout effects typically suppress the initial production of the DM asymmetry even if the branching ratio into the hidden sector is large. In principle, such washout effects can be suppressed if the two sectors are in the weak-washout regime or if the branching ratio into the SM sector is large while at the same time ϵ_L is small. Both of these possibilities are harder (but not impossible) to realize in our thermal scenario with see-saw neutrino masses, but can easily be found in deformations of this setup. In Fig. 5.6 we show scatter plots that demonstrate the

mass reach in the thermal leptogenesis case. In these scans we assume hierarchical sterile neutrino masses, $M_{N_1} : M_{N_2} : M_{N_3} = 1 : 10 : 100$, which implies $\epsilon_\chi \lesssim 10^{-2}$ and thus a slightly larger lower bound $m_\chi \gtrsim 10$ keV. We see that the lower reach of m_χ is indeed roughly 10 keV.

Before closing this subsection, a few remarks are in order.

- Throughout the chapter we have ignored finite-temperature effects which may play a significant role in some corners of the parameters space [144]. Nonetheless, we don't expect the conclusions to change qualitatively.
- The conclusions and plots in the above discussion rely strongly on the thermal leptogenesis scenario with neutrino masses arising from the see-saw mechanism. It is straightforward to consider other, less limiting scenarios. For instance the assumed hierarchy of the sterile neutrino masses does not need to exist, additional Higgs fields may be present, or other leptogenesis scenarios can be the dominant source for the asymmetry. In such cases, the DI bound takes a different form and the concluded possible DM mass spectrum may be very different.
- Adding the hidden sector is not exactly the same as adding an additional flavor, as the hidden sector comes with a new scalar field. Nevertheless, many effects present in the context of 3-flavor leptogenesis [182, 183] are valid in this case too.
- In the above we integrated out $N_{2,3}$, ignoring the asymmetry produced from their decays. As in the SM case, this is not always justified and special care may be needed if the Yukawa couplings in one sector display a large hierarchy [184].

5.4 Symmetric Dark Matter from an Asymmetry

In this section, we consider several simple variations of the framework introduced above. In sections 5.2 and 5.3, we described the class of models where the decays of a right-handed neutrino, N_1 , result in a dark matter asymmetry through the operator $N_1\chi\phi$, where ϕ is a scalar belonging to the dark matter sector, taken to satisfy $m_\phi > m_\chi$. We

assumed that ϕ carries no asymmetry due to the presence of fast interactions that convert $\phi \leftrightarrow \bar{\phi}$. We further assumed that ϕ does not receive a VEV, so that DM is stable. In this section, we relax these two assumptions and consider models where:

1. **An asymmetry for ϕ is generated.**
2. **ϕ obtains a VEV.**

We will see below that these simple modifications have important consequences for dark matter phenomenology. In models of type (1), where ϕ also carries an asymmetry, the decays of ϕ to $\bar{\chi}$, at low temperature, will reintroduce symmetric dark matter at late times. As we discuss in section I., models of this type predict a large DM annihilation rate in the present day. In models of type (2), the VEVs of $\langle\phi\rangle$ and the SM higgs, $\langle h\rangle$, cause DM to inherit a small mixing with neutrinos. In a sense, DM becomes a sterile neutrino with a large Dirac mass, $m_\chi\chi\tilde{\chi}$. This has two important phenomenological consequences which we discuss in section II.: DM can decay into SM fermions giving observable signatures, and χ can oscillate into $\tilde{\chi}$ at late times, also repopulating symmetric dark matter.

In both cases discussed here, the symmetric DM component is obtained at late times from the dominating asymmetric one. Of course, symmetric DM is also produced directly through N_1 decays and may dominate the energy density already at earlier times. The predictions of such a scenario are distinct from the ones considered here, and will be presented in future work [185].

I. Restoring Symmetric Dark Matter with Late Decays

Above, in our example model of thermal leptogenesis, we assumed that ϕ has interactions that are efficient at low energy and set $n_\phi = n_{\phi^\dagger}$. This is roughly the situation for the SM Higgs, but does not need to hold in the hidden sector. Consider the case where ϕ number is preserved, so that $n_{\Delta\phi} = n_\phi - n_{\phi^\dagger}$ can be nonzero at low temperatures. As we discuss below, the asymmetry in ϕ results in the restoration of $\bar{\chi}$ after χ decouples. This leads to symmetric DM with some interesting phenomenological possibilities that we discuss

in this section: a large annihilation rate at the present day and mixed warm/cold dark matter.

We now outline the cosmology of this scenario. Suppose, as above, that CP violation in right-handed neutrino decays produce a χ asymmetry, $n_{\Delta\chi} > 0$. In the absence of strong washout processes, there will also be an asymmetry of ϕ , $n_{\Delta\phi} > 0$. In fact, if the BEs for the two asymmetries are invariant under the exchange of χ and ϕ , the resulting asymmetries are equal:

$$n_{\Delta\phi} = n_{\Delta\chi}. \quad (5.4.24)$$

One can then check that a sufficient condition for the exchange symmetry to exist, is for the low energy interactions to preserve a $U(1)_L \times U(1)_\phi$ symmetry under which the fields transform as $\phi(0, 1)$ and $\chi(1, -1)$ ⁴. These symmetries further guarantee that $n_{\Delta\bar{\chi}} = 0$. Incidentally the mass term, $m_\chi \chi \tilde{\chi}$ violates the above condition but keeps Eq. (5.4.24) intact. If, however, other interactions exist that involve $\tilde{\chi}$, Eq. (5.4.24) is modified by an order one amount, reflecting the redistribution of the χ asymmetry into that of $\tilde{\chi}$. Assuming no such interactions, when the temperature reaches the χ and ϕ masses, the symmetric components annihilate and freezeout, leaving asymmetric abundances of χ and ϕ . Then, at temperatures below χ and ϕ decoupling, the scalar ϕ can decay to $\bar{\chi}$ as shown in Fig. 5.7, repopulating symmetric DM. Eq. 5.4.24 implies that the final abundances of χ and $\bar{\chi}$ are equal.

The Boltzmann equation for $\Delta\chi$ now also depends on $\Delta\phi$, but given Eq. 5.4.24, it can be expressed in a very similar form to equation Eq. 5.2.7,

$$\frac{sH_1}{z} Y'_{\Delta\chi} = \gamma_D \left[\epsilon_\chi \left(\frac{Y_{N_1}}{Y_{N_1}^{eq}} - 1 \right) - \frac{Y_{\Delta\chi}}{Y_\chi^{eq}} \text{Br}_\chi \right] + (2 \leftrightarrow 2 \text{ washout} + \text{transfer}). \quad (5.4.25)$$

The only difference, from above, is that the $2 \rightarrow 1$ washout term is twice as big as when ϕ had no asymmetry.

For simplicity, in the rest of this section, we assume the hierarchical limit $M_{N_1} \ll M_{N_{2,3}}$, and only include the lightest right-handed neutrino, N_1 . Furthermore, we suppress lepton flavor indices. It is straightforward to extend our discussion to the more general case. In our example model, ϕ can decay to $\bar{\chi}$ through a dimension 5 operator that is

⁴Here we assume a Maxwell-Boltzmann distribution for the equilibrium values of the two fields.

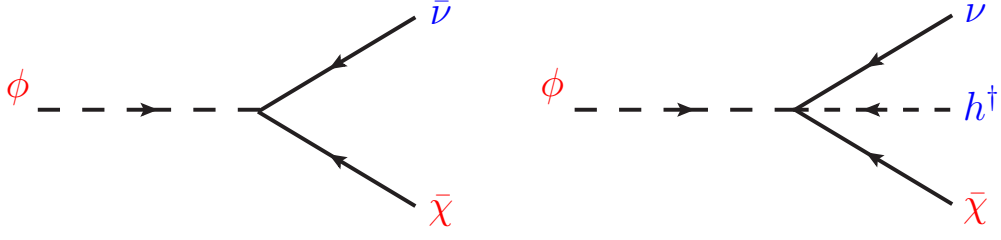


Figure 5.7: *Two-body and three-body decay modes of ϕ into DM and SM particles. In the absence of washout processes for ϕ , its asymmetry is equal to that of χ . Consequently, the above decays, which occur after annihilations have decoupled, repopulate the symmetric component of DM, allowing for an observable annihilation signal.*

generated by integrating out the right-handed neutrinos,

$$\mathcal{L} \supset -y\lambda \frac{\chi\phi LH}{M_{N_1}} + h.c.. \quad (5.4.26)$$

Inserting the Higgs VEV, ϕ can two-body decay to $\bar{\chi}$ and a neutrino,

$$\Gamma(\phi \rightarrow \bar{\chi}\bar{\nu}) = \frac{y^2\lambda^2 v_{\text{EW}}^2}{32\pi M_{N_1}^2} m_\phi \left(1 - \frac{m_\chi^2}{m_\phi^2}\right)^2 = \frac{\lambda^2}{16\pi} \frac{m_\nu}{M_{N_1}} m_\phi \left(1 - \frac{m_\chi^2}{m_\phi^2}\right)^2, \quad (5.4.27)$$

where $m_\nu = y^2 v_{\text{EW}}^2 / M_{N_1}$ is the see-saw contribution to the neutrino mass matrix, along the diagonal in flavor space, from integrating out N_1 . Decays to neutrinos are only weakly constrained by Big Bang Nucleosynthesis (BBN), and decays as late as $\tau \lesssim 10^6$ sec are allowed if ϕ decays entirely through this mode [186]. Decays can easily proceed fast enough,

$$\tau_\phi \simeq 7 \times 10^{-4} \text{ sec} \times \left(\frac{0.1}{\lambda}\right)^2 \left(\frac{0.05 \text{ eV}}{m_\nu}\right) \left(\frac{M_{N_1}}{10^9 \text{ GeV}}\right) \left(\frac{100 \text{ GeV}}{m_\phi}\right). \quad (5.4.28)$$

Equation 5.4.26 also introduces a three-body decay mode where the Higgs is produced, $\phi \rightarrow \bar{\chi}\nu h$. This decay is of course suppressed by three-body phase space, but is enhanced, relative to the two body decay, when $m_\phi \gg v$,

$$\frac{\Gamma(\phi \rightarrow \bar{\chi}\bar{\nu}h)}{\Gamma(\phi \rightarrow \bar{\chi}\bar{\nu})} \simeq \frac{m_\phi^2}{24\pi^2 v^2} \quad (5.4.29)$$

This three-body decay mode is strongly constrained by BBN because of the hadronic decays of the Higgs [187, 81], implying that ϕ must decay faster than about a second if the branching fraction to three-body decays is appreciable.

Recall that in the asymmetric DM scenario, χ and $\bar{\chi}$ annihilate with a large enough cross-section, σ_{ann} , such that the symmetric component of DM is subdominant at the present day,

$$\langle\sigma_{ann}v\rangle\gg 3\times 10^{-26}\text{ cm}^3\text{ s}^{-1}.\quad (5.4.30)$$

We must make sure that ϕ decays late enough such that these χ annihilations are decoupled (and furthermore, late enough to avoid their recoupling after the decay), so that the χ abundance is determined by the asymmetry, instead of the annihilation rate. This decoupling temperature is defined by the relation, $sY_{\Delta\chi}\langle\sigma_{ann}v\rangle=H(T_{dec})$, which implies that,

$$T_{dec}=\text{GeV}\frac{m_\chi}{100\text{ GeV}}g_*^{-1/2}\left(\frac{10^{-24}\text{ cm}^3/\text{sec}}{\langle\sigma_{ann}v\rangle}\right),\quad (5.4.31)$$

where we've assumed that $g_*\sim g_{*S}$ at T_{dec} . Consequently,

$$\tau_{dec}=6\times 10^{-6}\text{ sec}g_*^{1/2}\left(\frac{100\text{ GeV}}{m_\chi}\right)^2\left(\frac{\langle\sigma_{ann}v\rangle}{10^{-24}\text{ cm}^3/\text{sec}}\right)^2.\quad (5.4.32)$$

Requiring that ϕ decays occur after this decoupling temperature leads to a nontrivial constraint on the parameters,

$$g_*^{1/2}\frac{m_\phi}{m_\chi}\left(\frac{\lambda}{0.1}\right)^2\left(\frac{100\text{ GeV}}{m_\chi}\right)\left(\frac{\langle\sigma_{ann}v\rangle}{10^{-24}\text{ cm}^3/\text{s}}\right)^2\left(\frac{10^9\text{ GeV}}{M_{N_1}}\right)\left(\frac{m_\nu}{0.05\text{ eV}}\right)\quad (5.4.33)$$

$$< 100,$$

where we've assumed that the three-body decay mode is not dominating, for this estimate.

If DM is dominantly asymmetric today, then DM annihilations are suppressed at the current epoch, making it difficult to observe indirect signatures of dark matter annihilations. But when $\bar{\chi}$ is restored by decays of ϕ , DM annihilation signals are also restored and proceed at a boosted rate relative to a thermal WIMP, as in Eq. 5.4.30. This provides a novel mechanism for producing a large dark matter annihilation rate today.

In this scenario, such annihilations may account for the leptonic cosmic ray excesses observed by PAMELA [14], FERMI [16], and HESS [85]. The requirement is simply that DM has a TeV scale mass and that its annihilations produce leptons. This provides an attractive alternative to the scenario where the DM annihilation rate experiences a Sommerfeld enhancement at low velocities [20]. In models with a Sommerfeld enhancement,

there can be tension between producing the correct relic density and a large enough annihilation rate in our Galaxy [188, 189]. But in our framework, this tension is resolved because the DM abundance follows from the asymmetry produced by leptogenesis, not from the annihilation rate at decoupling. We note that both models with Sommerfeld enhancement, and our framework, are constrained by the Cosmic Microwave Background (CMB) [115] (and other astrophysical constraints, see e.g. [18]) because ϕ decays before the time of recombination.

Finally, we emphasize that decays of ϕ provide a mechanism for generating mixed warm/cold DM when there is a mass hierarchy: $m_\phi \gg m_\chi$. In this regime, $\bar{\chi}$ is produced carrying a large kinetic energy set by m_ϕ . If the decay occurs late enough, such that $\bar{\chi}$ is kinetically decoupled, then it will not thermalize and there will not be enough time to redshift away its kinetic energy. This opens up the possibility for χ to constitute cold dark matter while $\bar{\chi}$ is warm. Parametrically, the velocity of $\bar{\chi}$ at the present epoch is given by [190],

$$v_{\bar{\chi}} \sim 2 \times 10^{-5} \frac{\text{km}}{\text{s}} \left(\frac{m_\phi}{m_\chi} \right) \sqrt{\frac{\tau_\phi}{1 \text{ s}}}, \quad (5.4.34)$$

where τ_ϕ is the ϕ lifetime. For example, if $m_\phi = 100 \text{ GeV}$, $m_\chi = 1 \text{ MeV}$, and τ_ϕ is one second, then $\bar{\chi}$ will have a free-streaming velocity of about 1 km/sec, large enough to impact the matter power spectrum [190]. These parameters have some tension with the limit of Eq. 5.4.33, but the limit can be satisfied at small λ and large M_{N_1} . This scenario of mixed warm/cold dark matter, where half of dark matter is warm and the other half cold, may have interesting phenomenological consequences for structure formation, which would be worthwhile to further explore.

II. Asymmetric Sterile Neutrinos from Leptogenesis

So far, we have assumed that the scalar in the hidden sector, ϕ , does not obtain a VEV at low-energy. This permits DM to be stable when $m_\phi > m_\chi$. In this section, we relax this assumption by allowing ϕ to receive a nonzero VEV. We will see that this simple change leads to several new phenomenological possibilities. Because of the nonzero $v_\phi \equiv \langle \phi \rangle$, DM now mixes with the left-handed neutrinos. Therefore, it constitutes a Dirac sterile

neutrino (we continue to assume that DM has a Dirac mass, which is necessary for its abundance to be set by an asymmetry). This scenario thus provides a novel mechanism to account for the correct relic abundance of sterile neutrino DM (for a nice review and references see Ref. [177]). DM stability is no longer guaranteed, and several decay modes open up due to the mixing with neutrinos. For the appropriate DM lifetime, this leads to observable cosmic rays at the present epoch. Another consequence of $v_\phi \neq 0$ is that DM inherits a small Majorana mass, $\mu_\chi \chi^2$, where $\mu_\chi \ll m_\chi$. As we discuss below, this leads to oscillations at late times, allowing for a large annihilation rate at the present day, as in section I. We consider the above effects in detail below.

Recall that the seesaw Lagrangian (here simplified to the one-flavor case) is given by,

$$\mathcal{L} \supset -m_\chi \chi \tilde{\chi} + \frac{1}{2} M_{N_1} N_1^2 + \lambda N_1 \chi \langle \phi \rangle + y N_1 L \langle h \rangle + h.c., \quad (5.4.35)$$

where we have included an explicit Dirac mass for χ , and we emphasize that both ϕ and the SM higgs, h , receive VEVs. After integrating out the heavy right-handed neutrino, N_1 , we have the following mass terms,

$$\mathcal{L} \supset -m_\chi \chi \tilde{\chi} - \frac{\mu_\chi}{2} \chi^2 - \frac{m_\nu}{2} \nu^2 - \mu_{\chi\nu} \chi \nu + h.c., \quad (5.4.36)$$

where $\mu_\chi \ll m_\chi$ constitutes a small Majorana mass for χ , m_ν is the usual Majorana mass for left-handed the neutrino, and $\mu_{\chi\nu}$ represents a mass-mixing between χ and ν . These masses are given by,

$$\mu_\chi = \lambda^2 \frac{v_\phi^2}{M_{N_1}}, \quad m_\nu = y^2 \frac{v_{\text{EW}}^2}{M_{N_1}}, \quad \mu_{\chi\nu} = \left(\frac{\lambda}{y} \frac{v_\phi}{v_{\text{EW}}} \right) m_\nu. \quad (5.4.37)$$

The χ Majorana mass, μ_χ , leads to DM particle/antiparticle oscillations $\chi \leftrightarrow \tilde{\chi}$. Similarly, the DM-neutrino mass mixing, $\mu_{\chi\nu}$, leads to DM/neutrino oscillations, $\chi \leftrightarrow \bar{\nu}$. We now discuss how these oscillations can modify the cosmological history of this model.

We begin by considering only the $\chi \leftrightarrow \tilde{\chi}$ oscillations (we will see below that the $\chi \leftrightarrow \bar{\nu}$ oscillations can be neglected for the parameters of interest). It is important that the oscillations do not turn on until after DM annihilations decouple, because otherwise the χ asymmetry, resulting from leptogenesis, is erased. As a consequence, we shall now see that the rate of oscillations are slow relative to the Hubble rate at all times.

Nonetheless, the probability to oscillate becomes sizable at late times, thereby enabling a large annihilation rate at the present day, as in Eq. 5.4.30. This provides an alternative mechanism, compared to the late ϕ decays discussed in section I, for generating large cosmic ray fluxes at the present epoch [165, 191].

In order to verify that DM does not oscillate too soon, we briefly review the formalism for treating particle oscillations in the expanding universe [192, 193, 194]. Consider a generic oscillation of the type $\alpha \rightarrow \beta$. The BE for production of β , through oscillations, is given by,

$$\frac{dY_\beta}{dz} = \frac{z}{2} \langle P_{\alpha \rightarrow \beta}(t) \rangle \frac{\Gamma_\alpha}{H_1} (Y_\alpha - Y_\beta), \quad (5.4.38)$$

where $P_{\alpha \rightarrow \beta}(t)$ is the probability that α oscillates into β after time t , Γ_α is the total interaction rate of α , $z = m/T$ is defined in terms of an arbitrary mass scale m , and $H_1 \equiv H(T = m)$. The oscillation probability, P , is averaged over the interaction time, $\langle P \rangle = \Gamma_\alpha \int_0^\infty dt e^{-\Gamma_\alpha t} P$. We see that the BE is driven by $P \times \Gamma$. Therefore, oscillations are in equilibrium whenever $P\Gamma \gg H$ and are frozen out whenever $P\Gamma \ll H$. The general expressions for P and $\langle P \rangle$ are:

$$\begin{aligned} P_{\alpha \rightarrow \beta}(t) &= \sin^2(2\theta_{\alpha\beta}) \sin^2\left(\frac{\Delta E_{\alpha\beta}}{2} t\right) \\ \langle P_{\alpha \rightarrow \beta}(t) \rangle &= \frac{\sin^2(2\theta_{\alpha\beta})}{2} \frac{\Delta E_{\alpha\beta}^2}{\Delta E_{\alpha\beta}^2 + \Gamma_\alpha^2}, \end{aligned} \quad (5.4.39)$$

where $\theta_{\alpha\beta}$ is the mixing angle and $\Delta E_{\alpha\beta} = t_{osc}^{-1}$ the energy difference between the states α and β , or equivalently the inverse oscillation time. Note that for simplicity, we neglect the effects of finite temperature and density. These corrections are considered, for example, in many studies of sterile neutrino production through neutrino/sterile neutrino oscillations [192, 193, 194].

We now apply the above formalism to understand $\chi \leftrightarrow \tilde{\chi}$ oscillations. The mixing angle and the energy splitting in this case are given by

$$\theta_{\chi\tilde{\chi}} \simeq \frac{\pi}{4}, \quad \Delta E_{\chi\tilde{\chi}} \simeq \begin{cases} \mu_\chi m_\chi / T & T > m_\chi \\ \mu_\chi & T \leq m_\chi \end{cases} \quad (5.4.40)$$

In order to insure that these oscillations are slow before DM annihilations decouple, it is sufficient to require that $\Gamma P < H$ at the temperature of decoupling,

$$\langle P_{\chi \rightarrow \bar{\chi}}(t) \rangle \Gamma_{\chi}(T_{\text{dec}}) \lesssim H(T_{\text{dec}}). \quad (5.4.41)$$

Since the asymmetric component of χ cannot be neglected, T_{dec} must be calculated by comparing the total number density times the annihilation rate to Hubble, $\Gamma_{\text{ann}} = [n_{\text{asym}}(T_{\text{dec}}) + n_{\text{sym}}(T_{\text{dec}})] \langle \sigma_{\text{ann}} v \rangle = H(T_{\text{dec}})$. For our case, where the asymmetric component dominates at low temperatures one finds, $m_{\chi}/T_{\text{dec}} \gg 20$ implying that even at temperatures below that at which the symmetric component decouples, $m_{\chi}/T_{\text{dec}}^{\text{sym}} \sim 20$, oscillations may recouple the annihilation process, thereby significantly altering the DM abundance. Using Eqs. (5.4.39) and (5.4.40), Eq. (5.4.41) reads at $T = T_{\text{dec}}$,

$$\mu_{\chi} \lesssim \sqrt{\Gamma_{\chi} \Gamma_{\text{ann}}(T = T_{\text{dec}})}. \quad (5.4.42)$$

This condition can be converted into a limit on the size of λv_{ϕ} , which enters the oscillation probability through μ_{χ} . Using Eqs. 5.4.37 one finds the limit,

$$\frac{\lambda v_{\phi}}{m_{\chi}} \lesssim 3 \times 10^{-7} \left(\frac{M_{N_1}}{10^{10} \text{ GeV}} \right)^{1/2} \left(\frac{10^{-24} \text{ cm}^3/\text{s}}{\langle \sigma_{\text{ann}} v \rangle} \right) \left(\frac{\langle \sigma_{\text{tot}} v \rangle}{\langle \sigma_{\text{ann}} v \rangle} \right)^{1/4} \left(\frac{g_*^{3/4}}{g_{*S}} \right), \quad (5.4.43)$$

where σ_{ann} is the $\chi + \bar{\chi}$ annihilation cross-section, σ_{tot} is the overall χ interaction cross-section (which determines the total DM interaction rate Γ_{χ}), and g_* and g_{*S} are evaluated at the temperature that DM annihilations decouple. We see that the requirement that DM particle/antiparticle oscillations are slow, before DM decouples, presents a rather stringent limit on the quantity λv_{ϕ} relative to the DM mass, m_{χ} .

We note that if Eqs. 5.4.41 and 5.4.43, are satisfied, then $P\Gamma \ll H$, also at temperatures below DM decoupling, due to the drop in Γ relative to H as the Universe cools. This means that, given the condition Eq. 5.4.41 is satisfied, oscillations always remain slow in the expanding universe, and never produce a significant yield of $Y_{\bar{\chi}}$. Still, there is a large annihilation rate today, as long as $t_{\text{osc}} = \mu_{\chi}^{-1}$ is much shorter than the age of the universe. In this regime, whenever two DM particles collide at the present day, there is an $\mathcal{O}(1)$ probability that one has oscillated. We also comment that if μ_{χ} is chosen so that t_{osc} is longer than the timescale for recombination, then the constraints from the CMB [115] are alleviated.

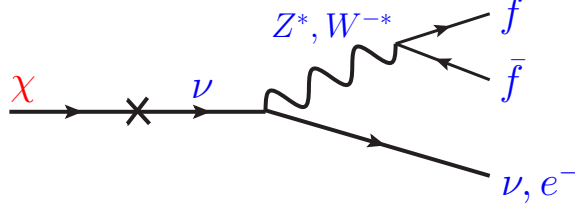


Figure 5.8: *Dark matter decay modes in the case where $\langle\phi\rangle \neq 0$. These modes occur due to mixing of DM with SM neutrinos and place stringent constraints on the mixing angle for $m_\chi \gtrsim 0.1$ GeV. For lighter DM, oscillations into $\tilde{\chi}$ are more constraining.*

Now we consider oscillations between DM and neutrinos, $\chi \leftrightarrow \bar{\nu}$. Oscillations of this type are highly suppressed by the small mixing angle between DM and neutrinos,

$$\theta_{\chi\nu} \simeq \frac{\mu_{\chi\nu}}{m_\chi}, \quad \Delta E_{\chi\nu} \simeq \begin{cases} m_\chi^2/T & T > m_\chi \\ m_\chi & T \leq m_\chi \end{cases} \quad (5.4.44)$$

In particular, combining the constraint of Eq. 5.4.43 with Eqs. 5.4.37, 5.4.39, and 5.4.44, we learn that,

$$\langle P_{\chi \rightarrow \bar{\nu}}(t) \rangle \simeq 2 \left(\frac{\mu_{\chi\nu}}{m_\chi} \right)^2 \lesssim 10^{-33} \left(\frac{m_\nu}{0.05 \text{ eV}} \right) \left(\frac{10^{10} \text{ GeV}}{M_{N_1}} \right) \quad (5.4.45)$$

This oscillation probability is small enough that $P\Gamma \ll H$ for all temperatures. This shows, *a posteriori*, that we were justified to neglect DM/neutrino oscillations in the above discussion.

There is, however, one very important effect of DM/neutrino mixing, $\theta_{\chi\nu}$. This mixing opens up several decay modes for DM. For example, suppose that χ is lighter than the electroweak gauge bosons. Then as shown in Fig. 5.8, DM can three-body decay through off-shell Z^*/W^* , $\chi \rightarrow \nu(Z^* \rightarrow f\bar{f})$ and $\chi \rightarrow e^-(W^{+*} \rightarrow f\bar{f}')$, where f/f' are SM fermions. The rate for these decays is given, parametrically, by the expression,

$$\Gamma_{\chi \rightarrow \nu f \bar{f}} \simeq \frac{\alpha_2^2 \theta_{\chi\nu}^2}{4\pi} \left(\frac{m_\chi}{m_Z} \right)^4 m_\chi \quad (5.4.46)$$

Of course, these decays are constrained to not proceed too quickly. In order to be consistent with cosmic ray and diffuse gamma observations, $\tau_\chi \gtrsim 10^{26}$ s [18, 195]. This

limit can also be expressed as a constraint on the size of λv_ϕ relative to m_χ ,

$$\frac{\lambda v_\phi}{m_\chi} \lesssim 10^{-9} \left(\frac{\text{GeV}}{m_\chi} \right)^{5/2} \left(\frac{M_{N_1}}{10^{10} \text{ GeV}} \right)^{1/2} \left(\frac{0.05 \text{ eV}}{m_\nu} \right)^{1/2} \left(\frac{10^{26} \text{ s}}{\tau_\chi} \right)^{1/2} \quad (5.4.47)$$

We see that the DM lifetime is a stronger constraint than DM particle/antiparticle oscillations, when $m_\chi \gtrsim 0.1 \text{ GeV}$, while oscillations present the dominant constraint on light DM. For DM above the GeV scale, the cosmic rays are observable, by ongoing and future observations, when λv_ϕ saturates the above limit. We note that sterile neutrino DM of this type can also decay, at one loop, to a photon line, $\chi \rightarrow \nu\gamma$ [177]. However, this decay is suppressed, relative to the above three-body decays, by a factor of $\sim \alpha/4\pi$. We also note that in the regime where $m_\chi > m_Z$, DM will dominantly decay two-body to longitudinal electroweak gauge bosons and the Higgs, $\chi \rightarrow Z\nu$, $\chi \rightarrow W^+e^-$, and $\chi \rightarrow h\nu$. In this regime, the decays proceed faster than above, and the constraint on λv_ϕ is significantly stronger.

5.5 Cosmology and Light Dark Matter

As we have seen, asymmetric DM populated by leptogenesis can accommodate a wide range of DM masses, between about keV and 10 TeV. Within this broad framework, cosmology, astrophysics, and colliders can all constrain the properties of DM, and the hidden sector within which it resides. In particular, the hidden sector must contain additional degrees of freedom, lighter than DM, which the symmetric DM component can annihilate into. While the constraints on weak-scale DM are well-known (for a review see [19]), light (keV to 10 GeV) DM raises several interesting issues, which are the subject of this section.

For concreteness, we specialize to models with a hidden $U(1)_d$ gauge symmetry [148], where the symmetric DM component annihilates predominantly into a pair of hidden sector photons, γ_d . The hidden sector couples to the visible sector through the vector portal,

$$\mathcal{L} \supset \frac{\epsilon}{2} F'_{\mu\nu} F^{\mu\nu}, \quad (5.5.48)$$

where $F'_{\mu\nu}(F^{\mu\nu})$ is the γ_d (electromagnetic) field strength. The above coupling allows γ_d to decay into kinematically available SM fields with non-zero electric charge. The width and lifetime of γ_d is determined by its mass m_{γ_d} and by the mixing parameter ϵ .

We will find it helpful to consider two cases separately, depending on whether m_χ is heavier than, or lighter than, the MeV scale. First, we consider $m_\chi \gtrsim \text{MeV}$. In this regime, we are also free to assume that $m_{\gamma_d} \gtrsim \text{MeV}$, and in particular that no sub-MeV hidden states exist. This means that there are no new relativistic DOF present during BBN, and the only constraint from BBN is that the the lightest state in the hidden sector decays to the SM fast enough to avoid late dissociation processes [187, 81]. This requirement is not hard to fulfill. For instance, if the hidden photon is the lightest hidden state, it decays to electron pairs before $T \sim \text{MeV}$ for [3]

$$\epsilon > 3 \times 10^{-11} \left(\frac{\text{GeV}}{m_{\gamma_d}} \right)^{1/2}. \quad (5.5.49)$$

Further constraints on γ_d are summarized in [196, 84]. For a hidden photon heavier than $\sim \text{GeV}$, the constraints come from B-factories and muon anomalous magnetic moment and imply $\epsilon \lesssim 10^{-3}$. For m_{γ_d} between MeV and GeV, beam dump experiments (typically assuming a 2-body decay of the lightest state) require $\epsilon \lesssim 10^{-7}$. Finally, for m_{γ_d} between $\sim 1 - 50 \text{ MeV}$, constraints from supernovae cooling imply $\epsilon \lesssim 4 \times 10^{-9}$.

Now we consider very light DM, $m_\chi \in [\text{keV}, \text{MeV}]$. In this regime, there are two important changes to the above discussion: (1) there are additional light DOF present during BBN, and (2) for $m_{\gamma_d} < 2m_e$, the hidden photon becomes cosmologically long-lived because there remain no lighter states with electric charge. Both of these facts are potentially hazardous, and we now discuss how to evade the danger.

The model can be ruled out by BBN, because DM plus the hidden photon exceed the number of relativistic DOF allowed during BBN at the SM temperature. This constraint can be avoided if the hidden sector is cooler than the SM when $T \sim \text{MeV}$. This is only possible if kinetic equilibrium is not maintained between the two sectors, which requires that the following type of reaction be inefficient: $\gamma_d e^\pm \leftrightarrow \gamma e^\pm$. This reaction is decoupled when $T \gtrsim (\epsilon^2 \alpha_{\text{EM}}^2 / \pi^2 g_*^{1/2}) M_{\text{Pl}}$. Therefore, the two sectors are not in kinetic equilibrium

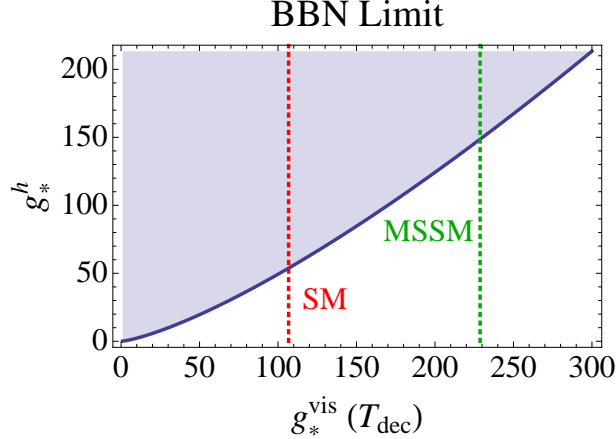


Figure 5.9: *The BBN limit on the effective number of degrees of freedom in the hidden sector, g_*^h , as a function of the number of degrees of freedom in the visible sector, g_*^{vis} , at the temperature the two sectors decouple, T_{dec} . For reference, the vertical dashed lines indicate the sizes of the full SM and MSSM. Here we have assumed that the entire hidden sector is lighter than the BBN scale $\sim \text{MeV}$.*

at $T_{\text{BBN}} \sim 1 \text{ MeV}$ if

$$\epsilon < \epsilon_{\text{BBN}} \simeq 7 \times 10^{-9}. \quad (5.5.50)$$

Suppose that this condition is satisfied, and that the two sectors begin at the same temperature (for example at the leptogenesis scale) and decouple at a lower temperature, $M_{N_1} > T_{\text{dec}} > T_{\text{BBN}}$. If more DOF freezeout in the SM than the hidden sector, before BBN, then by the separate conservation of entropy in the two sectors, $T_h < T$. The limit from BBN becomes, at 95% CL [197],

$$g_*^h(T_{\text{BBN}}^h) \left(\frac{T_{\text{BBN}}^h}{T_{\text{BBN}}} \right)^4 < 2.52. \quad (5.5.51)$$

Here T_{BBN}^h is the temperature in the hidden sector at BBN, while $g_*^h(T)$ is the effective number of relativistic degrees of freedom in the hidden sector, as defined in [197]. In Fig. 5.9 we use this relation to show the constraint on the size of the hidden sector, g_*^h , as a function of the number of DOF in the SM when the two sectors decouple, $g_*^{\text{vis}}(T_{\text{dec}})$, assuming that all hidden particles are lighter than the temperature of BBN. We see that rather large hidden sectors can be accommodated, $g_*^h \sim 50$ if the two sectors decouple above the electroweak scale.

The bottom line of the above discussion is that the two sectors cannot be in thermal equilibrium at the time of BBN, which enforces the constraint $\epsilon < \epsilon_{BBN}$. We note that even stronger constraints arise from bounds on the lifetime of the sun and horizontal branch stars that require $\epsilon \lesssim 10^{-13}$ [196, 84].

Finally, we discuss how to avoid overclosing the Universe, since the hidden photon is cosmological long-lived below the MeV scale. One possibility is to drop the assumption that the hidden sector has only one mass scale. Then we can make the lightest state in the hidden sector sufficiently light, such that it does not overclose the universe even if it is cosmologically stable⁵. An estimate for the upper bound on the mass of the lightest state, h' , can be found by assuming it follows a thermal distribution. At temperatures above its mass, $T^h > m_{h'}$, the number density is related to the photon number density through,

$$n_{h'}(T^h) = C_{h'} \frac{g}{2} \left(\frac{T^h}{T} \right)^3 n_\gamma(T), \quad (5.5.52)$$

with $C_{h'} = 3/4$ ($C_{h'} = 1$) for a fermion (boson) h' . Below $m_{h'}$, the energy density scales as a^{-3} and is therefore proportional to $n_\gamma(T_0)$. Comparing to the measured DM energy density, one finds,

$$m_{h'} \leq 3 \text{ eV} \left(\frac{2}{g} \right) C_{h'}^{-1} \xi_{h'}^{-3}, \quad (5.5.53)$$

where $\xi_{h'} = T^h/T$ at the time when h' becomes non-relativistic. This result is in agreement with the more precise calculation of [198].

Another intriguing possibility exists. Above we assumed that the hidden sector was in thermal equilibrium with the SM at the time of leptogenesis. However if the hidden sector couples only weakly to the right-handed neutrino, the two sectors may have never been in equilibrium with each other. In that case the hidden sector can easily be much colder than the SM, so as to allow for a heavier $m_{h'}$, cf. Eq. (5.5.53). Furthermore, it is interesting to note that if the DM annihilation rate is slow (or even vanishing), the symmetric component can dominate over the asymmetric one. Then the symmetric component would be responsible for the observed relic abundance, while at the same time it would be related to generation of the baryon asymmetry. This possibility is however outside the ADM paradigm, therefore we postpone its study to future work [185].

⁵The lightest state may reside in a distinct sector thus explaining the hierarchy of scales.

As a final remark, we note that the above discussion assumed a hidden gauge group coupled to the visible sector through gauge kinetic mixing. Other portals, such as the Higgs portal may be considered. The Higgs portal can have very different (and potentially weaker) astrophysical constraints than the vector portal. This is because γ_d couples to electric charge and therefore equally to electrons and protons, whereas a hidden sector scalar, that couples through the Higgs portal, will couple more strongly to protons than electrons.

5.6 Outlook

In this chapter we discussed the ADM scenario in the context of 2-sector leptogenesis. The asymmetries in the SM and DM sectors depend on several factors, such as the branching fractions and decay asymmetries of the sterile neutrinos, and the strength of washout effects in each sector. Consequently, the ratio of dark matter number density to the baryon number density is very sensitive to the model parameters, thereby accommodating a wide range of dark matter masses from keV to 10 TeV. Our findings suggest that the spectrum of predictions of ADM, especially of those concerning the dark matter mass, is much wider than previously thought. This is very important for planning direct and indirect experimental searches that target the ADM scenario.

Here, we have chosen to focus on the concrete scenario of thermal leptogenesis with hierarchical neutrino masses. There are several variations and open questions that remain unexplored:

- Other leptogenesis scenarios, such as soft leptogenesis, resonant leptogenesis or Dirac leptogenesis, may be accommodated within the 2-sector leptogenesis framework. It would be interesting to study the above variations as they are expected to admit different dynamics and in some cases produce very different phenomenology.
- It would be interesting to extend our treatment of the BEs to include finite temperature corrections and the full flavor structure of the theory. These corrections

are well-studied for traditional leptogenesis and may have interesting consequences for 2-sector leptogenesis as well.

- In one of the variations studied here, the DM mixes with the active neutrinos, providing a novel realization of sterile neutrino DM. It is worthwhile to investigate this scenario further. In particular, it would be interesting to understand how the constraints derived from late time oscillations or decays can be ameliorated in other leptogenesis scenarios.
- It is possible to imagine a similar mechanism for populating ADM in a single-sector leptogenesis model [199]. Clearly the phenomenology of such a scenario would be distinct.
- Another deformation studied here predicts dark matter to be a mixture of cold and warm components with roughly equal numbers. This may have interesting phenomenological consequences for structure formation, which would be worthwhile to explore.
- It may also be interesting to consider variants of this scenario where the symmetric DM component dominates the relic density. In particular, the symmetric component originally produced by the decays of the heavy sterile neutrinos may not annihilate away. In such a case, the asymmetric lepton density is suppressed (due to the usual bounds on the decay asymmetry into the SM sector) with respect to the DM number density, thereby predicting light DM. We postpone a study of the details of such scenarios to future work [185].

PART II: LEPTON JETS

Introduction to Lepton Jets

6.1 Lepton Jets from a Non-Abelian Dark Sector

In this section we discuss the collider phenomenology associated with the models presented in the previous sections. In the first part of this section we analyze the generic predictions associated with a non-abelian dark sector that is linked to the SM only via kinetic mixing. In the second part we present the signals expected in supersymmetric versions of such models. Throughout, we limit the discussion to the Tevatron and LHC. It is important to realize that in the case of a GeV scale dark sector such high-energy accelerators are needed more for their luminosity than their energy reach, which is considerably higher than the dark sector scale. In supersymmetric implementations, colored MSSM superpartners can be copiously produced at hadron colliders. Their subsequent decay into dark states can produce spectacular signals involving multiple lepton jets. We leave it for future work to investigate the phenomenology of these models at low-energy experiments, but see Ref. [35] for low-energy signatures of similar models.

A new sector of light particles with very weak couplings to the Standard Model have been discussed in detail in the context of the “Hidden Valley” models [10]. Their collider phenomenology was investigated in [11, 12]. In particular, the modifications such models can introduce to the decay chains of the MSSM was clarified in Ref. [13]. Here, we focus on the particular scenario which uses the kinetic mixing as the essential link between the SM and the dark sector. In addition, motivated by astrophysical observations, we allow the dark sector to decay back to light leptons (e^\pm and μ^\pm) only. For the purpose of this chapter, we do not concern ourselves with a possibly small branching fraction into pions.

The pair production of the dark matter states at colliders is certainly possible if they happen to carry SM weak charge. However, their detection proves extremely difficult since they are not accompanied by any hard object. Even if the excited states of its SM multiplet are produced, their decays are too soft to trigger on since they are separated

by only $\sim \text{GeV}$ (notice that this splitting is generated by the SM gauge interactions and are of order αM_Z [56]).

I. Production and decay of dark gauge bosons and Higgses

As discussed in detail in appendix A.1, the kinetic mixing induces two important, ϵ suppressed, couplings: The SM electromagnetic current is now also charged under the dark gauge bosons; the SM Z^0 boson is now coupled to the dark hypercharge current. Before discussing each of these couplings and their impact on collider signals, let us briefly discuss the decays of the dark gauge boson and the dark Higgses.

Dark gauge boson and Higgs decay chains

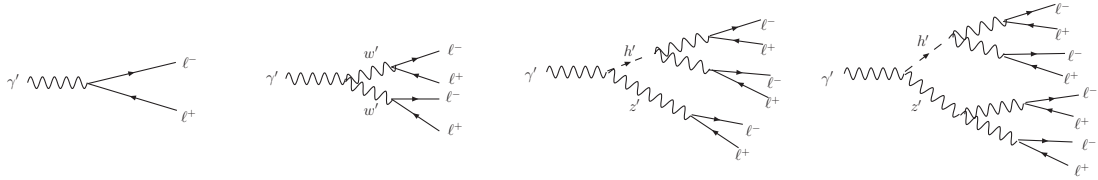


Figure 6.1: Typical decay chains starting with a dark gauge boson, labelled γ' in this plot. The dark decay chain can have several stages and involve additional dark sector states, such as other dark gauge bosons (labeled w' , z' in this figure), and dark Higgses (labelled h').

The non-abelian nature of the dark sector implies the presence of complicated decay chains. Some of the typical decays chains are shown in Fig. 6.1. In the dark sector, gauge boson mass eigenstates are generically mixtures of all four $SU(2)_{\text{dark}} \times U(1)_y$ gauge eigenstates. In Fig. 6.1 and the rest of this section, we have used γ' (and also w' and z' in this figure) to denote any one of these mass eigenstates. For an abelian dark sector with kinetic mixing with the SM, γ' decay leads to a di-lepton final state, shown in the first panel from the left of Fig. 6.1. On the other hand, a non-abelian dark sector, like one of the examples considered in this chapter, leads to complicated decay chains, such as the ones shown in the rest of Fig. 6.1. The dark Higgs sector, necessary to break the non-abelian group, may also participate in such cascades as shown in the right two panels

of Fig. 6.1. Such cascades inevitably produce multiple, easily > 2 and possibly 8, final state leptons, which provides a unique signature of the non-abelian nature of the dark sector¹. We expect the decay between dark states to be generically prompt. Therefore, the decay length is dominated by the very last decays back into SM leptons. A rough estimate for a generic decay is then,

$$c\tau_{2\text{-body}}^{\gamma' \rightarrow n\ell} \sim \frac{1}{\alpha\epsilon^2 m_{\gamma'}} = 2.7 \times 10^{-6} \text{ cm} \left(\frac{\text{GeV}}{m_{\gamma'}} \right) \left(\frac{10^{-3}}{\epsilon} \right)^2. \quad (6.1.1)$$

With moderate boost $\gamma \sim \mathcal{O}(10)$, this may lead to a displaced vertex if $\epsilon \lesssim 10^{-4}$.

To be observable at hadron colliders, the dark boson which initiates such a cascade must carry $p_T \sim \mathcal{O}(10\text{s})$ GeV. Therefore, regardless of the precise nature of the cascade which ensues, its decay products have small opening angles $\delta\theta \sim m_{\gamma'}/p_T < 0.1$. Those decay products will eventually decay into several collimated SM leptons. A collection of more than 2 hard and collimated leptons is dubbed a “lepton jet” [21].

Displaced vertices and missing energy

While Eq. (6.1.1) is the generic estimate for the resulting decay length of dark cascades, there are several exceptions which may result in more noticeably displaced vertices or missing energy in lepton jets.

If it is kinematically forbidden for a dark gauge boson to have 2-body on-shell decays within the dark sector, then the dark gauge boson may decay directly into two leptons. However, a noticeable exception occurs when the 3-body decay $\gamma' \rightarrow a'^* b'_1 \rightarrow b'_1 b'_2 b'_3$ is kinematically allowed, where a' , b' can be either dark gauge boson or dark Higgs states. In this case, there is an additional suppression of $(\delta m/m_{a'})^5 \times (\text{3-body phase space})$ on the decay width, where $\delta m \sim m_{\gamma'} - \sum_i m_{b'_i}$, and we have used $m_{\gamma'} \sim m_{a'}$ in this estimate. This decay channel can be competitive and even dominate over the direct decay into 2 leptons. In particular, when the decay into SM leptons is strongly suppressed (dark pseudoscalar decay) or all together forbidden (dark fermion decay), the 3-body process may dominate and lead to a displaced vertex. The impact parameters of multiple leptons

¹Sometimes phase space constrains the flavor of the lepton. For example, a GeV dark gauge boson cannot decay into more than 4 muons

associated with this displaced vertex will not be correlated with each other since they come from the decays of different resonances $b'_{1,2,3}$.

If the lightest dark sector state is a dark Higgs, h'_0 , it cannot directly decay into SM leptons (unless it mixes the SM Higgs, see Ref. [43,20]). In this case, the dark Higgs will either decay into 4 leptons through two off-shell gauge bosons, shown in the left panel of Fig. 6.2, or into 2 leptons through a one-loop decay. Either way, such a decay leads to a very long life-time, $c\tau \sim \mathcal{O}(\text{km})$ for $m_{h'_0} \lesssim \text{GeV}$. In this case, dark cascades which involve this lightest scalar contain missing energy as it escapes the detector. These cascades can still produce observable lepton jets because, in addition to missing energy, one still gets leptons from the intermediate steps of the decay, such as $h'_i \rightarrow a'h'_0$ followed by $a' \rightarrow$ lepton pairs. In this case, the lepton jet contains missing energy that is collimated with the leptons of the same cascade.

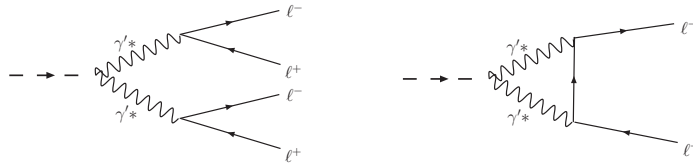


Figure 6.2: Two possible decay channels if the lightest dark sector state is a scalar from the dark Higgs sector.

An additional source of missing energy comes in a supersymmetric dark sector with R-parity. The lightest dark supersymmetric particle (LDSP) may be stable if the gravitino is heavier. Otherwise, it may eventually decay into the gravitino. Either way, it carries with it missing energy. Unless the MSSM sector decays directly into the LDSP, in which case there may be no lepton jets, missing energy due to the LDSP will be collimated with the visible lepton jets, very similarly to the non-SUSY case. Such correlations provide an additional handle on the reconstruction of these events since we know the direction of the missing particles and can treat them as having vanishing masses. We provide an example of such a reconstruction in the case of rare Z^0 decays below.

Direct Production

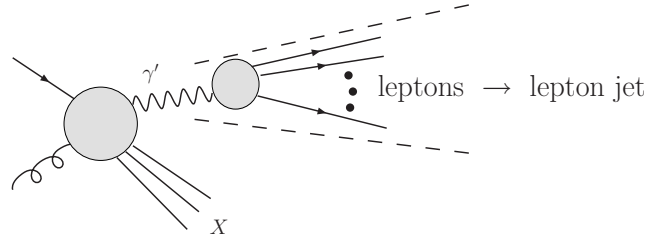


Figure 6.3: Direct production of a dark gauge boson in a process very similar to prompt photon production in the Standard Model.

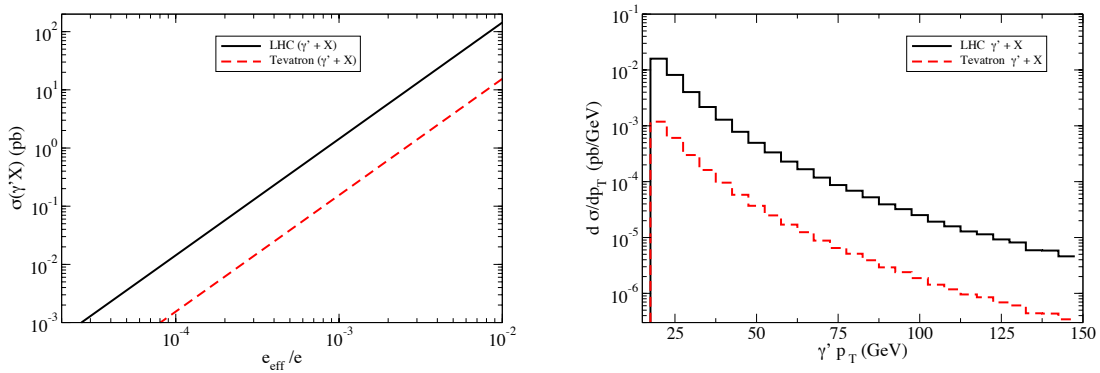


Figure 6.4: In the left pane, we show the rate of direct production of the dark gauge boson as a function of e_{eff}/e , where e_{eff} is the effective coupling of dark gauge boson to the Standard Model fields.

The kinetic mixing between the dark force carrier and the SM photon induces a small dark charge for electromagnetically charged SM fields. Consequently, the dark gauge boson can be directly produced in colliders via a process analogous to prompt photon production in the SM, shown in Fig. 6.3.

In the left panel of Fig. 6.4, we present the production rate of dark gauge bosons as a function of e_{eff}/e , where $e_{\text{eff}} = \epsilon e \cos \theta_W f_b$ is their effective gauge coupling to SM fields² and f_b is the fraction of the dark hypercharge gauge boson b_μ in a given dark gauge boson mass eigenstate. In the right panel of Fig. 6.4 we plot the inclusive differential cross-section of dark photon (γ') production at the LHC and the Tevatron with $e_{\text{eff}} = 10^{-3}e$.

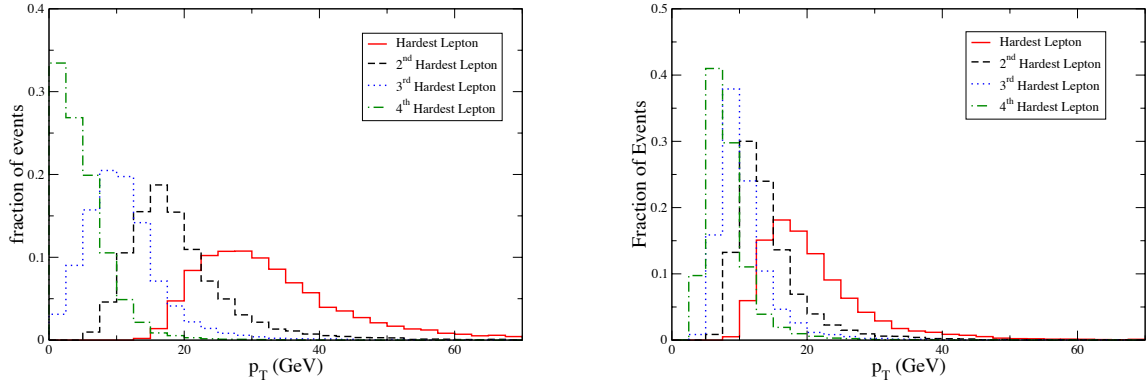


Figure 6.5: p_T distributions for cascades resulting in 4 (left) and 8 (right) leptons, for events with $p_T > 50$ GeV for γ' .

After dark vector bosons are produced, they typically cascade down to multiple leptons that form a lepton jet as discussed above. These leptons carry a significant amount of p_T , as shown in Fig. 6.5. At CMS, the Level 1 Dimuon trigger (2 muons with $p_T > 3$ GeV in $|\eta| < 2.4$) or single muon trigger (1 muon with $p_T > 7$ GeV and $|\eta| < 2.4$) should be able to detect those events that contain muons [63]. The electron triggers are single e (isolated $E_T > 26$ GeV), double e (isolated $E_T > 14.5$) and double relaxed e (not isolated $E_T > 21.8$ GeV). Since the resulting electrons are unlikely to be isolated “electromagnetic” objects, the double relaxed e is probably necessary. We will conservatively assume that muons alone are triggered on. In Fig. 6.6, we show the differential cross section of dark γ' , taking into account the simple requirements on muon triggering.

²The simulation was actually of prompt photon production with PYTHIA [62] and the resulting cross-section was multiplied by a factor of e_{eff}^2/e^2 .

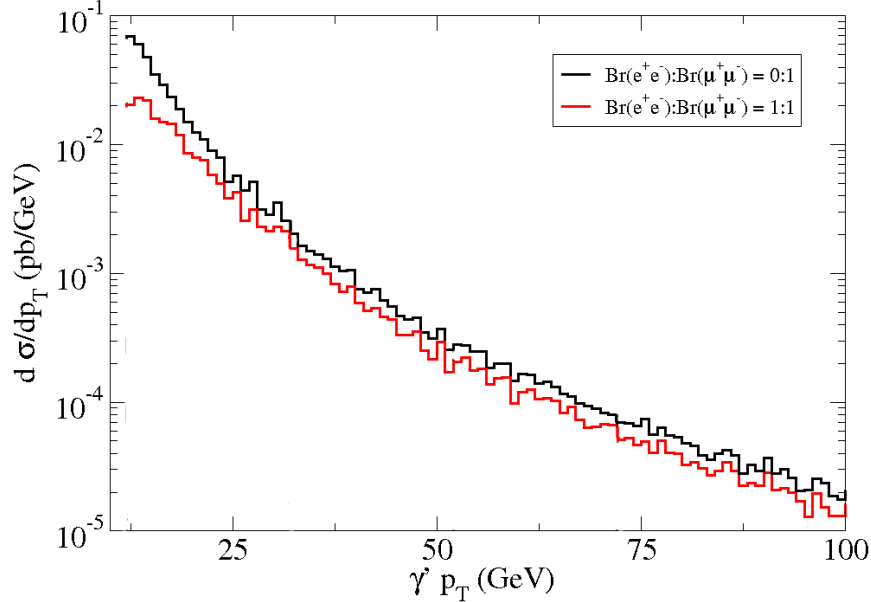


Figure 6.6: The differential cross-section as a function of the p_T of γ' at the LHC ($\sqrt{s} = 14$ TeV) after including muon triggers, demanding either a single muon with $p_T > 7$ GeV or two muons with $p_T > 3$ GeV. Proper η cuts were imposed and each event was required to contain at least 3 leptons.

Distinguishing Leptons

Let us discuss the issue of discriminating individual leptons within a given lepton jet³. In our present discussion, we focus on muons. In Fig. 6.7 we plot the maximal opening angle between any two of the four leptons. At such high momenta, the resulting decay products are highly collimated with an initial opening angle of approximately $\theta \sim m_{\gamma'}/p_T < 0.1$, which can be as small as 10^{-2} . By the time these muons reach the first layer of the muon system, they typically acquire a sufficient separation to be distinguished. For example, as depicted in Fig. 6.5, a typical scenario will have two muons with average $p_T \sim 20$ GeV and $\Delta p_T \sim 5$ GeV. Without even including the initial lepton jet opening angle, we estimate that the acquired separation is about 10 cm (in the CMS detector), which is greater than the cell size of ~ 4.5 cm. The separation between two same sign muons is proportional to $\Delta p_T / (p_T^{\mu_1} p_T^{\mu_2})$. For a given lepton jet p_T , since both Δp_T and p_T are

³We are grateful for valuable discussions with Jim Olsen on this subject.

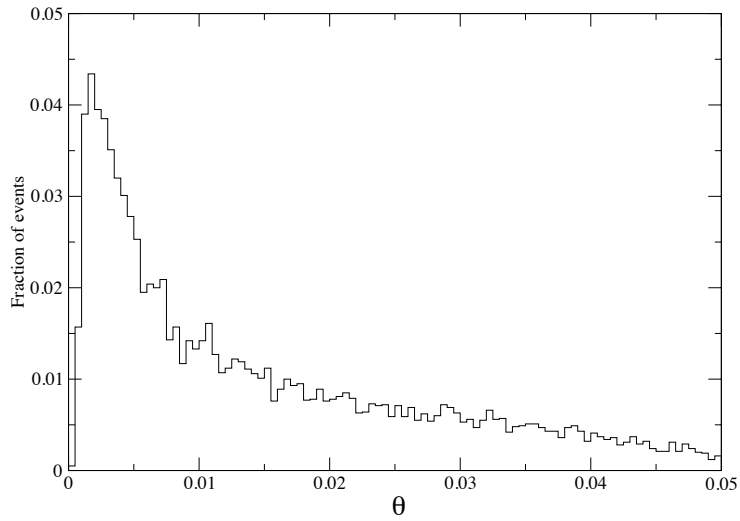


Figure 6.7: The fraction of events with a maximum opening angle θ between leptons in a lepton jet, which contains 4 leptons.

inversely proportional to the number of leptons, higher multiplicities actually result in larger separations. We also notice from Fig. 6.5 that leptons in lepton jets typically have different p_T , such that $\Delta p_T/p_T \sim 20\%$ or so. LHC detectors can achieve better muon momentum resolution. For example, CMS can achieve $\Delta p_T/p_T \sim 1\%$ (about 10% with muon system only) in the momentum regime of interest [64]. ATLAS can achieve a similar precision [65]. Finally, the muon isolation separation defined by CMS can be as small as $\Delta R = 0.01$. The angular resolution is even smaller, about 2 mrad [64]⁴. Thus, it is reasonable to assume that CMS will be capable of resolving several, if not all of the muons. The primary background arises from K and π decays and $J/\psi \rightarrow \mu^+\mu^-$ (muons coming off soft jets can be vetoed with isolation cuts), and possibly from other heavy flavor decays. The high lepton multiplicity in those events and the lack of hadronic activity around the lepton jet should be sufficient to fight these backgrounds and obtain

⁴This is the resolution quoted for a single hit. It is beyond our abilities to evaluate how the resolution deteriorates with multiple collimated muons.

a clean sample. However, a more careful collider analysis is certainly warranted, but is beyond the scope of the present work.

Rare Z^0 decay

As discussed in Appendix A.1, the kinetic mixing also induces a coupling $\epsilon Z_\mu J_b^\mu$, where J_b^μ is the dark hypercharge current. Thus, we can produce dark hypercharged states through rare decays of the Z^0 , shown schematically in Fig. 6.8. The ϵ^2 suppression makes LEP searches irrelevant due to luminosity limits, but the Tevatron and LHC may probe such events. The decay branching ratio to any particular dark sector state d_i can be written as

$$\text{BR}(Z^0 \rightarrow d_i d_i) = \frac{c_{d_i} \epsilon^2 g_y^2 y_{d_i}^2 \sin^2 \theta_W}{\Gamma_Z^0 48\pi} M_{Z^0}, \quad (6.1.2)$$

where c_{d_i} depends on decay matrix element and is proportional to the number of degrees of freedom of d_i . The total branching ratio into the dark sector will scale linearly with the number of dark sector states, which could be easily $\mathcal{O}(10)$ in our scenario.

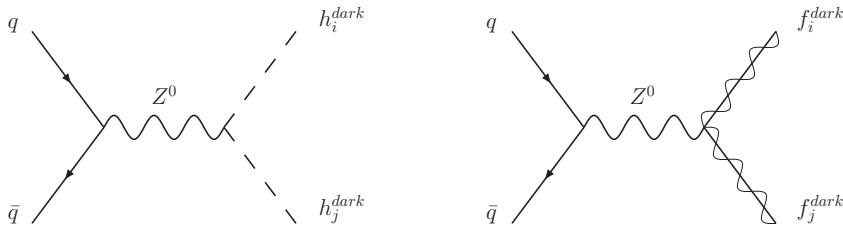


Figure 6.8: Z^0 production and two possible decay channels into the dark sector. On the left we depict a decay into the dark Higgs sector. Fermionic channels, such as the one shown on the right, are dominantly associated with the Higgsino states possible in supersymmetric versions of the model.

The SM photon does not couple to the dark sector states. However, there is a “continuum” contribution to the same amplitude through off-shell dark photon, $q\bar{q} \rightarrow \gamma'^* \rightarrow d_i d_i$, which is proportional to $e_{\text{eff}}^2 \propto \epsilon^2$. Depending on the spectrum and couplings in the dark sector, it could have important contributions to the signal off the Z-peak. In this section, we will focus on the contribution within the Z resonance.

The production rates of dark sector states at the Tevatron and LHC are shown in Fig. 6.9 [66]. We present rates coming from decays into bosonic (denoted by h') and fermionic (denoted by f') dark sector states. In the context of the SUSY models discussed later in this section, these bosonic and fermionic states could refer to dark Higgs bosons or Higgsinos, respectively. On the other hand, the collider phenomenology is similar if other possible dark sector states decay into lepton jets. A cut of $|\eta| < 2.4$ has been imposed on the direction of the lepton jets. The difference in rates between the fermionic and bosonic channels results from the η cut, the boost of the Z^0 in the lab frame, and the fact that fermions are more likely to be emitted along the boost direction because of angular momentum conservation.

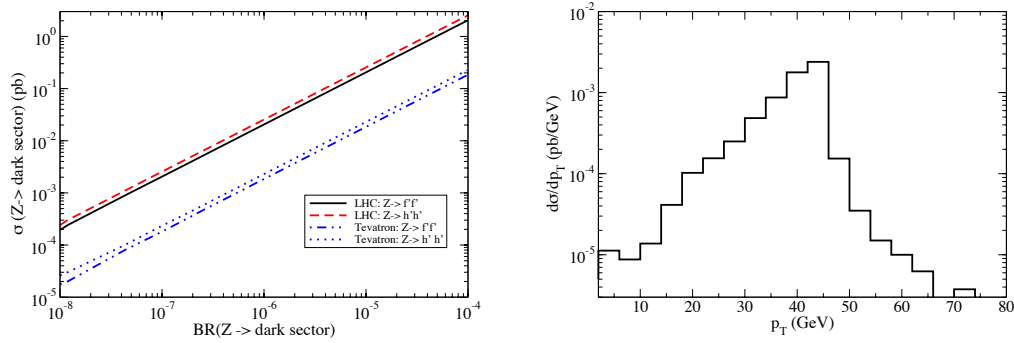


Figure 6.9: Left: The production rate as a function of the branching ratio of the decay: $Z^0 \rightarrow$ dark states. The solid and dashed lines are for Z^0 decays into dark sector scalars and fermions, respectively. Right: lepton jet p_T distribution resulting from Z^0 decays.

As can be seen from Fig. 6.9, the lepton jets produced in this way are peaked towards $p_T^{\text{lepton jet}} \sim 0.5 M_Z$. Therefore, they are typically harder than the lepton jets resulting from the prompt production of dark gauge bosons. As we have discussed in Section I., such harder lepton jets will be easier to trigger on. However, we expect the efficiency of identifying different leptons in a lepton jet will be lowered as it is $\propto 1/p_T$.

Reconstructing the Z^0 is not difficult and helps to reduce the background. With enough statistics, it is even possible to study the angular distribution of the resulting lepton jets and get a handle on the spin of the dark sector states as demonstrated in

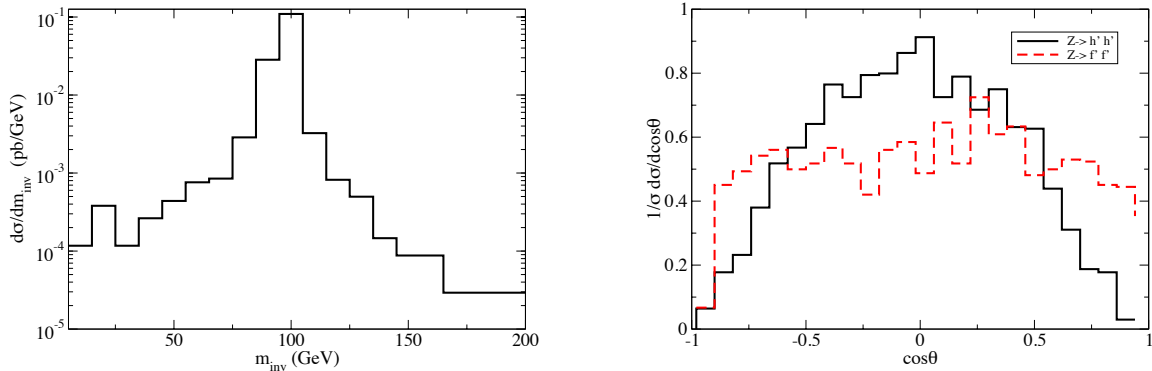


Figure 6.10: Left: Reconstructed Z^0 boson. Right: Normalized lepton jet angular distribution in the Z^0 boson's rest-frame.

Fig. 6.10. About 5000 events are used in this plot. We see that the expected rise for $\cos\theta \sim \pm 1$ from the fermionic decay channels is washed out due to the large boost of Z^0 and the $|\eta|$ cut. However, the resulting distribution is still quite different from that of the bosonic decay channel.

II. Collider signals of supersymmetric models

In this section, we discuss the collider signals associated with supersymmetric models. In Section 2.3, we have focused on models with low supersymmetry breaking scale. However, the present discussion of the resulting collider signatures is largely independent of that scale or other MSSM details since we will not consider any specific superpartner spectrum. In that sense, models with higher supersymmetry breaking scales, such as the Planck slop option suggested in Ref. [21], are only different in that the gravitino is heavier. Hence, the end of the dark sector decay chain will not involve the gravitino. However, this does not have a visible effect on the collider signals. Even in the low scale models where the gravitino is light, the decay length of the dark sector LSP to the gravitino is much larger than the detector size. That said, it is important to note that the collider signatures discussed in this section are based on the assumption that the MSSM LSP dominantly decays into the dark sector.

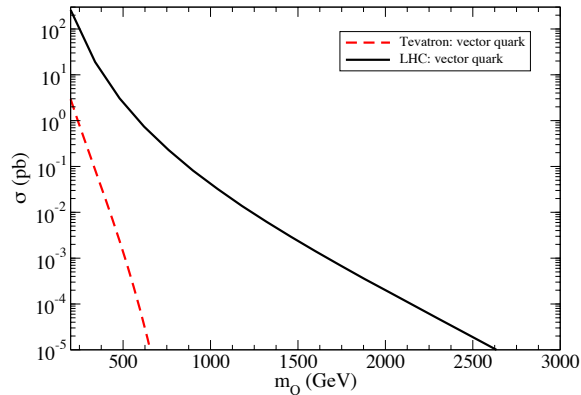


Figure 6.11: Production rate of one set of $\mathbf{3} + \bar{\mathbf{3}}$ vector-like quarks, which can be part of the dark matter multiplet. The rate should be scaled by the number of such representations and the dimension of the dark matter representation under G_{dark} .

With supersymmetry, the dark sector states are dominantly produced from cascade decays of MSSM colored superpartners, such as gluinos and squarks. These particles follow typical MSSM decay chains down to the MSSM LSP (not the gravitino). The effect of the GeV dark sector is to extend and/or modify the decay chains following MSSM LSP production [21]. We begin by summarizing the main features of such cascades.

Let us first note, however, that a notable exception occurs if dark matter is part of a pair of $\mathbf{5} + \bar{\mathbf{5}}$ under the SM gauge groups. An example of such a model was presented in the benchmark of Section II. The rate for the production of the colored components of such a pair is shown in Fig. 6.11. Thus, the LHC has great potential for producing such states up to about 2 TeV. As pointed out in Ref. [21], as long as the colored particles decay only through higher dimensional operators they will be long-lived and may have decays with very distinct signatures [67]. We will not elaborate on these possibilities but refer the interested reader to the detailed discussion in Ref. [21].

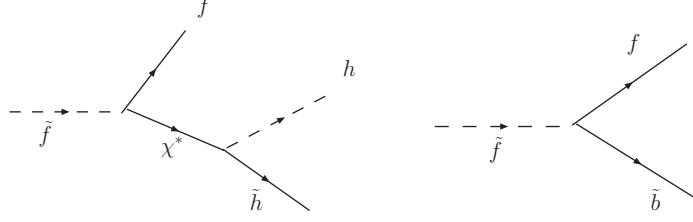


Figure 6.12: Decay of sfermion LSP.

MSSM decays into the dark sector

Kinetic mixing implies that if the MSSM LSP is a neutralino then it decays into dark sector states with a lifetime of

$$\begin{aligned} \tau_{\text{LSP} \rightarrow h + \tilde{h}} &\sim (\alpha_y^{\text{dark}} f_{\tilde{B}}^2 \epsilon^2 M_{\text{LSP}})^{-1} \\ &= 7 \times 10^{-19} \text{ s} \left(\frac{100 \text{ GeV}}{M_{\text{LSP}}} \right)^2 \left(\frac{0.01}{\alpha_y^{\text{dark}}} \right) \left(\frac{1.0}{f_{\tilde{B}}} \right)^2 \left(\frac{10^{-3}}{\epsilon} \right)^2, \end{aligned} \quad (6.1.3)$$

where $f_{\tilde{B}}$ is the bino fraction of the MSSM LSP. In the low-scale gauge mediation models constructed earlier in this chapter, it is possible for the gravitino to be significantly lighter than the MSSM LSP. When the gravitino is light, another possible decay channel for the MSSM LSP is $\text{LSP} \rightarrow X_{\text{SM}} \tilde{G}$, where X_{SM} can be a photon, Z, or Higgs, depending on the model parameters and phase space. The decay lifetime can be estimated as

$$\tau_{\text{LSP} \rightarrow \gamma, Z, h + \tilde{G}} \sim \left(\frac{M_{\text{LSP}}^5}{16\pi F^2} \right)^{-1} = 3.3 \times 10^{-13} \text{ s} \left(\frac{100 \text{ GeV}}{M_{\text{LSP}}} \right)^5 \left(\frac{\sqrt{F}}{100 \text{ TeV}} \right)^4. \quad (6.1.4)$$

We see that the LSP dominantly decays into the dark sector instead of the gravitino. However, the two channels can be comparable in certain regions of parameter space, such as $f_{\tilde{B}} \sim 0.1$ and a low supersymmetry breaking scale $\sqrt{F} \sim \sqrt{m_{3/2} M_P} \sim 10 \text{ TeV}$.

When the MSSM LSP is a sfermion ($\tilde{\ell}$ or \tilde{q}), things become more subtle. One possible decay channel is through an off-shell gaugino with a significant bino fraction, $\tilde{f} \rightarrow f + \tilde{\chi}^* \rightarrow f + [\text{dark sector states}]$, shown the left panel of Fig. 6.12. Its decay lifetime can be estimated to be

$$\begin{aligned} \tau_{\tilde{f} \rightarrow 3\text{-body}} &\sim \left[\alpha_y^{\text{dark}} g_Y^2 c_{f\chi}^2 f_{\tilde{B}}^2 \epsilon^2 \frac{m_{\tilde{f}}}{16\pi^2} P(m_{\tilde{f}}/M_\chi) \right]^{-1} \\ &= 8.3 \times 10^{-16} \text{ s} \left(\frac{100 \text{ GeV}}{m_{\tilde{f}}} \right) \left(\frac{0.01}{\alpha_y^{\text{dark}}} \right) \left(\frac{1.0}{c_{f\chi} f_{\tilde{B}}} \right)^2 \left(\frac{10^{-3}}{\epsilon} \right)^2 \frac{1}{P(m_{\tilde{f}}/M_\chi)}, \end{aligned} \quad (6.1.5)$$

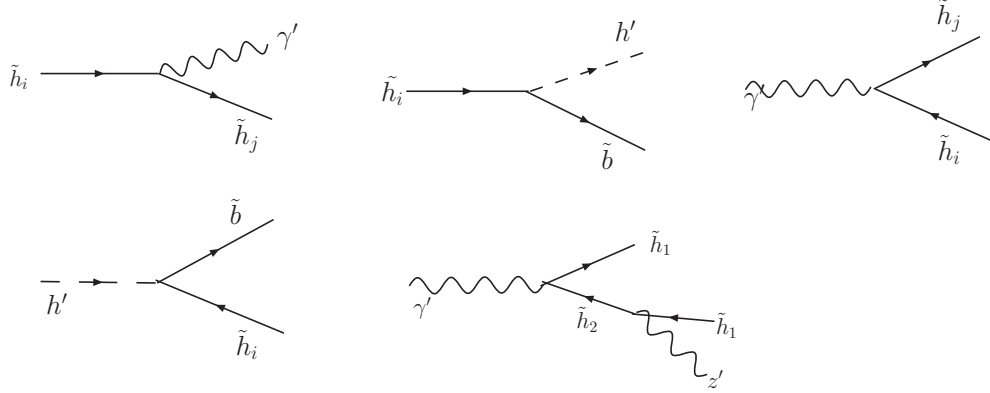


Figure 6.13: Typical SUSY dark sector decay chains. The dark sector states, γ' , h' and z' , can be either on or off shell. They will cascade further to produce lepton jets, similarly to the non-SUSY case.

where $c_{f\chi}$ is the effective fermion- χ coupling, and $P(m_{\tilde{f}}/M_\chi)$ is a function with the limit $P \rightarrow (m_{\tilde{f}}/M_\chi)^4$ for $M_\chi \gg m_{\tilde{f}}$. Another possible decay channel is $\tilde{f} \rightarrow f + \tilde{b}$, shown in the right panel of Fig. 6.12, where \tilde{b} is the dark bino. However, as explained in Appendix A.1, in addition to kinetic mixing, this coupling has an additional suppression of order $M_{\tilde{b}}/M_{\tilde{B}}$. Hence, its lifetime is

$$\begin{aligned} \tau_{\tilde{f} \rightarrow f + \tilde{b}} &\sim \left[\alpha_Y \epsilon^2 m_{\tilde{f}} \left(\frac{M_{\tilde{b}}}{M_{\tilde{B}}} \right)^2 \right]^{-1} \\ &= 6.6 \times 10^{-15} \text{ s} \left(\frac{100 \text{ GeV}}{m_{\tilde{f}}} \right) \left(\frac{10^{-3}}{\epsilon} \right)^2 \left(\frac{1 \text{ GeV}}{M_{\tilde{b}}} \right)^2 \left(\frac{M_{\tilde{B}}}{100 \text{ GeV}} \right)^2. \end{aligned} \quad (6.1.6)$$

Notice that when the off-shell gaugino state is dominantly bino, we have

$$\frac{\tau_{\tilde{f} \rightarrow 3\text{-body}}}{\tau_{\tilde{f} \rightarrow f + \tilde{b}}} \sim \frac{4\pi}{\alpha_y^{\text{dark}}} \frac{M_{\tilde{b}}^2 M_{\tilde{B}}^2}{m_{\tilde{f}}^4}. \quad (6.1.7)$$

Therefore, these two channels can be either quite different or comparable, depending very sensitively on the details of the model. In principle, these two decay channels are distinguishable experimentally, as the three (two) body decay gives rise to three (two) different lepton jets, respectively. Notice also that in this case, it is easier for the channel that decays into the gravitino to be competitive as well, if F is close to tens of TeV.

Once the cascade has progressed into the dark sector, it will decay through the mass hierarchy there. Several typical cascades in the supersymmetric dark sector are shown

in Fig. 6.13. For example, the center panel on the second row is important when the fermionic dark superpartners are lighter than the dark gauge boson. An example of such a scenario is discussed in Section II.. All of the decay products in the same chain are collimated into one lepton jet with typical $p_T \sim 100$ GeV. Therefore, it is difficult to uncover the details of the decay chain that produces a given lepton jet.

Finally, we discuss the endpoint of the dark sector decay chain. First, consider the situation where the lightest dark sector particle is the LDSP, as in the benchmarks of sections II. and II.. If the gravitino is heavier than the LDSP, then the decay chain will end there with the LDSP escaping the detector, producing missing energy along the direction of the lepton jet. If the gravitino is lighter than the LDSP, as in the case of low scale supersymmetry breaking models, the last step of the cascade will be $\text{LDSP} \rightarrow X_{\text{SM}} \tilde{G}$, where X_{SM} corresponds to a light SM particle, such as a photon or lepton. For simplicity, we consider the case where the LDSB is mostly dark bino. We can estimate its decay lifetime as

$$\tau_{\tilde{b} \rightarrow \gamma \tilde{G}} \sim \left[\frac{\epsilon^2}{16\pi} \frac{M_{\tilde{b}}^5}{F^2} \right]^{-1} = 3.3 \times 10^3 \text{ s} \left(\frac{10^{-3}}{\epsilon} \right)^2 \left(\frac{1 \text{ GeV}}{M_{\tilde{b}}} \right)^5 \left(\frac{\sqrt{F}}{100 \text{ TeV}} \right)^4, \quad (6.1.8)$$

which is clearly not relevant on the collider timescale. Second, we consider the case where there is also a dark sector gauge boson, b , that is lighter than the LDSP. This situation is not realized in our benchmarks of Section II., but is certainly a possibility. In this case, the LDSP can decay through the channel, $\tilde{b} \rightarrow b \tilde{G}$, where b subsequently decays to leptons. There is no ϵ^2 suppression here, but setting ϵ to 1 in Eq. (6.1.8) gives a decay length inside the detector only for $\sqrt{F} \lesssim 10$ TeV. Therefore, we can effectively think of the LDSP as the endpoint of the dark sector decay chain for most of parameter space.

Extended discovery reach for direct electroweak-ino production

The direct production of electroweak-inos is an important channel since it is independent of the existence of colored superpartners and may provide additional information on the properties of those electroweak-inos. In the conventional MSSM, it is usually difficult to see events with direct pair-production of electroweak-inos. In the case of direct MSSM LSP production, one has to trigger on some additional hard radiation, which has a lower

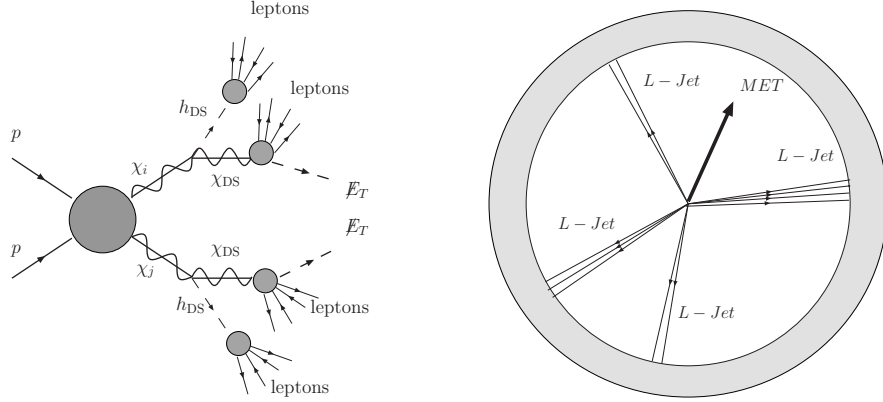


Figure 6.14: Pair-production of the SM LSP can result in spectacular lepton jet + MET events. On the left we depict the event topology. On the right we show a schematic representation of the resulting geometry.

rate and a large background. The pair-production of heavier electroweak-ino states which cascade down to the LSP may be easier to observe but suffers from large SM background. However, in the scenario we consider, the LSP of the MSSM, which we denote by χ_0 , will decay further into the dark states [13] whose decays result in leptons and missing energy [21]. Such events are easy to trigger on since all the leptons carry significant amounts of p_T . Since χ_0 is produced almost on threshold, its boost factor is order unity and the opening angle in the decay $\chi_0 \rightarrow h_{DM}\chi_{DM}$ is fairly large. The resulting event geometry is striking and is depicted schematically in Fig. 6.14).

In the left panel of Fig. 6.15, we show the rate of electroweak-ino pair production at the Tevatron. In the case of pure wino-like and Higgsino-like LSP, we have also included the production of the closely degenerate charginos and neutralinos. We then decay each LSP into a pair of lepton jets and study their kinematics. At the Tevatron, the neutralinos and charginos produced from $q\bar{q}'$ initial states are expected to have small boosts. Therefore, the majority of the resulting lepton jets are expected to be very central as shown in the right panel of Fig. 6.15, where we have required $|\eta| < 2.4$ for the lepton jets. In addition we see that the majority $> 90\%$ of the events have 4 lepton jets within the central region as illustrated in the left panel of Fig. 6.15. Since the presence of such lepton jets greatly enhances the possibility of triggering on such events and separating them from

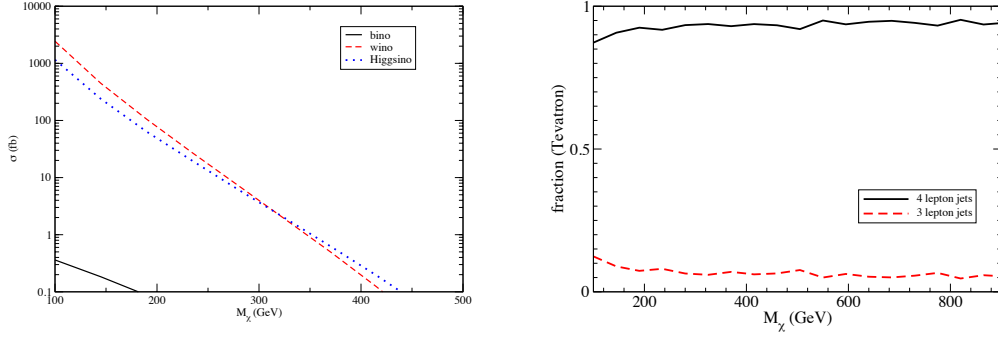


Figure 6.15: Left: The cross-sections for electroweak-ino production at the Tevatron. We have included both LSP pair production and, in the case of wino and Higgsino LSP, the production of closely degenerate states, as a function of M_χ . We choose the squark mass to be 750 GeV. Right: the fraction of events with 3 and 4 lepton jets within the central region $|\eta| < 2.4$.

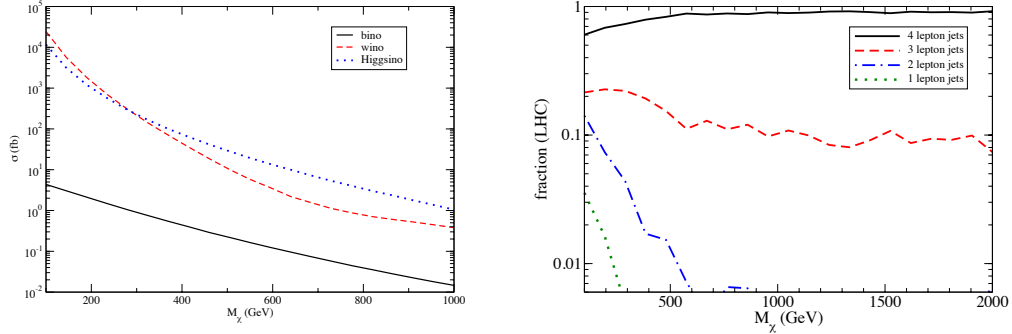


Figure 6.16: Left: The cross-sections for electroweak-ino production at the LHC. We have included both LSP pair production and, in the case of wino and Higgsino LSP, the production of closely degenerate states, as a function of M_χ . We choose the squark mass to be 750 GeV. Right: the fraction of events with 1, 2, 3 and 4 lepton jets within the central region $|\eta| < 2.4$.

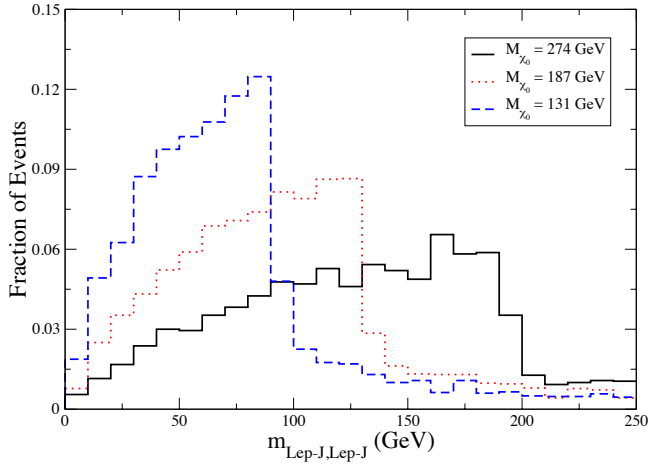


Figure 6.17: Forming the invariant mass of all the lepton jets in the events can lead to a measurement of the mass of χ_0 , shown here as an edge at M_{χ_0} . Incorrect pairings of the lepton jets are included. However, we assumed that individual leptons are properly bunched with the correct lepton jet.

the background, we estimate a reach of about 300 GeV for pure Higgsino or wino LSP at the Tevatron. The case of pure bino is still difficult because of the suppression in rate.

We have shown a similar study for the LHC in Fig. 6.16. At the LHC, the $q\bar{q}'$ initial state will carry significant boost. Therefore, as can be seen in the right panel of Fig. 6.16, there is a significant fraction of events with 3 or less lepton jets in the central region, especially for the smaller electroweak-ino mass $M_\chi \leq 400$ GeV. On the other hand, as M_χ increases, the effect of the boost quickly decreases and the fraction of events with 4 lepton jets increases. Such lepton jets will give the LHC the amazing ability to probe bino production up to $M_{\tilde{B}} \sim 1$ TeV, and wino or Higgsino production up to 2 TeV.

Measuring the mass of the MSSM LSP

In the sorts of SUSY events shown in Fig. 6.14, it is possible to use lepton jets for a measurement of the mass of χ_0 . There are two lepton jets in each decay chain. There is a clear edge in their invariant mass distribution at M_{χ_0} , as shown in Fig. 6.17. This provides

an absolute mass measurement and helps to remove some of the degeneracies discussed in the literature [68]. In addition, such reconstructions can be very useful in other precision measurements of the properties of the MSSM superpartners. For example, since we now have information about the LSP mass, and the direction of its decay products, it is easier to reconstruct the kinematics of the full event. In fact, we can fully recover the kinematics of the event using the same reconstruction method mentioned in the case of Z^0 +jets associated production in section I. Gaining such information will significantly improve the prospect of measuring the spin of the LSP, which can be very challenging in the conventional scenario.

Lepton Jet Showering and Experimental Definition

7.1 Introduction

In light of recent astrophysical observations, the authors of [20] have proposed a broad class of theories in which the annihilation of $\sim\text{TeV}$ scale dark matter in the galactic halo accounts for the anomalous excess of cosmic ray leptons. While this dark matter is probably inaccessible to colliders, it is accompanied by a $\sim\text{GeV}$ scale dark sector which couples, albeit very weakly, to the standard model (SM). The dark sector states are relatively light and can be produced at high energy colliders, only to cascade decay through the dark sector and ultimately return to the visible sector as electrons, muons, and possibly pions. The outgoing leptons emerge in the detector as lepton jets [21], which are highly collimated multiple muons or electrons that result from the decay of these highly boosted dark sector states. As observed in ref. [21] and later elaborated on in ref. [1], the addition of supersymmetry also bears with it a number of interesting and novel collider signatures. Some of the phenomenology is also relevant for scenarios with hidden valleys [10] or where DM decays into a GeV scale sector [3], and as such may describe a large class of models. Recently, experimental effort in searching for such objects has been reported in [200].

The aim of the present work is to provide a quantitative study of the collider phenomenology of a typical event involving the GeV scale sector and resulting in lepton jets. We consider the minimal scenario whereby the SM sector and the dark sector are coupled only via kinetic mixing terms as detailed below. Effectively, dark sector fermions and scalars have a small coupling to the Z^0 boson and the minimal supersymmetric standard model (MSSM) bino, while the dark sector gauge boson couples weakly to the SM elec-

tromagnetic current. As a result of these couplings, a typical event factorizes into three modular stages, which are illustrated in Fig. 7.1:

- **Electroweak Production**

Once Z^0 bosons and electroweak-inos are produced, they decay into the dark sector via the aforementioned coupling. Rare Z^0 decays and electroweak-ino pair production are the cleanest channels in which to observe the production of dark sector states due to the limited hadronic activity. Decays into the dark sector depend weakly on the dark sector details.

- **Dark Sector Evolution**

Once the electroweak states have decayed into the dark sector, the resulting dark states are highly boosted and cascade decay down to the bottom of the dark sector spectrum. A universal feature of these dark matter scenarios is that there is log enhanced soft emission of dark gauge bosons, which increases the multiplicity of light dark sector states and ultimately yields a greater number of final state leptons. We simulate these dark sector showers and discuss their characteristics.

- **Outgoing Lepton Jets**

Cascade decays and soft emissions through the dark sector result in radiated dark gauge bosons which return to the visible sector as collimated lepton jets. After studying the shape and distribution of simulated lepton jets and taking into account the possible dilution and contamination from the decay of the dark bosons into pions, we suggest a concrete definition for a lepton jet which can be used in inclusive experimental searches for these objects. While much of the phenomenology we consider is independent of the details and spectra of the particular dark sector model, this is not the case for the bottom of the dark sector spectrum, which may be probed by studying lepton jet shapes.

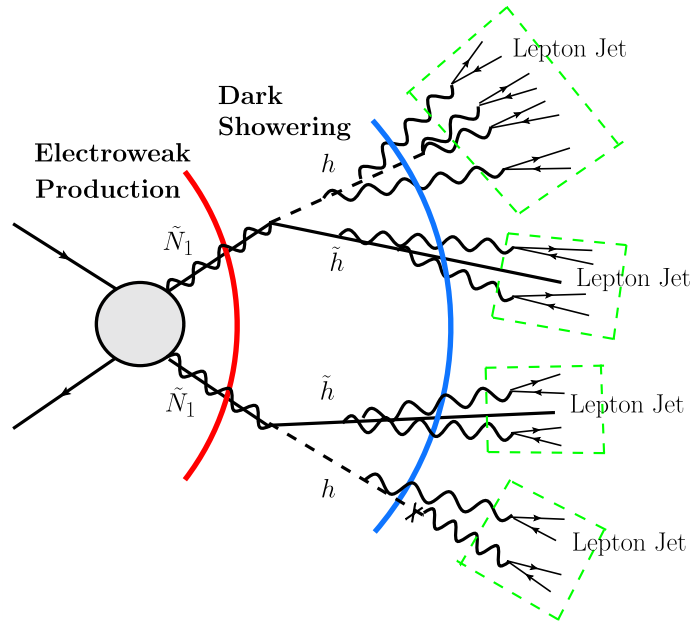


Figure 7.1: A schematic illustration of the type of events we consider in this work. The time evolution can be divided into three stages: electroweak boson or -ino production and subsequent decay into the dark-sector, evolution through the dark sector, and finally the formation of lepton jets, as delineated by the dashed boxes. Such events may also include missing energy.

In section 7.2 we review how the dark sector couples to the visible sector and discuss the production of dark sector states in rare Z^0 decays at LEP, the Tevatron and the

LHC. We also consider electroweak-ino pair production at the Tevatron and LHC. In section 7.3 we consider the evolution in the dark sector which includes dark showering and cascade decays in the dark sector itself. Section 7.4 begins with an analysis of the final state leptons and the formation of lepton jets and ends with some proposals for experimental searches. Section 7.5 contains our conclusions.

7.2 Electroweak Production

Let us first review how the visible sector and dark sector are coupled. For a detailed treatment, see [1]. As in [20], we assume the existence of a new dark gauge group which contains a $U(1)$ factor that is spontaneously broken at $\sim \text{GeV}$. The associated dark gauge boson kinetically mixes with the SM photon and the Z^0 vector-boson. We parameterize these couplings as

$$\mathcal{L}_{\text{gauge mix}} = -\frac{1}{2}\epsilon_1 b_{\mu\nu} A^{\mu\nu} - \frac{1}{2}\epsilon_2 b_{\mu\nu} Z^{\mu\nu} \quad (7.2.1)$$

$$= -\frac{1}{2}\epsilon'_1 b_{\mu\nu} B^{\mu\nu} - \frac{1}{2}\epsilon'_2 b_{\mu\nu} W_3^{\mu\nu} \quad (7.2.2)$$

where $b_{\mu\nu}$ denotes the field strength for the dark gauge boson and $\epsilon_{1,2}$ and $\epsilon'_{1,2}$ are related by the Weinberg angle. In particular, when only ϵ'_1 is present, we have $\epsilon_1 = \epsilon'_1 \cos \theta_W$ and $\epsilon_2 = \epsilon'_1 \sin \theta_W$. The first parameterization (mass basis) is more useful when discussing SM processes while the second (gauge basis) comes in handy when considering the MSSM¹. With the addition of supersymmetry, the above coupling implies a kinetic mixing between the dark bino, \tilde{b} and the MSSM gauginos, \tilde{B} and \tilde{W}_3 :

$$\mathcal{L}_{\text{gaugino mix}} = -2i\epsilon'_1 \tilde{b}^\dagger \bar{\sigma}^\mu \partial_\mu \tilde{B} - 2i\epsilon'_2 \tilde{b}^\dagger \bar{\sigma}^\mu \partial_\mu \tilde{W}_3 + \text{h.c.} \quad (7.2.3)$$

The gauge and gaugino kinetic mixings can both be eliminated by a set of field redefinitions which induce the portal to the dark sector which will be relevant to this collider

¹The operator involving W_3 is not gauge-invariant with respect to $SU_L(2)$. It should be thought of as the result of a higher dimensional operator $b_{\mu\nu} \text{tr}(H^\dagger W^{\mu\nu} H)/\Lambda^2$, where Λ is some high-scale. After the higgs condenses one obtains an effective mixing between $b_{\mu\nu}$ and $W_{3\mu\nu}$.

study:

$$\mathcal{L}_{\text{portal}} = \epsilon_1 b_\mu J_{\text{EM}}^\mu + \epsilon_2 Z_\mu J_b^\mu + \epsilon'_1 \tilde{B} \tilde{J}_{\tilde{b}} + \epsilon'_2 \tilde{W}_3 \tilde{J}_{\tilde{b}} \quad (7.2.4)$$

$$J_b^\mu = g_d \sum_i q_i \left(i(h_i^\dagger \partial^\mu h_i - h_i \partial^\mu h_i^\dagger) + \tilde{h}_i^\dagger \bar{\sigma}^\mu \tilde{h}_i \right) \quad (7.2.5)$$

$$\tilde{J}_{\tilde{b}} = -i\sqrt{2}g_d \sum_i q_i \tilde{h}_i^\dagger h_i \quad (7.2.6)$$

where J_{EM} is the SM electromagnetic current and J_b and $\tilde{J}_{\tilde{b}}$ are the bosonic and fermionic components of the dark gauge current. In particular, J_b contains dark scalar and dark fermion bilinears, while $\tilde{J}_{\tilde{b}}$ contains mixed dark scalar-fermion bilinears.

Since the dark sector scalars and fermions couple to the Z^0 boson and the MSSM bino, they will be produced in rare Z^0 decays and electroweak-ino decays, which we now consider in detail.

I. Rare Z^0 Decays

The strongest bound on kinetic mixing with a new $\sim \text{GeV}$ scale vector-boson comes from the muon $g - 2$ ratio [35], which constrains the photon mixing to be

$$\epsilon_1^2 \lesssim 3 \times 10^{-5} \frac{m_b}{100 \text{ MeV}} \quad (7.2.7)$$

On the other hand, the branching ratio of Z^0 into a pair of dark fermions charged under the dark gauge group is fixed by the mixing parameter, ϵ_2 , which is not directly limited by this bound and can be somewhat larger. The branching fraction of Z^0 to dark fermions is

$$\text{BR}(Z \rightarrow f\bar{f}) = \frac{\epsilon_2^2 g_d^2 M_{Z^0}}{12\pi \Gamma_{Z^0}} \quad (7.2.8)$$

while the branching fraction into a pair of dark scalars is a quarter of this. This has implications for LEP, as well as the Tevatron and LHC:

LEP: With a nominal value of $\alpha_d = \alpha_{\text{EM}}(M_Z)$ and $\epsilon_2^2 = 10^{-4}$ the 17M on-shell Z^0 bosons produced at LEP [201] will yield about 150 events of dark fermion pairs. While the LEP data can at the very least place stronger bounds on the couplings, it is not clear that existing searches covered the type of event topologies involved. Collimated leptons

coming off of dark sector states may have been missed in exclusive searches requiring isolated leptons.

Tevatron and LHC: The cross-section for production of a pair of dark sector states off the Z^0 at Tevatron and LHC is shown in Fig. 7.2. To a good approximation, the interfering diagram involving an off-shell dark vector-boson can be neglected since it produces final states which are too soft. With several fb^{-1} of data, the Tevatron can already probe this production channel for $\text{BR}(Z^0 \rightarrow \text{dark sector}) > 10^{-6}$. The LHC should be sensitive to the same parameter region with several hundreds pb^{-1} of data.

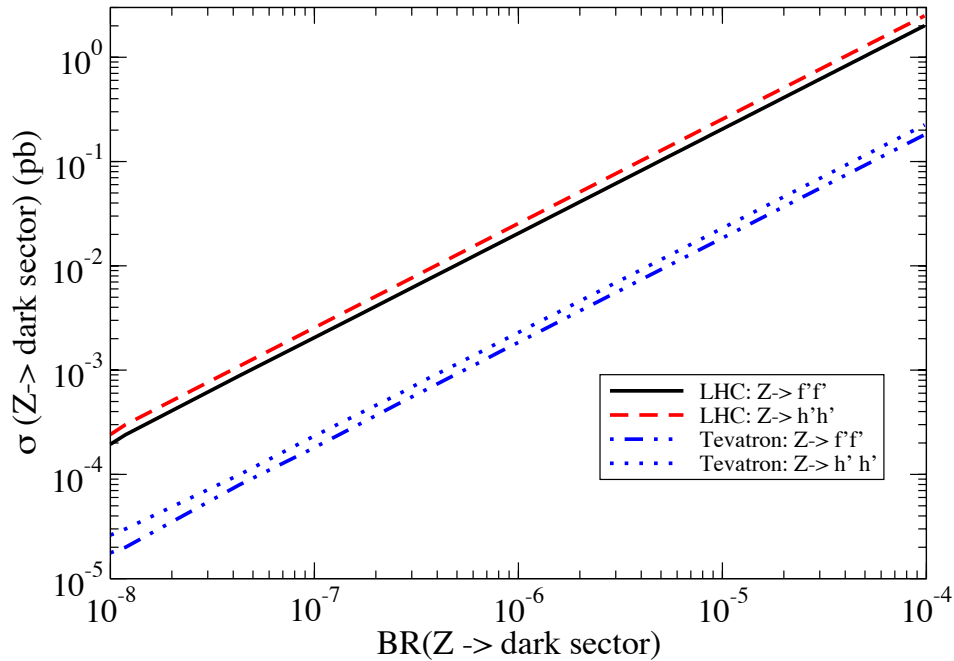


Figure 7.2: The cross-section for production of dark sector states via Z^0 as a function of the branching ratio for both the Tevatron and LHC. The vertical green dashed lines mark the branching ratio for $\epsilon_2 = 10^{-3}, 10^{-2}$, and 10^{-1} from left to right, using Eq.(7.2.8) with $\alpha_d = \alpha_{\text{EM}} = 1/127$.

II. Electroweak-ino Pair Production

Electroweak-ino pair production is well understood and has been discussed extensively in the literature. In particular, the tri-lepton final state with its low SM background offers one of the better discovery channels for the conventional MSSM [202].

In order to minimize the hadronic activity it is useful to focus on the production of colorless particles. While strong production channels yield much larger cross-sections, they result in more complicated events. At this early stage of the investigation, we prefer to concentrate on the lepton jets by themselves. At the Tevatron and LHC, the colliding particles certainly carry color, so the possibilities are few. One possibility is the Drell-Yan production of sleptons. Another is the pair production of electroweak-inos, which are superpositions of winos, binos, and higgsinos. After these -inos are produced, they will promptly cascade decay through the visible sector until they reach the lightest superpartner of the MSSM, which in turn decays into dark sector superpartners. The precise details of the MSSM cascade depend on the exact MSSM spectrum², but we will assume that it only produces isolated leptons, as is the case for example in decays of the chargino to the neutralino.

We divide the electroweak production channels into three categories, neutralino-pair, chargino-pair, and neutralino-chargino associate production. In Figs. 7.3 and 7.4 we depict the production cross-sections for the different pure gaugino states at the Tevatron and LHC, respectively. The purpose of these graphs is to give an estimate for the cross-sections involved for general MSSM spectra rather than concentrate on a particular benchmark scenario. In the case of neutralino pair production, the pure bino and wino states are produced only through a t-channel exchange of a squark, and their production cross-section is therefore suppressed compared with the higgsino state which enjoys its coupling to the Z^0 . Charged wino pair production has a much larger cross-section due to the large coupling of charged winos to the electroweak vector-bosons. For the purpose

²In this work, we will limit ourselves to no more than a single step by assuming that the spectrum contains at most one additional ino below the ones produced. It is important to realize that since DM is no longer associated with the MSSM per say, any of the MSSM sparticles can be the lightest as long as it is unstable and can decay into the dark sector.

of computing the neutralino-chargino associate production we assume a degeneracy between the charged and neutral state, however, in realistic spectra those are usually split and the cross-sections are somewhat modified.

Both Tevatron and early LHC data should be sensitive to large parts of the parameter space. It is clear that generically, -ino production is dominated by channels with at least one chargino. This fact has important implications on the type of event topologies we can expect to encounter in association with lepton jets. As the chargino cascades down to the lightest neutralino it will emit a hard isolated lepton or other SM particles as we now discuss.

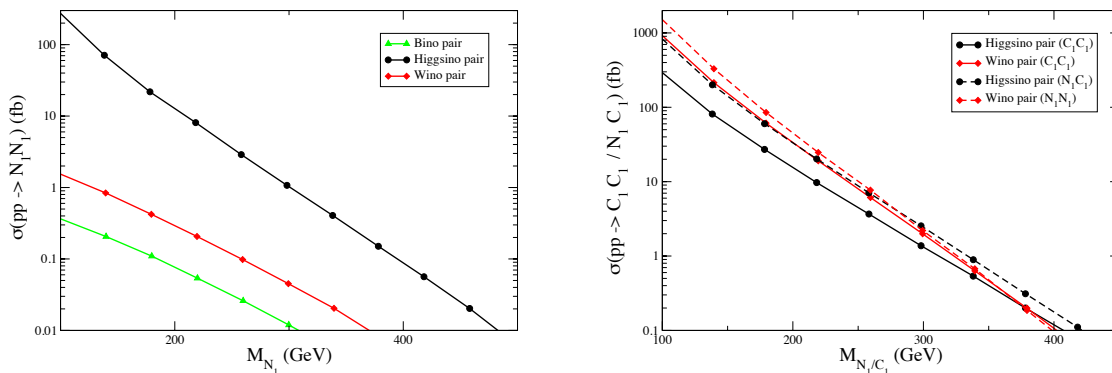


Figure 7.3: Production cross-sections for the different ino states at the Tevatron. The left pane includes neutralino pair production for the different gauginos. The right pane shows chargino pair production as well as neutralino-chargino associated production. A squark mass of 750 GeV was assumed. Cross-sections were computed with Pythia [62].

III. Neutralino Decays into the Dark Sector

Once produced, electroweak-inos will promptly cascade down to the lightest neutralino, \tilde{N}_1 . In the process, they may emit leptons, quarks, or Z^0/W^\pm (on-shell or off-shell) depending on the precise MSSM mass spectrum. Therefore, some of the events contain

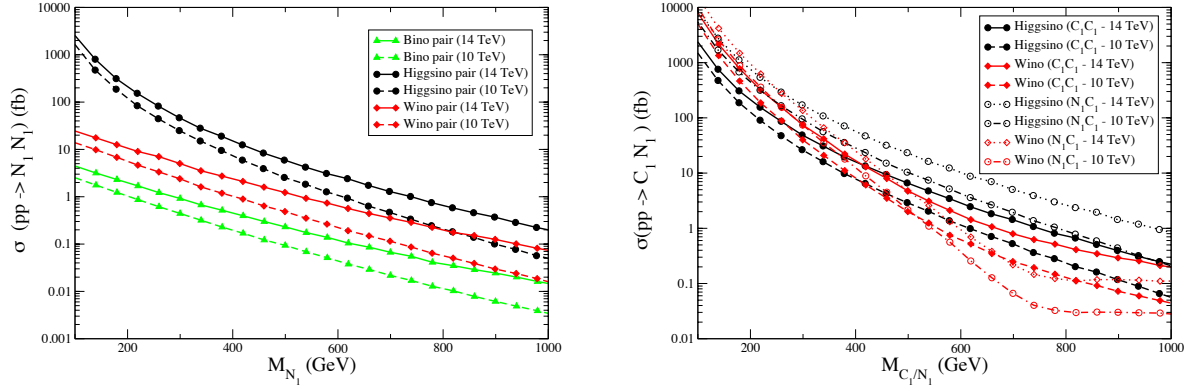


Figure 7.4: Same as Fig. 7.3, but for the LHC with center of mass energy of 14 TeV as well as 10 TeV.

isolated leptons in addition to the lepton jets generated at a later stage of the event. Such isolated leptons should not cause any complications in a properly inclusive search. The cascades to \tilde{N}_1 may also result in colored particles and hence QCD-jets, but for the purpose of the current study we will assume that a substantial fraction of such cascades result in no colored particles. This is not a strong assumption as it is satisfied in many concrete examples of MSSM spectra [203], and may even be discarded altogether in actual lepton jet searches including QCD-jets.

The couplings in eq. 7.2.4 imply that the lightest neutralino decays into the dark sector via its bino or wino fraction. The higgsino state is rendered unstable through its mixing with the wino and bino, as depicted in Fig. 7.5. The complex scalar fields shown in this figure are dark gauge eigenstates separated into real and imaginary parts. The precise linear combinations of fields which define the mass eigenstates are described in the appendix. In particular, one combination is the eaten goldstone boson of the dark gauge symmetry. As we will see, it is conceptually simpler to work in the gauge basis, especially when describing the ensuing radiation.

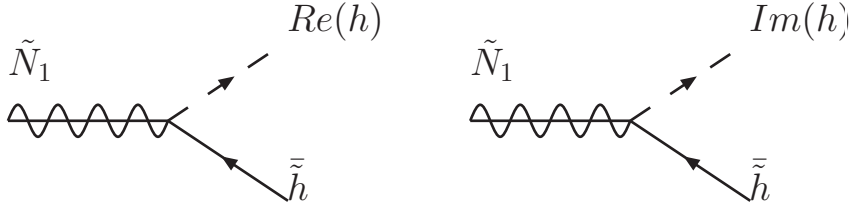


Figure 7.5: The MSSM neutralino can decay to the light elements in the dark sector. We distinguish between the real and imaginary part of the dark higgses, because one linear combination is in fact the goldstone boson eaten by the broken dark gauge group. Thus, it can decay directly into lepton pairs while the other higgses cannot.

The event shape is determined to a large degree by production, since the electroweakinos are produced almost at threshold. Therefore, the lightest neutralino \tilde{N}_1 is **not** very boosted in the lab frame and so its decay products are **not** collimated. Each of the two neutralinos gives off a pair which yields a total of four highly-boosted dark sector particles which are well-separated in the lab frame. They form the seeds of the dark showers described in the next section. The final outgoing lepton jets will consist of some isolated leptons coming from the electroweak-ino cascades together with up to four lepton jets created by the boosted dark sector states.

We conclude this section by considering some special cases in which the decay into the dark sector proceeds slightly differently, resulting in alternative final configurations. For instance, in low-scale SUSY breaking scenarios, the gravitino is light and so the lightest neutralino can decay into a gravitino with the emission of a real photon. This process competes with neutralino decays into the dark sector. Generally, those two decay rates are vastly different [1], but in some instances they may be comparable [204]. If so, the events will contain a single hard photon, lepton jets and possibly other isolated leptons. This topology was the basis for a recent analysis looking for lepton jets in the Tevatron [205].

Second, there are cases where the degeneracy between the charged and neutral winos is lifted only by electromagnetic loop corrections, as is the case for instance in anomaly mediated supersymmetry breaking. The decay $\tilde{W}^\pm \rightarrow \tilde{W}^0 + \pi^\pm$ proceeds with an approx-

imate lifetime of 10^{-10} sec and results in a displaced vertex. Thus, the lepton jets that emerge out of the decay of \tilde{W}^0 into the dark sector reconstruct this displaced vertex and are themselves displaced. We do not consider such scenarios further in this work, but only comment that lepton jets with displaced vertices may require special consideration when designing an experimental search because triggers usually assume the leptons to come from the primary interaction point³.

7.3 Dark Sector Dynamics

In this section we discuss the evolution of dark sector states that arise from visible sector decays. As observed in [1] these states can seed long cascades if the dark sector happens to have a rich particle spectrum. Such a scenario is generic if the dark sector has non-abelian gauge dynamics. Along and at the end of these cascades, numerous leptons are produced from the resulting dark gauge bosons, yielding highly collimated lepton jets. A primary observation of this chapter is that dark sectors with relatively sparse spectra, for example abelian theories, also provide a sizeable production of lepton jets due to soft particle emission.

To see this, consider the scenario described in the previous section, where each neutralino arising from a supersymmetric cascade in the visible sector decays into a well-separated and boosted dark scalar and fermion pair. Each of these carries an energy of roughly half the neutralino mass (~ 100 's GeV). Furthermore, since these dark sector states are so highly boosted (and have mass \lesssim GeV) they will radiate soft and collinear dark photons with high probability [108, 80]. Each dark photon brehmsstrahlung eventually decays into a pair of leptons, and contributes substantially to the final lepton multiplicity of the resulting lepton jet. This part of the evolution is universal and depends only very weakly on the precise details of the symmetry breaking.

Once the shower completes, we dress the dark scalars and fermions with the proper mass eigenstates as detailed below in section II.. Depending on the final state, there may or may not be a pair of leptons at the termination point of the dark sector cascade. For

³We thank Roger Moore for pointing this out to us.

example, if the final state is the eaten goldstone boson of the dark symmetry breaking, then it will decay to a lepton pair directly. If instead it is a scalar which lacks a direct coupling to leptons, then it decays through an intermediate (on-shell or off-shell) dark vector-boson (see Fig. 7.8).

In this section we discuss each stage of the dark sector evolution: showering, dressing, and their combined effect on the structure of the lepton jet. For our analysis we employ the simple abelian model described in the appendix with the necessary field content to spontaneously break the dark gauge symmetry. As such, much of the abelian model phenomenology is indicative of a broad class of models, including more complicated extensions such as non-abelian theories.

I. Dark Showering

Decays into the dark sector produce highly boosted dark particles which radiate soft dark photons. The number of photons radiated off a dark higgs, h , or dark higgsino, \tilde{h} , can be understood parametrically in terms of the Sudakov double logarithm:

$$N_{b_\mu} \sim \frac{\alpha_d}{2\pi} \log \left(\frac{M_{\text{EW}}^2}{M_{\text{dark}}^2} \right)^2 \simeq 1.4 \left(\frac{\alpha_d}{0.1} \right) \quad (7.3.9)$$

which is the expected number of soft dark photon emissions occurring within an energy window defined by M_{dark} and M_{EW} . More precisely, M_{EW} is the invariant mass of the initial dark sector state, for example the mass of the Z^0 or \tilde{N}_1 that decays into the dark sector, and M_{dark} is the the scale of dark sector masses, which regulates the soft and collinear divergences. For the estimate in the final step of Eq. (7.3.9), we have taken $M_{\text{EW}}/M_{\text{dark}} \sim 10^2$. For $M_{\text{dark}} \sim \text{GeV}$, the only parameters that determine the amount of showering are therefore α_d and $M_{\tilde{N}_1}$. Since the ratio of scales, $M_{\text{EW}} \gg M_{\text{dark}}$, is independent of the details of the GeV-scale spectrum, showering is a universal process. Furthermore, due to the logarithmic enhancement, it is clear that showering is an $\mathcal{O}(1)$ effect, even for weakly coupled $U(1)_d$.

In order to perform a detailed study of dark sector evolution, we have implemented the virtuality ordered parton shower employed by Sherpa [206] and Pythia [62]. This algorithm is given by the repeated application of the following: 1) given an on-shell

“mother” particle, sample the Sudakov form factor to obtain the mother’s new virtuality t and the energy fraction z (and $1 - z$) going to each of its daughters, and 2) re-shuffle kinematics to be consistent with four-momentum conservation. We use the kinematic expressions of [207]. For a substantially more detailed description of the virtuality ordered parton shower, refer to the above references.

For a weakly coupled dark sector with a GeV-scale mass gap, we have found several simplifications to the parton shower which have little effect on lepton jet observables. First, we note that the dark shower is dominated by splitting functions with both a soft and collinear divergence, $h \rightarrow h\gamma'$ and $\tilde{h} \rightarrow \tilde{h}\gamma'$. Other splittings are only enhanced by the collinear log, and therefore constitute a $\lesssim 10\%$ effect. Second, massive splitting functions and the precise GeV-scale virtuality cutoff have little effect. This is because the amount of radiation depends only logarithmically on M_{dark} . We have found that varying the virtuality cutoff of the shower by an order of magnitude around a GeV only has a noticeable effect on the p_T distribution of radiated dark photons for $p_T \lesssim 5$ GeV, where the dependence is $\mathcal{O}(1)$. Third, the running of the dark gauge coupling is negligible, since the theory is weakly coupled in the relatively small range between M_{EW} and M_{dark} , and also constitutes a $\lesssim 10\%$ effect on the amount of showering. Based on the above discussion, we adopt several simplifications for what follows, allowing us to keep the showers as model independent as possible. In particular, we only include splitting functions that are double log enhanced, we neglect massive splitting functions and fix the virtuality cutoff to 1 GeV, and we neglect the running of the dark gauge coupling.

Lastly, we mention a notable difference between abelian and non-abelian theories pertaining to angular ordering. In particular, consider a soft emission of the form $A \rightarrow BC$. In the case that B and C are both charged (for instance in a non-abelian theory), then any subsequent soft emission at large transverse wavelength from either B or C is suppressed by a Chudakov-like effect. This is due to interference in the matrix element, and is simulated in virtuality ordered parton showers by enforcing ‘angular ordering,’ where subsequent emissions are required to occur at smaller opening angles than prior emissions. In our case, however, the theory is abelian, and the dominant process consists

of a hard dark-charged h or \tilde{h} line emitting dark photons. Since dark photons are neutral, there is no suppression arising from angular ordering.

In Fig. 7.6 we present the average number of radiated dark photons in rare Z^0 decays and neutralino pair production events. The amount of radiation increases with the dark coupling as can be expected. It also increases with larger neutralino mass since the initial dark higgs and higgsinos are more energetic. In Fig. 7.7 we plot the p_T distributions for the radiated photons for different parameters.

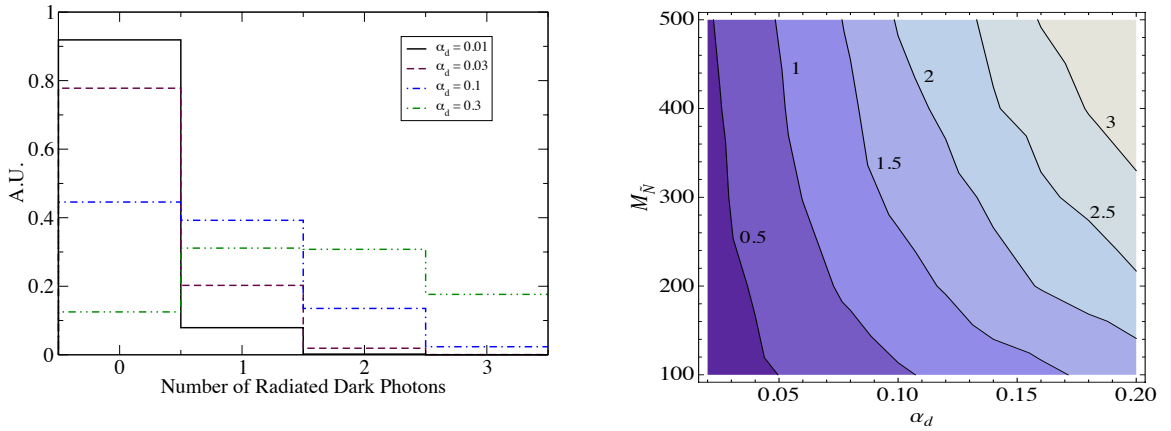


Figure 7.6: On the left we depict the normalized distributions for the expected number of radiated dark photons in rare Z^0 decays into the dark sector. On the right is a contour plot of the number of soft dark photon emissions per neutralino as a function of the dark gauge coupling α_d and the neutralino mass $M_{\tilde{N}}$. The linear dependence on α_d and logarithmic dependence on $M_{\tilde{N}}$ is in accord with the naive expectation, Eq. (7.3.9). The plots were produced using a 3 GeV p_T cut on the dark photons. Both plots are for LHC at 10 TeV center of mass energy.

Altogether, the effects of radiation in rare Z^0 decays into the dark sector are rather mild. The energy scale involved is somewhat lower as compared with neutralino pair

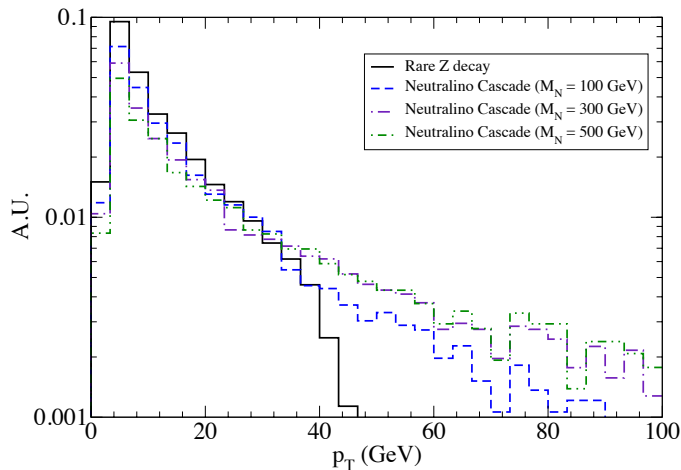


Figure 7.7: The p_T distribution of radiated dark photons for rare Z^0 decays and neutralino cascades.

production and subsequently the radiation is softer and less pronounced. On the other hand, for neutralino cascades into the dark sector the effects of radiation are important. The presence of these extra radiated photons modifies and enriches the structure of the resulting lepton jets as we discuss in the next section.

II. Decay of dark states back into leptons and pions

Once the virtuality reaches the dark state's mass ($\sim \text{GeV}$) no further radiation is possible and the state is placed on-shell. At this point, it may decay back into light standard model particles such as leptons and pions⁴ via the kinetic mixing operators, Eq. (7.2.1). The characteristics of the decay depend on the identity of the dark particle involved since not all are directly mixed with the standard model. For illustrative purposes we consider the two dark scalar model presented in the appendix, in which case the bosonic spectrum consists of a heavy dark higgs, H_d , a dark pseudo-scalar a_d , a dark vector-boson b_μ and a

⁴In what follows we mention leptons only for the sake of brevity, but pions are also possible. We discuss this issue more carefully below.

lighter dark higgs h_d . The fermionic spectrum might involve the superpartners of these particles, the dark higgsinos and gauginos.

Since only b_μ mixes with hypercharge, it alone can decay directly into leptons. H_d on the other hand we take to first decay into two on-shell b_μ 's which later also decay, resulting in 4 leptons. h_d can also decay through two b_μ 's, but if it is lighter than the dark vector-boson then the decay is off-shell and results in a very long lifetime [1, 208]. This typically means that h_d escapes detection and is counted as missing energy. The pseudo-scalar, a_d , can typically decay into h_d and two leptons through either on-shell or off-shell b_μ . These different decay modes are shown in Fig. 7.8. While the specifics of the decay are fairly model dependent, we believe that the resulting phenomenology it describes is fairly universal in that each dark particle can do one of three things: 1) decay into an even multiplicity of leptons (2,4,6 . . . leptons); 2) constitute missing energy; 3) a combination of the two.

In the next section we analyze the structure of lepton jets that results from the decay of the dark states back into leptons. The lepton jets are produced by first simulating the hard production process, followed by the decay into the dark sector, followed by a simulation of the dark radiation. Finally, in the last step we randomly assign the bosons to H_d , b_μ , a_d , or h_d and decay them accordingly, thus producing lepton jets. We take the dark fermions to be stable and only account for their radiation.

III. Lepton jets' morphology

Before moving on to discuss the results of the simulations, we briefly discuss the qualitative differences between the resulting lepton jets and the type of jets one can expect from QCD. Lepton jets differs from QCD jets by both composition and shape.

The composition of the lepton jet is affected by the ratio of electrons/muons to pions which is determined by the decay modes of the dark vector-boson. The decay branching ratio of the vector-boson b_μ into pions is dictated by the electromagnetic form-factor at $q^2 = m_b^2$, also known as the R ratio [209]. If the vector-boson mass is very close to the ρ -meson resonance, then its decay is mostly into pions and speaking of "lepton jets" is not very appropriate. In general, however, a sizable branching fraction into leptons can

be expected and in what follows we consider several benchmarks with different branching fractions ($\text{Br}(b_\mu \rightarrow \pi^+\pi^-) = 1/7, 1/3, 3/5$ and taking the muon vs. electron branching fraction to be equal.). This is an important effect to model because pion contamination will reduce the efficiency for lepton jet searches with hadronic isolation cuts as we discuss in the next section.

Regarding the shape of lepton jet, they are usually made of a "hard core" of tightly packed high energy leptons coming from the primary dark bosons, and a "soft-shell" of somewhat sparse and less energetic lepton pairs coming from dark radiation. This configuration is quite different from usual QCD jets and can be used to search for this objects as we discuss in the next section. The "soft-shell" itself may contain additional discriminating power. Since the dark photon is relatively light \lesssim GeV, even the soft radiation usually results in fairly collimated leptons. We therefore expect the pattern of energy deposition in the "soft-shell" to be of fairly isolated hits.

It is important to realize that there are certain regions of parameter space where the resulting jets look very similar to QCD jets and their discovery is difficult at best. As we just mentioned, when the dark vector-boson mass is very close to the ρ -meson mass, it decays mostly into pions. If the dark coupling is very large, radiation is a substantial effect which will smear out the distinction between the "hard core" and "soft shell". In this case, the resulting jets resemble QCD jets in both composition (mostly mesons) and shape (smeared energy deposition). That said, in most other parts of parameter space, lepton jets are sufficiently different from QCD jets by both composition and shape that their discovery should be possible.

7.4 Lepton Jets and Experimental Searches

In this penultimate section we present the results of simulations for the different processes discussed above. Production of the dark states was simulated using Madgraph [210]. The later cascade and decay back into the SM was simulated with a private code using Mathematica.

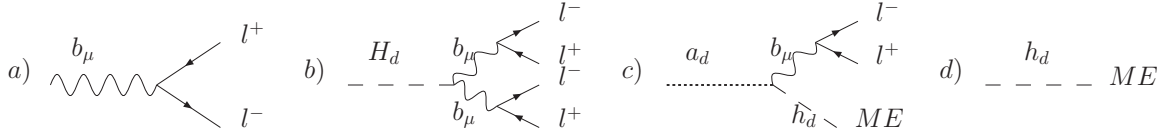


Figure 7.8: The different decay modes associated with the dark bosons: a) b_μ direct decay into leptons through kinetic mixing; b) H_d decays into two on-shell b_μ which then decay into two leptons each; c) a_d decays into h_d and dileptons through an on-shell or off-shell dark vector-boson depending on the detailed spectrum; d) h_d if lighter than the other bosons typically decays outside the detector and constitutes missing energy.

I. Lepton jets from rare Z^0 decays

As discussed in the previous section, the effects of dark radiation in the case of rare Z^0 decays into the dark sector are mild with possibly one radiated dark photon in a fraction of the events (left pane of Fig. 7.6). The structure of the lepton jets in this case is therefore straightforward to understand. If the decay is into dark fermions, the event contains large amounts of missing energy and possibly one or two dileptons from the fermions cascade. On the other hand the decay into dark bosons lead to 4 distinct topologies. Assuming CP conservation, the Z^0 must decay into one CP-even and CP-odd boson. On one side of the event we can expect either b_μ or a_d and on the other side H_d or h_d . Their decays are depicted in Fig. 7.8 and the corresponding lepton jets are comprised of 2 or 4 collimated leptons with some of the events containing missing energy. Radiation will increase the lepton multiplicity in some of the events, but should not substantially affect the event topology and lepton jet structure. We consider this an important channel for lepton jet searches since it is rather clean with a simple event topology as depicted on the left of Fig. 7.9.

II. Lepton jets from neutralino cascades

In the case of neutralino cascades, shown on the right of Fig. 7.9, the effects of dark radiation are more substantial. If not for radiation, one would expect two clean lepton

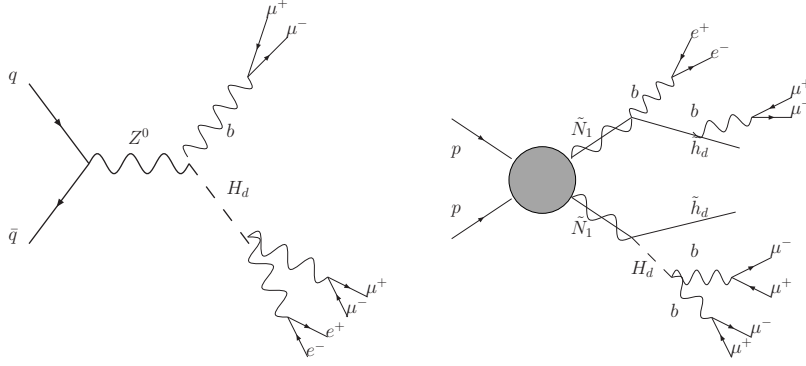


Figure 7.9: The event topologies discussed in section 7.4. On the left we depict a rare Z^0 decay into dark states which subsequently decay as in Fig. 7.8. This would result in two isolated lepton jets recoiling against each other. On the right is a neutralino pair production event with the neutralino ultimately decaying into the dark sector. We allow the dark bosons to decay as usual, but keep the dark fermions stable, aside from possible radiation. The events therefore consist of 2 hard lepton jets, missing energy, and softer leptons coming from radiation of the dark fermions (radiation from the dark bosons would normally be clumped together with the harder leptons coming from the cascade.).

jets in almost every event, coming from the scalars decaying into leptons (with the exception of h_d which would constitute missing energy, and any decays involving pions). Including radiation, the dark fermions may also produce lepton jets (albeit softer) which would increase the lepton jet multiplicity. On the other hand, dark radiation might also deteriorate the signal. In particular, a justified concern is the pollution of lepton jets by pions coming from radiated dark photons. Such contaminants will make the distinction between lepton jets and QCD-jets difficult.

In order to investigate these effects in detail, we simulated the entire process, starting from production, going through the dark states' radiation and cascade, and ending with the decay back into leptons and pions. We assume that the neutralino always decays into the dark sector via its coupling to the dark current, Eq. (7.2.4). In simulating the cascades we included all 4 decays shown in Fig. 7.8 in equal proportions and kept

the dark fermions stable. The results are presented in Tables 7.1 and 7.2 where we present the probability of finding clean lepton jets per event for different values of the dark gauge-coupling and the branching ratio into pions. Clean lepton jets are defined as follows: at least two leptons with $p_T > 10$ GeV each in a cone of $\Delta R < 0.1$ with hadronic *and* leptonic isolation of $\sum p_T < 3$ GeV in $0.1 < \Delta R < 0.4$. The number in brackets represents the same probability, but where leptonic isolation has been removed and only hadronic isolation is required. Not surprisingly, the efficiency without lepton isolation is higher compared with the case where isolation is required. This is especially so when α_d is large and more radiation is expected in the isolation annulus. This effect may be important when looking for light sectors which are strongly coupled and radiate copiously. On the left of Fig. 7.10 we show the differential lepton jet number per event as a function of the lepton jet p_T . As the dark coupling increases, the p_T tends to decrease since the stronger radiation dilutes the hard core of the lepton jet. On the right of Fig. 7.10 we depict the missing energy distribution in these events. It depends strongly on the mass of the neutralino and only weakly on the dark gauge coupling.

The probability of finding lepton jets decreases with increasing dark gauge-coupling since more radiation results in a lower average p_T and softer leptons. A larger branching ratio into pions tends to pollute the lepton jets. At $\text{Br}(b \rightarrow \pi^+\pi^-) = 3/5$, for example, it becomes very unlikely to observe more than one lepton jet per event. The probability of observing more than two lepton jets is rather small throughout the parameter space and is not depicted. However, it is important to realize that this is to some extent a consequence of the strict definition of clean lepton jets. Such a strict definition is probably necessary to trigger and search inclusively for the harder lepton jets, but it may be desirable to relax the requirements somewhat for the other lepton jets in the events. In Fig. 7.11 we plot the probability of finding more than one lepton jet as a function of the p_T cut on the second hardest lepton in the jet.

Another important characteristic of a lepton jet is its lepton multiplicity. Higher multiplicity helps with background rejection since few standard model processes can give more than 2 hard and collimated leptons. In Tables 7.3 and 7.4 we show the lepton multiplicity distribution in the hardest jet for different values of the gauge-coupling and

Lepton Jet Efficiencies						
$\alpha_d \backslash \text{Br}_{b \rightarrow \pi\pi}$	1 Lepton-Jet			2 Lepton-Jet		
	1/7	1/3	3/5	1/7	1/3	3/5
0	0.46 (0.46)	0.36 (0.36)	0.26 (0.26)	0.18 (0.18)	0.08 (0.08)	0.02 (0.02)
0.01	0.46 (0.47)	0.39 (0.39)	0.26 (0.26)	0.15 (0.15)	0.1 (0.11)	0.03 (0.03)
0.03	0.41 (0.42)	0.37 (0.37)	0.25 (0.26)	0.14 (0.17)	0.09 (0.1)	0.03 (0.03)
0.1	0.39 (0.41)	0.36 (0.37)	0.21 (0.24)	0.14 (0.18)	0.06 (0.1)	0.02 (0.02)
0.3	0.31 (0.38)	0.27 (0.37)	0.17 (0.25)	0.07 (0.21)	0.04 (0.11)	0.02 (0.03)

Table 7.1: Clean lepton jet efficiencies for different values of the dark gauge-coupling and $\text{Br}(b \rightarrow \pi^+ \pi^-)$. The neutralino mass was set to $\tilde{M} = 100$ GeV. For $\alpha_d = 0$ dark radiation was switched off. The number of lepton jets increases with α_d as radiation becomes more likely. The requirement for “clean” lepton jets, as described in the text, results in a decrease in efficiency with the growth of the branching ratio into pions. In brackets are efficiencies for the case where only hadronic isolation is required in the $0.1 < \Delta R < 0.4$ annulus. The statistical error on the efficiencies is ± 0.03

branching fraction into pions. A sizable fraction of the events ($\sim \mathcal{O}(10\%)$) have at least one lepton jet with 4 hard leptons in it coming mostly from H_d decay. The number of such lepton jets diminishes as the gauge-coupling increases because dark radiation pollutes the annulus $0.1 < \Delta R < 0.4$. This reduction is less significant if one removes the requirement of leptonic isolation in the $0.1 < \Delta R < 0.4$ region. In Fig. 7.12 we show the differential distribution of lepton jets with a given number of leptons as a function of p_T .

Lepton Jet Efficiencies						
	1 Lepton-Jet			2 Lepton-Jet		
$\text{Br}_{b \rightarrow \pi\pi}$ α_d	1/7	1/3	3/5	1/7	1/3	3/5
0	0.49 (0.49)	0.47 (0.47)	0.31 (0.31)	0.28 (0.28)	0.14 (0.15)	0.05 (0.05)
0.01	0.47 (0.47)	0.44 (0.45)	0.31 (0.32)	0.3 (0.31)	0.16 (0.16)	0.04 (0.04)
0.03	0.43 (0.41)	0.47 (0.48)	0.3 (0.3)	0.27 (0.3)	0.14 (0.16)	0.04 (0.05)
0.1	0.43 (0.39)	0.41 (0.44)	0.29 (0.32)	0.23 (0.3)	0.13 (0.18)	0.05 (0.07)
0.3	0.38 (0.32)	0.34 (0.36)	0.25 (0.34)	0.16 (0.3)	0.11 (0.22)	0.05 (0.09)

Table 7.2: Same as Table 7.1, but with $\tilde{M} = 300$ GeV

III. Experimental Searches

These findings suggest that it is possible to look for lepton jets in a fairly inclusive fashion and compel us to put forward some suggestions for such experimental searches. One such search was in fact already done in the Tevatron [200] where a fairly similar definition for lepton jets as the one discussed below was employed. We believe that many of the conclusions arrived at here will remain true and carry over in the case of a non-abelian dark gauge group as long as it does not condense. It is useful to try and arrive at some quantitative definition of a lepton jet and we suggest the following⁵:

Two or more leptons each with $p_T > 10$ GeV inside a cone of $\Delta R < 0.1$ with hadronic/leptonic isolation cut of $\sum p_T < 3$ GeV in an annulus of $0.1 < \Delta R < 0.4$ around the lepton jet.

We view this definition as a template to which more adequate figures can be added later once issues of backgrounds, triggering and other experimental difficulties are thoroughly analyzed and resolved. In particular, it will be important to bring the following parts under control:

1. “Two or more leptons” - Muons likely suffer from less background than electrons (either instrumental or physical) so we may require fewer of them than we do

⁵We thank the participants of Boost09 and especially, B. Demirkoz, A. Haas, R. Moore, P. Schuster, N. Toro, and J. Wacker for very fruitful discussions concerning these issues.

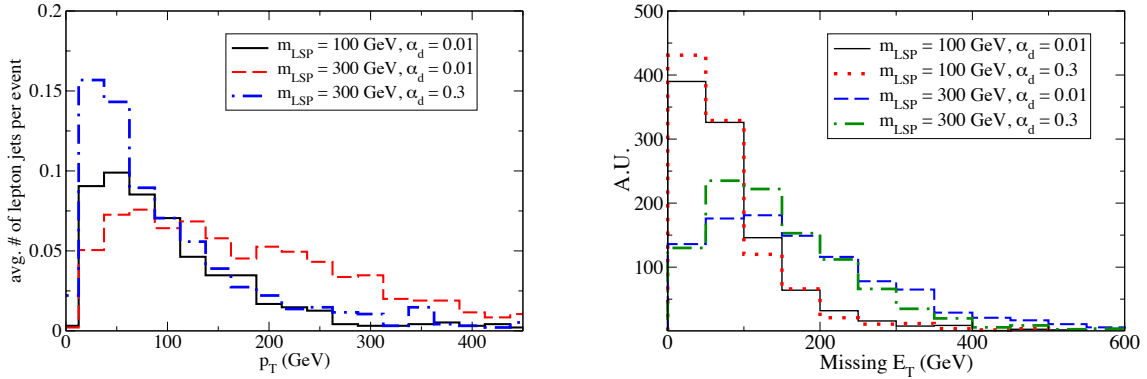


Figure 7.10: On the left pane we plot the differential lepton jet number per event as a function of their p_T for different values of the neutralino mass and gauge coupling. Increasing the mass tends to increase the average p_T as expected, while a larger gauge-coupling tends to soften it because more radiation is generated. On the right pane we show the missing energy distribution in the events. The distributions are fairly insensitive to the dark gauge coupling.

electrons. When only two hard leptons are present, one might demand the hardest two leptons to have the same flavor and opposite sign as this may prove useful in reconstructing the tracks as they separate in the magnetic field⁶. This might be more difficult to do in the case of H_d decay (or non-abelian scenarios) where more than one pair of hard leptons is expected.

2. “ $p_T > 10$ GeV” - This figure can be changed depending on the lepton species under consideration. Also, it may be refined to allow for a softer secondary lepton.
3. “ $\Delta R < 0.1$ ” - This figure may be tuned depending on the process under consideration and the expected size of the opening angle. Also, one may want to define a lower limit in order to reduce background.

⁶We thank Andy Haas for pointing this out to us.

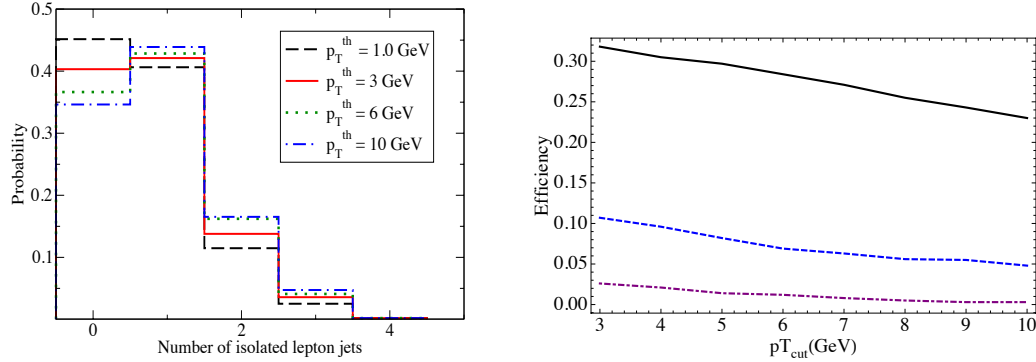


Figure 7.11: On the left pane we show the dependence of the lepton jet efficiency on the isolation cut $\sum p_T$. On the right pane we plot the efficiency for 2 (black-solid), 3 (blue-dashed), and 4 (purple-dotted) clean lepton jets as a function of the $p_{T_{\text{cut}}}$ of the second hardest lepton in the jet. The parameters used are $\tilde{M} = 300$ GeV, $\alpha_d = 0.1$, and $\text{Br}(b \rightarrow \pi^+\pi^-) = 1/7$. This plot shows that by lowering the p_T requirement on the second lepton in the lepton jets, one can increase the efficiency for their observation.

4. “ $\sum p_T < 3$ GeV” - A hadronic/leptonic isolation cut around the lepton jet core is necessary in order to fight background. It may be possible to relax the requirement for leptonic isolation if the background is not too large. The precise annulus in which this isolation cut is required (tentatively, $0.1 < \Delta R < 0.4$) should be thought of carefully especially since dark radiation leads to more dispersed lepton jets.
5. “around the lepton jet” - In this work we defined the cone as follows: We first used an iterative algorithm to build the lepton jet 4-vector. Starting with the hardest lepton we collected all leptons within $\Delta R = 0.1$ around it and added their 4-vectors to the lepton jet. This was repeated until no further leptons were found within $\Delta R = 0.1$ around the lepton jet 4-vector. This same 4-vector was then used to define the isolation cone $0.1 < \Delta R < 0.4$. This choice was motivated by the physics since the combined 4-vectors reconstruct the dark state. However, other definitions are possible, for example the one employed by Ref. [200] where several isolation cones were defined, one about each lepton in the lepton jet.

Lepton Multiplicity in Clean Lepton Jets									
	2 Leptons			4 Leptons			6 Leptons		
$\alpha_d \backslash \text{Br}_{b \rightarrow \pi\pi}$	1/7	1/3	3/5	1/7	1/3	3/5	1/7	1/3	3/5
0	0.41	0.31	0.21	0.22	0.13	0.06	0.	0.	0.
0.01	0.37	0.33	0.23	0.23	0.15	0.05	0.	0.	0.
0.03	0.33	0.31	0.22	0.2	0.14	0.06	0.01	0.	0.
0.1	0.29	0.26	0.18	0.18	0.12	0.04	0.02	0.01	0.
0.3	0.22	0.19	0.14	0.09	0.08	0.03	0.02	0.01	0.

Table 7.3: Lepton multiplicity in the hardest lepton jet for different values of the dark gauge-coupling and $\text{Br}(b \rightarrow \pi^+\pi^-)$. The neutralino mass was set to $\tilde{M} = 100$ GeV. Odd number of leptons is fairly unlikely since the vector-boson always decays into a pair of leptons.

6. Lepton jets can have a displaced vertex as well. This case should be carefully studied by itself since in general the trigger algorithms assume that electrons and muons have a track in the inner detector and therefore displaced lepton jets may fail to trigger⁷.

This definition is likely to be revised and modified once collider effects are studied and a better understanding of the different backgrounds is developed. Once a proper operational definition of a lepton jet is formed, and maybe several interesting subclasses are identified, it is possible to conduct inclusive searches for these objects:

1. Lepton jet recoiling against a QCD-jet would be an inclusive search for a prompt dark photon production [1].
2. Two lepton jets recoiling against each other and reconstructing the Z^0 would be an interesting signal of rare Z^0 decays into the dark sector and can be looked for at LEP, Tevatron, and LHC.

⁷We thank Roger Moore for pointing this out to us.

Lepton Multiplicity in Clean Lepton Jets									
	2 Leptons			4 Leptons			6 Leptons		
$\alpha_d \backslash \text{Br}_{b \rightarrow \pi\pi}$	1/7	1/3	3/5	1/7	1/3	3/5	1/7	1/3	3/5
0	0.49	0.44	0.29	0.28	0.17	0.07	0.	0.	0.
0.01	0.53	0.43	0.29	0.25	0.18	0.06	0.	0.	0.
0.03	0.47	0.46	0.29	0.26	0.16	0.06	0.01	0.01	0.
0.1	0.42	0.43	0.32	0.25	0.16	0.06	0.04	0.02	0.
0.3	0.35	0.38	0.34	0.21	0.11	0.05	0.07	0.04	0.01

Table 7.4: Same as Table 7.3, but for $\tilde{M} = 300$ GeV.

- Two (or more) lepton jets together with missing energy and possibly other isolated final states (e.g. a muon, an electron, and etc.) can be the result of electroweak-ino production and their eventual cascade into the dark sector.
- Lepton jets in association with QCD-jets could be the result of strong production of colored particles which eventually cascade into the dark sector. This production mode was not investigated in this chapter, but is important to investigate in future works on the subject since it enjoys a very large cross-section.

7.5 Conclusions

In this chapter we investigated the (supersymmetric) production of dark states through electroweak processes. We carefully included the dark radiation that accompanies highly boosted dark states as well as their cascade evolution back into leptons and pions. This allows for a more realistic characterization of the resulting lepton jets and their properties. In particular, we put forward an operational definition for lepton jets that should aid in performing inclusive searches for these objects. We simulated the relevant processes (without including detector effects) and conclude that the efficiency for identifying clean

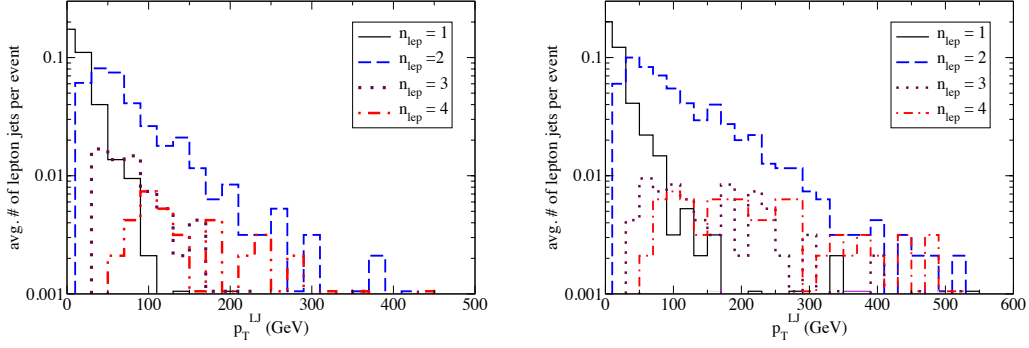


Figure 7.12: The average number of lepton jets with a given number of leptons in them $n_{lep} = 1, 2, 3,$ and 4 for $M_{\tilde{N}_1} = 100$ GeV (300 GeV) on the left (right) with $\alpha_d = 0.1$ and $\text{Br}(b \rightarrow \pi^+\pi^-) = 1/3$. Most lepton jets contain 2 leptons. The $n_{lep} = 1$ case does not really satisfy the requirements needed to be identified as a lepton jet, but is included here to illustrate that isolated leptons in those events are fairly soft. They originate from soft radiated dark photons which have decayed into two, fairly separated leptons. This does not include the possibility of a hard isolated lepton originating from chargino to neutralino cascade, a possibility which was not simulated here.

lepton jets is rather high throughout the parameter space, even when possible pollution from pions and other leptons is included.

The entire process depends on several disjoint assumptions and we have attempted to keep the discussion modular throughout. The production of dark states depends of course on the existence of the dark sector and its coupling to the standard model. The dark radiation is a result of the \sim GeV scale gauge group and depends on the gauge coupling and (logarithmically) on the energy carried by the dark states. The cascade back into the standard model depends on the details and spectrum of the dark sector which in this work we took to consist of two dark chiral multiplets (scalars and fermions). Finally, the decay branching fraction into pions vs. leptons is determined by the electromagnetic form-factor at the dark gauge-boson mass and we have modeled this effect by considering several pion branching fractions.

However, while our analysis depends on numerous assumptions, we believe that the resulting phenomenology is rather robust and depends mostly on the existence of such a light sector with a small, but not negligible, interaction with the standard model. As such, the present work should aid future searches for lepton jets in high energy colliders irrespective of the precise details of the light sector.

Hiding the Higgs with Lepton Jets

8.1 Introduction

Within the Standard Model (SM) the mass of the Higgs boson is constrained by the LEP experiments to be larger than 114.4 GeV [212]. This limit, however, varies in a model-dependent manner. For example, the limit can be relaxed if the production cross-section of the Higgs particle is suppressed. A more interesting possibility is that the *Higgs is hidden: it has been copiously produced at LEP and the Tevatron but has evaded detection due to non-standard decays*. There are at least two hints that the Higgs might be lighter than the naive LEP limit. On the experimental side, the best fit to electroweak precision observables corresponds to a Higgs mass of 80 GeV [213]. On the theoretical side, typical supersymmetric models require fine-tuning to accommodate a Higgs boson substantially heavier than m_Z .

The naive LEP limit on the Higgs mass is based on studies of the associated production of the Higgs and Z -boson, with the Higgs decaying to a pair of b quarks (as in the SM). In theories beyond the SM, the Higgs decay pattern can be greatly modified [214, 215, 216, 217, 218]. Then, as long as the $h \rightarrow b\bar{b}$ branching ratio is below $\lesssim 20\%$, the standard Higgs search strategies and mass limits may not directly apply [219]. The LEP collaborations have put considerable effort into constraining non-standard Higgs decays into invisible particles or into final states with two SM particles. However, Higgs decays into higher multiplicity final states have not been systematically searched for. Consequently, it is conceivable that the Higgs decaying in a non-standard way may have been missed at colliders, if it decays into a final state that has not been targeted. In reality, it is not necessarily easy for a light Higgs to remain hidden, because the collective body of LEP searches constrain many different final state topologies. Even if a specific Higgs decay mode has not been searched for directly, it may still be captured by a multitude of LEP searches.

There are a few proposals for a hidden Higgs in the literature (for a review see [220, 221]). The most studied scenario (and the first one to point out the improved naturalness with a hidden Higgs) is in the context of the NMSSM [222, 223, 224]. Additional examples include more general singlet extensions of the MSSM [225], supersymmetric little Higgs models [226, 227], the R-parity violating MSSM [228], and the CP-violating MSSM [229, 230]. In all of these scenarios the Higgs decays into a pair of light non-SM particles, e.g. pseudoscalar singlets or neutralinos, which then decay into two or more visible SM particles. Recently, the hidden Higgs scenario has triggered enough interest in the community to prompt the revisiting of LEP data in search of certain 4-body Higgs decay topologies. The $h \rightarrow 4b$ [219] and $h \rightarrow 4\tau$ [231] possibilities are now excluded for Higgs masses $\lesssim 110$ GeV. Other scenarios, however, are constrained only by the model-independent Higgs search of OPAL [232], requiring that the Higgs mass be above ~ 82 GeV.

The hidden Higgs idea is most naturally expressed in the context of supersymmetry (SUSY) where the existence of a light Higgs, $m_h \simeq m_Z$, ameliorates the little hierarchy problem. In this case it is natural to wonder whether *SUSY could also be hidden*: some of the SM superpartners may have been copiously produced at colliders and evaded detection due to non-standard decays. In this chapter, we realize hidden Higgs and hidden SUSY in a supersymmetric model with a light hidden sector. The lightest ‘visible’ superpartner (LVSP – the equivalent of the LSP in the MSSM) is allowed to cascade into the hidden sector, typically producing visible particles in the process. The sensitivity of standard SUSY searches can then be greatly diminished when the LVSP decays partly into visible energy.

We consider three distinct scenarios where the lightest MSSM Higgs boson decays dominantly into the hidden sector. In the *singlet channel* scenario the Higgs decays to the hidden sector through direct couplings. In the other two scenarios the Higgs first decays to a pair of LVSPs which, having no visible decay channels open, decay into the hidden sector. The MSSM contains two types of electrically neutral and colorless superpartners which leads to the *neutralino channel* and the *sneutrino channel* scenarios. In all of the models we consider, hidden sector cascades produce a large multiplicity of

boosted hidden sector particles. Some of these hidden sector particles decay to leptons, and the final state of the Higgs decay is therefore characterized by several groups of collimated leptons plus missing energy. The name *lepton jet* has been coined for these spectacular objects [21, 5, 1].

The striking phenomenology of light hidden sectors has been studied in the past [10, 11, 13]. More recently, the existence of such sectors was motivated by the observed astrophysical anomalies [14, 233, 85, 16]. Indeed, the observed excesses in the positron and electron cosmic ray fluxes may be signatures of dark matter annihilations [20, 18, 41, 234, 2, 74, 73] or decays [18, 3, 95, 96] into a light hidden sector which is weakly coupled to the visible sector. In this chapter we do not address the aforementioned anomalies and concentrate instead, on the collider signatures of such hidden sectors.

As a simple example, we consider a hidden sector with $U(1)_d$ gauge symmetry broken at the GeV scale. $U(1)_d$ couples to the visible sector through kinetic mixing with hypercharge, implying that (i) the hidden photon can decay to the light SM fermions, and (ii) the LVSP can decay to the hidden sector. Consequently, once the Higgs decays, it initiates a hidden sector cascade, producing in addition to the true LSP, many hidden photons and scalars which decay to highly boosted lepton jets. An example of such a Higgs decay is shown in Fig. 8.1. To demonstrate that a light Higgs can be accommodated in the above scenario, we simulate Higgs decays to lepton jets and determine the sensitivity of a wide range of LEP and Tevatron searches. We consider the experimental observables that are relevant for Higgs decays into lepton jets, and identify the viable region in the space of these observables. This procedure allows us to write benchmark models for the neutralino and singlet channels in which the Higgs as light as 100 GeV is allowed by all existing searches. (The sneutrino channel is harder to accommodate with the specific hidden sector we consider.) One should stress that the final states in these models are so spectacular that a *dedicated* analysis at LEP or the Tevatron could quickly discover the Higgs signal, or place a far more stringent bound on the Higgs boson mass.

Several previous studies have considered Higgs decays to light hidden sectors. Ref. [235] considers decays that produce very displaced vertices. While it is conceivable that such a scenario can accommodate a light Higgs, this possibility was not explored by the authors

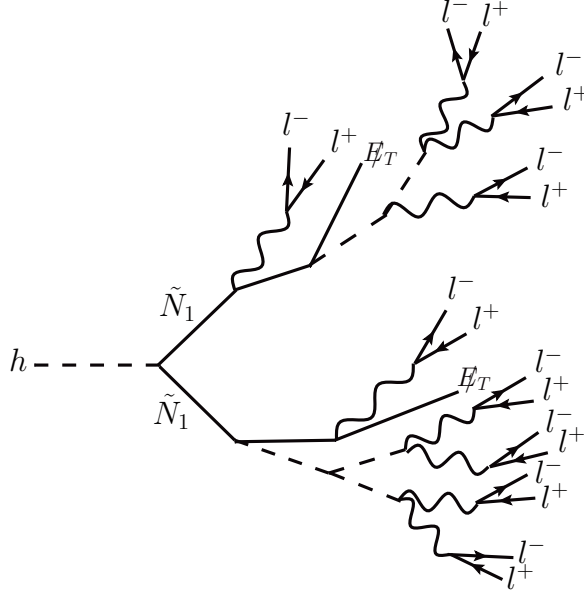


Figure 8.1: An example of a Higgs decay to lepton jets, through the neutralino production portal of Section I.. The hidden sector cascades can lead to many leptons per Higgs decay, in this case 18. This example uses the particle content and vertices of the minimal $U(1)_d$ hidden sector described in section II.. A larger hidden sector can lead to even larger multiplicities. If the neutralinos are heavy enough to be produced close to rest, their decay products will be well-separated, and the leptons will partition into 4 distinct lepton jets. Alternatively, if the neutralinos are light and boosted, the event will consist of two groups of collimated leptons, *neutralino jets*.

of [235] and we do not consider it here. Ref. [236] discusses Higgs decays to two hidden sector photons which subsequently decay to four SM leptons [236]. The authors do not attempt to hide a light Higgs in this scenario (but see comments in [221]). We take a complimentary approach by considering different models that yield a larger variety of final state topologies and multiplicities than these previous works, and in doing so, we identify scenarios that allow for a light Higgs boson with prompt decays.

This chapter is organized as follows. In Section 8.2 we review the concept of a GeV-scale hidden sector that communicates with the SM through kinetic mixing, and introduce a minimal phenomenological model with a $U(1)_d$ gauge symmetry. In Section 8.3 we describe the channels via which the Higgs can decay into the hidden sector. In Section

8.4 we discuss the collider phenomenology of Higgs decays to lepton jets by defining the experimental observables that characterize this scenario. In Section 8.5 we briefly explain why a light Higgs decaying into lepton jets is not obviously excluded by LEP and Tevatron searches, as one may naively suspect. We then review the relevant LEP and Tevatron searches in Section 8.6. In Section 8.7, we discuss how these searches constrain the experimental observables, and construct benchmark models with a 100 GeV Higgs that satisfy these constraints. In Section 8.8 we discuss search strategies at LEP and the Tevatron that can differentiate lepton jets from QCD jets and allow for discovery of a light Higgs decaying to lepton jets. We conclude in Section 8.9. We describe our hidden sector notations in Appendix A.6 and list benchmark signal efficiencies for LEP and Tevatron searches in Appendix A.7.

8.2 The Hidden Sector

We begin by reviewing the framework in which we will later embed a hidden Higgs. In Section I., we discuss portals that can connect a light hidden sector to the visible sector. These portals take the form of operators composed of both hidden sector fields and SM fields. We focus on the vector portal – kinetic mixing between hidden sector gauge fields and SM gauge fields. Then, in Section II., we specialize to a minimal phenomenological hidden sector, with $U(1)_d$ gauge symmetry, and discuss the interactions among hidden sector fields. These hidden sector interactions will be important for the collider phenomenology discussed later in the chapter.

I. Portals

To trigger non-conventional Higgs decays, we study a hidden sector with a gauge group G_d broken at the GeV scale and weakly coupled to the SM. Here and below we work in the supersymmetric framework, which allows one to stabilize both the weak and GeV scales. For simplicity, we will focus on $G_d = U(1)_d$. We will see that this simple case is rich enough to allow for Higgs decays with tens of lepton tracks. Non-Abelian models

generalize the structure and provide a simple way to further soften and increase the multiplicity of the produced leptons. We return to this scenario in Section III.

The hidden sector may couple to the visible sector through various portals (for a useful discussion see [237]). Here we concentrate on the so-called *vector portal* which has been studied extensively [34, 36, 237, 20, 1, 208, 238, 80, 83, 84, 239, 240, 242, 243, 2, 74, 133]. It is straightforward to extend this scenario to other portals. The communication of the hidden sector with the MSSM is through kinetic mixing of the hidden photon, γ_d , of mass m_{γ_d} and the hypercharge field B_μ ,

$$\mathcal{L}_{mix} = \frac{1}{2}\epsilon\gamma_d^{\mu\nu}B_{\mu\nu} = \frac{1}{2}\epsilon\gamma_d^{\mu\nu}(\cos\theta_W A_{\mu\nu} - \sin\theta_W Z_{\mu\nu}). \quad (8.2.1)$$

Here $\gamma_d^{\mu\nu}$ ($B_{\mu\nu}$) is the field strength of γ_d (B_μ) and θ_W is the Weinberg angle. The mixing parameter, ϵ , is assumed to be small, $\epsilon \lesssim 10^{-3}$. The mixing with the photon can be removed by a shift of the photon field,

$$A_\mu \rightarrow A_\mu + \epsilon \cos\theta_W \gamma_d. \quad (8.2.2)$$

As a consequence, the hidden photon couples to all electrically charged particles with the strength $\epsilon e \cos\theta_W$. The smallness of ϵ implies millicharged couplings, consistent with all current bounds [208, 238, 80, 83, 84, 239, 240, 242, 243]. The main significance of the above mixing is to trigger the decay of the hidden photon, γ_d , to kinematically accessible leptons and hadrons. This is illustrated with the left diagram of Fig. 8.2. Decays of the hidden photon to electrically neutral particles that couple to the Z , such as neutrinos, are suppressed by $m_{\gamma_d}^2/m_Z^2$ and will not play an important role. Similarly, we can ignore the mixing between the hidden and visible Higgses through the D-terms.

Upon supersymmetrizing Eq. (8.2.1), the hidden gaugino and visible bino (and therefore neutralinos) mix. One finds the kinetic mixing terms

$$-i\epsilon\tilde{\gamma}_d^\dagger\bar{\sigma}^\mu\partial_\mu\tilde{B} - i\epsilon\tilde{B}^\dagger\bar{\sigma}^\mu\partial_\mu\tilde{\gamma}_d. \quad (8.2.3)$$

Much as before, it is convenient to shift the hidden bino

$$\tilde{\gamma}_d \rightarrow \tilde{\gamma}_d + \epsilon\tilde{B}, \quad (8.2.4)$$

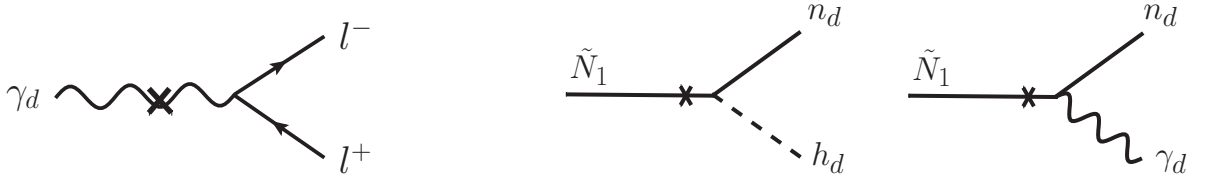


Figure 8.2: Interactions that follow from kinetic mixing between the hidden photon and hypercharge. The hidden photon couples to the electromagnetic current, including lepton pairs, as in the diagram on the *left*. The cross on the diagram indicates the ϵ suppression. The *right* two diagrams show possible decays of the SM bino to the hidden sector, which follow from gaugino kinetic mixing. The SM LSP is no longer stable, and all SUSY cascades can end in the hidden sector.

which removes the kinetic mixing, while keeping the mass matrix diagonal to order m_{γ_d}/m_Z . Consequently, hidden fields charged under $U(1)_d$ interact with the visible neutralinos with ϵ -suppressed couplings. In particular, all hidden sector scalars h_d^i , with charges q_i , couple to the visible bino,

$$- \epsilon \gamma_d \tilde{B} \sum_i q_i h_d^{i\dagger} \tilde{h}_d^i. \quad (8.2.5)$$

Thus the visible neutralino may decay to the hidden neutralinos and either a Higgs or the longitudinal mode of the hidden photon, as in the right two diagrams of Fig. 8.2. In addition to the above, the small off-diagonal terms in the mass matrix induce m_{γ_d}/m_Z -suppressed couplings of the form

$$- \epsilon g' \frac{m_{\gamma_d}}{m_Z} \tilde{\gamma}_d \sum_i Y_i f^i \tilde{f}^i, \quad (8.2.6)$$

where $f^i(\tilde{f}^i)$ are MSSM (s)fermions, Y_i are the corresponding hypercharges, and g' is the hypercharge gauge coupling. This coupling will play a role in the sneutrino decay channel discussed in Section II. below.

Finally, the hidden sector may have additional couplings to the visible sector. For instance, couplings of singlets in the superpotential,

$$W \supset S (y \chi \bar{\chi} + \lambda H_u H_d), \quad (8.2.7)$$

can lead to the *higgs portal*, $H_u H_d \chi^* \bar{\chi}^* + \text{c.c.}$, where χ and $\bar{\chi}$ are charged under the hidden sector. If χ and/or $\bar{\chi}$ get VEVs, this operator can trigger mixing between the MSSM

Higgses and hidden particles. If $\chi, \bar{\chi}$ are relatively heavy the presence of the mixing does not change the decay branching fractions of the low-lying hidden states. The Higgs portal can, however, lead to Higgs decays into hidden sector particles. From now on we will refer to this mechanism as the *singlet channel*, which we return to in Section III.

II. A Minimal Model

We now introduce the field content of a minimal hidden sector that leads to Higgs decays to lepton jets. In order to break the $U(1)_d$ gauge group, two Higgs chiral superfields, $h_{1,2}$ with charges ± 1 , are added. Generally, both Higgs fields obtain VEVs. This hidden sector setup was also studied in [5] (and we give further details in Appendix A.6). The hidden spectrum contains

- One massive photon γ_d ,
- Three hidden neutralinos \tilde{n}_d^i , which are mixtures of the hidden gaugino and Higgsinos,
- Three hidden scalars h_d^i : taking the hidden sector vacuum to preserve CP, there are two CP-even scalars, h_d, H_d , and one CP-odd scalar, A_d .

All these particles have masses which, for definiteness, are assumed to lie in the 100 MeV to few GeV ballpark. Supersymmetry is softly broken in the hidden sector, and we assume completely general soft and μ terms. This gives sufficient freedom to organize the masses in the hidden sector into various patterns leading to different types of cascades. The interactions within the hidden sector are fully dictated by gauge symmetry and supersymmetry. The neutralinos interact via,

$$\tilde{n}_d^i \tilde{n}_d^j h_d^k, \quad \tilde{n}_d^{i\dagger} \sigma_\mu \tilde{n}_d^j \gamma_d^\mu, \quad (8.2.8)$$

where the couplings are fixed by the hidden gauge couplings and mixing angles. Through these vertices the hidden neutralinos can cascade down to the lightest one (which we assume to be the true LSP¹, emitting hidden scalars and photons). Whenever it is

¹If visible-sector SUSY is broken by gauge mediation, there will also be a light gravitino. Hidden fermions decay to the gravitino well outside the detector [1], so here we can neglect the gravitino.

kinematically available, the scalars can also decay through the vertices

$$h_d^i h_d^j h_d^k, \quad h_d^i \gamma_d^\mu (\gamma_d)_\mu, \quad (8.2.9)$$

that originate from the D-term and from the scalar kinetic terms.

Thus, depending on the mass spectrum, the cascades may lead to a large multiplicity of hidden particles in each event. The mass spectrum controls, for example, the typical length of the hidden cascade, the multiplicity of visible final states, and the amount of missing energy. The minimal model can be deformed by considering a non-Abelian hidden gauge group or by adding more chiral multiplets, both of which increase the number of scalar and fermionic eigenstates and can lengthen the hidden cascades, thereby producing a larger final state multiplicity. We study an example with such a modification in Section III.

8.3 Higgs Decays to the Hidden Sector

The MSSM by itself allows for a rich variety of Higgs decay modes, depending on the visible spectrum. In particular, if the LVSP is sufficiently light, the Higgs can decay to it with a sizable branching fraction, much larger than to the SM channels like $b\bar{b}$ or $\tau^+\tau^-$. If the LVSP is stable, such a scenario is strongly constrained by invisible Higgs searches at LEP [244]. The mixing of the hidden sector with the MSSM, however, makes the LVSP unstable. Then the Higgs can decay predominantly into complicated high-multiplicity final states. Such a possibility has not been experimentally studied at LEP or the Tevatron, therefore a priori a Higgs boson can be lighter than the naive LEP limit of 114.4 GeV. Below we identify three possible channels through which the lightest CP-even Higgs of the MSSM can decay into the hidden sector.

I. Neutralino Channel

In principle, there is no model-independent bound on the mass of the LVSP neutralino (this is because the bino is an MSSM singlet). The bounds on the Higgs boson mass can then be significantly relaxed, if the LVSP neutralino is sufficiently light, such that the

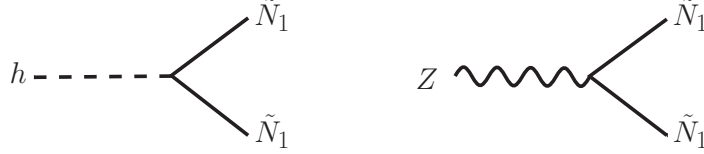


Figure 8.3: Higgs and Z decays to neutralinos. The neutralinos then decay into the hidden sector as in figure 8.2. We consider the region of the MSSM parameter space where the Higgs dominantly decays to neutralinos while the charginos are above the LEP bound of ~ 100 GeV. In this region, we find $m_{\tilde{N}_1} < m_Z/2$, such that the Z can also decay to neutralinos, as in the *right* diagram. This is consistent with LEP-1 constraints when $\text{BR}(Z \rightarrow 2\tilde{N}_1) \lesssim 10^{-3}$.

Higgs branching fraction into it is $\gtrsim 75\%$, while a sizable fraction of the neutralino energy comes back in the form of visible SM states. A similar scenario with a light Hidden Higgs was considered in Ref. [228] within the R-parity violating MSSM, where the neutralino decays into three SM quarks, leading to the Higgs-to-6-jets signature. Higgs decays to neutralinos have also been considered in the framework of gauge mediation in [245]. Here we revisit the neutralino channel in the context of the Higgs decaying to lepton jets.

The coupling of the lightest MSSM Higgs boson to the lightest neutralino arises from the Higgs-Higgino-Bino/Wino couplings and takes the form,

$$g_{h11}h\tilde{N}_1\tilde{N}_1 + \text{h.c.}, \quad g_{h11} = \frac{1}{2}(gc_W - g'c_B)(c_\alpha c_U + s_\alpha c_D). \quad (8.3.10)$$

We parametrized the embedding of the lightest CP-even Higgs boson into the Higgs doublets as $H_u^0 = (s_\beta v + c_\alpha h + \dots)/\sqrt{2}$, $H_d^0 = (c_\beta v - s_\alpha h + \dots)/\sqrt{2}$. The angles c_i describe the composition of the lightest neutralino in terms of the original gauginos and Higgsinos: $\tilde{N}_1 = c_B\tilde{B} + c_W\tilde{W}^3 + c_U\tilde{H}_u^0 + c_D\tilde{H}_d^0$. The Higgs partial decay width is,

$$\Gamma(h \rightarrow \tilde{N}_1\tilde{N}_1) = \frac{g_{h11}^2 m_h}{4\pi} \left(1 - 4\frac{\tilde{m}_{\tilde{N}_1}^2}{m_h^2}\right)^{3/2}. \quad (8.3.11)$$

This should be compared with the decay width into a pair of b -quarks,

$$\Gamma(h \rightarrow b\bar{b}) = c_{\text{QCD}} \frac{3}{8\pi} y_{hbb}^2 \left(1 - 4\frac{m_b^2}{m_h^2}\right)^{3/2}, \quad (8.3.12)$$

where $y_{hbb} = c_\alpha m_b/c_\beta v$ and c_{QCD} is a fudge factor that captures higher-order QCD effects. The latter are numerically relevant; for example, $c_{\text{QCD}} \approx 1/2$ for the SM Higgs

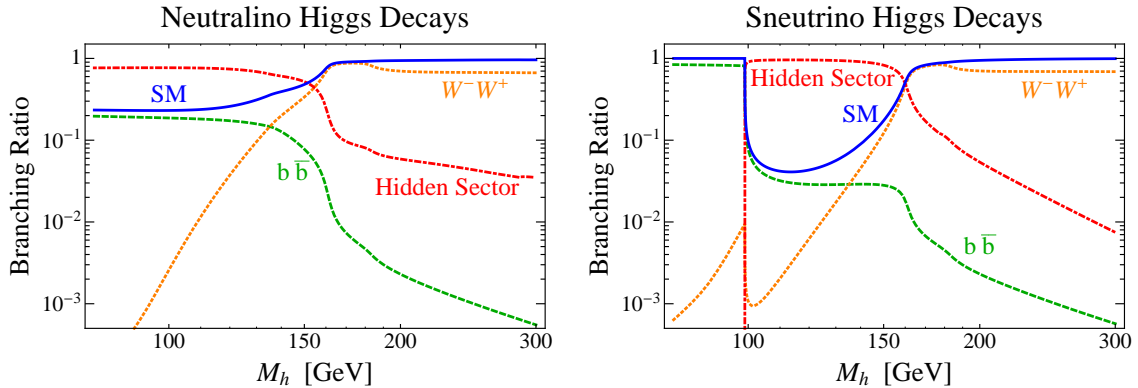


Figure 8.4: Higgs branching ratios for the neutralino and sneutrino channels. Each plot shows the total Higgs branching ratios to the SM and hidden sector, as functions of the Higgs mass. The SM width is dominated by the branching fractions to $b\bar{b}$ and W^+W^- , which are also shown separately. The parameters are fixed according to the benchmark models of Section III. For each model, the Higgs decays dominantly to the hidden sector below the W^+W^- threshold, and a 100 GeV Higgs satisfies the LEP constraint $\text{BR}(h \rightarrow b\bar{b}) < 0.2$. The Higgs widths to SM states are taken from HDECAY [246].

of $m_h = 100$ GeV and for $m_b \approx 4.6$ GeV. The neutralinos then subsequently decay to the hidden sector through the couplings in Eq. (8.2.5). The decays are illustrated in Fig. 8.3.

Even if $m_{N_1} < m_h/2$ (which is fairly easy to arrange) it is not automatic that the Higgs decays to neutralinos with a sizable branching fraction. Indeed, the coupling g_{h11} vanishes if the lightest neutralino is a pure gaugino or a pure Higgsino. The decays into neutralinos are therefore relevant only if the latter is a mixture of gauginos and Higgsinos. LEP constraints on a light SM Higgs require that

$$\Gamma(h \rightarrow b\bar{b})/\Gamma(h \rightarrow \tilde{N}_1\tilde{N}_1) \lesssim 0.25 \quad (8.3.13)$$

This is possible for example, if the lightest neutralino is dominantly a bino, with a 10% Higgsino fraction. A corollary is that the second visible neutralino and the lightest visible chargino cannot be arbitrarily heavy as otherwise the mixing angles $c_{U,D}$ would be suppressed. Thus there is tension between Eq. (8.3.13) and the LEP constraints on light charginos and the Tevatron constraints on trilepton signals from decays of the

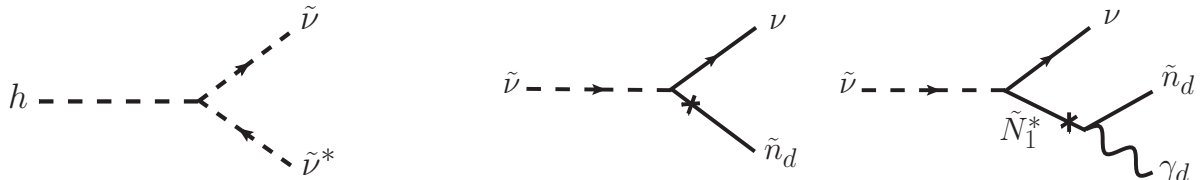


Figure 8.5: Diagrams relevant for Higgs cascade decays into the hidden sector via the sneutrino channel. The *left* diagram shows the Higgs decaying into a sneutrino pair. The *right* two diagrams are examples of two and three body decays of the sneutrino into hidden particles plus a SM neutrino. The neutrino production implies an irreducible missing energy component for this channel, which is constrained by LEP $h \rightarrow \cancel{E}_T$ searches, as discussed in Section II.

second to lightest neutralino². Nevertheless, numerically one can find large portions of the parameter space where the Higgs decay into the lightest neutralino dominates, and at the same time the lightest chargino and the second neutralino are significantly heavier than 100 GeV, and thus beyond LEP reach. Trilepton constraints from the Tevatron, on the other hand, are model-dependent, because they depend on the branching fraction to trileptons and their kinematics. In Section III., we will consider an example spectrum that is not constrained by trilepton searches.

Interestingly, all the viable points we have found correspond to the lightest visible neutralino mass below 40 GeV (this is consistent with the results of [228]). In consequence, the neutralino channel is constrained by LEP-1 searches (the Z boson can decay to neutralinos via its Higgsino component), but in the following we show that all existing experimental constraints can be satisfied. In the left plot of Fig. 8.4 we show the Higgs decay branching fractions as a function of the Higgs mass for the neutralino channel. The benchmark parameters of the specific model used are described in Section III..

II. Sneutrino Channel

The MSSM contains another class of neutral supersymmetric particles – the sneutrinos – which are the scalar partners of the SM left-handed neutrinos. If at least one of the sneutrinos is lighter than half the Higgs mass, another channel is open for the Higgs to

²Although the standard supersymmetry searches are not necessarily sensitive to these models, we require the charginos to be heavier than the LEP reach ~ 100 GeV.

decay into the hidden sector. In the MSSM, the Higgs couples to the sneutrinos through the $SU(2)_W \times U(1)_Y$ D-terms,

$$V_D \supset \frac{1}{8} (g'^2 + g^2) (|H_u|^2 - |H_d|^2 - |\tilde{\nu}_i|^2 + \dots)^2, \quad (8.3.14)$$

where $g'(g)$ is the hypercharge (weak) gauge coupling and the ellipses stand for additional terms which involve the sleptons and additional MSSM fields. The above term induces a tri-linear coupling between the lightest MSSM Higgs and two sneutrinos,

$$\frac{m_Z^2}{v} \sin(\alpha + \beta) h \tilde{\nu}^\dagger \tilde{\nu}, \quad (8.3.15)$$

where the resulting Higgs decay width is

$$\Gamma(h \rightarrow \tilde{\nu}\tilde{\nu}) = \frac{m_Z^4}{16\pi m_h v^2} \sin^2(\alpha + \beta) \left(1 - 4 \frac{m_{\tilde{\nu}}^2}{m_h^2}\right)^{1/2}. \quad (8.3.16)$$

The Higgs-sneutrino coupling is typically large, thus the $h \rightarrow \tilde{\nu}\tilde{\nu}$ decay normally dominates over $h \rightarrow b\bar{b}$ as soon as it is kinematically allowed. This is shown in the right plot of Fig. 8.4 for the benchmark model described in Section III.. The sneutrino cannot be lighter than $m_Z/2$ as this is excluded by the LEP-1 measurement of the Z -width. This leaves the window $m_Z/2 < m_{\tilde{\nu}} < m_h/2$ where the decay into sneutrinos can potentially lead to a hidden and light Higgs.

Much as in the neutralino LVSP case, the sneutrino is not stable and hence the Higgs decaying into sneutrinos is not invisible. There are two ways for the sneutrino to decay into the hidden sector, both illustrated in Fig. 8.5. Since the bino is heavy in this scenario, Eq. (8.2.6) induces a three-body decay into a neutrino, a hidden neutralino and a hidden boson (scalar or photon). Conversely, the sneutrino can decay directly into a SM neutrino and a hidden neutralino, through the interaction in Eq. (8.2.6), however, the coupling is suppressed by an additional m_{γ_d}/m_Z factor. As a consequence, the 3-body decay is dominant, unless the lightest visible neutralino is significantly heavier than 100 GeV. The sneutrino decay may be followed by a cascade in the hidden sector leading to a final state with a number of visible leptons and missing energy from the true LSP in the hidden sector. Due to the SM neutrino in the final state, the sneutrino channel is characterized by more missing energy than the neutralino channel.

As we will discuss below, the sneutrino channel, together with the minimal $U(1)_d$ hidden sector of Section II., suffers from considerable tension with several LEP searches. Two reasons are the typically larger missing energy in the Higgs decays through the sneutrino channel and the independent sneutrino production cross-section through off-shell Z 's, which is comparable in rate to Higgs-strahlung. An extended hidden sector, with additional cascades, can resolve this tension. We return to these issues in Section 8.7.

III. Singlet Channel

Finally, new Higgs decay modes are possible, if there are additional mediators that couple both to the Higgs and to the hidden sector. A simple example is constructed starting from the NMSSM in which an additional singlet, S , couples to the Higgs doublets. S obtains a VEV, thereby ameliorating the so called μ -problem. To enable the Higgs decays, consider, as an example, the following superpotential,

$$W_{\text{singlet}} = S(y\chi\bar{\chi} + \lambda H_u H_d) + \kappa_1 \bar{\chi} h_1^2 + \kappa_2 \chi h_2^2. \quad (8.3.17)$$

Here $\chi, \bar{\chi}$ are chiral superfields with charges ± 2 under G_d and $h_{1,2}$ are the two hidden Higgses. Once the visible Higgses and the singlet acquire VEVs, masses for $\chi, \bar{\chi}$ are generated: the fermionic degrees of freedom get a mass $y\langle S \rangle$, while the scalar masses are split by the F -term of S , $m_\chi^2 = y^2\langle S \rangle^2 \pm y F_S$. If the lightest scalar state is lighter than $m_h/2$, the Higgs can decay into a pair of these fields with a large branching fraction, as long as the couplings y and λ are sizeable. Quite generically, the branching fraction into the hidden sector is close to unity. The branching fraction for the benchmark model described in Section 8.7 is shown in the right plot of Fig. 8.7.

Subsequently, the χ states decay via the $\kappa_{1,2}$ couplings into hidden Higgsinos and Higgses, which finally decay to SM fermions. Once again the final state of the Higgs decay is a number of leptons plus missing energy. The virtue of this model is that it requires a minimal deformation of the NMSSM (or other variants which address the μ -problem), and is by and large independent of the visible spectrum. It can therefore accommodate heavy SM superpartners which are beyond the LEP and Tevatron reach,

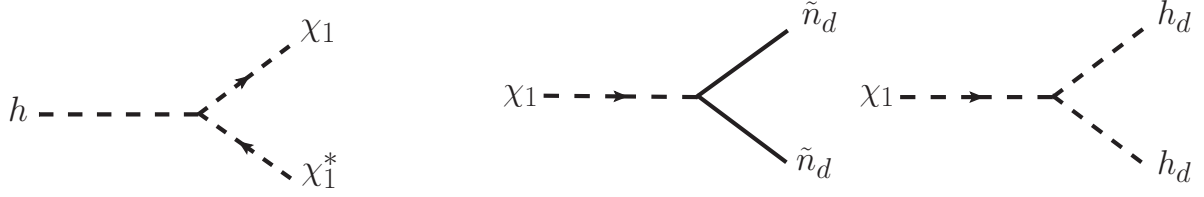


Figure 8.6: Diagrams relevant for Higgs cascade decays into the hidden sector via the singlet channel of Eq. (8.3.17). The scalars that couple to the Higgs are split by the NMSSM singlet F -term, such that the lighter one, χ_1 , is easily lighter than half the Higgs mass. The scalars couple to light hidden sector Higgses through the superpotential, and the *right* two diagrams are examples of the resulting decays of χ_1 into hidden fermions and scalars.

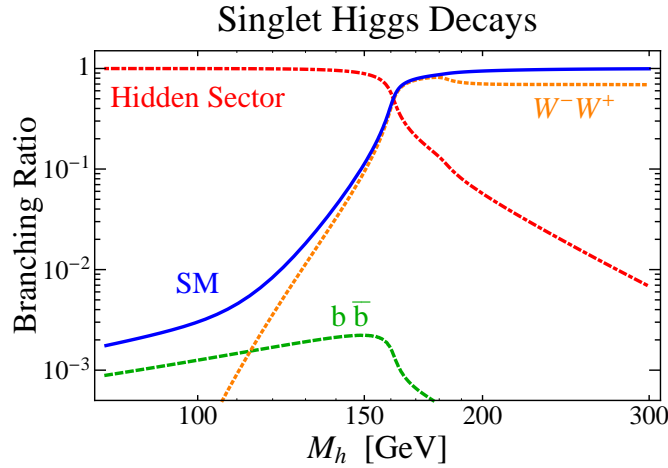


Figure 8.7: Same as in Fig. 8.4, for the singlet channel, with the parameters fixed according to the benchmark of Section III.

while allowing the Higgs to decay dominantly into the hidden sector. Such a model is therefore in principle less constrained by existing searches.

8.4 Collider Phenomenology

In order to establish models where the Higgs and possibly SUSY are hidden, we must understand how the phenomenology of this scenario is experimentally constrained. In this section, we describe the collider physics of a Higgs decaying to lepton jets. We begin, in Section I., with a general description of lepton jets and neutralino jets, which are a

particular subclass defined below. Then, in Section II., we describe the most prominent experimental variables of this scenario, defining a space of observables. After discussing the relevant LEP and Tevatron searches in Section 8.6, we continue in Section 8.7 by identifying the allowed region in this space of experimental observables. We then construct benchmark models that reside in this allowed region.

I. Lepton Jets and Neutralino Jets

The Higgs can avoid detection at LEP and the Tevatron if it decays into final states that are relatively unconstrained by existing searches. Here we focus on one such class of final state objects: *lepton jets*, which are defined as high-multiplicity clusters of boosted and collimated leptons [21, 5, 1]. Lepton jets can be produced when the Higgs decays through low lying hidden sector states with masses (in particular the hidden gauge boson) below $\lesssim 1$ GeV. These hidden sector states then decay to leptons. The picture is the following. First, the Higgs boson is produced, alone or in association with Z or W , and decays into a pair of SM superpartners or singlets. We discussed three such channels in Section 8.3. The pair promptly decays into the hidden sector, cascading through hidden sector interactions to produce highly boosted hidden scalars, photons and neutralinos. These appear in the detector either as missing energy or produce boosted leptons which populate lepton jets. An example of such a Higgs cascade decay is depicted in Fig. 8.1.

The number of lepton jets per Higgs decay depends on the cascading spectrum, and the resulting topology is easily deduced by recalling that particles produced at rest decay to well-separated objects while boosted particles decay to collimated objects. For example, if the Higgs decays to two weak scale SM superpartners or singlets, each will decay to well-separated hidden particles that seed distinct lepton jets. Subsequent decays will be collimated, and the event topology can contain as many as four lepton jets. Alternatively, for example, if the Higgs decays to two very light neutralinos, $m_{\tilde{N}_1} \lesssim 10$ GeV, then each neutralino's decay products will be clustered, and the event topology will contain two lepton jets, one for each neutralino. In this situation, we refer to the lepton jets as *neutralino jets*. We consider an example with neutralino jets in Section III..

γ_d Branching Ratio

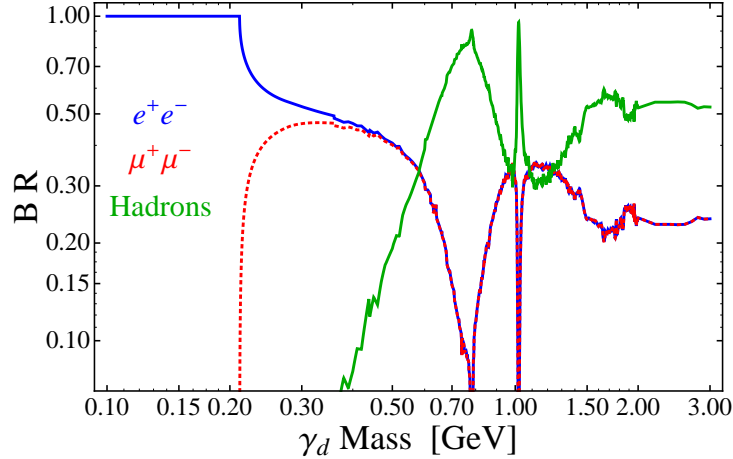


Figure 8.8: Hidden photon branching ratios to electrons, muons, and hadrons through the electromagnetic current, as a function of the hidden photon mass. The hadronic branching ratio is derived from the measured $R \equiv \text{BR}(e^+e^- \rightarrow \text{had})/\text{BR}(e^+e^- \rightarrow \mu^+\mu^-)$ [209]. We see that for $m_{\gamma_d} \lesssim 500$ MeV, the hidden photon decays dominantly to leptons, including muons for $m_{\gamma_d} > 211$ MeV.

II. Experimental Observables

Concentrating on the lepton jets, we identify the following relevant collider variables,

- **Visible Final States: Electrons vs. Muons**

The hidden photon decays through the kinetic mixing, Eq. (8.2.1), into all kinematically allowed SM states with electric charge. Thus, the mass of the hidden photon is the only parameter controlling which visible particles appear at the end of the Higgs cascade decay. For $m_{\gamma_d} < 2m_e$ the hidden photon is stable on collider scales, which would amount to a purely invisible Higgs signature. This scenario is strongly constrained, as we review in Section 8.6, and we do not consider this possibility here. For $2m_e < m_{\gamma_d} < 2m_\mu$ the hidden photon decays exclusively into electrons. For $2m_\mu < m_{\gamma_d} < 2m_{\pi^\pm}$ the hidden photon decays into a pair of muons or electrons, roughly in equal amounts. For $m_{\gamma_d} > 2m_{\pi^\pm}$ the branching fractions are determined by $R \equiv \text{BR}(e^+e^- \rightarrow \text{had})/\text{BR}(e^+e^- \rightarrow \mu^+\mu^-)$ [108, 208] which is measured experimentally [209]. As long as $m_{\gamma_d} \lesssim 400$ MeV, $\text{BR}(\gamma_d \rightarrow \pi^+\pi^-)$ is

less than 10% and can be safely neglected, as we do below. The branching fractions are shown in Fig 8.8.

- **Lepton Multiplicity**

This observable is extremely sensitive to the details of the hidden sector spectrum. One important factor is the identity of the lightest hidden neutralino. Since the visible bino couples to hidden Higgsinos, see Eq. (8.2.5), model realizations where the hidden bino is lighter than the hidden Higgsinos have longer cascades, and therefore tend to produce more visible leptons. Another crucial factor is the ratio of the masses of the lightest hidden scalar and hidden photon. When $m_{h_d} < m_{\gamma_d}$, the hidden Higgs, h_d , dominantly decays to 2 leptons at one-loop [208], and is stable on collider scales. On the other hand, for $m_{h_d} > m_{\gamma_d}$ the 3-body decays with one on-shell hidden photon are allowed, which leads to prompt decays of h_d into 4 leptons, as long as the mixing parameter ϵ is not too small. The spectrum of the other hidden scalars is also important. For example, when $m_{H_d} > 2m_{h_d}$ the dominant decay mode of H_d is $H_d \rightarrow 2h_d \rightarrow 8l$, while for $m_{\gamma_d} < m_{H_d} < 2m_{h_d}$ the 4-lepton decay via the hidden photons dominates. Depending on the mass spectra, the average lepton multiplicities can thus range from zero to a few tens of leptons per Higgs decay. Going beyond the minimal $U(1)_d$ model, for example by making the hidden group non-Abelian, only increases the number of possibilities. Additionally, if the hidden gauge coupling is sizeable ($g_d^2/4\pi \gtrsim 0.1$), hidden sector showering also increases the number of leptons [108,5]. Example lepton multiplicity distributions are given in Fig. 8.9.

- **Missing Energy**

The average missing energy per Higgs decay is also very sensitive to the hidden spectrum. The missing energy can range anywhere from being very small, less than 10 GeV, to where it dominates over visible energy. The most important factor determining the amount of missing energy is how many hidden particles are collider-stable. Furthermore, missing energy depends on the Higgs decay channel into the hidden sector. For the sneutrino channel the amount of missing energy

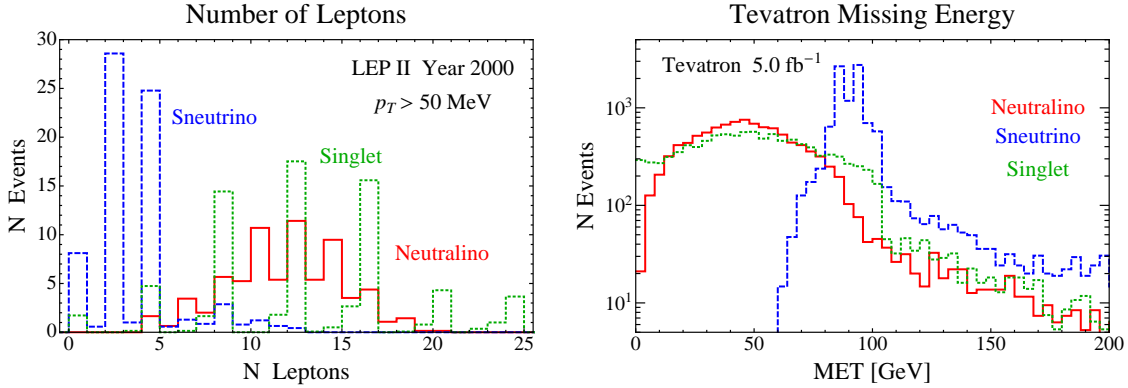


Figure 8.9: The lepton multiplicity and missing transverse energy distributions of Higgs decays for the three benchmarks of section III.. The *left* panel shows the multiplicity of leptons with $p_T > 50$ MeV, which is roughly the threshold for detecting tracks at LEP. The event counts correspond to the data collected in the year 2000 at LEP-2, corresponding to $\mathcal{L} \approx 214 \text{ pb}^{-1}$ at $\sqrt{s} = 205 - 207$ GeV. The *right* panel shows the missing energy distribution at Tevatron Run II, $\sqrt{s} = 1.96$ TeV, and the event counts correspond to $\mathcal{L} = 5 \text{ fb}^{-1}$. The sneutrino benchmark has the most missing energy because of the irreducible missing energy carried by the neutrinos.

is typically larger, because a hard neutrino is emitted when the sneutrino decays into the hidden sector. For typical hidden spectra the average missing transverse energy per Higgs decay is on the order of 10-50 GeV, and displays a large variation on an event-by-event basis, see Fig. 8.9.

- **Event Topology: Number of Lepton Jets**

The directions of final state lepton momenta are not distributed randomly. Hidden sector particles are produced with large boosts, and their clustered decay products populate distinct lepton jets containing highly collimated leptons. The final state topology is characterized by the number of lepton jets, which depends on the spectrum and first steps of the cascade decay. A two-jet topology arises when the Higgs decays directly into two GeV scale objects, or if the superpartners decay into one hidden particle that decays visibly along with other invisible particles. The former possibility is most easily realized with the neutralino jets discussed in Section I.. Indeed, if the lightest MSSM neutralino mass is below 10 GeV (which is possible without compromising naturalness, and without conflicting experiment), its visible

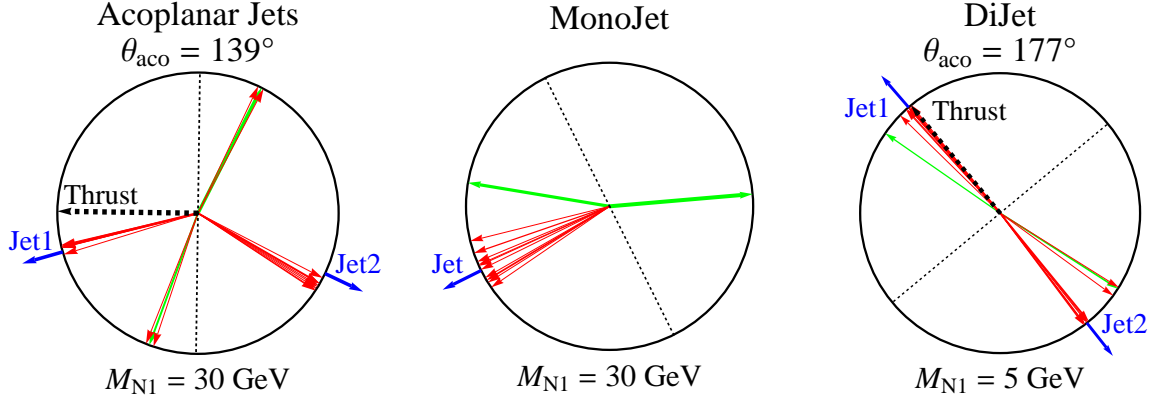


Figure 8.10: Transverse event displays for Z decays to neutralinos at LEP-1. The red vectors show the transverse momenta of leptons and the green vectors correspond to long-lived hidden sector particles that escape the detector as missing energy. The *left* display shows a 4-lepton-jet event, with $m_{\tilde{N}_1} = 30$ GeV, that would have been detected by the ALEPH acoplanar jet search [247]. The thrust (black) is used to define two jets (blue). In an acoplanar event, the jets are separated by $\theta_{\text{aco}} < 175^\circ$ in the transverse plane. The *central* display shows an event that would have been detected by the ALEPH monojet search [248] because all visible energy falls in the same hemisphere. Here, both neutralinos produce exactly one visible lepton jet in the same hemisphere, balanced by missing energy. Both acoplanar jets and monojets are avoided if $m_{\tilde{N}_1} \lesssim 5$ GeV with both neutralinos decaying (partly) visibly, as in the *right* display. The topology of the back-to-back neutralino jets mimic the hadronic dijet background.

decay products form a jet along its direction of motion. On the other hand, when the Higgs decays into neutralinos heavier than 10 GeV, or when the three-body decays of the sneutrino channel dominate, the event topology will contain 3 or more jets. Finally, if one of the two primary Higgs decay products (neutralinos, sneutrinos or hidden fields) decays invisibly, while the other decays into one lepton jet, the final state will display a monojet topology. All three possibilities are shown in Figure 8.10.

- **Lepton Isolation**

Yet another consequence of their boosted origin is that lepton jets are narrow, with constituent leptons that are not isolated. Tevatron searches for new physics that produces leptons, such as the trilepton and like-sign dilepton searches discussed in

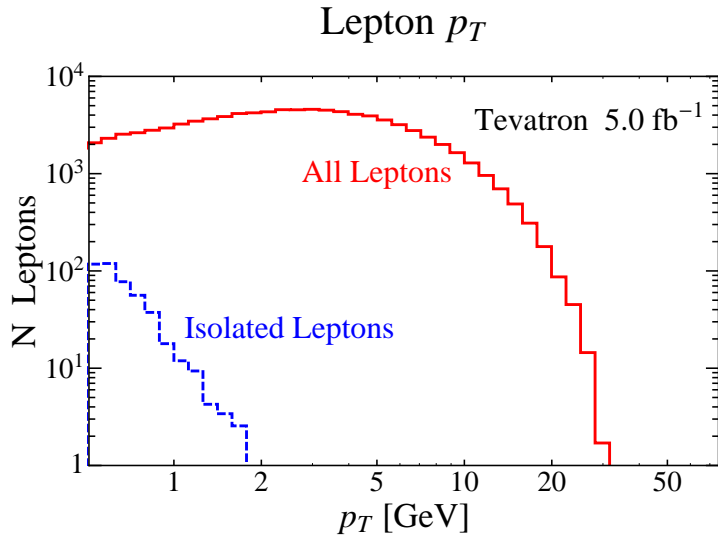


Figure 8.11: The p_T distributions of all leptons (solid, red) and isolated leptons (dashed, blue) produced in gluon fusion Higgs decays at Tevatron Run II, $\mathcal{L} = 5 \text{ fb}^{-1}$, for the singlet benchmark of section III. Tevatron searches for trileptons and like-sign dileptons impose strict isolation requirements in order to fight the SM heavy flavor and in-flight-decay backgrounds. For this plot, we use a track-based isolation definition where the scalar p_T sum of all other tracks in a cone surrounding the lepton, $\Delta R < 0.4$, must not exceed 10% the p_T of the lepton [249]. We see that Higgs decays to lepton jets produce few isolated leptons, all of which are soft.

Section III., require isolated leptons in order to fight the backgrounds from heavy-flavor decays and in-flight meson decays. These searches typically require leptons to be isolated within cones of $\Delta R < 0.4$. Some searches require total isolation in this cone [250], while other searches put limits on the energy deposition in the calorimeters [251], or the sum of track p_T [249]. Lepton jets violate these isolation definitions because each hidden photon decays into a pair of close leptons separated by $\Delta R \lesssim 0.1$. Thus, almost all leptons in the final state have at least one companion track within the isolation cone³. Furthermore, the bulk of our parameter space leads to large lepton multiplicities with numerous leptons in a $\Delta R \sim 0.1$ cone, further spoiling the isolation. In Fig. 8.11 we show the distribution of the total number of

³Isolated leptons are sometimes produced when soft leptons are emitted at wide angles from the rest of the lepton jet or when nearby leptons are too soft to reach the calorimeter (e.g. $p_T \leq 0.5 \text{ GeV}$ at Tevatron), and are therefore interpreted as missing energy.

leptons as a function of the transverse momenta together with leptons that satisfy the track-based isolation of Ref. [249]. One can see that only a small fraction of the leptons are isolated, and these are typically soft leptons that would not pass the p_T cuts for most new physics analyses. The other isolation definitions give similar results.

- **Displaced Vertices**

A final feature of this class of models is the possible existence of displaced vertices. For instance, displaced vertices are produced if the kinetic mixing, ϵ , is small enough. The hidden photon decay length scales as $1/\epsilon^2$, so that for hidden photon mass $m_{\gamma_a} \simeq 0.1$ GeV, displaced vertices show up for $\epsilon \lesssim 10^{-5}$. Displaced vertices can also appear for a subset of final state particles, in three-body decays, if mass splittings in the hidden sector are small compared to the GeV scale. This can occur without tuning. For example, the splitting between two hidden neutralinos can be naturally small if they are both Higgsino-like. The presence of displaced vertices would avoid most of the existing LEP and Tevatron constraints, as such signal events would not be selected by most analyses. Higgs decays with displaced vertices were studied in [235, 252, 253]. To keep our discussion simple we do not consider them in this chapter. Nonetheless, one should keep in mind that this possibility could be realized in nature and would relax the constraints on new physics. Conversely, designing collider search strategies that would be sensitive to a Higgs decaying to lepton jets with displaced vertices is an important task that we postpone for future work.

8.5 Can Lepton Jets Really Hide the Higgs?

Before considering specific searches, it is natural to ask whether Higgs decays to lepton jets would have been trivially seen at LEP and/or the Tevatron. In other words, one might think that it is naive to imagine that such spectacular events can remain undetected. To address this worry let us first consider LEP-2, which sets the strongest limits on a light Higgs. The production cross-section, for a 100 GeV Higgs, is around $0.3 - 0.4$ pb. The

total luminosity at LEP-2 is on the order of 450 pb^{-1} , per experiment. The number of Higgs-strahlung events before cuts is therefore ~ 130 . Preliminary cuts typically reduce the number of events by an order of magnitude, leaving only a handful of events and making detection nontrivial without a dedicated search. Furthermore, due to the relatively poor quality of the hadronic calorimeters at the LEP experiments, hadronic activity is typically identified by the number of tracks. For this reason, even at LEP-1 where the neutralino channel allows for as many as 10^4 lepton jet events, these events are easily hidden beneath the large hadronic background.

At the Tevatron, Higgs production is dominated by gluon fusion with a cross-section of $\sim 2 \text{ pb}$ for a 100 GeV Higgs. With 5 fb^{-1} this implies 10^4 Higgs events. Of course, the large QCD background does not allow one to search for such events ‘by eye’. Even so, one may worry that the existence of many leptons would, naively, allow for an easy discovery. The key point is that Tevatron searches for leptons require them to be isolated. This is true, in particular, for the Vista/Sleuth global searches which take a model-independent approach [254]. The leptons produced by Higgs decays to lepton jets are typically not isolated, and thereby evade the standard searches. The small number of Higgs events that do produce isolated leptons are buried beneath the QCD and electroweak backgrounds.

8.6 Experimental Constraints

The strongest constraints on the Higgs mass and decay branching fractions come from LEP-2 searches. These are obtained assuming the Higgs is dominantly produced through the Higgs-strahlung process, $e^+e^- \rightarrow Zh$, with the SM cross section. Three well known results should be kept in mind:

1. The most robust constraint on the Higgs mass comes from the model independent search by OPAL [232], $m_h \geq 82 \text{ GeV}$. This bound is independent of the Higgs decay modes.
2. The mass of the SM Higgs is constrained to be $m_h \geq 114.4 \text{ GeV}$ [255]. This bound is obtained by studying the dominant $h \rightarrow b\bar{b}$ SM decay. Conversely, the study can

be interpreted as a bound on the $h \rightarrow b\bar{b}$ branching ratio, which for a 100 GeV Higgs is bounded to be $\text{BR}(h \rightarrow b\bar{b}) \lesssim 20\%$ [219].

3. Finally, the invisible Higgs (where the Higgs decays exclusively into missing energy) must be heavier than 115 GeV [256]. Again, the bound can be interpreted also as the bound on the branching ratio of Higgs to invisible states. For a 100 GeV Higgs the bound is $\text{BR}(h \rightarrow \cancel{E}) \lesssim 15\%$.

The LEP collaborations have performed several searches for Higgs decaying into 2 SM particles other than the b quarks, always placing a bound on the Higgs mass almost as stringent as the SM one, see [220] for a review. Higgs decaying into a larger number of SM states is considerably less constrained, with the exception of $h \rightarrow 4b$ and $h \rightarrow 4\tau$ channels. Thus, Higgs decaying into high multiplicity final states offers a way to circumvent the LEP limits, as long as 2-body decay channels are sufficiently suppressed.

Higgs decaying to lepton jets has not been searched for at LEP or the Tevatron. In this scenario the Higgs mass is in principle constrained only by the OPAL model-independent limit. But the final states predicted by this scenario could well be picked up by some existing Higgs or new physics searches. This section provides an overview of the most relevant searches at LEP and the Tevatron together with a brief explanation why they could be sensitive to the Higgs decaying to lepton jets.

I. LEP-1 Searches

The LEP-1 searches are relevant for the neutralino channel, Section I., because in this scenario the lightest MSSM neutralino is necessarily lighter than $m_Z/2$ [228]. The Z boson can then decay into a pair of neutralinos, each of which decays via the hidden sector cascade into a hidden neutralino and lepton jets. Even though $BR(Z \rightarrow \tilde{N}_1\tilde{N}_1)$ can be as small as $10^{-3} - 10^{-4}$, this still leaves $10^3 - 10^4$ neutralino/lepton jets at LEP-1. For the sneutrino channel, Section II., the measurement of the Z width at LEP-1 constrains the branching ratio of Z into any new particle to be smaller than 10^{-3} [201]. This immediately implies $m_{\tilde{\nu}} > m_Z/2$. For the singlet channel, Section III., the LEP-1 searches are not important since the hidden fields do not couple to Z at leading order.

We have identified the following searches that could be sensitive to $Z \rightarrow \tilde{N}_1 \tilde{N}_1 \rightarrow$ lepton jets + \cancel{E} decays in our scenario

- **Monojets**

In [248] the ALEPH collaboration analyzed the so-called monojet events where no energy is detected in the hemisphere opposite to the direction of the total visible momentum. This can happen, if the neutralinos are produced at rest or in those corners of the parameter space where the hidden cascade yields a low multiplicity of visible states, in particular, if one of the neutralinos decays invisibly. Conversely, these constraints are typically avoided, if the neutralino decays to a large number of visible states.

- **Acoplanar Jets**

Events can be clustered into two jets by summing the total momenta in each of the two hemispheres defined by the plane perpendicular to the thrust axis. Acoplanar jets are then defined by requiring that the angle between transverse momenta of the two jets is smaller than, e.g., 175° [247]. In Ref. [247] the ALEPH collaboration searched for acoplanar jets accompanied by missing energy. The signal events often contain a large number of charged tracks (especially if the model satisfies the monojet constraints). Therefore they may be efficiently picked up by this analysis, even though it was designed to search for hadronic events.

- **Energetic Lepton Pairs**

Also in Ref. [247], ALEPH made a search for energetic lepton pairs in hadronic events. In the neutralino channel, Section I., two of the multiple leptons from the neutralino jet can readily meet the definition of the energetic pair.

II. LEP-2 Searches

The following LEP-2 Higgs searches are sensitive to the events $e^+e^- \rightarrow Zh$ with $h \rightarrow$ lepton jets + \cancel{E} and could potentially constrain our scenario.

- **Flavor-independent Higgs**

LEP has constrained the Higgs boson decaying into generic jets without relying on b -tagging. These searches can be relevant since our signal often displays a two-jet topology. The analysis of the OPAL collaboration [257] is the most straightforward to interpret in our framework, because it does not rely on neural network techniques. However the presence of missing energy makes the $H \rightarrow 2j$ searches less sensitive to the signal, as compared for example with the squark searches described later in this subsection.

- **Invisible Higgs**

Searches for the Zh final state where h decays entirely into missing energy have been performed by all collaborations [256]. The most relevant for us is the OPAL invisible Higgs search [244], because its visible mass cut is the least aggressive, $50 \text{ GeV} < M_{\text{vis}} < 120 \text{ GeV}$. This search can strongly constrain our models, especially the sneutrino channel where the invisible energy fraction is typically larger due to the neutrinos produced by sneutrino decays. This search can also pick up the signal events in the case of the neutralino and the singlet channel models, if the associated Z boson decays invisibly.

- **Higgs to WW^***

In Ref. [258] the ALEPH collaboration performed a search for $h \rightarrow WW^*$ decays in the context of fermiophobic Higgs models. Leptonic decays of W lead to final states with electrons/muons and missing energy, so that the ALEPH search targets final states similar to our signal — lepton jets and missing energy. Furthermore, the data sample is systematically divided into distinct classes corresponding to different decay topologies of the WW^* system. The $h \rightarrow WW^*$ search thus turns out to be very sensitive to Higgs decaying to lepton jets.

- **Higgs to 4τ**

Very recently, an analysis of the $h \rightarrow AA \rightarrow 4\tau$ decay was presented by the ALEPH collaboration [231]. This search targets the case where the intermediate pseudoscalar A is very light, 10 GeV or less, in which case Higgs decays into two

pairs of nearly overlapping τ^\pm . Since tau leptons decay into 1 or 3 charged particles most of the time, the analysis focuses on 2-jet events that contain 2 or 4 tracks per jet, while the associated Z is assumed to decay invisibly or leptonically. From our perspective, the analysis is very relevant, since no τ identification is attempted, other than constraining the number of tracks. Therefore, Higgs-to-lepton jets signal might be picked up, if the Higgs decays to a small enough number of charged states.

Apart from the Higgs searches, certain SUSY searches could also be sensitive to the Higgs-to-lepton jet final state,

- **R-parity Violation**

If there is R-parity violating operator LLE^c in the superpotential, the lightest neutralino or sneutrino decay to leptons and neutrinos. In that context, ALEPH [259] and DELPHI [260] analyzed final states with multiple leptons and missing energy.

- **Six-Leptons**

Multilepton final states can also arise from slepton decays in (R-parity conserving) gauge mediated SUSY breaking scenarios, where the missing energy is carried away by a gravitino. The ALEPH search for 6 lepton final states is described in Ref. [261].

- **Squark Searches**

Squark pair production at LEP can lead to a final state with two acoplanar jets, where each jet has small invariant mass, accompanied by missing energy (and possibly additional leptons). The searches of OPAL [262] and ALEPH [263] can pick up the signal when the Higgs decays to lepton jets carrying a large number of leptons, while the associated Z decays invisibly. The OPAL search turns out to be especially constraining, due to the fact that the number of observed events is well below the expected SM background.

III. Tevatron Searches

The Tevatron experiments search for lepton jets in a noisier hadronic environment. Even so, due to the large Higgs production cross-section and the high luminosity, discovery may be within reach with possibly many light Higgs-to-lepton jets events already on tape. We identify the following relevant searches⁴

- **Dark Photon Search**

Recently, the D0 collaboration has made a search [205] for hidden photons produced in neutralino decays. In addition to the lepton jet, a requirement for an isolated (ordinary) photon is made. The photon requirement reduces significantly the expected signal from Higgs-to-lepton jets decays, where the photon can come only from initial state radiation. In addition, the D0 search requires the lepton jet to have only two leptons which is uncommon in our scenario.

- **NMSSM Hidden Higgs**

Ref. [200] targeted a Higgs boson decaying into 4μ and $2\tau 2\mu$ final states via an intermediate pair of pseudoscalar singlets of the NMSSM. The search focused on the case where the pseudoscalar is fairly light, so that the muon and tau pairs to which it decays are highly collimated. Consequently, Ref. [200] looked for isolated muons with close companion tracks. This topology can readily arise in Higgs-to-lepton jet decays as long as the hidden photon is heavy enough to decay into muon pairs.

Studies of multilepton final states have been routinely performed at the Tevatron, mostly in the context of SUSY searches. The SM processes are unlikely to produce 3 or more energetic and *isolated* leptons, therefore such topologies offer clean channels to search for new physics. Although these searches typically target isolated high- p_T leptons,

⁴Multilepton signatures were also addressed in Ref. [264] where an excess of multi-muon events was reported. This search focuses on events with displaced vertices, and therefore it is not relevant for the Hidden Higgs signal we consider in this chapter. In any case, cross sections required to address the CDF multi-muon excess are orders of magnitude larger than the Higgs production cross section at the Tevatron.

it is conceivable that a subset of our signal events may yield muons and electrons passing the selection criteria. The most interesting from our perspective are

- **Trilepton Searches**

Of all trilepton searches Ref. [250] is singled out because it is based on the largest data sample of 3.2 fb^{-1} . Moreover, the cuts on lepton p_T and on missing transverse energy are relatively soft. However, the isolation requirements are quite severe. In particular, all objects in the analysis are required to be separated by $\Delta R > 0.4$, which decreases the sensitivity to the Higgs-to-lepton jets signal. Another search in Ref. [251] focused on di-muon pairs accompanied by a third lepton with a very low p_T threshold of 5 GeV. In this case lepton isolation is determined by calorimeter deposits: less than 10 percent of the lepton p_T should be detected in the $\Delta R = 0.4$ cone around the lepton.

- **Like-Sign Dilepton Searches**

Ref. [249] focused on events with two energetic electrons or muons of the same electric charge and large invariant mass. Such a pair can arise in the signal when the two selected leptons come from separate lepton jets, or when a lepton in a lepton jet is paired with another lepton from W or Z decays. Again the sensitivity to our signal is reduced by the isolation requirements: the sum of the transverse energy within $\Delta R = 0.4$ around the leptons must be less than 10 percent of the lepton p_T .

8.7 Hiding the Higgs

In this section we discuss the implications of the experimental searches, listed in Section 8.6, for viable models where the Higgs decays dominantly to lepton jets. After introducing our methodology in Section I., we show in Section II. that the set of observables (listed in Section II.) are constrained by LEP and the Tevatron, to a particular region which can accommodate a light Higgs decaying to lepton jets. In Section III. we then present concrete benchmark models that hide the Higgs.

I. Methodology

We are interested in how well the LEP and Tevatron searches listed in Section 8.6 constrain the Higgs decaying to lepton jets. No searches have explicitly placed limits on this signal, thus the limits must be inferred from simulation. We simulate Higgs production and decays to lepton jets using Monte Carlo and evaluate the efficiency of the above searches by making the appropriate cuts on the produced signal events. We use `Madgraph` [210] to simulate the Higgs production and decay into the hidden sector, `BRIDGE` [265] to simulate the hidden sector cascades that populate lepton jets, `Slowjet` [266] for event analysis, including kinematic cuts, jet clustering, and lepton isolation. We do not simulate hidden sector showering, which can be important for $g_d^2/4\pi \gtrsim 0.1$ [5, 108]. It is important to keep in mind that, due to the collimated nature of lepton jets, some tracks may fail to reconstruct and some leptons may fail lepton identification. While we work with the ideal situation where this is not the case, but to set reliable limits on scenarios where the Higgs decays to lepton jets, a more comprehensive study with full detector simulation is necessary. Such a study is beyond the scope of this chapter.

II. Constraints on Experimental Observables

We now discuss how the experimental searches constrain viable Higgs-to-lepton jets signatures. We consider the observables: event topology, lepton multiplicity, lepton species, and missing energy listed in Section II.. The discussion includes all three production channels discussed in Section 8.3.

We begin by arguing that several searches lead one to consider a two-jet topology for the lepton jets. For instance, the neutralino channel is strongly constrained by the acoplanar jet search at LEP-1 [247], where neutralino pairs can be produced in rare Z decays. While constraints on the Z -width allow the Z branching fraction to neutralinos to be as large as 10^{-3} , the branching fraction to 3 or more lepton jets must be suppressed by $\sim 10^{-6}$ in order for the model not to be excluded. Such low branching ratios are obtained for a very light neutralino, $m_{\tilde{N}_1} \lesssim 5$ GeV, where the resulting event topology

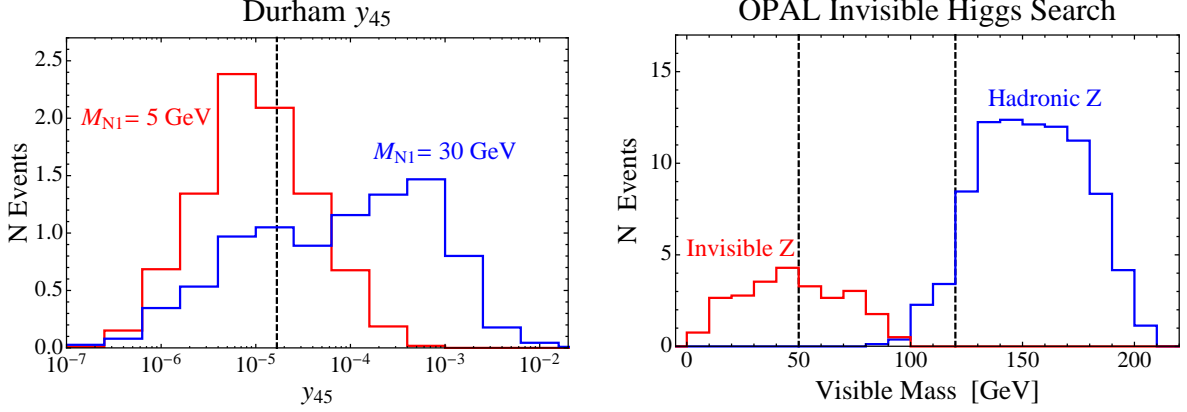


Figure 8.12: *Left:* The Durham y_{45} jet clustering parameter [267] for Higgs-strahlung events with leptonic Z 's. The ALEPH $h \rightarrow WW^*$ search [258], class **2c**, cuts on $y_{45} > 2 \times 10^{-5}$, selecting events with 5 well-separated objects (y_{45} is small, if the event has less than 5 well-separated jets). Due to the leptonic Z , this search is less sensitive to models where the Higgs decays to two or less lepton jets. *Right:* The visible mass distribution for Higgs-strahlung events with hadronic or invisible Z 's in the neutralino benchmark of Section III. The OPAL $h \rightarrow \cancel{E}_T$ search [244] selects events with $50 \text{ GeV} < M_{\text{vis}} < 120 \text{ GeV}$. Some, but not too much, missing energy per Higgs decay, $E_T \sim 50 \text{ GeV}$, helps evade this search by keeping most invisible Z events below the window and hadronic (or leptonic) Z events above the window.

consists of two back-to-back neutralino-jets (shown in the third panel of Figure 8.10). Decays with such a topology are not excluded because of the kinematical similarity to the large hadronic Z background. A two-jet topology is also favored by the $h \rightarrow WW^*$ search at LEP-2 [258]. Especially constraining is a search subclass consisting of a final state with two hard leptons, ($E_T > 25 \text{ GeV}$ and $E_T > 20 \text{ GeV}$), a softer lepton ($E_T > 8 \text{ GeV}$), and at least two additional tracks. This selection has a small SM background, which is further reduced by using the Durham jet clustering algorithm to select events with at least 5 well separated jet-like or single track objects. This subclass is sensitive to our signal from $e^+e^- \rightarrow Zh$ production, if the Z decays leptonically (forming two well-separated objects), while h decays to three or more lepton jets. Higgs production is therefore safe if the Higgs decays to less than three lepton jets, as shown on the left panel of Figure 8.12. We see that final states with two lepton jets are favored by both LEP-1 and LEP-2.

We note, however, that the two-lepton jet topology is partially constrained by LEP-2. In particular, searches for squark pair production target topologies with two QCD jets and missing energy, and these searches can be sensitive to Higgs decays to lepton jets accompanied by an invisible Z . We find that the OPAL squark search, [262], is most constraining, although because of the substantial SM background it does not have the sensitivity to exclude a 100 GeV Higgs decaying to lepton jets. An exception is the sneutrino channel, which is particularly constrained by [262], because of the extra lepton jet events due to direct sneutrino production through off-shell Z 's. The ALEPH squark search, [263], is less sensitive to all channels due to tighter cuts that largely reduce the signal. LEP-2 has also searched for Higgs decays to two QCD jets. These searches do not seriously constrain Higgs decays to lepton jets because they require heavy flavor tagging and/or focus on Higgs decays without missing energy [257].

The lepton multiplicity within lepton jets is also strongly constrained by LEP-1 and LEP-2. In particular, the neutralino cannot have a large branching fraction to invisible matter. Indeed, at LEP-1, the monojet topology must be suppressed by $\sim 10^{-6}$, and therefore the neutralino branching fraction to purely missing energy, by $\sim 10^{-3}$. The ALEPH search for $h \rightarrow 4\tau$ [231] at LEP-2 constrains the multiplicity further since the search is evaded by lepton jets containing more than 4 leptons. Meanwhile, the flavor of leptons within lepton jets is most constrained at the Tevatron, where the D0 search for $h \rightarrow 4\mu, 2\mu 2\tau$ [200] sets stringent limits on final states containing muons with companion tracks. Models where lepton jets are electron only, $m_{\gamma_d} < 2m_\mu$, are unconstrained by this search. When $m_{\gamma_d} > 2m_\mu$, lepton jets consisting of exactly two muons must be suppressed by $\sim 10^{-3}$, while lepton jets with more than two leptons can spoil the track and calorimeter isolation requirements placed on the muon pairs [200]. We therefore find that high multiplicity lepton jets are the least constrained, and are necessary for models where lepton jets include muons.

The amount of missing energy per Higgs decay is most constrained by the OPAL search for $h \rightarrow \cancel{E}_T$ which selects events with a visible mass in a wide window around the Z mass, $50 \text{ GeV} < M_{\text{vis}} < 120 \text{ GeV}$. Our signal can fall within this window when Higgs decays include too much missing energy. For a light Higgs, $m_Z \sim m_h$, this search is also

sensitive to the situation where the Z decays invisibly and the Higgs decays to lepton jets. Then, some missing energy can lead to a signal with $M_{\text{vis}} < 50$ GeV, evading the search. We therefore find that hadronic and invisible Z decays constrain the missing energy from opposite directions, and the optimal value is $E_T \sim 50$ GeV, as in the right panel of Figure 8.12. We also find that the sneutrino channel is more difficult to accommodate with this search than the other channels, because the sneutrino decays produce neutrinos that carry substantial missing energy. We note that a hidden Higgs decaying to final states that include missing energy is also considered by Ref. [268].

Finally, we comment that trilepton searches [250, 251] and like-sign dilepton searches [249], are easily evaded by lepton jets due to the strong isolation requirements of these searches. Consequently, most Tevatron searches do not constrain the Higgs-to-lepton jets scenario. We summarize the consequences of existing searches at LEP and the Tevatron for a light Higgs decaying to lepton jets,

- **Two-Jet Topology:** The Higgs should decay to two lepton jets. For the neutralino channel, $m_{\tilde{N}_1} \lesssim 10$ GeV.
- **High Lepton Multiplicity:** The lepton jets should have high lepton multiplicities, $\gtrsim 4$ leptons per lepton jet.
- **All Electron or Very High Multiplicity:** All-electron lepton jets, $m_{\gamma_d} < 2 m_\mu$, are the least constrained. Very high multiplicity lepton jets can include muons, if the rate of events with isolated muon pairs, is suppressed by $\sim 10^{-3}$.
- **Some \cancel{E}_T :** The Higgs decays should produce some, but not too much, missing energy, $\cancel{E}_T \sim 50$ GeV.

III. Benchmarks Models

We now present one benchmark model with a 100 GeV Higgs for each of the decay channels: the neutralino channel (Section I.), the sneutrino channel (Section II.), and the singlet channel (Section III.). For the neutralino and sneutrino benchmarks the hidden photon decays only to electrons, whereas for the singlet benchmark muons are

also produced. The neutralino and singlet benchmarks pass all searches of sections I., II., and III. at the 2σ level, hiding the Higgs from LEP and the Tevatron. Efficiencies of the searches for each of the benchmarks are given in Appendix A.7. For the sneutrino model, we find some tension at accommodating all searches, when using the simple $U(1)_d$ hidden sector of Section II. We present a benchmark model which is excluded by the ALEPH $h \rightarrow 4\tau$ search [231] and the OPAL $2j + \cancel{E}_T$ squark search [262] at more than 3σ , but passes all the other searches within 2σ . The tension is due to the extra lepton jet events following from $e^+e^- \rightarrow Z^* \rightarrow \tilde{\nu}\tilde{\nu}$, the missing energy carried by the neutrinos produced in the sneutrino decays, and the difficulty at achieving a 2-jet structure with sufficient lepton multiplicity. It is to be stressed that this latter difficulty is an artifact of the particular hidden sector model we are considering, and can be ameliorated in models with longer hidden sector cascades or substantial showering.

The three benchmark models occur within the supersymmetric framework. The constraints on these models are, in principle, sensitive to all soft parameters because SUSY partners may be produced at LEP and the Tevatron, and decay to lepton jets. For this discussion, because we are interested specifically in the constraints on Higgs decays to lepton jets, we decouple all unrelated SUSY partners and only consider light soft parameters that play a role in Higgs decays. For the neutralino channel, we specify the -ino spectrum, for the sneutrino channel we specify the left-handed slepton spectrum, and for the singlet channel we specify the parameters that determine the singlet VEV and F -term. It would be interesting to relax this assumption, and study the constraints on a light Higgs accompanied by additional light SUSY partners decaying to lepton jets, and we leave this for future study.

Neutralino Benchmark. For the neutralino benchmark we take $m_h = 100$ GeV, while the relevant electroweak MSSM parameters are

$$\mu = 149 \text{ GeV}, \quad M_1 = 13 \text{ GeV}, \quad M_2 = 286 \text{ GeV}, \quad \tan \beta = 3.5, \quad \sin \alpha = -0.28, \quad (8.7.18)$$

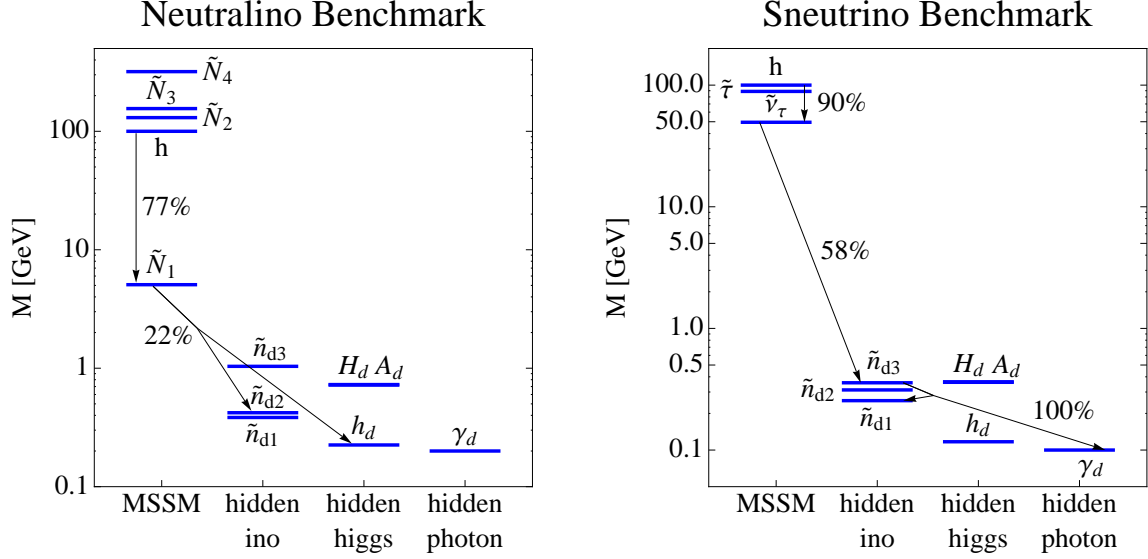


Figure 8.13: Spectra in the neutralino and sneutrino benchmark models. The dominant decay chain of the Higgs is denoted by arrows, labeled with branching ratios. Only the lowest lying states in the MSSM are shown. We also do not show the final decays into visible states in the last step of the decay chain. For the neutralino benchmark one has: $\tilde{n}_{d2} \rightarrow \tilde{n}_{d1}e^+e^-$, $h_d \rightarrow \gamma_d e^+e^-$ where in both benchmarks $\gamma_d \rightarrow e^+e^-$ and \tilde{n}_{d1} is stable.

and the hidden sector parameters are,

$$m_{\gamma_d} = 0.2 \text{ GeV}, \quad \mu_d = 0.4 \text{ GeV}, \quad M_d = 1 \text{ GeV}, \quad \tan \beta_d = 4, \quad \sin \alpha_d = -0.27, \quad (8.7.19)$$

where the hidden sector parameterization is defined in Appendix A.6. The resulting spectrum is shown in the left panel of Figure 8.13. Since $m_{\gamma_d} < 2m_\mu$ the lepton jets are composed entirely of electrons. Note that $m_{\tilde{N}_1} = 5 \text{ GeV}$, so that the Higgs decays produce boosted neutralinos. The resulting topology consists of 2 neutralino jets, avoiding the searches at LEP-1 and LEP-2. The lightest chargino has a mass of $m_{\tilde{C}_1} = 123 \text{ GeV}$, while the second lightest neutralino has a mass of $m_{\tilde{N}_2} = 130 \text{ GeV}$. These masses are above the LEP-2 reach. Also the Tevatron trilepton constraints do not apply because \tilde{N}_2 dominantly decays to \tilde{N}_1 and an on-shell Z . Trilepton searches veto events where opposite sign leptons reconstruct an on-shell Z , in order to control the electroweak background [250, 251]. For this benchmark, the Z decays to neutralinos with branching fraction $\Gamma_{Z \rightarrow 2\tilde{N}_1} = 8 \times 10^{-4}$, which is consistent with the LEP-1 measurement of the Z

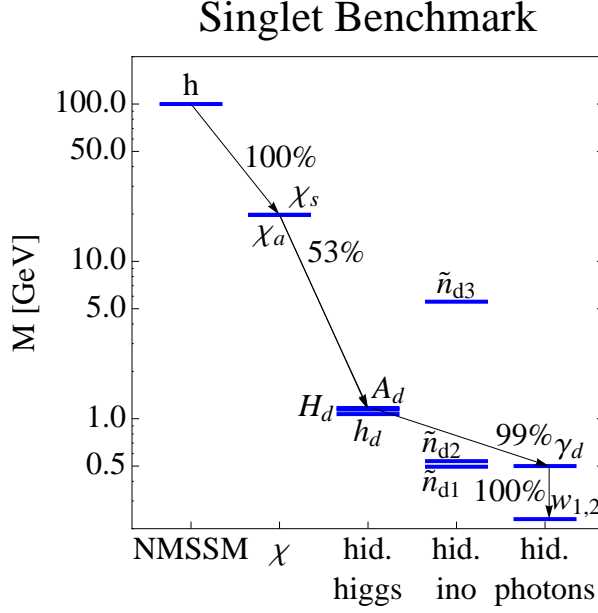


Figure 8.14: Spectrum of the singlet benchmark model. From the NMSSM states only the Higgs is shown, while other low lying states are also possible. The dominant decay chain of the Higgs is denoted by arrows, labeled with branching ratios. At the end of the decay chain $w_{\text{hid}}^{1,2}$ decay to e^+e^- . The LSP is \tilde{n}_{d1} .

width [201].

Sneutrino Benchmark. For the sneutrino benchmark, we also take $m_h \sim 100$ GeV. Here the Higgs decays into a pair of light tau sneutrinos. The relevant MSSM parameters are given by,

$$m_{L_3} = 77.3 \text{ GeV}, \quad \tan \beta = 3.5, \quad \sin \alpha = -0.28, \quad (8.7.20)$$

and the parameters that determine the hidden sector spectrum are,

$$m_{\gamma_d} = 0.1 \text{ GeV}, \quad \mu_d = 0.3 \text{ GeV}, \quad M_d = 0.3 \text{ GeV}, \quad \tan \beta_d = 4, \quad \sin \alpha_d = -0.27. \quad (8.7.21)$$

The spectrum is shown in the right panel of Figure 8.13. The hidden photon decays only to electrons. The tau sneutrino has a mass of $m_{\tilde{\nu}_\tau} = 49.5$ GeV and the stau a mass of $m_{\tilde{\tau}} = 89$ GeV. The stau and tau sneutrino are pair produced at LEP through an off-shell Z , leading to a lepton jet signal. For reference, the LEP-2 cross-sections of Higgsstrahlung, tau sneutrino pair production, and stau pair production are, at $\sqrt{s} = 206$ GeV,

$\sigma_{hZ} \simeq 0.3$ pb, $\sigma_{\tilde{\nu}\tilde{\nu}} \simeq 0.3$ pb, and $\sigma_{\tilde{\tau}\tilde{\tau}} \simeq 0.1$ pb. We find that this benchmark is ruled out by the ALEPH $h \rightarrow 4\tau$ search [231] and the OPAL $2j + \cancel{E}_T$ squark search [262], both at more than 3σ , while it passes all other searches at or below 2σ . The ALEPH search is only sensitive to lepton jets with low multiplicity and can be evaded by models that produce extra leptons through longer cascades or sufficient hidden sector showering.

Singlet Benchmark. The singlet benchmark also has a SM like Higgs at 100 GeV. In this model, the NMSSM singlet S couples to hidden sector messengers χ and $\bar{\chi}$, which couple to the hidden sector Higgses $h_{1,2}$ (see equation 8.3.17). The relevant NMSSM parameters [9] are given by,

$$\begin{aligned} \langle S \rangle = 150 \text{ GeV}, \quad \lambda = 1, \quad \kappa = 2, \quad \tan \beta = 5, \\ A_\lambda = 10, \quad A_\kappa = 1, \end{aligned} \tag{8.7.22}$$

and the hidden sector parameters are given by,

$$\begin{aligned} m_\chi = 160 \text{ GeV}, \quad \mu_d = 0.5 \text{ GeV}, \quad m_{\gamma_d} = 0.5 \text{ GeV}, \quad \tan \beta_d = 2, \\ M_d = 5.5 \text{ GeV}, \quad B\mu_d = -0.5, \text{ GeV}^2, \quad \kappa_1 = 0.1, \quad \kappa_2 = 0.1. \end{aligned} \tag{8.7.23}$$

Here, m_χ denotes the mass of the fermionic messengers, which are proportional to $\langle S \rangle$. The spectrum is shown in Figure 8.14. The scalar messengers, χ_\pm , are split by $\langle F_S \rangle$. The lighter scalar messenger has a mass of 20 GeV, allowing for the Higgs decays, $h \rightarrow \chi - \chi^*$. For this benchmark, we include muon production, which as discussed above, requires substantial lepton multiplicity in order to evade the D0 search for $h \rightarrow 4\mu, 2\mu 2\tau$ [200]. We find this difficult to achieve with the simplest $U(1)_d$ hidden sector, so for this benchmark we extend the hidden sector to a larger non-Abelian group, $SU(2)_d \supset U(1)_d$, where we take hidden sector cascades to dominantly end with decays of the form $\gamma_d \rightarrow w_d^1 w_d^2 \rightarrow 2l^- l^+$.

8.8 Suggested Search Strategies

We have argued that signatures of the Higgs decaying into lepton jets could have gone unnoticed by existing collider searches, especially if the leptons are collimated into two

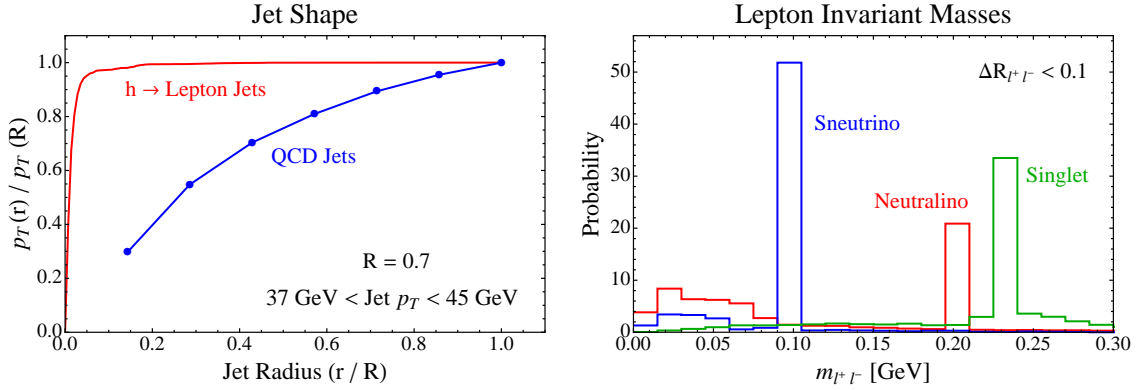


Figure 8.15: Lepton jet shape and constituent invariant masses. *Left:* We compare the shape of lepton jets produced by Higgs decays to the shape of QCD jets, as measured by CDF [269]. Jets of size $R = 0.7$ are identified by clustering the event with a midpoint-cone algorithm. The jet shape is then defined as the p_T fraction contained in smaller cones. We see that lepton jets are much narrower than QCD jets. *Right:* The invariant masses of all opposite sign lepton pairs, separated by $\Delta R < 0.1$, in Higgs decays to lepton jets. We see clear invariant mass peaks corresponding to the hidden sector photon masses, despite the background of wrong-pair combinatorics. Both jet shape and invariant mass peaks can be used to overcome the QCD background and discover lepton jets.

jets, mimicking the topology of certain hadronic backgrounds. Nevertheless, several properties of the lepton jets set them apart from QCD jets, and dedicated searches could very likely extract the signal from the SM background. Below we point out some features of the signal that could be targeted by experiments in order to increase the sensitivity. The discussion is concise and qualitative; a more quantitative study is beyond the scope of this chapter and will appear in chapter 9.

- **Hadronic energy deposition.** An obvious consequence of the high lepton content of the jets is a small energy fraction deposited in the hadronic calorimeter. Typical electrons stop in the electromagnetic calorimeter, while typical muons deposit of order 1-2 GeV in the hadronic calorimeter. Therefore experiments could search for jets with an anomalously small $E_{\text{had}}/E_{\text{em}}$ ratio.
- **Event shapes.** Since the leptons originate from highly boosted objects, lepton jets are slimmer than typical QCD jets. This is shown in Fig. 8.15 where we compare

the transverse momentum as a function of the jet radius for lepton jets and QCD jets [269]. The main parameter setting the size (defined, e.g., by the cone where 90% of the jet energy resides) is the ratio of the hidden photon mass to the electroweak scale. For the parameter choices considered in this chapter, typical lepton jet sizes are $\Delta R \lesssim 0.1$, compared to $\Delta R \sim 0.7$ for QCD jets. We stress that this estimates will change if hidden sector showering is significant, $g_d^2/4\pi \gtrsim 0.1$. An experiment could therefore impose cuts on the energy or p_T in the $0.1 < \Delta R < 0.4$ cone, as proposed in [5].

- **Pair invariant mass.** Many lepton pairs in the jets originate from two-body decays of the hidden photons. Therefore the invariant mass of the pair reconstructs the hidden photon mass. One can pair opposite sign same flavor leptons separated by, say, $\Delta R = 0.1$, and compute the invariant mass of all the pairs. The signal sample displays a prominent peak at the invariant mass of the hidden photon despite the combinatoric background. The peaks are clearly visible in Fig. 8.15 for the three benchmark points described in Section 8.7.
- **Leptons in jets.** Lepton jets in our scenario are composed of electrons, and possibly muons, with high multiplicities of leptons within each jet. QCD jets also contain leptons, but many of them originate from decays of pions and kaons in-flight. Prompt or almost prompt leptons can be produced by semileptonic decays of bottom and charm mesons, but these typically lead to 1 or 2 prompt leptons per jet. Experiments could therefore search for jets with an anomalous lepton content. Repeating the analysis of [231] without demanding the small number of tracks inside the lepton jet, but using instead the jet shape, hadronic energy or lepton ID information to control the background, could allow for sufficient sensitivity to discover a light Higgs decaying to lepton jets.

The above characteristics of lepton jets can be used to develop Tevatron searches, and to re-analyze old LEP-1 and LEP-2 data. For a 100 GeV hidden Higgs there are enough potential signal events to make such searches promising. We predict on the order of 100 Higgs events at LEP-2, and on the order of 10^4 Higgs events at the Tevatron.

Furthermore, the light neutralino scenario could lead to up to 10^4 lepton jet events at LEP-1. This is substantially more than in the case where no light SUSY state is present in which case the Z branching fraction to the hidden sector is suppressed by $\epsilon^2 \lesssim 10^{-6}$ and the number of lepton jets at LEP-1 is at most $\mathcal{O}(1)$ [1]. We conclude that a huge event sample might be buried in the existing data waiting to be uncovered! The precise sensitivity of experiments crucially depends on the experimental ability to reconstruct nearby tracks, untangle overlapping calorimetric showers, and identify nearby leptons. These issues are difficult to estimate without a full and accurate detector simulation and therefore input from the experimental community is vital.

8.9 Conclusions and Outlook

The mass and the decay width of a SM-like Higgs are strongly constrained by LEP and Tevatron searches. In the supersymmetric framework the existing bounds imply the need for fine tuning. These bounds (and hence the fine tuning) may be ameliorated if the Higgs has non-standard decays. Similarly, existing bounds on the masses of SM superpartners may be evaded if they decay unconventionally. It is therefore conceivable that both the Higgs and (possibly some of) the superpartners are sufficiently light to have been copiously produced at LEP and the Tevatron. Searches for standard decays could have missed such hidden states.

In this chapter we studied the prospects for the Higgs, and possibly the lightest neutralino or sneutrino, to be hidden at colliders due to their dominant decays into states that are part of a low scale hidden sector weakly coupled to the SM. The hidden states then subsequently cascade decay back to electrons and muons. The low, $\mathcal{O}(\text{GeV})$, mass gap in the hidden sector together with the hidden cascade decays, imply a significant number of collimated final state leptons known as lepton jets. Here we have considered three channels where the Higgs first decays to two light neutralinos, light sneutrinos or directly to the hidden sector fields. Due to the mixing between the SM and the hidden sector, the lightest visible supersymmetric particle is no longer stable and hidden cascade

decays occur. In all cases, the branching fraction of the Higgs to the hidden sector can dominate.

To test these scenarios we have identified the main experimental observables that characterize the collider signals of these models. We then simulated and studied existing SUSY and Higgs searches at LEP and the Tevatron that are potentially sensitive to lepton jets. Quite surprisingly, we found that the Higgs can evade detection if it *decays to some amount of missing energy together with many non-isolated electron or muons, all residing in two jet-like structures*. The topology and the lepton multiplicity depend on the spectrum of both the hidden and the visible sectors. Interestingly, the required phenomenology is easily produced by the minimal hidden sector model. Our study suggests that bounds on many additional SM superpartners may be significantly weakened in the presence of a low scale hidden sector. Consequently, other superpartners, not studied in this work, may be hidden at LEP or the Tevatron.

We will find it interesting to assess the potential for a discovery of this scenario in colliders, and we will address this assessment in chapter 9. We comment that one very effective path would be to reanalyze the old LEP data. A dedicated LEP-2 search for Z +lepton jets should easily extract the signal of Higgs-to-lepton jet decays from the background or significantly improve the bound on the mass of the Higgs in this scenario. Revisiting LEP-1 data may also be rewarding, because in the light neutralino scenario as many as 10^4 lepton jets (which we dub neutralino jets) could have been produced. Finally, the prospects at the Tevatron and the LHC also look promising, given the large number of final-state leptons. All experiments could increase their sensitivity to our scenario by zooming in on narrow jets with small hadronic deposits, attempting reconstruction of prompt leptons inside jets, counting their multiplicities, and studying the invariant mass distribution of close lepton pairs. So far dedicated experimental searches were limited to finding isolated lepton pairs. Our work suggests that this approach could be too narrow, and higher multiplicities of collimated leptons should also be targeted. To do so a serious study incorporating detector simulation is therefore warranted.

Finally, we stress that the relevance of our work extends beyond this particular hidden Higgs scenario. Even if the Higgs boson is heavier than 115 GeV, Higgs and/or SM

superpartners decaying to light SM states via a hidden sector is a phenomenological possibility that deserves attention. The standard new physics signatures may be altered or completely absent, and the signal would be missed unless it is specifically searched for. Multiple theoretical possibilities should be explored in order to ensure that such a scenario is not overlooked at the LHC.

Discovering Higgs Decays to (Electronic) Lepton Jets

9.1 Introduction

The Higgs boson is currently being searched for at the Tevatron and LHC, and its discovery may well complete the experimental verification of the Standard Model (SM). Alternatively, the Higgs couplings and branching fractions may differ from the SM predictions. In fact, the Higgs couplings to the light SM fermions are predicted to be very small (e.g. the Yukawa coupling to the bottom quark is $y_b \sim 0.02$). The presence of new light particles can thus drastically change the Higgs decay pattern. For this reason, Higgs decays present a promising opportunity for the discovery of new physics. In Ref. [6], we discussed a scenario where the Higgs boson decays dominantly into *two or more lepton jets plus missing energy*. The purpose of this chapter is to propose a concrete search strategy for this Higgs channel at hadron colliders.

A lepton jet (LJ) is a cluster of highly collimated charged particles: electrons, and possibly muons and pions [21, 1, 2, 80]. LJs can arise, if there exists a light hidden sector composed of unstable particles with masses in the MeV to GeV range. A well-motivated class of such models contains a massive vector particle (a hidden photon) that has a small kinetic mixing with the SM photon [34]. Due to this mixing, the hidden photon can decay to lighter particles with electric charge. For example, a 100 MeV hidden photon decays exclusively to electrons, whereas a 1 GeV one decays to electrons, muons and pions. At the Tevatron and LHC, hidden photons and other light hidden particles are produced with large boosts, causing their visible decay products to form jet-like structures. This feature makes LJs similar to ordinary QCD jets and the challenge is to develop experimental techniques that efficiently isolate the new physics signal from the hadronic background.

As of today, Higgs decays to LJs have not been targeted by any experimental analysis, and the efficiency of existing searches for this sort of signal is low. The notable exception is the latest LJ search at D0 [25], which constrains the parameter space of models in Ref. [6]. The D0 search looks for $\Delta R \lesssim 0.2$ clusters, containing an electron or muon of $p_T > 10$ GeV and at least one companion track of $p_T > 4$ GeV. These clusters are required to be isolated in an annulus, $0.2 < \Delta R < 0.4$. LJs, however, can be wider than $\Delta R \simeq 0.2$ and/or can contain a large multiplicity of leptons with $p_T < 10$ GeV. While the D0 search is sensitive to narrow LJs with low multiplicities, it would have missed LJs that are wide or more populated, as can be generic with a non-minimal or strongly coupled hidden sector. A Higgs boson decaying to such LJs could have escaped all existing searches even if it is very light, $m_h \simeq 100$ GeV [6].

In this note we concentrate on Higgs production in association with a W or Z and show that the Tevatron or early LHC is sensitive to Higgs decays to LJs for Higgs masses $\lesssim 155$ GeV. Moreover, we demonstrate that despite missing energy in the Higgs decays, it is possible to reconstruct the Higgs mass. The proposed search utilizes Higgs-specific kinematic cuts and additional cuts designed to identify LJs with the use of electromagnetic fraction (EMF) and charge ratio (CR). EMF is defined as the ratio of jet energy deposited in the electromagnetic calorimeter (ECAL) to the total jet energy. CR is defined as the ratio of the sum of the charged track p_T in the jet to the transverse energy deposited in the ECAL. We focus on the scenario where the LJs consist of electrons only (this happens when the hidden photon mass is below the $2m_\mu$ threshold). In this case the signal has EMF and CR $\simeq 1$, while QCD jets with EMF near one typically have CR different from 1. As we show, combining EMF and CR discriminates lepton jets from QCD jets, with a background efficiency on the order of a few $\times 10^{-3}$ per jet.

9.2 Models

The LJ structure is very sensitive to the details of the hidden sector. The signal we study is partially motivated by the weakly coupled models of Ref. [6]: the MSSM supplemented by a hidden $U(1)_d$ sector consisting of the hidden photon γ_d , 2 hidden Higgs scalars and

their superpartners. The SM Higgs boson decays into the hidden sector particles, which cascade down, increasing the final state multiplicity. At the end of the cascade, the hidden photons decay to electrons while the lightest hidden fermions carry off missing energy. As a result, the Higgs boson decays into 2 or more LJs plus missing energy. Alternatively, LJs can arise from a more complicated hidden sector (e.g. with a non-abelian gauge group) or from a strongly coupled hidden sector which could result in even larger final state multiplicities or wider jet shapes due to showering.

To be able to explore a wide range of LJ collider signatures we use an *N-step cascade* effective model. The hidden sector includes the hidden photon γ_d mixing with the SM photon, a stable scalar n mimicking the lightest hidden fermion described above, and a set of $N - 1$ hidden scalars $h_{d,i}$, that populate the cascade in the hidden sector. The Higgs boson first decays to a pair of hidden scalars $h_{d,1}$, which then decay to another pair of scalars $h_{d,2}$, and so forth. Finally, $h_{d,N-1}$ decays to either a pair of γ_d or n and subsequently, the hidden photons decay to pairs of electrons, while n counts as missing energy.

The tunable parameters of the effective model include the number of cascade steps (controlling the electron multiplicity and p_T), the hidden particle masses (controlling the number and width of LJs) and the branching fraction of $h_{d,N-1}$ into n (controlling the amount of missing energy). The effective model is thus flexible enough to simulate the multitude of LJ signatures available in the parameter space of [6] and in more general hidden sectors.

In this chapter, we present our results assuming a particular 3-step benchmark model. The masses of the two unstable scalars are chosen to be 10 and 4 GeV, while the hidden photon and stable scalar have masses of 100 and 90 MeV, respectively. The branching fraction of $h_{d,2}$ to n is 20%. This benchmark typically produces wide LJs with $\Delta R \sim 0.3 - 0.4$. Due to this feature, our benchmark is consistent with the D0 LJ search of Ref. [25] for the Higgs mass as low $m_h \sim 100$ GeV. We note that the D0 search has an even lower efficiency for models with longer cascades (more steps), such that the leptons are softer than the search's p_T requirement of 10 GeV.

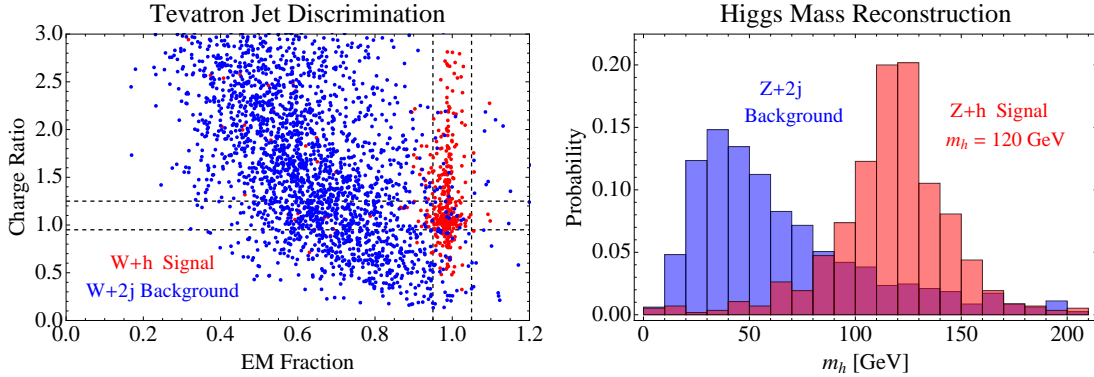


Figure 9.1: *Left*: scatter in electromagnetic fraction (EMF) and charge ratio (CR) for lepton jets (red) and background QCD jets (blue) in the $W+h$ channel at the Tevatron ($m_h = 120$ GeV). These events have passed the kinematic cuts of Eq. 9.4.1 and 9.4.2 and the jets have at least 4 tracks. EMF is the fraction of jet energy deposited in the ECAL and CR is the ratio of the sum of track p_T to the transverse energy deposited in the ECAL. The signal is clustered at EMF, $CR \simeq 1$, while these variables are anti-correlated for the QCD background. The cuts used in the analysis are denoted by dashed lines. *Right*: reconstruction of Higgs mass in the $h+Z$ channel at the Tevatron for $m_h = 120$ GeV, obtained using the approximation that the MET is collinear with the observed lepton jets. The signal (red) is clearly separated from the Z +jets background (blue).

9.3 Electron jets vs. QCD jets

To discover Higgs decays to LJs we need to tell LJs apart from ordinary QCD jets initiated by quarks and gluons. This is not completely straightforward as closely-spaced leptons do not satisfy the usual isolation criteria and will not be reconstructed as leptons by the experiments. In Ref. [6], we discussed a number of properties of LJs that may distinguish them from average QCD jets, e.g. EMF, jet shapes, and the pair invariant masses of nearby tracks. As we show below, the combination of EMF and CR is a particularly powerful discriminating tool that may open the way to a Higgs discovery. This approach is orthogonal to the one taken in Ref [25] and captures a different part of the LJ parameter space.

For the signal jets, the electrons typically leave all of their energy in the ECAL, so that $\text{EMF} \simeq 1$. This gets corrected by occasional leakage of electromagnetic showers into the HCAL, HCAL noise, or lepton jets overlapping with ordinary jets. Nonetheless, most of the signal has $\text{EMF} > 0.95$ (see Fig. 9.1).

For the background, the picture is more complicated. By the time a QCD jet reaches the detector, it mainly consists of charged pions and photons from π^0 decay. Most π^\pm deposit a sizable fraction of their energy in the HCAL, while photons deposit almost all their energy in the ECAL. The precise jet composition, and consequently EMF, fluctuates highly event-by-event. The distribution is further broadened by fluctuations of the electromagnetic and hadronic cascades, and by energy smearing in the detector (the latter also leads to a fraction of jets having $\text{EMF} > 1$). The end result is that the EMF distribution of QCD jets peaks around 0.5 – 0.8, depending on the detector. A few percent of jets have $\text{EMF} \simeq 1$. Thus the EMF alone provides only limited discriminatory power.

The high EMF tail of QCD is due to jets with a high photon content. These jets leave few tracks and are therefore expected to have small CR. In contrast, LJs composed of electrons have $\text{CR} \simeq 1$. The QCD jets and the electron jets are thus well separated in the EMF-CR plane, as shown in Fig. 9.1.

9.4 Analysis and Results

At hadron colliders, the dominant Higgs production mechanism is via gluon fusion, but the overwhelming dijet background makes this channel very challenging. Instead, we turn to Higgs production in association with electroweak gauge bosons. We search for a leptonically decaying W or Z accompanied by 2 LJs. The main background is W/Z +jets that mimic LJs.

We generated event samples for the D0 detector at the Tevatron and the ATLAS detector at the LHC with 7 TeV center-of-mass energy. Signal and background are generated at the parton level using `MadGraphv4` [66] and `BRIDGE` [265], and then showered and hadronized in `Pythia 6.4.21` [62], including multiple interactions and pileup. The

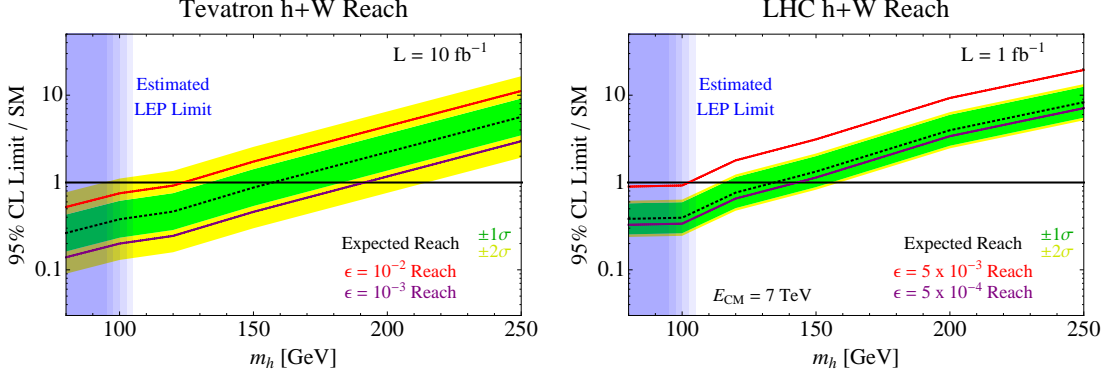


Figure 9.2: Higgs mass reach at the Tevatron (*left*) and the early LHC (*right*) with luminosities of 10 and 1 fb^{-1} , respectively. The limits are for the $h + W$ channel and are normalized to the SM Higgs production cross-section, assuming a 100% branching ratio into lepton jets. The expected 95% CL exclusion limit (black, dashed) assumes the EMF and CR rejection efficiencies, per QCD jet, extracted from our simulation and shown in Table 9.1: $\epsilon = 3.7 \times 10^{-3}$ at the Tevatron and $\epsilon = 1.2 \times 10^{-3}$ at the LHC. The green and yellow bands show the 1σ and 2σ deviations due to statistical fluctuations of the background. For comparison, the limits derived from more optimistic (lower) and more pessimistic (higher) values of ϵ are shown in purple and red, respectively. Although this signal has not been searched for at LEP, we estimated that the limit is $m_h \simeq 100 \text{ GeV}$ in Ref. [6], and this regime is shaded blue.

cross-sections are normalized to NLO using MCFM [272]. For detector simulation we use PGS4 [273] and a private code described below. We first employ kinematic cuts that target the $Z/W+h$ signal. For the search in the $Z+h$ channel we require two opposite sign same flavor isolated leptons ($l = e, \mu$) and exactly 2 jets satisfying:

$$p_T(j) > 15 \text{ GeV}, \quad \Delta R_{j_1, j_2} > 0.7, \quad (9.4.1)$$

$$p_T(l) > 10 \text{ GeV}, \quad |m(l^+l^-) - m_Z| < 10 \text{ GeV}. \quad (9.4.2)$$

The rapidity cuts are $|\eta| < 2.5$ for D0 (but removing the $1.1 < |\eta| < 1.5$ region where ECAL coverage is worse and the measurement of EMF and CR may be degraded), and $|\eta| < 2$ for ATLAS for all jets and leptons. For the $W+h$ channel we use the same cuts

on jets, but require one lepton and missing p_T satisfying,

$$p_T(l) > 20 \text{ GeV}, \quad p_{T,\text{miss}} > 20 \text{ GeV}, \quad (9.4.3)$$

and veto on additional isolated leptons harder than 10 GeV. The above cuts have efficiency of $\mathcal{O}(10 - 20\%)$ for the signal, see Table 9.1.

The kinematic cuts are insufficient to overcome the background. We therefore also employ EMF and CR cuts that are targeted at LJs. We stress that these cuts are not directly related to LJs arising from Higgs decays and would be suitable in any LJ search at hadron colliders.

The PGS4 implementation of calorimeter depositions is too simplistic for our purpose as it does not take into account realistic EM and hadronic cascades which are essential for EMF predictions. We therefore implement a fast calorimeter simulation for both D0 and ATLAS using a parametrization of EM showers in sampling calorimeters [274] and the Bock parametrization of hadronic cascades tuned to D0 [275] and ATLAS [276]. We allow fluctuations of all parameters and take into account detection efficiency of hadronic and EM energy (the non-compensation parameter h/e). Moreover, we simulate EM energy loss of heavy particles using the Landau-Vavilov distribution and detector smearing effects tuned to the detectors. For further details and references, see [209]. Finally we tune our simulation, in particular h/e , to D0 and ATLAS EMF data in dijets, obtaining accurate fits.

In order to ensure that our results are not significantly modified by photon conversions in the tracker, which we do not simulate, we require at least 4 tracks per jet. Next we use the code, described above, to estimate the EMF of the signal and background jets that pass the track cut and the kinematic cuts (9.4.1)- (9.4.3). We estimate the CR of the jets using track p_T from PGS4 divided by jet ECAL deposits obtained from our code. Sample results for $W+h$ at the Tevatron are plotted in Fig. 9.1. The electron jets are concentrated near EMF, $\text{CR} \simeq 1$, while the QCD jets display clear anti-correlation of the two variables: most of the QCD jets with EMF of order unity have CR different from 1. Due to the difference in detector performances, we tune the EMF cut differently for D0 and ATLAS. In particular, we find that a tighter EMF cut is required for ATLAS;

$m_h = 120 \text{ GeV}$		$W + h$		$Z + h$	
		Signal(Eff.)	Bckg.	Signal(Eff.)	Bckg.
Tevatron (10 fb^{-1})	Kinematic	87 (18%)	4.4×10^5	10.6 (18%)	2.8×10^4
	EMF+CR	14.4 (3%)	5.9	3.5 (6%)	1.4
LHC (1 fb^{-1})	Kinematic	35 (17%)	4.9×10^5	5.2 (25%)	3.6×10^4
	EMF+CR	4.9 (2%)	0.7	1.5 (7%)	0.7

Table 9.1: The number of signal and background events for the $W+h$ and $Z+h$ channels, with $m_h = 120 \text{ GeV}$, at the Tevatron and LHC. Event counts are shown after the cuts of Eqs. (9.4.1) - (9.4.3) and requiring at least 4 tracks per jet (Kinematic), and also after including the cuts on electromagnetic fraction and charge ratio (EMF+CR).

for D0 we take $0.95 < \text{EMF} < 1.05$, while for ATLAS, $0.99 < \text{EMF} < 1$. The CR cut is kept the same for both detectors, but different for the $W+h$ and $Z+h$ channels. The latter has smaller cross-section and requires looser cuts to retain enough statistics. We take $0.9 < \text{CR} < 1.9$ for $Z+h$ and $0.95 < \text{CR} < 1.25$ for $W+h$.

The efficiencies of our kinematic and LJ cuts are summarized in Table 9.1 for a Higgs, of mass of 120 GeV, decaying into LJs modeled by the 3-step cascade described above. In Fig. 9.2 we show the Higgs mass reach plot for 10 fb^{-1} of Tevatron data and 1 fb^{-1} of LHC data using the $W+h$ channel. As can be seen, a $\sim 155 \text{ GeV}$ (perhaps as high as 190 GeV) Higgs is accessible at the Tevatron, and $\sim 135 \text{ GeV}$ Higgs can be probed at the early LHC. The reach is much smaller in the $Z+h$ channel due to the smaller cross-section: $\sim 110 \text{ GeV}$ at the Tevatron and $\sim 80 \text{ GeV}$ at the early LHC. With more LHC data, the reach will improve significantly for both channels.

9.5 Higgs Mass

Finally, we comment that the Higgs mass can be reconstructed from the LJs in the $Z+h$ channel. Although there is missing energy in the final state carried by the n 's, we can assume that it is collinear with the two LJs (much like the $h \rightarrow \tau\tau$ channel in the

SM [277]). This gives 2 unknowns (the magnitudes of the two missing 4-vectors which are taken to be massless), that are fixed by transverse momentum conservation. The result of applying this procedure is shown in Fig. 9.1 for our benchmark model, and the Higgs mass peak is clearly visible. The limiting factor is the small cross-section in the leptonic $Z+h$ channel, which may render the mass reconstruction feasible only for light Higgs mass ($\lesssim 120$ GeV) or with more data.

Appendices

A.1 Kinetic Mixing

In this appendix we give a detailed description of kinetic mixing and its effect on dark sector/SM couplings. To begin, we consider the non-SUSY case. Following the proposal of [20], we couple the dark sector to the SM via a gauge kinetic mixing between the dark and SM hypercharges (see Eq. (2.1.1)), much like what happens in the SM between the photon and the rho meson. This scheme is attractive because it does not break any symmetries of the SM and is hence less phenomenologically constrained. Moreover, since this operator is marginal, it can be generated at a very high scale, and will persist in the infrared. This implies that if both $U(1)$'s are fundamental, the kinetic mixing is a UV boundary condition sensitive to physics at the highest scales. But if either $U(1)$ is ultimately embedded in a GUT, kinetic mixing is only induced below the GUT scale by fields charged under both $U(1)$'s. For example, by integrating out a multiplet of heavy fields Φ_i of mass M_i that is charged under both dark and SM hypercharge, we find that

$$\epsilon = -\frac{g_Y g_y}{16\pi^2} \sum_i Q_i q_i \log\left(\frac{M_i^2}{\mu^2}\right) \quad (1.1.1)$$

where Q_i and q_i are the charges of Φ_i under dark and SM hypercharge, and μ is the renormalization scale. If for example, SM hypercharge is generated by symmetry breaking of some GUT group under which Φ_i is charged, then $\sum_i Q_i = 0$. If this multiplet has uniform q_i charge, then the μ dependence cancels and the argument of the log becomes some ratio of scales in the multiplet, M/M' . For reasonable sizes of g_Y and g_y , and a log contribution $\log M/M' \sim 1$, this implies $\epsilon \sim 10^{-4} - 10^{-3}$, which is in the right range to explain DAMA.

Next, let us consider how the kinetic mixing induces couplings between the dark sector and SM. At the electroweak scale, the terms involving the kinetic mixing are

$$\mathcal{L}_{\text{gauge mix}} = -\frac{1}{4}W_{3\mu\nu}W_3^{\mu\nu} - \frac{1}{4}B_{\mu\nu}B^{\mu\nu} - \frac{1}{4}b_{\mu\nu}b^{\mu\nu} + \frac{\epsilon}{2}B_{\mu\nu}b^{\mu\nu} \quad (1.1.2)$$

$$\begin{aligned} &= -\frac{1}{4}Z_{\mu\nu}Z^{\mu\nu} - \frac{1}{4}F_{\mu\nu}F^{\mu\nu} - \frac{1}{4}b_{\mu\nu}b^{\mu\nu} \\ &\quad + \frac{\epsilon}{2}(\cos\theta_W F_{\mu\nu} - \sin\theta_W Z_{\mu\nu})b^{\mu\nu} \end{aligned} \quad (1.1.3)$$

where $F_{\mu\nu}$ and $Z_{\mu\nu}$ are the fields strengths for the SM photon and Z boson, and in the second line we have gone from gauge eigenstate to mass eigenstate. Performing a field redefinition on the photon and the dark hypercharge gauge boson

$$A_\mu' = A_\mu - \epsilon \cos\theta_W b_\mu \quad (1.1.4)$$

$$b_\mu' = b_\mu + \epsilon \sin\theta_W Z_\mu \quad (1.1.5)$$

removes the kinetic mixing between the photon and Z , and removes the kinetic mixing between the b and Z up to order ϵ^3 . In addition, these shifts will modify the gauge-current couplings, $A_\mu J_{\text{em}}^\mu + Z_\mu J_Z^\mu + b_\mu J_b^\mu + w_\mu J_w^\mu$, as well as the gauge boson mass matrix. Since the photon is exactly massless, the shift of A has no effect on the mass matrix and simply couples b to the electromagnetic current of the SM. This is precisely the channel that will generate the leptons seen in astrophysical data.

Analogously, the shift of b induces a coupling of the Z boson to the dark sector b current. However, unlike the photon, the b actually acquires a mass at $\sim \text{GeV}$, and furthermore mixes maximally with the dark w 's. For this reason shifting b induces a new mass mixing term between all the dark gauge bosons and Z_μ of order $\epsilon m_b^2/m_Z^2 = (1 \text{ GeV}/100 \text{ GeV})^2 \times \epsilon$. This in turn generates a mass suppressed coupling between b and the Z current and between Z and the w current! Thus, after removing the kinetic mixing, all the terms that couple the SM to the dark sector are

$$\begin{aligned} \mathcal{L}_{\text{coupling}} &= \epsilon b_\mu (\cos\theta_W J_{\text{em}}^\mu + \mathcal{O}(m_b^2/m_Z^2)J_Z^\mu) \\ &\quad + \epsilon Z_\mu (-\sin\theta_W J_b^\mu + \mathcal{O}(m_b^2/m_Z^2)J_w^\mu) \end{aligned} \quad (1.1.6)$$

where we have suppressed the mixing angles corresponding to the higher order contributions.

If we now add SUSY, then the kinetic mixing becomes the expression shown in Eq. (2.3.14). This induces a mixing term for gauginos and D-terms. Since we have already considered the D-term mixing in Section I, we focus on the gauginos. The new term is

$$\mathcal{L}_{\text{gaugino mix}} = -2i\epsilon\lambda_{\tilde{b}}^\dagger\bar{\sigma}^\mu\partial_\mu\lambda_{\tilde{B}} + \text{h.c.} \quad (1.1.7)$$

where $\lambda_{\tilde{b}}$ and $\lambda_{\tilde{B}}$ are the dark and MSSM bino, respectively. Once again, since the dark bino is effectively massless at the electroweak scale, it is natural to shift it by $\lambda_{\tilde{b}} \rightarrow \lambda_{\tilde{b}} + \epsilon\lambda_{\tilde{B}}$. This yields a coupling term

$$\mathcal{L}_{\text{coupling}} = \epsilon\left(\lambda_{\tilde{B}}\tilde{J}_b + \mathcal{O}(M_{\tilde{b}}/M_{\tilde{B}})\lambda_{\tilde{b}}\tilde{J}_B\right) \quad (1.1.8)$$

$$\tilde{J}_b = g_y \sum_i q_i \tilde{h}_i^\dagger h_i \quad (1.1.9)$$

$$\tilde{J}_B = g_Y \sum_i Q_i \tilde{H}_i^\dagger H_i \quad (1.1.10)$$

where \tilde{J}_b and \tilde{J}_B are the fermionic components of the dark and SM hypercharge supercurrents. Here the term that is $\mathcal{O}(M_{\tilde{b}}/M_{\tilde{B}})$ arises from new mass mixing terms that arise from the gaugino shift.

A.2 Charge Breaking in the Dark Sector

In general it is straightforward to achieve “electroweak” breaking for $G_{\text{dark}} = SU(2) \times U(1)$, simply by introducing a negative mass squared at the origin of Higgs field space. In the non-SUSY case this tachyon is inserted by hand, while in the SUSY case it arises naturally in the gauge mediation or kinetic mixing mediation scenarios mentioned in chapter 2.

However, breaking G_{dark} completely, i.e. breaking charge, is a more difficult task. To see this, let us first consider the two Higgs doublet model. We can parameterize the vevs by

$$h_1 = v_1 \begin{pmatrix} \cos \alpha \\ \sin \alpha \end{pmatrix}, \quad h_2 = v_2 \begin{pmatrix} 0 \\ 1 \end{pmatrix} \quad (1.2.11)$$

where h_1 and h_2 are $\mathbf{2}_{-1/2}$ and $\mathbf{2}_{1/2}$, respectively. For simplicity we have assumed that CP is preserved, and we have applied an $SU(2)$ transformation to rotate h_2 into a single

real component. For a given Higgs potential it is possible to determine whether charge is broken by considering the effective potential for the charge breaking angle α . Charge is preserved only if $\alpha = 0$ or π at the minimum of the potential. Since $|h_1|^2$ and $|h_2|^2$ are independent of α , only two renormalizable potential terms can contribute: $|h_1^T \epsilon h_2|^2$ and $h_1^T \epsilon h_2$. Naively, $|h_1^\dagger h_2|^2$ contributes as well, but this term can be written as $|h_1^\dagger h_2|^2 = |h_1|^2 |h_2|^2 - |h_1^T \epsilon h_2|^2$. Expanding these contributions in terms of α , the effective potential becomes

$$V_{\text{eff}}(\alpha) = -\frac{1}{2}A \cos^2 \alpha + B \cos \alpha \quad (1.2.12)$$

where A and B are a function of $v_{1,2}$ and the couplings. There is an extremum at $\alpha = \arccos B/A$. Checking that this point is stable, we find that a necessary condition for charge breaking is $A < 0$ and $|B/A| < 1$.

Next, let us consider this in an example. In the MSSM, the quartic couplings are fixed by the D-terms, which turns out to fix $A = g^2 > 0$, which is why charge is left unbroken. However, it is possible to push A below zero by introducing appropriate quartic contributions to the MSSM. In our SUSY benchmarks we accomplish this by including triplets. The one triplet SUSY benchmark has the superpotential:

$$W = \mu_\Phi \text{Tr}(\Phi\Phi) + \mu H_1^T \epsilon H_2 + \lambda H_1^T \epsilon \Phi H_2 \quad (1.2.13)$$

Let us consider the case where the triplet is heavy and we can integrate it out; this yields an effective theory of doublets in which charge breaking is simply determined. Our SUSY benchmarks are not in this decoupling limit, but nonetheless the physics of charge breaking in the low-energy doublet model appears to persist even as the triplet mass is lowered. Integrating out the triplet yields a quartic for the doublet with a coupling of $\lambda^2 m_\Phi^2 / \mu_\Phi^2$, where m_Φ is the soft mass for the triplet. Thus in $V_{\text{eff}}(\alpha)$ for this model we find

$$A = g^2 + \lambda^2 \frac{m_\Phi^2}{\mu_\Phi^2} \quad (1.2.14)$$

We see that $A < 0$ only if there is a negative soft mass for the triplet that is appropriately large. While this can be easily engineered using gauge mediation, this not always possible

generically. For example, if SUSY breaking is communicated in this theory via kinetic mixing mediation, then m_{Φ}^2 is not generated at the leading order, since Φ is a singlet under the dark hypercharge. On the other hand, we can easily remedy this by charging Φ under dark hypercharge—however, for anomaly cancellation we must also introduce a second triplet of opposite charge. In this model of two complex triplets, the kinetic mixing mediation will generate soft masses for the triplets.

A.3 Hidden \mathbb{Z}_2 Symmetry in the $\tan\beta = 1$ Limit

When $\tan\beta = 1$, there is an enhanced \mathbb{Z}_2 symmetry of the two Higgs doublet model that makes it phenomenologically inviable. In particular, under this symmetry the $w_{\pm\mu}$ have charge -1 and the z_{μ} and a_{μ} (dark photon) have charge $+1$. Since only z and a contain a component of the dark hypercharge, b , only these states couple to SM electric charge. On the other hand, transitions between the different dark matter states are mediated by w_{\pm} alone. Thus it is necessary to break this \mathbb{Z}_2 .

The origin of this \mathbb{Z}_2 is as follows. When $\tan\beta = 1$, then h_1 and h_2 have the same magnitude; thus, they can be simply thought of as two spinors that correspond to two unit vectors in 3-space. Next, h_1 and h_2 uniquely define a third direction which bisects the angle α between them. Rotations of 180° around this axis, followed by $h_1 \leftrightarrow h_2$, leave the vacuum invariant. Thus, all states in the low-energy theory are eigenstates of this \mathbb{Z}_2 . Since this \mathbb{Z}_2 is a subgroup of $SU(2)$, it acts nicely on $\{w_1, w_2, w_3\}$. It is obvious by choosing a basis where w_3 points along the axis of rotation, that two of the $SU(2)$ gauge bosons are odd under this \mathbb{Z}_2 and the remaining one is even. Thus, the latter is the only state that can mix with the dark hypercharge, b , since it is also \mathbb{Z}_2 neutral.

A.4 SUSY Contribution to DM Mass Splitting

In this appendix we present the supersymmetric contributions to the mass corrections of a Dirac fermion, Ψ . We show that in the parameter region we are interested in, those are negligible. These results are well-known (see for example [56]) and are presented

here for completeness. We begin with the non-supersymmetric contributions. Consider, therefore, a theory with a SM-like weak gauge-group $SU(2) \times U(1)$ which in general is broken down to nothing at some scale. Also, for simplicity, we take the Dirac fermion to be charged as $\mathbf{2}_{1/2}$ with a mass M_Ψ much larger than the Higgs scale of the theory. Similar conclusions hold for any representation of the gauge-group. At low energies, the masses of the two components are split. There are both wave-functions and mass insertion diagrams, given by,

$$\begin{array}{c} \text{Diagram 1: A wavy line labeled 'A' connects two fermion lines labeled '\Psi, \Psi^c'. The fermion lines are horizontal and have arrows pointing right. The wavy line is above the fermion lines.} \end{array} = -\frac{ig_A^2}{8\pi^2} \not{p} \int dx x \log \Delta \quad (1.4.15)$$

$$\begin{array}{c} \text{Diagram 2: A wavy line labeled 'A' connects two fermion lines labeled '\Psi, \Psi^c'. The fermion lines are horizontal and have arrows pointing right. The wavy line is above the fermion lines. There is a cross symbol on the fermion line between the two vertices.} \end{array} = \frac{ig_A^2}{4\pi^2} M_\Psi \int dx \log \Delta \quad (1.4.16)$$

where $\Delta = ((1-x)^2 M_\Psi^2 + x M_A^2)$, M_A is the mass of the gauge boson, and g_A is its coupling to the fermion. We neglected the divergent part since it cancels when considering the mass splitting. The propagating gauge boson is any one of the four massive vector bosons.

For the rest of this section we consider the simple case where one gauge boson is left massless. In that case we have,

$$\delta M_\Psi = \frac{\alpha M_\Psi}{2\pi} \int dx \log \left(1 + \frac{x M_Z^2}{(1-x)^2 M_\Psi^2} \right) \xrightarrow{M_\Psi \gg M_Z} \frac{\alpha M_Z}{2} \quad (1.4.17)$$

Where α is associated with the massless gauge boson coupling to matter. For a general multiplet of the gauge group the mass splitting between two eigenstates, i and j of T_3 is given by,

$$\begin{aligned} \delta M_{ij} &= \frac{\alpha}{2} (q_i^2 - q_j^2) M_z \\ &- \frac{\alpha_2}{2} ((T_i^3)^2 - (T_j^3)^2) (M_z - M_w), \end{aligned} \quad (1.4.18)$$

where the notation is explained after Eq. (2.2.9) in Section 2.2. When the ‘‘photon’’ is also massive the correction goes as the splitting between the gauge boson masses,

$$\delta M_\Psi \approx \frac{\alpha}{2} (M_Z - M_\gamma) + \dots \quad (1.4.19)$$

A.5 Decaying Models: Superpotentials and Charges

In each of the models of section 4.3, the DM can decay through dimension-6 GUT suppressed operators into GeV states in the hidden sector. For these models to work, it is necessary that renormalizable or dimension-5 operators that allow DM decays are absent. Such dangerous decays can be forbidden by global discrete symmetries at the GUT scale. Such symmetries also forbid a GUT scale mass for the DM. In this appendix we verify that the above models are generic and safe, by presenting such global symmetries that forbid both dangerous DM decays and GUT scale masses for light fields. We also collect the full superpotentials of each model, for easy reference.

$U(1)_d$

The superpotential of our minimal $U(1)_d$ model is given by:

$$\begin{aligned}
 W &= W_{\text{decay}} + W_{\text{DM}} + W_{\text{split}} , \\
 W_{\text{decay}} &= (M_{\text{GUT}} + X) Y \bar{Y} + M_{\text{GUT}} X \bar{X} + \bar{X} \chi_1 \bar{\chi}_2 , \\
 W_{\text{DM}} &= S (\chi_1 \bar{\chi}_1 + \chi_2 \bar{\chi}_2) + n h \bar{h} , \\
 W_{\text{split}} &= \sum_{i=1}^2 (S N_i^2 + N_i \chi_i \bar{h}) .
 \end{aligned} \tag{1.5.23}$$

There are several dangerous operators that are allowed by $U(1)_d$ gauge invariance. These include a GUT scale mass of the form, $\chi_i \bar{\chi}_j$, a TeV scale mass for the light Higgses, $S h \bar{h}$, renormalizable DM decay, $\chi_2 \bar{h} n$, and dimension-5 DM decay operators, $\chi_2 h \bar{h}^2$. All dangerous operators of these types are forbidden by the $\mathbb{Z}_4^R \times \mathbb{Z}_4$ symmetry displayed in the upper left of table A.1.

$$SU(2)_d \rightarrow U(1)_d$$

The superpotential of our $SU(2)_d \rightarrow U(1)_d$ model is:

$$\begin{aligned}
W &= W_{\text{decay}} + W_{\text{GUT}} + W_{\text{DM}} + W_{\text{split}} , \\
W_{\text{decay}} &= f(H) + HX^2 , \\
W_{\text{GUT}} &= \text{Tr} [g(H) (\Phi\bar{\Phi} + S_{\Phi}\bar{\Phi} + n'\bar{n} + s_n\bar{n}' + s_N N + s_{\bar{N}}\bar{N})] , \\
W_{\text{DM}} &= (\Phi + S_{\Phi})\chi\bar{\chi} + (n' + s_n)h^2 , \\
W_{\text{split}} &= (\Phi + S_{\Phi})N\bar{N} + N(\chi^2 + \bar{\chi}^2) + \bar{N}h^2 .
\end{aligned} \tag{1.5.24}$$

W_{split} is not discussed in section II., and is necessary to generate a DM splitting that evades the constraints from direct detection, as described in section II.. We also add the final two terms to W_{GUT} . Once H obtains a VEV, N_3 and \bar{N}_3 receive GUT scale masses while the charged components remain light. At low energies, W_{split} takes the form

$$W_{\text{split}}^{\text{eff}} = S(N_-\bar{N}_+ + N_+\bar{N}_-) + N_-(\chi_1^2 + \bar{\chi}_2^2) + N_+(\chi_2^2 + \bar{\chi}_1^2) + \bar{N}_-h_1^2 + \bar{N}_+h_2^2, \tag{1.5.25}$$

where S is the light linear combination of Φ_3 and S_{Φ} , as in Eq. (4.3.27). Expanding around the true minimum with $\langle S \rangle \sim \text{TeV}$ and $\langle h_2 \rangle \sim \text{GeV}$, we see that \bar{N}_- has a tadpole term which induces a VEV for N_- of order $\text{GeV}^2 / \text{TeV}$. Consequently, $\langle N_- \rangle$ contributes to the mass of χ_1 and $\bar{\chi}_2$, which splits the χ_i and $\bar{\chi}_i$ multiplets. These splittings allow the model to evade the constraints from direct detection, and to possibly incorporate the iDM and/or XDM proposals. In the upper right of table A.1, we display a \mathbb{Z}_{16} symmetry which forbids GUT scale masses for light fields and dangerous decays for DM.

In order to avoid a Landau pole below the GUT scale, the field content of this model requires that $\alpha_d \lesssim 1/100$. If DM annihilates only into light gauge fields, a gauge coupling of this size is insufficient to produce the correct DM relic density. Fortunately, W_{split} introduces DM annihilations into the light Higgses, which can dominate the annihilation cross-section and lead to the correct relic density.

SM Charged DM: $SU(5)_{\text{SM}} \times U(1)_d$

The superpotential and Kähler term of our model with DM charged under the SM are given by:

$$\begin{aligned}
W &= W_{\text{decay}} + W_{\text{DM}} + W_{\text{SM}}, \\
W_{\text{decay}} &= (M_{\text{GUT}} + X)Y\bar{Y} + M_{\text{GUT}}X\bar{X} + \bar{X}\chi\bar{\mathbf{5}}_f, \\
W_{\text{DM}} &= S(\chi\bar{\chi} + N^2 + s_1^2) + \chi H_d N + nh\bar{h}, \\
W_{\text{SM}} &= SH_u H_d + \mathbf{10}_f \bar{\mathbf{5}}_f H_d + \mathbf{10}_f^2 H_u + \frac{H_u^2 \bar{\mathbf{5}}_f^2}{M_{\text{GUT}}}, \\
K &\supset \frac{\bar{\chi} \bar{\mathbf{5}}_f^\dagger s_1}{M_{\text{GUT}}}. \tag{1.5.26}
\end{aligned}$$

Here W_{SM} denotes the usual $SU(5)$ GUT superpotential with Majorana neutrino masses and the NMSSM singlet for generating the μ term. Dangerous decay operators now include renormalizable Yukawa couplings between DM and the SM, such as $10_f \bar{\chi} H_d$. Such operators must be forbidden, and for this reason DM cannot be a fourth flavor. In table A.1, we list the charges under a $\mathbb{Z}_2^R \times \mathbb{Z}_3^R \times Z_6$ symmetry that forbids all dangerous decays and GUT scale masses, where the \mathbb{Z}_2^R extends the usual R-parity to the new fields.

$U(1)_\chi \times U(1)_d$

The superpotential of our $U(1)_\chi \times U(1)_d$ model is given by:

$$\begin{aligned}
W &= W_{\text{decay}} + W_{\text{DM}}, \\
W_{\text{decay}} &= (M_{\text{GUT}} + X)Y\bar{Y} + M_{\text{GUT}}X\bar{X} + \bar{X}\chi_1\bar{\chi}_2, \\
W_{\text{DM}} &= S_2 \chi_2 \bar{\chi}_2 + S_1(\chi_1 \bar{\chi}_1 + S_2^2) + nh\bar{h}. \tag{1.5.27}
\end{aligned}$$

This model is particularly simple since no DM splitting is required to evade the constraints from direct detection. There is a \mathbb{Z}_9^R symmetry, listed in the lower left side of table A.1, that forbids both dangerous DM decays and GUT scale masses for the light fields.

	$U(1)_d$	\mathbb{Z}_4^R	\mathbb{Z}_4	
GUT	X	0	0	0
	\bar{X}	0	2	0
	Y	1	0	0
	\bar{Y}	-1	2	0
TeV	χ_1	1	2	3
	$\bar{\chi}_1$	-1	0	3
	χ_2	1	0	1
	$\bar{\chi}_2$	-1	2	1
	S	0	0	2
	N_1	0	3	3
	N_2	0	1	1
GeV	h	1	1	1
	\bar{h}	-1	1	2
	n	0	0	1

	$SU(2)_d$	\mathbb{Z}_{16}	
GUT	H	Adj	0
	X	\square	8
	$\bar{\Phi}$	Adj	2
	\bar{n}	Adj	4
TeV	χ	\square	13
	$\bar{\chi}$	\square	5
	Φ	Adj	14
	S_Φ	1	14
	N	Adj	6
	\bar{N}	Adj	12
GeV	h	\square	2
	n'	Adj	12
	s_n	1	12

	$U(1)_\chi$	$U(1)_d$	\mathbb{Z}_9^R	
GUT	X	0	0	0
	\bar{X}	0	0	2
	Y	0	1	8
	\bar{Y}	0	-1	3
TeV	χ_1	1	0	0
	$\bar{\chi}_1$	-1	0	5
	χ_2	1	0	4
	$\bar{\chi}_2$	-1	0	0
	S_1	0	0	6
S_2	0	0	7	
GeV	h	0	1	2
	\bar{h}	0	-1	6
	n	0	0	3

	$SU(5)$	$U(1)_d$	\mathbb{Z}_2^R	\mathbb{Z}_3^R	\mathbb{Z}_6	
GUT	X	1	0	0	0	0
	\bar{X}	1	0	0	2	0
	Y	1	1	0	2	2
	\bar{Y}	1	-1	0	0	4
TeV	χ	\square	0	1	2	4
	$\bar{\chi}$	$\bar{\square}$	0	1	1	0
	S	1	0	0	2	2
	N	1	0	1	0	2
	s_1	1	0	0	0	2
GeV	h	1	1	1	0	4
	\bar{h}	1	-1	0	1	1
	n	1	0	1	1	1
SM	H_u	\square	0	0	0	4
	H_d	$\bar{\square}$	0	0	0	0
	$\bar{\mathbf{5}}_f$	$\bar{\square}$	0	1	1	2
	$\mathbf{10}_f$	\square	0	1	1	4

Table A.1: The gauge charges and example global charges for each model. Clockwise from the upper left, are the $U(1)_d$, $SU(2)_d \rightarrow U(1)_d$, $SU(5)_{\text{SM}} \times U(1)_d$, and $U(1)_\chi \times U(1)_d$ models. For each model, the charges forbid renormalizable and dimension 5 dark matter decays and GUT scale masses for light fields.

A.6 Notation for Hidden Higgs

The visible sector is the ordinary MSSM, and we follow the notation of [9]. The hidden sector is a broken supersymmetric U(1) gauge theory with 2 Higgs multiplets $h_{1,2}$ of opposite U(1) charge and the superpotential $W = \mu_d h_1 h_2$ [5]. Such a theory is completely specified by 3 scalar soft mass terms $m_{1,2}^2$, $B\mu_d$, the hidden bino mass M_d , the mu-term μ_d and the gauge coupling g_d . We do not impose any constraints on these parameters, in particular we do not assume any specific mechanism of supersymmetry breaking mediation to the dark sector. The scalar potential takes the form

$$V = (m_1^2 + \mu_d^2)|h_1|^2 + (m_2^2 + \mu_d^2)|h_2|^2 + (B\mu_d h_1 h_2 + \text{h.c.}) + \frac{g_d^2}{2} (|h_1|^2 - |h_2|^2)^2 \quad (1.6.28)$$

We are interested in the regions of the parameter space where the hidden scalars acquire vevs, $\langle h_1 \rangle = \sin \beta_d v_d$, $\langle h_2 \rangle = \cos \beta_d v_d$, which gives the hidden photon the mass $m_{\gamma_D} = g_d v_d$. In the broken phase, it is convenient to trade the scalar soft mass terms for more physical parameters: v_d , β_d and the mixing angle α_d of the two CP-even mass eigenstates h_d, H_d . The physical scalars are embedded in the Higgs fields as

$$\begin{aligned} h_1 &= \frac{\sin \beta_d v_d + \cos \alpha_d h_d + \sin \alpha_d H_d + i \cos \beta_d A_d}{\sqrt{2}} \\ h_2 &= \frac{\cos \beta_d v_d - \sin \alpha_d h_d + \cos \alpha_d H_d + i \sin \beta_d A_d}{\sqrt{2}} \end{aligned} \quad (1.6.29)$$

where A_d is the CP-odd scalar eigenstate. At the tree level the mass of the lighter Higgs h_d is constrained to be $\leq m_{\gamma_D}$, in analogy with the MSSM. However loop corrections from the hidden gauge and Higgs multiplets or from additional multiplets in the hidden sector can change that relation. Additional couplings to heavier hidden states can also contribute to the hidden Higgs mass. Therefore we take m_{h_d} as a free parameter of order m_{γ_D} when constructing our benchmark models. In the fermionic sector the mass terms after U(1) breaking are

$$- m_{\gamma_D} \sin \beta_d \tilde{h}_1 \tilde{b} + m_{\gamma_D} \cos \beta_d \tilde{h}_2 \tilde{b} - \frac{M_d}{2} \tilde{b} \tilde{b} - \mu_d \tilde{h}_1 \tilde{h}_2 + \text{h.c.} \quad (1.6.30)$$

The physical fermions are 3 dark neutralinos who are mixtures of hidden binos and higgsinos.

A.7 Efficiencies of Existing Searches for Hidden Higgs

LEP-1 searches							
Search	Ref.	Obs.	Bckg.	Neutr.	Sneutr.	Singlet	Max.
Monojets	[248]	3	2.8	< 1	0	0	6.6
Acoplanar	[247]	0	0.2	< 1	0	0	3.8
LEP-2 searches							
Search	Ref.	Obs.	Bckg.	Neutr.	Sneutr.	Singlet	Max.
$H \rightarrow 4\tau$	[231]	2	5.09	1	15	1	5.0
$H \rightarrow \cancel{E}$	[244]	8	11	2	5	3	7.5
$H \rightarrow WW^*2c$	[258]	0	0.3	2	< 1	2	3.8
$H \rightarrow WW^*2t$	[258]	1	1.2	1	1	3	5.0
6l	[261]	1	1.1	< 1	4	< 1	5.0
$2j + \cancel{E}$ (OPAL)	[262]	13	19.8	8	35	7	7.8
$2j + \cancel{E}$ (ALEPH)	[263]	19	15.9	7	3	1	14.5
$2j + 2l + \cancel{E}$	[263]	5	3	2	4	5	9.0
Tevatron searches							
Search	Ref.	Obs.	Bckg.	Neutr.	Sneutr.	Singlet	Max.
Dark photon	[205]	7	8	~ 1	< 1	< 1	7.9
$H \rightarrow 4\mu$	[200]	2	2.2	0	0	2	5.8
Unified 3l	[250]	1	1.47	< 1	< 1	< 1	3.7
Low p_T 3l	[251]	1	0.4	< 1	< 1	< 1	5.4
Like-sign 2l	[249]	13	7.8	1	< 1	< 1	14.7

Table A.2: A compilation of relevant searches for constraining the Higgs-to-lepton jet events.

In this appendix we quote the efficiencies of selected experimental analyses to the signals from the 3 benchmark models of Section 8.3. In Table A.2 we list the number of the observed events in each of the searches after all the cuts are applied (Obs.), the

expected number of SM background events (Bckg.), and the predicted number of signal events for the three benchmarks: the neutralino channel (Neutr.), the sneutrino channel (Sneutr.) and the singlet channel (Singlet). This should be compared to the maximum number of signal events (Max.) allowed at the 97.7% confidence level. This corresponds to a $2\text{-}\sigma$ one sided "exclusion" for Gaussian errors. The confidence level is determined using the CL_s prescription used at LEP for Higgs searches and takes into account downward fluctuations in the data compared to the expected background [270, 271]. The searches that do not pass the 2-sigma threshold are denoted in bold.

The numbers of observed events and the background estimates given in Table A.2 refer to the following:

- $H \rightarrow 4\tau$ search: invisible Z channel, $n_{1,2}^{\text{track}} = 2$ or 4, see Table 3 of [231],
- Invisible Higgs search in OPAL: more-than-2-jet events with M_{miss} in the 100-104 GeV bin, see Fig.4 in [244],
- $H \rightarrow WW^*$ search in ALEPH: the class 2c and 2t defined in Table 3 of [258],
- Six-lepton search in ALEPH: small Δm selection defined in Table 3.4 of [261],
- $2j + \cancel{E}$ search in OPAL and ALEPH: selection A, see Table 2 of [262], and large Δm AJ selection (years 1999-2000), see Table 5 of [263],
- $2j + 2l + \cancel{E}$ in ALEPH: to the large Δm selection (years 1999-2000), see Table 5 of [263]
- Dark photon search in D0: electron pairs with 0.2-0.4 GeV invariant mass, see Fig. 2 of [205],
- Unified trilepton search in CDF: trileptons defined by the (least tight) ttt cut, see Table 1 of [250],
- Like-sign dilepton search in CDF: dilepton events with missing energy, see Table 2 of [249].

The signal predictions were obtained using monte carlo as explained in Section I..

Bibliography

- [1] M. Baumgart, C. Cheung, J. T. Ruderman, L. T. Wang and I. Yavin, JHEP **0904**, 014 (2009) [arXiv:0901.0283 [hep-ph]].
- [2] C. Cheung, J. T. Ruderman, L. T. Wang and I. Yavin, Phys. Rev. D **80**, 035008 (2009) [arXiv:0902.3246 [hep-ph]].
- [3] J. T. Ruderman and T. Volansky, JHEP **1002**, 024 (2010) [arXiv:0908.1570 [hep-ph]].
- [4] A. Falkowski, J. T. Ruderman and T. Volansky, arXiv:1101.4936 [hep-ph].
- [5] C. Cheung, J. T. Ruderman, L. T. Wang and I. Yavin, JHEP **1004**, 116 (2010) [arXiv:0909.0290 [hep-ph]].
- [6] A. Falkowski, J. T. Ruderman, T. Volansky and J. Zupan, JHEP **1005**, 077 (2010) [arXiv:1002.2952 [hep-ph]].
- [7] A. Falkowski, J. T. Ruderman, T. Volansky and J. Zupan, Phys. Rev. Lett. **105**, 241801 (2010) [arXiv:1007.3496 [hep-ph]].
- [8] P. J. Fox *et al.*, arXiv:hep-th/0503249.
- [9] S. P. Martin, arXiv:hep-ph/9709356.
- [10] M. J. Strassler and K. M. Zurek, Phys. Lett. B **651**, 374 (2007) [arXiv:hep-ph/0604261].
- [11] T. Han, Z. Si, K. M. Zurek and M. J. Strassler, JHEP **0807**, 008 (2008) [arXiv:0712.2041 [hep-ph]].
- [12] M. J. Strassler, arXiv:0806.2385 [hep-ph].
- [13] M. J. Strassler, arXiv:hep-ph/0607160.
- [14] O. Adriani *et al.* [PAMELA Collaboration], Nature **458**, 607 (2009) [arXiv:0810.4995 [astro-ph]].

- [15] I. V. Moskalenko and A. W. Strong, *Astrophys. J.* **493**, 694 (1998) [arXiv:astro-ph/9710124].
- [16] A. A. Abdo *et al.* [The Fermi LAT Collaboration], *Phys. Rev. Lett.* **102**, 181101 (2009) [arXiv:0905.0025 [astro-ph.HE]].
- [17] A. W. Strong, I. V. Moskalenko, O. Reimer, *Astrophys. J.* **613**, 962-976 (2004). [astro-ph/0406254].
- [18] P. Meade, M. Papucci, A. Strumia and T. Volansky, arXiv:0905.0480 [hep-ph].
- [19] G. Jungman, M. Kamionkowski and K. Griest, *Phys. Rept.* **267**, 195 (1996) [arXiv:hep-ph/9506380].
- [20] N. Arkani-Hamed, D. P. Finkbeiner, T. R. Slatyer and N. Weiner, *Phys. Rev. D* **79**, 015014 (2009) [arXiv:0810.0713 [hep-ph]].
- [21] N. Arkani-Hamed and N. Weiner, *JHEP* **0812**, 104 (2008) [arXiv:0810.0714 [hep-ph]].
- [22] A. Sommerfeld, *Annalen der Physik* **403**, 257 (1931).
- [23] D. Tucker-Smith and N. Weiner, *Phys. Rev. D* **64**, 043502 (2001) [arXiv:hep-ph/0101138].
- [24] R. Bernabei *et al.* [DAMA Collaboration], *Eur. Phys. J. C* **56** (2008) 333 [arXiv:0804.2741 [astro-ph]].
- [25] D0 Note, 6079-CONF
- [26] CMS Collaboration, <https://twiki.cern.ch/twiki/bin/view/CMSPublic/PhysicsResultsEX011013>.
- [27] J. Chang *et al.*, *Nature* **456**, 362 (2008).
- [28] O. Adriani *et al.*, *Phys. Rev. Lett.* **102**, 051101 (2009) [arXiv:0810.4994 [astro-ph]].
- [29] D. P. Finkbeiner, *Astrophys. J.* **614**, 186 (2004) [arXiv:astro-ph/0311547].

- [30] D. P. Finkbeiner, arXiv:astro-ph/0409027.
- [31] G. Dobler and D. P. Finkbeiner, *Astrophys. J.* **680**, 1222 (2008) [arXiv:0712.1038 [astro-ph]].
- [32] I. Cholis, G. Dobler, D. P. Finkbeiner, L. Goodenough and N. Weiner, *Phys. Rev. D* **80**, 123518 (2009) [arXiv:0811.3641 [astro-ph]].
- [33] E. A. Baltz *et al.*, *JCAP* **0807**, 013 (2008) [arXiv:0806.2911 [astro-ph]].
- [34] B. Holdom, *Phys. Lett. B* **166**, 196 (1986).
- [35] M. Pospelov, *Phys. Rev. D* **80**, 095002 (2009) [arXiv:0811.1030 [hep-ph]].
- [36] M. Pospelov, A. Ritz and M. B. Voloshin, *Phys. Lett. B* **662**, 53 (2008) [arXiv:0711.4866 [hep-ph]].
- [37] J. Hisano, S. Matsumoto, M. Nagai, O. Saito and M. Senami, *Phys. Lett. B* **646**, 34 (2007) [arXiv:hep-ph/0610249].
- [38] J. Hisano, S. Matsumoto, M. M. Nojiri and O. Saito, *Phys. Rev. D* **71**, 063528 (2005) [arXiv:hep-ph/0412403].
- [39] M. Cirelli, A. Strumia and M. Tamburini, *Nucl. Phys. B* **787**, 152 (2007) [arXiv:0706.4071 [hep-ph]].
- [40] J. March-Russell, S. M. West, D. Cumberbatch and D. Hooper, *JHEP* **0807**, 058 (2008) [arXiv:0801.3440 [hep-ph]].
- [41] M. Pospelov and A. Ritz, *Phys. Lett. B* **671**, 391 (2009) [arXiv:0810.1502 [hep-ph]].
- [42] I. Cholis, L. Goodenough and N. Weiner, *Phys. Rev. D* **79**, 123505 (2009) [arXiv:0802.2922 [astro-ph]].
- [43] D. P. Finkbeiner and N. Weiner, *Phys. Rev. D* **76**, 083519 (2007) [arXiv:astro-ph/0702587].
- [44] G. Weidenspointner *et al.*, arXiv:astro-ph/0601673.

- [45] D. S. Akerib *et al.* [CDMS Collaboration], Phys. Rev. Lett. **96**, 011302 (2006) [arXiv:astro-ph/0509259].
- [46] Z. Ahmed *et al.* [CDMS Collaboration], Phys. Rev. Lett. **102**, 011301 (2009) [arXiv:0802.3530 [astro-ph]].
- [47] J. Angle *et al.* [XENON Collaboration], Phys. Rev. Lett. **100**, 021303 (2008) [arXiv:0706.0039 [astro-ph]].
- [48] D. N. Spergel and P. J. Steinhardt, Phys. Rev. Lett. **84**, 3760 (2000) [arXiv:astro-ph/9909386].
- [49] R. Dave, D. N. Spergel, P. J. Steinhardt and B. D. Wandelt, Astrophys. J. **547**, 574 (2001) [arXiv:astro-ph/0006218].
- [50] L. Ackerman, M. R. Buckley, S. M. Carroll and M. Kamionkowski, Phys. Rev. D **79**, 023519 (2009) [arXiv:0810.5126 [hep-ph]].
- [51] S. Chang, G. D. Kribs, D. Tucker-Smith and N. Weiner, Phys. Rev. D **79**, 043513 (2009) [arXiv:0807.2250 [hep-ph]].
- [52] I. F. Ginzburg and K. A. Kanishev, Phys. Rev. D **76**, 095013 (2007) [arXiv:0704.3664 [hep-ph]].
- [53] M. Kamionkowski and S. Profumo, Phys. Rev. Lett. **101**, 261301 (2008) [arXiv:0810.3233 [astro-ph]].
- [54] V. N. Lebedenko *et al.*, Phys. Rev. D **80**, 052010 (2009) [arXiv:0812.1150 [astro-ph]].
- [55] G. Angloher *et al.*, arXiv:0809.1829 [astro-ph].
- [56] S. D. Thomas and J. D. Wells, Phys. Rev. Lett. **81**, 34 (1998) [arXiv:hep-ph/9804359].
- [57] K. R. Dienes, C. F. Kolda and J. March-Russell, Nucl. Phys. B **492**, 104 (1997) [arXiv:hep-ph/9610479].

- [58] P. Meade, N. Seiberg and D. Shih, *Prog. Theor. Phys. Suppl.* **177**, 143 (2009) [arXiv:0801.3278 [hep-ph]].
- [59] K. M. Zurek, *Phys. Rev. D* **79**, 115002 (2009) [arXiv:0811.4429 [hep-ph]].
- [60] E. Poppitz and S. P. Trivedi, *Phys. Lett. B* **401**, 38 (1997) [arXiv:hep-ph/9703246].
- [61] Z. Komargodski and N. Seiberg, *JHEP* **0903**, 072 (2009) [arXiv:0812.3900 [hep-ph]].
- [62] T. Sjostrand, S. Mrenna and P. Z. Skands, *JHEP* **0605**, 026 (2006) [arXiv:hep-ph/0603175].
- [63] **CMS** Collaboration, G. L. Bayatian *et al.*, *J. Phys.* **G34** (2007) 995–1579.
- [64] **CMS** Collaboration, G. L. Bayatian *et al.*, CERN-LHCC-2006-001.
- [65] **ATLAS** Collaboration, CERN-LHCC-97-22.
- [66] F. Maltoni and T. Stelzer, *JHEP* **0302**, 027 (2003) [arXiv:hep-ph/0208156].
- [67] A. Arvanitaki, S. Dimopoulos, A. Pierce, S. Rajendran and J. G. Wacker, *Phys. Rev. D* **76**, 055007 (2007) [arXiv:hep-ph/0506242].
- [68] N. Arkani-Hamed, G. L. Kane, J. Thaler and L. T. Wang, *JHEP* **0608**, 070 (2006) [arXiv:hep-ph/0512190].
- [69] Y. Nomura and J. Thaler, *Phys. Rev. D* **79**, 075008 (2009) [arXiv:0810.5397 [hep-ph]].
- [70] E. Kraus and D. Stockinger, *Nucl. Phys. B* **626**, 73 (2002) [arXiv:hep-th/0105028].
- [71] Y. Cui, D. E. Morrissey, D. Poland and L. Randall, *JHEP* **0905**, 076 (2009) [arXiv:0901.0557 [hep-ph]].
- [72] M. Pospelov and A. Ritz, *Phys. Lett. B* **651**, 208 (2007) [arXiv:hep-ph/0703128].
- [73] E. J. Chun and J. C. Park, *JCAP* **0902** (2009) 026 [arXiv:0812.0308 [hep-ph]].
- [74] A. Katz and R. Sundrum, *JHEP* **0906**, 003 (2009) [arXiv:0902.3271 [hep-ph]].

- [75] A. de Gouvea, A. Friedland and H. Murayama, Phys. Rev. D **59**, 095008 (1999) [arXiv:hep-ph/9803481].
- [76] S. Dimopoulos and G. F. Giudice, Phys. Lett. B **393**, 72 (1997) [arXiv:hep-ph/9609344].
- [77] I. Jack and D. R. T. Jones, Phys. Lett. B **482**, 167 (2000) [arXiv:hep-ph/0003081].
- [78] B. Murakami and J. D. Wells, Phys. Rev. D **68**, 035006 (2003) [arXiv:hep-ph/0302209].
- [79] D. P. Finkbeiner, T. R. Slatyer, N. Weiner and I. Yavin, arXiv:0903.1037 [hep-ph].
- [80] Y. Bai and Z. Han, arXiv:0902.0006 [hep-ph].
- [81] K. Jedamzik, Phys. Rev. D **74**, 103509 (2006) [arXiv:hep-ph/0604251].
- [82] R. Essig, P. Schuster and N. Toro, Phys. Rev. D **80**, 015003 (2009) [arXiv:0903.3941 [hep-ph]].
- [83] M. Reece and L. T. Wang, JHEP **0907**, 051 (2009) [arXiv:0904.1743 [hep-ph]].
- [84] J. D. Bjorken, R. Essig, P. Schuster and N. Toro, Phys. Rev. D **80**, 075018 (2009) [arXiv:0906.0580 [hep-ph]].
- [85] F. Aharonian *et al.* [H.E.S.S. Collaboration], Astron. Astrophys. **508**, 561 (2009) [arXiv:0905.0105 [astro-ph.HE]].
- [86] F. Aharonian *et al.* [H.E.S.S. Collaboration], Phys. Rev. Lett. **101**, 261104 (2008) [arXiv:0811.3894 [astro-ph]].
- [87] L. Bergstrom, J. Edsjo and G. Zaharijas, arXiv:0905.0333 [astro-ph.HE].
- [88] D. Grasso *et al.* [FERMI-LAT Collaboration], Astropart. Phys. **32**, 140 (2009) [arXiv:0905.0636 [astro-ph.HE]].
- [89] V. Barger, W. Y. Keung, D. Marfatia and G. Shaughnessy, Phys. Lett. B **672** (2009) 141 [arXiv:0809.0162 [hep-ph]].

- [90] M. Cirelli, M. Kadastik, M. Raidal and A. Strumia, Nucl. Phys. B **813**, 1 (2009) [arXiv:0809.2409 [hep-ph]].
- [91] For other annihilating models of DM that address the cosmic ray excess, see the references of [18, 108].
- [92] D. Eichler, Phys. Rev. Lett. **63**, 2440 (1989).
- [93] E. Nardi, F. Sannino and A. Strumia, JCAP **0901** (2009) 043 [arXiv:0811.4153 [hep-ph]].
- [94] A. Arvanitaki, S. Dimopoulos, S. Dubovsky, P. W. Graham, R. Harnik and S. Rajendran, arXiv:0812.2075 [hep-ph].
- [95] X. Chen, arXiv:0902.0008 [hep-ph].
- [96] J. Mardon, Y. Nomura and J. Thaler, Phys. Rev. D **80**, 035013 (2009) [arXiv:0905.3749 [hep-ph]].
- [97] W. Buchmuller, L. Covi, K. Hamaguchi, A. Ibarra and T. Yanagida, JHEP **0703** (2007) 037 [arXiv:hep-ph/0702184].
- [98] K. Ishiwata, S. Matsumoto and T. Moroi, Phys. Rev. D **78**, 063505 (2008) [arXiv:0805.1133 [hep-ph]].
- [99] C. R. Chen, F. Takahashi and T. T. Yanagida, Phys. Lett. B **671**, 71 (2009) [arXiv:0809.0792 [hep-ph]].
- [100] P. f. Yin, Q. Yuan, J. Liu, J. Zhang, X. j. Bi and S. h. Zhu, Phys. Rev. D **79**, 023512 (2009) [arXiv:0811.0176 [hep-ph]].
- [101] M. Pospelov and M. Trott, JHEP **0904**, 044 (2009) [arXiv:0812.0432 [hep-ph]].
- [102] C. H. Chen, C. Q. Geng and D. V. Zhuridov, Phys. Lett. B **675**, 77 (2009) [arXiv:0901.2681 [hep-ph]].
- [103] B. Kyae, JCAP **0907**, 028 (2009) [arXiv:0902.0071 [hep-ph]].

- [104] S. Shirai, F. Takahashi and T. T. Yanagida, *Phys. Lett. B* **675**, 73 (2009) [arXiv:0902.4770 [hep-ph]].
- [105] A. Ibarra, A. Ringwald, D. Tran and C. Weniger, *JCAP* **0908**, 017 (2009) [arXiv:0903.3625 [hep-ph]].
- [106] D. Aristizabal Sierra, D. Restrepo and O. Zapata, *Phys. Rev. D* **80**, 055010 (2009) [arXiv:0907.0682 [hep-ph]].
- [107] S. L. Chen, R. N. Mohapatra, S. Nussinov and Y. Zhang, *Phys. Lett. B* **677**, 311 (2009) [arXiv:0903.2562 [hep-ph]].
- [108] P. Meade, M. Papucci and T. Volansky, arXiv:0901.2925 [hep-ph].
- [109] L. Bergstrom, G. Bertone, T. Bringmann, J. Edsjo and M. Taoso, arXiv:0812.3895 [astro-ph].
- [110] G. Bertone, M. Cirelli, A. Strumia and M. Taoso, *JCAP* **0903**, 009 (2009) [arXiv:0811.3744 [astro-ph]].
- [111] J. Mardon, Y. Nomura, D. Stolarski and J. Thaler, *JCAP* **0905**, 016 (2009) [arXiv:0901.2926 [hep-ph]].
- [112] S. Profumo and T. E. Jeltema, arXiv:0906.0001 [astro-ph.CO].
- [113] A. V. Belikov and D. Hooper, *Phys. Rev. D* **81**, 043505 (2010) [arXiv:0906.2251 [astro-ph.CO]].
- [114] G. Huetsi, A. Hektor and M. Raidal, *Astron. Astrophys.* **505**, 999 (2009) [arXiv:0906.4550 [astro-ph.CO]].
- [115] T. R. Slatyer, N. Padmanabhan and D. P. Finkbeiner, arXiv:0906.1197 [astro-ph.CO].
- [116] M. Cirelli, F. Iocco and P. Panci, *JCAP* **0910**, 009 (2009) [arXiv:0907.0719 [astro-ph.CO]].

- [117] T. Kanzaki, M. Kawasaki and K. Nakayama, *Prog. Theor. Phys.* **123**, 853 (2010) [arXiv:0907.3985 [astro-ph.CO]].
- [118] J. Hisano, S. Matsumoto and M. M. Nojiri, *Phys. Rev. Lett.* **92**, 031303 (2004) [arXiv:hep-ph/0307216].
- [119] P. Gondolo and G. Gelmini, *Nucl. Phys. B* **360** (1991) 145.
- [120] M. Ibe, H. Murayama and T. T. Yanagida, *Phys. Rev. D* **79**, 095009 (2009) [arXiv:0812.0072 [hep-ph]].
- [121] W. L. Guo and Y. L. Wu, *Phys. Rev. D* **79**, 055012 (2009) [arXiv:0901.1450 [hep-ph]].
- [122] D. Feldman, Z. Liu and P. Nath, *Phys. Rev. D* **79**, 063509 (2009) [arXiv:0810.5762 [hep-ph]].
- [123] K. Griest and D. Seckel, *Phys. Rev. D* **43** (1991) 3191.
- [124] L. J. Hall, T. Moroi and H. Murayama, *Phys. Lett. B* **424** (1998) 305 [arXiv:hep-ph/9712515].
- [125] J. T. Ruderman and T. Volansky, arXiv:0907.4373 [hep-ph].
- [126] M. Cirelli, N. Fornengo and A. Strumia, *Nucl. Phys. B* **753** (2006) 178 [arXiv:hep-ph/0512090].
- [127] S. Nussinov, L. T. Wang and I. Yavin, arXiv:0905.1333 [hep-ph].
- [128] A. Menon, R. Morris, A. Pierce and N. Weiner, *Phys. Rev. D* **82**, 015011 (2010) [arXiv:0905.1847 [hep-ph]].
- [129] G. D. Kribs and I. Z. Rothstein, *Phys. Rev. D* **55**, 4435 (1997) [Erratum-ibid. *D* **56**, 1822 (1997)] [arXiv:hep-ph/9610468].
- [130] T. K. Hemmick *et al.*, *Phys. Rev. D* **41**, 2074 (1990).
- [131] T. Yamagata, Y. Takamori and H. Utsunomiya, *Phys. Rev. D* **47**, 1231 (1993).

- [132] N. Seiberg, T. Volansky and B. Wecht, *JHEP* **0811** (2008) 004 [arXiv:0809.4437 [hep-ph]].
- [133] D. E. Morrissey, D. Poland and K. M. Zurek, arXiv:0904.2567 [hep-ph].
- [134] M. Dine, J. L. Feng and E. Silverstein, *Phys. Rev. D* **74** (2006) 095012 [arXiv:hep-th/0608159].
- [135] K. Schmidt-Hoberg and M. W. Winkler, arXiv:0907.3940 [astro-ph.CO].
- [136] R. E. Lingenfelter, J. C. Higdon and R. E. Rothschild, arXiv:0904.1025 [astro-ph.HE].
- [137] E. Witten, *Phys. Lett. B* **117** (1982) 324.
- [138] D. Shih, arXiv:0906.3346 [hep-ph].
- [139] B. Keren-Zur, L. Mazzucato and Y. Oz, arXiv:0906.5586 [hep-ph].
- [140] J. D. March-Russell and S. M. West, *Phys. Lett. B* **676** (2009) 133 [arXiv:0812.0559 [astro-ph]].
- [141] W. Shepherd, T. M. P. Tait and G. Zaharijas, *Phys. Rev. D* **79**, 055022 (2009) [arXiv:0901.2125 [hep-ph]].
- [142] M. Fukugita and T. Yanagida, *Phys. Lett. B* **174**, 45 (1986).
- [143] S. Davidson, E. Nardi and Y. Nir, *Phys. Rept.* **466**, 105 (2008) [arXiv:0802.2962 [hep-ph]].
- [144] G. F. Giudice, A. Notari, M. Raidal, A. Riotto and A. Strumia, *Nucl. Phys. B* **685**, 89 (2004) [arXiv:hep-ph/0310123].
- [145] S. Nussinov, *Phys. Lett. B* **165**, 55 (1985).
- [146] D. B. Kaplan, *Phys. Rev. Lett.* **68** (1992) 741.
- [147] D. E. Kaplan, M. A. Luty and K. M. Zurek, *Phys. Rev. D* **79**, 115016 (2009) [arXiv:0901.4117 [hep-ph]].

- [148] T. Cohen, D. J. Phalen, A. Pierce *et al.*, Phys. Rev. **D82**, 056001 (2010).
[arXiv:1005.1655 [hep-ph]].
- [149] G. R. Farrar and G. Zaharijas, arXiv:hep-ph/0406281.
- [150] D. Hooper, J. March-Russell and S. M. West, Phys. Lett. B **605**, 228 (2005)
[arXiv:hep-ph/0410114].
- [151] R. Kitano and I. Low, Phys. Rev. D **71** (2005) 023510 [arXiv:hep-ph/0411133].
- [152] K. Agashe and G. Servant, JCAP **0502** (2005) 002 [arXiv:hep-ph/0411254].
- [153] R. Kitano, H. Murayama and M. Ratz, Phys. Lett. B **669**, 145 (2008)
[arXiv:0807.4313 [hep-ph]].
- [154] J. Shelton and K. M. Zurek, arXiv:1008.1997 [hep-ph].
- [155] H. Davoudiasl, D. E. Morrissey, K. Sigurdson and S. Tulin, Phys. Rev. Lett. **105**,
211304 (2010) [arXiv:1008.2399 [hep-ph]].
- [156] N. Haba and S. Matsumoto, arXiv:1008.2487 [hep-ph].
- [157] P. H. Gu, M. Lindner, U. Sarkar and X. Zhang, arXiv:1009.2690 [hep-ph].
- [158] M. Blennow, B. Dasgupta, E. Fernandez-Martinez and N. Rius, arXiv:1009.3159
[hep-ph].
- [159] J. McDonald, arXiv:1009.3227 [hep-ph].
- [160] C. Cheung, G. Elor, L. J. Hall and P. Kumar, JHEP **1103**, 042 (2011)
[arXiv:1010.0022 [hep-ph]].
- [161] C. Cheung, G. Elor, L. J. Hall and P. Kumar, JHEP **1103**, 085 (2011)
[arXiv:1010.0024 [hep-ph]].
- [162] L. J. Hall, J. March-Russell and S. M. West, arXiv:1010.0245 [hep-ph].
- [163] B. Dutta and J. Kumar, arXiv:1012.1341 [hep-ph].

- [164] B. Feldstein and A. L. Fitzpatrick, JCAP **1009**, 005 (2010) [arXiv:1003.5662 [hep-ph]].
- [165] T. Cohen and K. M. Zurek, Phys. Rev. Lett. **104**, 101301 (2010) [arXiv:0909.2035 [hep-ph]].
- [166] M. R. Buckley and L. Randall, arXiv:1009.0270 [hep-ph].
- [167] N. Cosme, L. Lopez Honorez and M. H. G. Tytgat, Phys. Rev. D **72** (2005) 043505 [arXiv:hep-ph/0506320].
- [168] P. H. Gu, U. Sarkar and X. Zhang, Phys. Rev. D **80** (2009) 076003 [arXiv:0906.3103 [hep-ph]].
- [169] P. H. Gu and U. Sarkar, Phys. Rev. D **81** (2010) 033001 [arXiv:0909.5463 [hep-ph]].
- [170] H. An, S. L. Chen, R. N. Mohapatra and Y. Zhang, JHEP **1003**, 124 (2010) [arXiv:0911.4463 [hep-ph]].
- [171] E. J. Chun, arXiv:1009.0983 [hep-ph].
- [172] A. Pilaftsis and T. E. J. Underwood, Nucl. Phys. B **692** (2004) 303 [arXiv:hep-ph/0309342].
- [173] E. K. Akhmedov, V. A. Rubakov and A. Y. Smirnov, Phys. Rev. Lett. **81**, 1359 (1998) [arXiv:hep-ph/9803255].
- [174] K. Dick, M. Lindner, M. Ratz and D. Wright, Phys. Rev. Lett. **84**, 4039 (2000) [arXiv:hep-ph/9907562].
- [175] Y. Grossman, T. Kashti, Y. Nir and E. Roulet, Phys. Rev. Lett. **91**, 251801 (2003) [arXiv:hep-ph/0307081].
- [176] Y. Grossman, T. Kashti, Y. Nir and E. Roulet, JHEP **0411**, 080 (2004) [arXiv:hep-ph/0407063].
- [177] A. Kusenko, Phys. Rept. **481**, 1 (2009) [arXiv:0906.2968 [hep-ph]].

- [178] S. Davidson and A. Ibarra, Phys. Lett. B **535**, 25 (2002) [arXiv:hep-ph/0202239].
- [179] A. Arvanitaki, C. Davis, P. W. Graham, A. Pierce and J. G. Wacker, Phys. Rev. D **72** (2005) 075011 [arXiv:hep-ph/0504210].
- [180] J. Kang, M. A. Luty and S. Nasri, JHEP **0809** (2008) 086 [arXiv:hep-ph/0611322].
- [181] M. Viel, J. Lesgourgues, M. G. Haehnelt, S. Matarrese and A. Riotto, Phys. Rev. D **71** (2005) 063534 [arXiv:astro-ph/0501562].
- [182] A. Abada, S. Davidson, F. X. Josse-Michaux, M. Losada and A. Riotto, JCAP **0604** (2006) 004 [arXiv:hep-ph/0601083].
- [183] E. Nardi, Y. Nir, E. Roulet and J. Racker, JHEP **0601** (2006) 164 [arXiv:hep-ph/0601084].
- [184] G. Engelhard, Y. Grossman, E. Nardi and Y. Nir, Phys. Rev. Lett. **99**, 081802 (2007) [arXiv:hep-ph/0612187].
- [185] A. Falkowski, E. Kuflik, J. T. Ruderman, T. Volansky, *Work in progress*.
- [186] T. Kanzaki, M. Kawasaki, K. Kohri and T. Moroi, Phys. Rev. D **76**, 105017 (2007) [arXiv:0705.1200 [hep-ph]].
- [187] M. Kawasaki, K. Kohri and T. Moroi, Phys. Rev. D **71**, 083502 (2005) [arXiv:astro-ph/0408426].
- [188] J. L. Feng, M. Kaplinghat and H. B. Yu, Phys. Rev. D **82**, 083525 (2010) [arXiv:1005.4678 [hep-ph]].
- [189] D. P. Finkbeiner, L. Goodenough, T. R. Slatyer, M. Vogelsberger and N. Weiner, arXiv:1011.3082 [hep-ph].
- [190] K. Jedamzik, M. Lemoine and G. Moulhaka, JCAP **0607**, 010 (2006) [arXiv:astro-ph/0508141].
- [191] Y. Cai, M. A. Luty and D. E. Kaplan, arXiv:0909.5499 [hep-ph].

- [192] R. Barbieri and A. Dolgov, Phys. Lett. B **237**, 440 (1990).
- [193] S. Dodelson and L. M. Widrow, Phys. Rev. Lett. **72**, 17 (1994) [arXiv:hep-ph/9303287].
- [194] K. Abazajian, G. M. Fuller and M. Patel, Phys. Rev. D **64**, 023501 (2001) [arXiv:astro-ph/0101524].
- [195] M. Papucci and A. Strumia, JCAP **1003**, 014 (2010) [arXiv:0912.0742 [hep-ph]].
- [196] J. Jaeckel and A. Ringwald, Ann. Rev. Nucl. Part. Sci. **60** (2010) 405 [arXiv:1002.0329 [hep-ph]].
- [197] J. L. Feng, H. Tu and H. B. Yu, JCAP **0810**, 043 (2008) [arXiv:0808.2318 [hep-ph]].
- [198] S. Das and K. Sigurdson, arXiv:1012.4458 [astro-ph.CO].
- [199] C. Cheung, L. Hall, D. Pinner *Work in progress*.
- [200] V. M. Abazov *et al.* [D0 Collaboration], Phys. Rev. Lett. **103**, 061801 (2009) [arXiv:0905.3381 [hep-ex]].
- [201] [ALEPH Collaboration and DELPHI Collaboration and L3 Collaboration], Phys. Rept. **427**, 257 (2006) [arXiv:hep-ex/0509008].
- [202] H. Baer and X. Tata, Phys. Rev. D **47**, 2739 (1993).
- [203] B. C. Allanach *et al.*, in *Proc. of the APS/DPF/DPB Summer Study on the Future of Particle Physics (Snowmass 2001)* ed. N. Graf, Eur. Phys. J. C **25**, 113 (2002) [arXiv:hep-ph/0202233].
- [204] D. Shih and S. Thomas, *Private communication*.
- [205] V. M. Abazov *et al.* [D0 Collaboration], Phys. Rev. Lett. **103**, 081802 (2009) [arXiv:0905.1478 [hep-ex]].
- [206] F. Krauss, A. Schalicke and G. Soff, Comput. Phys. Commun. **174**, 876 (2006) [arXiv:hep-ph/0503087].

- [207] C. W. Bauer and F. J. Tackmann, Phys. Rev. D **76**, 114017 (2007) [arXiv:0705.1719 [hep-ph]].
- [208] B. Batell, M. Pospelov and A. Ritz, Phys. Rev. D **79**, 115008 (2009) [arXiv:0903.0363 [hep-ph]].
- [209] C. Amsler *et al.* [Particle Data Group], Phys. Lett. B **667**, 1 (2008).
- [210] J. Alwall *et al.*, JHEP **0709**, 028 (2007) [arXiv:0706.2334 [hep-ph]].
- [211] J. F. Gunion, H. E. Haber, G. L. Kane, and S. Dawson, SCIPP-89/13.
- [212] R. Barate *et al.* Phys. Lett. B **565**, 61 (2003) [arXiv:hep-ex/0306033].
- [213] H. Flacher, M. Goebel, J. Haller, A. Hocker, K. Moenig and J. Stelzer, Eur. Phys. J. C **60**, 543 (2009) [arXiv:0811.0009 [hep-ph]].
- [214] R. E. Shrock and M. Suzuki, Phys. Lett. B **110**, 250 (1982).
- [215] B. A. Dobrescu and K. T. Matchev, JHEP **0009**, 031 (2000) [arXiv:hep-ph/0008192].
- [216] D. O'Connell, M. J. Ramsey-Musolf and M. B. Wise, Phys. Rev. D **75**, 037701 (2007) [arXiv:hep-ph/0611014].
- [217] O. Bahat-Treidel, Y. Grossman and Y. Rozen, JHEP **0705**, 022 (2007) [arXiv:hep-ph/0611162].
- [218] K. Cheung, J. Song and Q. S. Yan, Phys. Rev. Lett. **99**, 031801 (2007) [arXiv:hep-ph/0703149].
- [219] S. Schael *et al.* Eur. Phys. J. C **47**, 547 (2006) [arXiv:hep-ex/0602042].
- [220] S. Chang, R. Dermisek, J. F. Gunion and N. Weiner, Ann. Rev. Nucl. Part. Sci. **58**, 75 (2008) [arXiv:0801.4554 [hep-ph]].
- [221] R. Dermisek, Mod. Phys. Lett. A **24**, 1631 (2009) [arXiv:0907.0297 [hep-ph]].

- [222] R. Dermisek and J. F. Gunion, Phys. Rev. Lett. **95**, 041801 (2005) [arXiv:hep-ph/0502105].
- [223] R. Dermisek and J. F. Gunion, Phys. Rev. D **75**, 075019 (2007) [arXiv:hep-ph/0611142].
- [224] R. Dermisek and J. F. Gunion, Phys. Rev. D **81**, 075003 (2010) [arXiv:1002.1971 [hep-ph]].
- [225] S. Chang, P. J. Fox and N. Weiner, JHEP **0608**, 068 (2006) [arXiv:hep-ph/0511250].
- [226] B. Bellazzini, C. Csaki, A. Falkowski and A. Weiler, Phys. Rev. D **80**, 075008 (2009) [arXiv:0906.3026 [hep-ph]];
- [227] B. Bellazzini, C. Csaki, A. Falkowski and A. Weiler, arXiv:0910.3210 [hep-ph].
- [228] L. M. Carpenter, D. E. Kaplan and E. J. Rhee, Phys. Rev. Lett. **99**, 211801 (2007) [arXiv:hep-ph/0607204].
- [229] M. S. Carena, J. R. Ellis, A. Pilaftsis and C. E. M. Wagner, Nucl. Phys. B **586**, 92 (2000) [arXiv:hep-ph/0003180].
- [230] M. S. Carena, J. R. Ellis, S. Mrenna, A. Pilaftsis and C. E. M. Wagner, Nucl. Phys. B **659**, 145 (2003) [arXiv:hep-ph/0211467].
- [231] ALEPH Collaboration, arXiv:1003.0705 [hep-ex].
- [232] G. Abbiendi *et al.* [OPAL Collaboration], Eur. Phys. J. C **27**, 311 (2003) [arXiv:hep-ex/0206022].
- [233] F. Aharonian *et al.* [H.E.S.S. Collaboration], Phys. Rev. Lett. **101**, 261104 (2008) [arXiv:0811.3894 [astro-ph]];
- [234] I. Z. Rothstein, T. Schwetz and J. Zupan, JCAP **0907**, 018 (2009) [arXiv:0903.3116 [astro-ph.HE]].

- [235] M. J. Strassler and K. M. Zurek, Phys. Lett. B **661** (2008) 263 [arXiv:hep-ph/0605193].
- [236] S. Gopalakrishna, S. Jung and J. D. Wells, Phys. Rev. D **78**, 055002 (2008) [arXiv:0801.3456 [hep-ph]].
- [237] B. Batell, M. Pospelov and A. Ritz, Phys. Rev. D **80** (2009) 095024 [arXiv:0906.5614 [hep-ph]].
- [238] M. Ahlers, J. Jaeckel, J. Redondo and A. Ringwald, Phys. Rev. D **78**, 075005 (2008) [arXiv:0807.4143 [hep-ph]].
- [239] M. Goodsell, J. Jaeckel, J. Redondo and A. Ringwald, JHEP **0911**, 027 (2009) [arXiv:0909.0515 [hep-ph]].
- [240] M. Freytsis, G. Ovanesyanyan and J. Thaler, JHEP **1001**, 111 (2010) [arXiv:0909.2862 [hep-ph]].
- [241] P. Schuster, N. Toro and I. Yavin, Phys. Rev. D **81**, 016002 (2010) [arXiv:0910.1602 [hep-ph]].
- [242] P. Meade, S. Nussinov, M. Papucci and T. Volansky, JHEP **1006**, 029 (2010) [arXiv:0910.4160 [hep-ph]].
- [243] R. Essig, P. Schuster, N. Toro and B. Wojtsekhowski, JHEP **1102**, 009 (2011) [arXiv:1001.2557 [hep-ph]].
- [244] G. Abbiendi *et al.* [OPAL Collaboration], arXiv:0707.0373 [hep-ex].
- [245] J. D. Mason, D. E. Morrissey and D. Poland, Phys. Rev. D **80** (2009) 115015 [arXiv:0909.3523 [hep-ph]].
- [246] A. Djouadi, J. Kalinowski and M. Spira, Comput. Phys. Commun. **108**, 56 (1998) [arXiv:hep-ph/9704448].
- [247] D. Buskulic *et al.* [ALEPH Collaboration], Phys. Lett. B **313**, 299 (1993).

- [248] D. Buskulic *et al.* [ALEPH Collaboration], Phys. Lett. B **334**, 244 (1994).
- [249] A. Abulencia *et al.* [CDF Collaboration], Phys. Rev. Lett. **98**, 221803 (2007) [arXiv:hep-ex/0702051].
- [250] The CDF Collaboration, CDF Public Note 9817 (2009),
- [251] T. Aaltonen *et al.* [CDF Collaboration], Phys. Rev. D **79**, 052004 (2009) [arXiv:0810.3522 [hep-ex]].
- [252] M. L. Graesser, Phys. Rev. D **76**, 075006 (2007) [arXiv:0704.0438 [hep-ph]];
- [253] M. L. Graesser, arXiv:0705.2190 [hep-ph].
- [254] G. Choudalakis, et al., [CDF Collaboration], CDF note 8763
- [255] R. Barate *et al.* [LEP Working Group for Higgs boson searches], Phys. Lett. B **565**, 61 (2003) [arXiv:hep-ex/0306033].
- [256] [LEP Higgs Working Group for Higgs boson searches], arXiv:hep-ex/0107032.
- [257] G. Abbiendi *et al.* [OPAL Collaboration], Phys. Lett. B **597**, 11 (2004) [arXiv:hep-ex/0312042].
- [258] S. Schael *et al.* [ALEPH Collaboration], Eur. Phys. J. C **49**, 439 (2007) [arXiv:hep-ex/0605079].
- [259] A. Heister *et al.* [ALEPH Collaboration], Eur. Phys. J. C **25**, 1 (2002) [arXiv:hep-ex/0201013].
- [260] J. Abdallah *et al.* [DELPHI Collaboration], Eur. Phys. J. C **36**, 1 (2004) [Eur. Phys. J. C **37**, 129 (2004)] [arXiv:hep-ex/0406009].
- [261] A. Garcia-Bellido, arXiv:hep-ex/0212024.
- [262] G. Abbiendi *et al.* [OPAL Collaboration], Phys. Lett. B **545** (2002) 272 [Erratum-*ibid.* B **548** (2002) 258] [arXiv:hep-ex/0209026].

- [263] A. Heister *et al.* [ALEPH Collaboration], Phys. Lett. B **537** (2002) 5 [arXiv:hep-ex/0204036].
- [264] T. Aaltonen *et al.* [CDF Collaboration], arXiv:0810.5357 [hep-ex].
- [265] P. Meade and M. Reece, hep-ph/0703031.
- [266] **SlowJet** is a private **Mathematica** package for event analysis, to be distributed upon demand.
- [267] S. Moretti, L. Lonnblad and T. Sjostrand, JHEP **9808**, 001 (1998) [arXiv:hep-ph/9804296].
- [268] S. Chang and N. Weiner, JHEP **0805**, 074 (2008) [arXiv:0710.4591 [hep-ph]].
- [269] D. E. Acosta *et al.* [CDF Collaboration], Phys. Rev. D **71** (2005) 112002 [arXiv:hep-ex/0505013].
- [270] A.L. Read, F. James, L. Lyons, and Y. Perrin (eds.), Workshop on Condence Limits, CERN Yellow Report 2000-005
- [271] T. Junk, Nucl. Instrum. Meth. A **434**, 435 (1999) [arXiv:hep-ex/9902006].
- [272] J. M. Campbell and R. K. Ellis, Phys. Rev. D **65**, 113007 (2002) [arXiv:hep-ph/0202176].
- [273] J. Conway, <http://www.physics.ucdavis.edu/~conway/research/software/pgs/pgs4-general.htm>.
- [274] G. Grindhammer and S. Peters, hep-ex/0001020.
- [275] D. M. Norman, Ph. D. Thesis, UMI-94-25106.
- [276] Y. A. Kulchitsky, M. V. Kuzmin, J. A. Budagov, V. B. Vinogradov and M. Nessi, hep-ex/0004009.
- [277] R. K. Ellis, I. Hinchliffe, M. Soldate and J. J. van der Bij, Nucl. Phys. B **297**, 221 (1988).